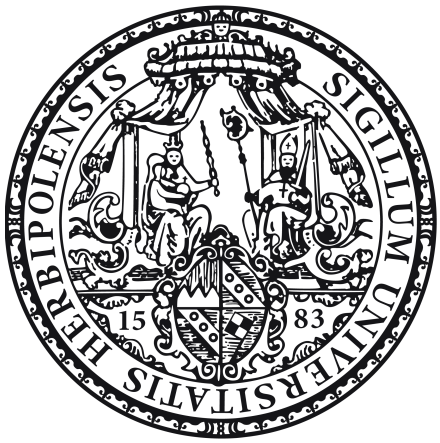

Identification of metabolic liabilities in 3D models of cancer

Identifikation metabolischer Abhängigkeiten in 3D Tumormodellen

Doctoral thesis
for a doctoral degree
at the Graduate School of Life Sciences,
Julius-Maximilians-Universität Würzburg,

Section Biomedicine

submitted by

Irem Kaymak
from Kdz Eregli, Turkey

Würzburg, 2019

Submitted on:

……..……..

Office stamp

Members of the *Promotionskomitee*:

Chairperson:

Primary Supervisor: Prof. Almut Schulze

Supervisor (Second): Dr. Mathias Rosenfeldt

Supervisor (Third): Prof. Thomas Rudel

Date of Public Defence: ……

Date of Receipt of Certificates:

…….

SUMMARY

Inefficient vascularisation of solid tumours leads to the formation of oxygen and nutrient gradients. In order to mimic this specific feature of the tumour microenvironment, a multicellular tumour spheroid (SPH) culture system was used. These experiments were implemented in p53 isogenic colon cancer cell lines (HCT116 p53 +/+ and HCT116 p53-/-) since Tp53 has important regulatory functions in tumour metabolism. First, the characteristics of the cells cultured as monolayers and as spheroids were investigated by using RNA sequencing and metabolomics to compare gene expression and metabolic features of cells grown in different conditions. This analysis showed that certain features of gene expression found in tumours are also present in spheroids but not in monolayer cultures, including reduced proliferation and induction of hypoxia related genes. Moreover, comparison between the different genotypes revealed that the expression of genes involved in cholesterol homeostasis is induced in p53 deficient cells compared to p53 wild type cells and this difference was only detected in spheroids and tumour samples but not in monolayer cultures. In addition, it was established that loss of p53 leads to the induction of enzymes of the mevalonate pathway via activation of the transcription factor SREBP2, resulting in a metabolic rewiring that supports the generation of ubiquinone (coenzyme Q10). An adequate supply of ubiquinone was essential to support mitochondrial electron transport and pyrimidine biosynthesis in p53 deficient cancer cells under conditions of metabolic stress. Moreover, inhibition of the mevalonate pathway using statins selectively induced oxidative stress and apoptosis in p53 deficient colon cancer cells exposed to oxygen and nutrient deprivation. This was caused by ubiquinone being required for electron transfer by dihydroorotate dehydrogenase, an essential enzyme of the pyrimidine nucleotide biosynthesis pathway. Supplementation with exogenous nucleosides relieved the demand for electron transfer and restored viability of p53 deficient cancer cells under metabolic stress. Moreover, the mevalonate pathway was also essential for the synthesis of ubiquinone for nucleotide biosynthesis to support growth of intestinal tumour organoids. Together, these findings highlight the importance of the mevalonate pathway in cancer cells and provide molecular evidence for an enhanced sensitivity towards the inhibition of mitochondrial electron transfer in tumour-like metabolic environments.

ZUSAMMENFASSUNG

In soliden Tumoren führt die ineffiziente Bildung von Blutgefäßen (Vaskularisierung) zu einem Nährstoff- und Sauerstoffgradienten im gesamten Tumor, welches eine spezifische Tumormikroumgebung schafft. Um diese Tumorumgebung nachzuahmen, wurde ein spezielles multi-zelluläres Tumorsphäroid (SPH) Zellkultursystem verwendet. Da Tp53 wichtige regulatorische Funktionen im Tumormetabolismus hat, wurde zur Generierung von Sphäroiden p53 isogene Darmkrebs-Zelllinen HCT116 (p53 +/+ und p53 -/-) verwendet. Zunächst wurden die Sphäroide mittels RNA Sequenzierung und Metabolomik charakterisiert, um die Genexpression und metabolischen Eigenschaften in verschiedenen Zellkulturbedingungen zu vergleichen. Diese Analyse hat gezeigt, dass gewisse Genexpressionsmuster in Tumoren wie beispielsweise Proliferations- und Hypoxia verwandte Gene in Sphäroiden übereinstimmen, nicht jedoch in Monolayer-Kulturen. Vergleicht man die zwei unterschiedlichen Genotypen miteinander, so sind Gene, die in der Cholesterinhomöostase involviert sind, in p53 defizienten Zellen induziert, nicht jedoch in p53 wildtypischen Zellen. Dieser Unterschied ist in Sphäroiden vorhanden, nicht jedoch in Monolayer-Kulturen. Verlust von p53 führt über die Aktivierung des Transkriptionsfaktors SREBP2 zur Induktion von Enzymen des Mevalonat-Synthesewegs und zudem zu einer neuen metabolischen Vernetzung, die die Generierung von Ubichinon (Coenzym Q10) unterstützt. Eine ausreichende Ubichinon-Versorgung ist wichtig, um den mitochondrialen Elektronentransport und die Pyrimidin-Biosynthese in p53-defizienten Krebszellen unter metabolischen Stressbedingungen zu unterstützen. Darüber hinaus induziert die Inhibition des Mevalonat-Synthesewegs durch Statine in p53-defizienten Darmkrebszellen, die Sauerstoff und Nährstoffmangel ausgesetzt sind, selektiv oxidativen Stress und Apoptose. Verursacht wird dies durch einen Mangel an Ubichinon, welches für den Elektronentransfer der Dihydroorotatdehydrogenase, einem essentiellen Enzym der Pyrimidinnukleotid-Biosynthese, notwendig ist. Gabe von exogenen Nukleosiden entlastete die Nachfrage an Elektronentransfer und stellte die Lebensfähigkeit von p53-defizienten Krebszellen unter metabolischem Stress wieder her. Darüber hinaus konnte gezeigt werden, dass der Mevalonat-Syntheseweg auch für die Synthese von Ubichinon für die Pyrimidinnukleotid-Biosynthese unerlässlich ist, um das Wachstum von Darmtumor-Organoiden zu unterstützen. Zusammengenommen interstreichen diese Ergebnisse die Bedeutung des Mevalonat-Syntheseweg in Krebszellen und liefern den molekularen Mechanismus für die erhöhte Empfindlichkeit von Tumorzellen gegenüber der Hemmung des mitochondrialen Elektronentransfers in einer Tumor-ähnlichen Stoffwechselumgebung.

1 INTRODUCTION

1.1 Cancer metabolism

Cell growth and proliferation is a tightly controlled process in normal cells. Extrinsic growth factors and intracellular signals are maintained in a balance during normal cell proliferation. However, cancer cells represent uncontrolled, high proliferation rates. Rapid cell proliferation requires energy in the form of ATP as well as the synthesis or uptake of amino acids, nucleotides and lipids as building blocks for the production of proteins, nucleic acids and biological membranes, respectively (Lunt et al., 2011). In order to synthesize these precursors for macromolecules, several processes of the intermediate metabolism are needed, including glycolysis, for the formation of pyruvate or lactate from glucose, the pentose phosphate pathway (PPP), for the formation of riboses and NADPH, the citric acid cycle, for the generation of metabolic precursors and reducing equivalents (NADH, $FADH_2$) and oxidative phosphorylation (OXPHOS) for the generation of ATP. Moreover, fatty acid synthesis is essential for the formation of phospholipids for membranes and triacylglycerides for energy storage, while cholesterol synthesis also provides membrane lipids as well as other important metabolic intermediates. Conversely, beta-oxidation contributes to the generation of ATP from fatty acid catabolism. Therefore, it is evident that metabolism and high proliferation rates of cancer cells are linked to each other. Similarly, cancer metabolism has been recognised as one of the emerging hallmarks of cancer (Hanahan et al., 2011).

Normal cells in a resting state direct glucose to mitochondria for oxidation in order to generate ATP via the electron transport chain and oxidative phosphorylation. This reaction also recycles NADH to NAD^+. In contrast, rapidly proliferating cells produce ATP mainly through glucose fermentation, which requires the conversion of pyruvate to lactate to regenerate NAD^+. Otto Warburg

stated that cancer cells metabolize glucose into lactate even in the presence of oxygen, presumably because of defective mitochondria in cancer cells (Otto Warburg, 1924) (O. Warburg, 1956). This phenomenon is called aerobic glycolysis. As a consequence, cancer cells display more glucose uptake and high lactate secretion compared to the normal cells and this phenomenon led to the invention of FDG-PET (Gallamini et al., 2014). Later, it has been proven that cancer cells do not switch to aerobic glycolysis because of defective mitochondria; it is rather because of the perturbed signaling pathways driven by the activation of oncogenes and loss of tumour suppressor function (Vander Heiden et al., 2009). Although aerobic glycolysis yields less energy than respiration, the reason cancer cells preferentially produce lactate via aerobic glycolysis remains to be explained. Taken together, cancer cells rewire their metabolism at different levels in order to satisfy their biosynthetic and bioenergetic demands and to maintain their redox balance.

1.1.1 Glycolysis

Cancer cells facilitate high rates of glycolysis by increasing the expression of glucose transporters (GLUT1 and GLUT3) and hexokinase 2 (HK2) (Patra et al., 2013). Another important rate-limiting step in glycolysis is the conversion of fructose 6-phosphate to fructose 1,6-bisphosphate by phosphofructokinase 1 (PFK1) (Mor et al., 2011) and this reaction involves hydrolysis of ATP. PFK1 is regulated at different levels to function as a gatekeeper of glycolysis and to regulate glycolytic flux. ATP levels inhibit PFK1 activity whereas AMP levels activate it (Hers et al., 1982). Moreover, citrate levels generated from the tricarboxylic acid cycle (TCA) cycle and long chain fatty acids inhibit the activity of the PFK1 (Jenkins et al., 2011). An important allosteric regulator of PFK1 is fructose 2,6-bisphosphate (F2,6BP) (Okar et al., 1999). Levels of F2,6BP are controlled by the 6-phosphofructo-2-kinase/fructose 2,6-bisphosphatases (PFK-2/FBPase-2), a family of bifunctional enzymes that have both kinase and phosphatase function (Ros et al., 2013). As ATP levels repress the activity of PFK-1, F2,6BP levels can release this inhibition and support the glycolytic flux in the presence of ATP.

PFK-2/FBPase-2 enzymes are expressed by different genes in mammals, *PFKFB1, PFKFB2, PFKFB3,* an*d PFKFB4*. Although there is a homology between these genes, they represent different regulatory and kinetic features (Ros et al., 2013). Another glycolytic enzyme TP53-Inducible Glycolysis and Apoptosis regulator (TIGAR) has been shown to have similar properties as the phosphatase activity of PFK-2/FBPase-2 enzymes (Bensaad et al., 2006). Expression of PFKFBs was reported be upregulated in several cancer types. PFKFB3, which has predominant kinase activity, increases the F2,6BP levels and glycolytic flux in cancer cells (Yalcin et al., 2009). On the other hand, PFKFB4 displays high expression levels in colon, lung and pancreatic cancer cell lines (Minchenko et al., 2005). Prostate cancer cells lose their viability when *PFKFB4* is silenced (Ros et al., 2012) and *PFKFB4* is an essential gene for the survival of p53 deficient colon cancer cells (Ros, Floter, et al., 2017). Interestingly, silencing of *PFKFB4* increased the glycolytic flux via increasing levels of F2,6BP. In the presence of high glycolytic flux, cancer cells lose viability, as the need for NADPH cannot be satisfied. The flux of glucose 6-phosphate to the oxidative branch of the PPP is decreased and this leads to decreased levels of NADPH and the formation of reactive oxygen species (ROS). Likewise, TIGAR functions as a similar manner to PFKFB4 by increasing the flux to the oxidative branch of PPP to promote the production of riboses and NADPH for DNA repair after DNA damage (Bensaad et al., 2006)

The last committed step in glycolysis is the conversion of phosphoenolpyruvate (PEP) to pyruvate by pyruvate kinases (PKM), a reaction that also generates ATP. In cancer cells, this reaction is attenuated by expression of a low affinity kinase isoform, PKM2. Although *PKM2* is widely expressed in tumour, knockout studies have demonstrated that the enzyme is dispensable for tumour growth in colon and breast cancer (Israelsen et al., 2013). In this study, however, exon specific deletion of *PKM2* also resulted in the ablation of the PKM1 isoform, demonstrating that low PKM activity is favourable for tumour growth. As affinity of PKM2 is low and can be completely deleted, an alternatively mechanism for the conversion of PEP to pyruvate can occur via phosphoglycerate mutase 1 (PGAM1), an enzyme known to catalyze the formation of 2-phosphoglycerate from 3-phosphoglycerate (Vander Heiden et al., 2010). Since the last step of glycolysis is

reduced in cancer cells, other anabolic reactions can use intermediates of the glycolytic reactions, including serine biosynthesis and the PPP (Hay, 2016).

Conversion of pyruvate to lactate is highly enhanced in cancer cells by the activity of lactate dehydrogenase enzymes (LDH), which are encoded by four different genes (*LDHA, LDHB, LDHC, LDHD*) and work bidirectional. Given the high affinity of LDHA towards pyruvate and of LDHB towards lactate, LDHA favours the forward reaction by converting NADH to NAD^+, whereas the reverse reaction is generally catalised by LDHB (McCleland et al., 2012). Tumour cells express high LDHA levels resulting for the production of lactate (Valvona et al., 2016). Lactate as well as protons are exported by the lactate transporters (MCTs) in glycolytic cells to prevent the accumulation of metabolic waste and to prevent a highly acidic intracellular environment (Marchiq et al., 2016). Different normal tissues express different isoforms of MCTs (Halestrap et al., 2004); for example, expression of MCT4 is high in white skeletal muscle fibers whereas MCT1 is expressed at low levels in most tissues (Ritzhaupt et al., 1998). High levels of MCT1 are detected in breast, colorectal, gastric, and cervical cancer as well as in neuroblastoma and glioma (Doherty et al., 2013). As MCTs can also import lactate, their expression can also be found in stromal cells and MCTs are involved in metabolic symbiosis between different cancer cell populations and between cancer and stromal cells (Perez-Escuredo et al., 2016). Therefore, several attempts have been made to target lactate transporters for cancer therapy.

1.1.2 Fate of pyruvate

Warburg has made the assumption that the production of lactate from glucose in cancer cells is the consequence of defective mitochondria. However, it has been demonstrated since that many cancer cells can perform respiration; in fact, the proportion of cancer cells that rely on glycolysis has been shown to be 60% (Busk et al., 2008), while the rest rely on mitochondrial metabolism for ATP production. Thus, pyruvate can enter two different directions that determine the rewiring of cancer metabolism. As mentioned before, pyruvate can be converted to lactate in the cytosol or it can be transported to mitochondria via mitochondrial pyruvate carrier (MPC) (Herzig et al., 2012). Pyruvate can then be converted to

either oxaloacetate (OAA) by pyruvate carboxylase (PC) or acetyl-CoA by the pyruvate dehydrogenase enzyme complex (PDH) (Olson et al., 2016). PDH is inhibited post-translationally through phosphorylation by pyruvate dehydrogenase kinases and expression of pyruvate dehydrogenase kinases isoform 1 (PDK1) is associated with oncogenesis (Hitosugi et al., 2011). Pyruvate dehydrogenase phosphatase isoform 2 (PDP2) reverses the activity of PDK1, thereby preventing inhibition of PDH leading to the direction of pyruvate to acetyl-CoA. In addition, PC dependent anaplerosis frequently occurs in cancer and the regulation of expression of PC is determined transcriptionally and also metabolically (Christen et al., 2016).

1.1.3 Regulation of the TCA cycle

In the first step of the TCA cycle, acetyl-CoA gets condensed with OAA to form citrate (Rauckhorst et al., 2016) via citrate synthase (CS) in an irreversible manner. Citrate then can be oxidized in the TCA in the mitochondrial matrix or can be exported to the cytosol to provide the substrate for fatty acid biosynthesis. In the cytosol, acetyl-CoA is produced from citrate by the activity of ATP citrate lyase (ACLY). Acetyl-CoA levels are determined mostly by glucose availability, fatty acid oxidation and mitochondrial respiratory function (Martinez-Reyes et al., 2018). Acetyl-CoA has also been shown to be an important regulator of histone acetylation (McDonnell et al., 2016). Acetate can also be converted to acetyl-CoA under metabolic stress (Schug et al., 2015) and contributes to histone acetylation when glucose availability is low (Galdieri et al., 2012).

The TCA cycle is a very important metabolic process for the generation of substrates for anabolic reactions in tumour cells. Among the anabolic output of the TCA cycle in aspartate, a non-essential amino acid, generated by the transamination of OAA. Aspartate is required for protein and pyrimidine biosynthesis. It has been shown that cancer cells require respiration to produce electron acceptors for aspartate synthesis (Sullivan et al., 2015). Moreover, malic enzymes have been shown to convert the TCA cycle intermediate malate to pyruvate, thereby producing NADPH in the mitochondria and cytoplasm (P. Jiang et al., 2013). This reaction is very important for the production of reducing

equivalents for the biosynthetic demands of cancer cells.

Furthermore, several intermediates of the TCA cycle have been shown to function as oncometabolites by modulating the activity of important regulatory processes. Succinate dehydrogenase (SDH) is an enzyme complex that converts succinate to fumarate with a conversion of FAD to $FADH_2$. SDH has been identified as a tumour suppressor, as mutations in SDH lead to the accumulation of the oncometabolite succinate (Frezza et al., 2009). Accumulation of succinate causes inhibition of histone demethylases (M. Xiao et al., 2012) and stabilisation of hypoxia inducible factor (HIF) (Selak et al., 2005). Malate is generated from fumarate by fumarate hydratase (FH) and mutations in FH have been demonstrated in hereditary leiomyomatosis and renal cell cancer (HLRCC) (Tomlinson et al., 2002). Like succinate, fumarate also inhibits histone demethylases and leads to the stabilisation of HIF (M. Xiao et al., 2012). In addition, fumarate leads to a phenomenon called succination and important transcription factor Kelch-like ECH-associated protein 1 (KEAP1) is subjected to succination in FH deficient cells and it represses its inhibitory effect on nuclear factor (erythroid-derived 2)-like 2 (NRF2), a transcription factor important for the antioxidant response. Through this mechanism, inhibition of KEAP1 activates expression of NRF2 targets and supports the survival of cancer cells under metabolic stress conditions (Adam et al., 2011).

The reactions of the TCA cycle produce reducing equivalents in the form of NADH and $FADH_2$. These reducing equivalents transfer their electrons to the electron transport chain (ETC). In the ETC, Complex I transfers two electrons from NADH to ubiquinone, an electron transfer molecule also known as coenzyme Q10. Complex I therefore functions as a NADH:ubiquinone oxidoreductase. Mutations or deficiency of complex I often result in electron leakage from the ETC and the formation of ROS (Gaude et al., 2014). Complex II known as succinate:uniquinone oxidoreductase (SQR) has four nuclear encoded subunits: SDHA, SDHB, SDHC and SDHD. In addition, complex II is responsible from oxidizing succinate to fumarate and it transfers electrons from succinate to ubiquinone (Kluckova et al., 2013). Transfer of electrons from reduced ubiquinone to cytochrome C is supported by Complex III, a coenzyme Q:cytochrome c oxidoreductase. Cytochrome C then transfers the electrons to cytochrome c oxidase,

Complex IV. This complex reduces oxygen to water and to four protons. Electron transfer is coupled to the pumping of protons across the inner mitochondrial membrane and generates a proton gradient, which can then be used to generate ATP by the mitochondrial complex V, the ATP synthase (Weinberg et al., 2015).

1.1.4 Fatty acid synthesis and its regulation

Fatty acids are building blocks of membrane lipids in the human body under physiological conditions. Fatty acids are carboxylic acids with a hydrocarbon chain ranging from four to 36 carbon atoms. This hydrocarbon chain can consist of carbon atoms connected by single bonds, thereby forming fully saturated fatty acids. However, the hydrocarbon chains can also contain one or more double bonds and the resulting fatty acids are then grouped into mono- or polyunsaturated fatty acids. Length and degree of unsaturation determines the physical properties of fatty acids. Fatty acids contribute to the formation of phospholipids. Therefore, synthesis and degradation of fatty acids are important processes for the body homeostasis.

Fatty acids can be provided exogenously from the diet or generated by the liver and distributed to different tissues via the circulation. Serum lipids are transported to peripheral tissues in the form of lipid/protein complexes, called lipoproteins, with a hydrophobic lipid core and hydrophilic protein side chains and lipid head groups at the surface. Fatty acids are stored as triacylglycerols in lipid droplets under normal physiological conditions. Lipid droplets contain a phospholipid monolayer that covers a core of triacylglycerols and sterol esters, and because of the chemical structure they are inert (Farese et al., 2009).

In the adult body, *de novo* synthesis of fatty acids only takes place in the liver, the lactating breast and the cycling endometrium (Swinnen et al., 2006). Malonyl-CoA, three-carbon intermediate, is required for fatty acid biosynthesis and the conversion of malonyl-CoA from acetyl-CoA is catalyzed by acetyl-CoA carboxylase (ACC). There are two isoforms of ACC in human body. ACC1 is predominantly responsible for the formation of malonyl-CoA for fatty acid synthesis while ACC2 produces this metabolite mainly for the inhibition of

carnitine palmitoyltransferase (CPT1), thereby inhibiting fatty acid degradation (Santos et al., 2012). ACCs are regulated allosterically in a positive manner by glutamate and citrate, while fatty acyl-CoAs inhibit ACC activity. AMP-activated protein kinase (AMPK) phosphorylates ACCs and this phosphorylation inhibits their activity (Zaugg et al., 2011)

After formation of malonyl-CoA, successive condensation steps take place in order to form the long carbon fatty acid chains. Palmitate, a fatty acid with 16 carbon atoms, is the product of fatty acid synthesis and gets released. Fatty acid synthase (FASN) is a 250-270 kD, homodimeric enzyme and catalyzes fatty acid biosynthesis and acetyl-CoA and NADPH are required for this reactions (Menendez et al., 2007). The principal product of fatty acid biosynthesis is palmitate and longer chain fatty acids can be formed by the fatty acid elongation systems in the endoplasmic reticulum (ER) and mitochondria. In mammals, palmitate and stearate are the important precursors for the formation of most common monounsaturated fatty acids (MUFA), palmitoleate (16:1) and oleate (18:1), having a cis double bond between Carbon 9 and 10. Generation of MUFAs from saturated fatty acids is catalyzed by the enzyme stearoyl-CoA desaturase (SCD). This reaction requires oxygen and NAD(P)-cytochrome b5 reductase and takes place in the smooth ER (Peck et al., 2016). Humans express two isoforms of SCD; *SCD1* that is ubiquitously expressed and *SCD5* expressed only in brain and pancreas (Paton et al., 2009). In mammals, only the double bond at carbon-9 position can be generated while other double bonds cannot be formed. Thus, mammals are unable to synthesize linoleate, 18:2 ($\Delta^{9,12}$), α-linolenate, 18:3 ($\Delta^{9,12,15}$) and, as they are important for the production of other metabolites, they must be taken up from the diet. Moreover, linoleate can be converted to other polyunsaturated fatty acids such as arachidonate, which is important for the formation of the eicosanoids, important signaling molecules (Baenke et al., 2013; Currie et al., 2013).

Fatty acid gets degraded via fatty acid oxidation (β-oxidation) in humans and β-oxidation is often in balance with fatty acid synthesis. Free long chain fatty acids get converted into fatty acyls-CoA esters by acyl-CoA synthetases (ACSLs). ACSLs have different affinities towards different saturated or unsaturated fatty acids. Once they get converted into fatty acyls-CoA esters, fatty acids become

substrates for either lipid synthesis or β-oxidation (Padanad et al., 2016). Fatty acyl-CoAs get transported into mitochondria from cytosol by the carnitine acylcarnitine translocase system. First, long chain acyl-CoAs are converted into acylcarnitines and free CoA by CPT1. Acylcarnitine gets to the mitochondrial matrix and converted back to acyl-CoA for β-oxidation by CPT2. Malonyl-CoA, the first metabolite for the fatty acid biosynthesis, is a strong inhibitor of CPT1 and determines the balance between fatty acid synthesis and β-oxidation (Qu et al., 2016). Moreover, β-oxidation contributes to the energy needs of the cell and increase the amount of NADPH.

1.1.5 Regulation of cholesterol biosynthesis

Another pathway that uses acetyl-CoA as a substrate is cholesterol synthesis. Two molecules of acetyl-CoA get combined to form acetoacetyl-CoA that gets condensed with another molecule of acetyl-CoA to form β-hydroxy-β-methylglutaryl-CoA (HMG-CoA) by the enzyme HMG-CoA synthase 1 (HMGCS1). Next, HMG-CoA reductase (HMGCR) catalyzes the conversion of HMG-CoA to mevalonate, requiring using two molecules of NADPH, and this is the rate-limiting step of the cholesterol synthesis pathway. HMGCR is located on the smooth ER and an important regulator of cholesterol biosynthesis. After several phosphorylation steps requiring ATP, isopentenyl pyrophosphate (IPP) is formed. This molecule gets condensed with dimethylallyl pyrophosphate to form geranyl pyrophosphate (GPP), and then another condensation reaction forms the fifteen-carbon molecule farnesyl pyrophosphate (FPP). This part of the cholesterol pathway produces important intermediates that are essential for many cellular functions. The hydrophobic chain in FPP and GGPP is important for the isoprenylation of proteins. The 15-C farnesyl or 20-C geranylgeranyl isoprenoid is covalently attached to cysteine residues or the carboxyl terminus of proteins by farnesyltransferases (FTase) or geranylgeranyltransferase 1 (GGTase 1). Mainly, small GTPases of the RAS and RHO/RAC families are subjected to this post-translational modification and isoprenylation affects their stability, attachment to different cellular membranes, subcellular trafficking and activity (M. Wang et al., 2016).

Another important molecule produced from intermediates of the cholesterol biosynthesis pathway is ubiquinone. In mammals, production of ubiquinone follows several sequential reactions. The quinone part of the molecule is formed from tyrosine that is converted via several steps to 4-hydroxybenzoate. The isoprenoid side chain is formed from polyprenyl, which is made from FPP. FPP is first converted to decaprenyl pyrophosphate, then condensed with 4-hydroxybenzoate to form ubiquinone (Ernster et al., 1995). After it was discovered, it has been shown that ubiquinone reversibly oxidizes and reduces electron transport chain complexes (Crane et al., 1957). Later, ubiquinone has been recognised as an important electron carrier from complex I and II to complex III (Kerscher et al., 1999). However, more functions that are related to the electron transfer via ubiquinone have been demonstrated (Y. Wang et al., 2016). For example, the enzyme dihydroorotate dehydrogenase, which is localized in the mitochondrial inner membrane, oxidises dihydroorotate to orotate and requires the transfer of electrons into the ETC via ubiquinone (Evans et al., 2004). Additionally, farnesyl chains contribute to the formation of heme A, an important component of the ETC via serving as a prosthetic group in cytochrome c oxidase (Complex IV).

In addition to serving as substrates for the synthesis of isoprenoid chains, FPP can also remain in the cholesterol biosynthesis pathway. Here, two FPP molecules condense head to head to form squalene with the elimination of pyrophosphate groups. This is then further converted to squalene 2,3 epoxide, circularized to form lanosterol, and eventually cholesterol is generated (Shimano et al., 2017). Cholesterol is an important metabolite for the regulation of membrane fluidity, the production of steroid hormones and has several fates in human body. As it cannot be simply digested, it is converted to bile acids in the liver or to cholesterol esters via acyl-CoA-cholesterol acyl transferase (ACAT) (Yamauchi et al., 2018). This enzyme triggers the addition of fatty acid from coenzyme A to the hydroxyl group of cholesterol to make it more hydrophobic. Cholesterol esters and cholesterol can be stored as lipid droplets or can be transported as lipoprotein particles in the body (Bensaad et al., 2014). In the case of excess lipids in the body, triacylglycerols, cholesterol and cholesterol esters are packaged into very-low-density lipoprotein (VLDL). Removal of triaclyglycerols from the VLDLs produces low-density lipoproteins (LDL) and these carry mostly cholesterol and cholesterol

esters. Cells can take up LDL particles by LDL receptors (LDLR) via endocytosis (Jeon et al., 2012). Endosomes containing LDL particles then fuse with the lysosome and release cholesterol and fatty acids to the cytosol if it is needed. Cholesterol synthesis and uptake is quite complex and tightly regulated by different mechanisms, which will be discussed later (Yamauchi et al., 2018).

1.2 Sterol regulatory binding proteins (SREBPS)

Three members of the family of sterol regulatory element binding proteins (SREBP) were identified via cDNA cloning by Goldstein and Brown (Hua et al., 1993). These proteins contain an N–terminal transcription activation domain, a middle hydrophobic region containing two hydrophobic transmembrane segments and a C-terminal regulatory domain. Human SREBP1a and SREBP1c are expressed from a single gene located on chromosome 17p11.2, *SREBF1*. Difference between SREBP1a and SREBP1c is a 113 amino acid stretch, due to the alternative splicing of the first exons (Yokoyama et al., 1993). Other member of SREBP family, SREBP2 is expressed by a different gene on human chromosome 22q13, *SREBF2*, and only a single transcript of this gene has been identified in humans and mice so far (Hua et al., 1995). Although there are differences in the gene length of *SREBF1* and *SREBF2* (26 kb versus 72 kb), exon-intron boundaries in both genes share high similarities. SREBPs have been demonstrated as evolutionary conserved transcription factors throughout different species.

1.2.1 SREBP isoforms and SREBP targets

SREBPs have basic-helix-loop-helix-leucine zipper (bHLH-Zip) N-terminal domains; this domain provides the ability to activate transcription (R. Sato et al., 1994). As the acidic part of the N-terminal domain in SREBP1c includes fewer amino acids, this isoform has a weaker transactivation ability compared to SREBP1a and SREBP2 (R. Sato, 2009). The bHLH-Zip domain is important for DNA binding and dimerization of SREBPs. Most proteins containing bHLH-Zip domains bind to E-boxes; however, SREBPs bind both E-boxes and Sterol

Regulatory Elements (SRE)(Rawson, 2003). The LDL receptor has been shown to have recognition sites consisting of 10 nucleic acids (5'-ATCACCCCAC-3') and this site was identified as SRE (Briggs et al., 1993). Later, Kim *et al* showed that the ability of SREBPs to bind to both sequences is due to a single amino acid substitution within the DNA binding domain of a tyrosine residue instead of arginine found in other bHLH-Zip proteins (J. B. Kim et al., 1995). SREBPs have several regulatory cofactors that enhance their efficiency in regulating the expression of target genes. NF-Y/CBF, CREB/ATF, and Sp1 have been demonstrated as regulatory cofactors at the promoters in different studies (Han et al., 2015; Sanchez et al., 1995)

Studies with transgenic mice overexpressing active truncated versions of SREBPs (nSREBPs) demonstrated the target specificity of different SREBP isoforms. SREBP2 thereby preferentially regulates genes involved in cholesterol synthesis (Horton et al., 2003), while SREBP1c mainly activates fatty acid biosynthesis genes (Shimano, Horton, et al., 1997). SREBP1a affects both cholesterol and fatty acid synthesis (Horton et al., 2003).

Additionally, a ChIP-chip study has confirmed that SREBP1 regulates the expression of targets in the cholesterol and fatty acid pathway, but also factors involved in insulin signaling and cell cycle control (Reed et al., 2008). Another study suggested NLR family protein as an SREBP1 target in addition to lipogenesis in macrophages (Im et al., 2011). Seo *et al* showed that genes involved in autophagy and apoptosis are SREBP2 targets, using a ChIP-sequencing approach in mouse liver (Seo et al., 2011). In addition, SREBP1 has been identified as a transcription factor affecting the expression of S-adenosylmethionine (SAM) in C. elegans (Walker et al., 2011). Likewise, SREBP1 but not SREBP2 has been shown to be a regulator of heme oxygenase 1 (HMOX1) and other stress regulator genes in fibroblasts. Moreover, *HMOX1* includes a consensus SREBP binding site (Kallin et al., 2007). As HMOX1-deficient cells are more sensitive to stress, induction of HMOX1 by SREBP1 could represent a protective role of SREBPs against stress conditions. Likewise, DnaJA4, a heat shock chaperone, has been identified as regulated by SREBP2 (Robichon et al., 2006). SREBPs also affect NADPH levels during lipogenesis in order to protect cells from oxidative stress (Gorrini et al.,

2013). Taken together, these findings demonstrate that SREBPs regulate genes involved in cellular stress response, autophagy and apoptosis in addition to their canonical function in fatty acid and cholesterol metabolism.

In vivo studies in mice demonstrated that *srebf* is an essential gene. For this purpose, several mouse models have been generated. Deletion of the *srebf1* gene expressing both SREBP1a and SREBP1c isoforms in the liver by homologous recombination led to death of most of the embryos at day 11. The small number of survivors had elevated levels of SREBP2 and increased expression of *hmgcs1* and *hmgcr* in the liver, leading to the induction of cholesterol but not fatty acid synthesis (Shimano, Shimomura, et al., 1997). The underlying reason why the deletion of SREBP1 is embryonic lethal is still not well known. Moreover, it has been suggested that the survival of some *srebf1* -/- embryos was due to compensation by SREBP2. In another study, Srebp1c was selectively deleted in mice while Srebp1a stayed intact; the resulting animals were viable in contrast to the complete SREBP1 deficient mice with a similar increase in cholesterol levels in addition to triacylgycerol levels (G. Liang et al., 2002). Lastly, tissue specific deletion of *srebf2* in the liver was shown to be embryonic lethal (Horton et al., 2002a). These experiments performed *in vivo* demonstrate the importance of SREBP1a and SREBP2 during mouse embryogenesis. However, more experiments are needed to understand the exact compensatory mechanism between SREBP2 and SREBP1.

SREBP1a is highly expressed in intestinal epithelial, heart, macrophage and bone marrow dendritic cells and activates lipid synthesis in fast proliferating and growing cells, whereas SREBP1c is expressed in most tissues at low level and plays an important role in nutritional regulation of liver metabolism. In contrast SREBP2 is present in every tissue and governs the sterol metabolism. Overall, the tissue specific expression of the different SREBP isoforms is more prominent *in vivo* than *in vitro* (Shimano et al., 2017).

1.2.2 Regulation of SREBP activity

Protein abundance and transcriptional activity of SREBPs is regulated by different mechanisms, including proteolytic cleavage, post-translational modifications and regulation of protein stability.

1.2.2.1 Proteolytic cleavage

As mentioned previously, SREBPs are translated as full-length precursors, which are found on the ER membrane, often bound in the vicinity of the nuclear envelope. They form a hairpin structure consisting of three main domains: the NH2 terminal domain (480 aminoacids), the COOH domain (590 aminoacids) projecting into the cytosol and a short loop (31 aminoacids) into ER lumen or nuclear envelope. After SREBPs are synthesized, they are bound by the SREBP cleavage activating protein (SCAP). SCAP consists of two domains, NH2 domain (730 aminoacids) with 8 membrane-spanning domains and more hydrophilic COOH terminal domain (546 aminoacids). SREBPs and SCAP interact at the cytoplasmic side of the ER. The structure of SCAP has been shown to resemble that of HMGCR, an ER membrane resident enzyme that also has a sterol sensing function. The NH2 terminal domain of SCAP has been shown to be a sterol sensor and (Sakai et al., 1997). When sterol levels are low in the cells, SCAP/SREBP leaves the ER in COP-II coated vesicles that bud from the ER membrane. This is initiated by Sar1, small GTP binding protein that mediates the COP-II binding with Sec23/24. Sec24 binds to SCAP via the hexapeptide sequence (MELADL) and Sec23 helps the attachment of other proteins (Shimano et al., 2017). In the presence of sterols, binding the transmembrane domains of SCAP alter their structure, leading to a conformational change, which results in the binding of SCAP to the insulin induced gene (INSIG-1). Binding of INSIG to SCAP causes detachment of the Sar1/Sec23/Sec24 complex from SCAP and retains the SREBP/SCAP complex at the ER (L. P. Sun et al., 2005).

INSIG-1 was first identified as a SREBP target that co-immunoprecipitates with SCAP at the ER. A closely related isoform, INSIG-2, was

discovered later with a similar SCAP binding feature (Yabe et al., 2002). At low sterol levels, SCAP and SREBP translocate from ER to Golgi for proteolytic cleavage; whereas, in the presence of sterols because of the conformational change SCAP binds to INSIG leading to accumulation of SCAP- SREBP complex in the ER (L. P. Sun et al., 2005). INSIGs make cholesterol binding to SCAP easier. Therefore, it can be concluded that cholesterol dissociates from SCAP easily unless SCAP is bound by INSIGs and the INSIG/SCAP/SREBP complex can be retained in the ER, when INSIG is bound to SCAP (Goldstein et al., 2006). INSIGs are regulated via ubiquitinylation and degraded by the proteasome when sterol levels are low (Gong et al., 2006). In the presence of sterols, SCAP binds to INSIG-1 and prevents its degradation. Therefore, when cells are deprived of sterols the half-life of the INSIGs is relatively short (less than 30 min), while the half-life of INSIGs in the condition of high sterol is longer than 2 hrs.

In the low sterol condition where INSIG are not bound to SCAP, the SREBP/SCAP complex moves from the ER to the Golgi. In the Golgi, a two-step proteolytic cleavage takes place via Golgi membrane proteins, site-1 and site-2 proteases (S1P and S2P). At first, SREBP is cleaved at the hydrophilic loop that projects into the ER lumen by S1P. This cleavage divides the SREBPs into two parts, leaving the NH2-terminal domain membrane bound and it is defined as intermediate fragment of SREBP. At this level of regulation, the COOH domain cannot precipitate with the membrane bound NH2 domain (Sakai et al., 1997). After the formation of intermediate form of SREBPs, S2P cleavage takes place of the NH2 terminal domain within the membrane spanning part. At the end of these two proteolytic cleavages, the N-terminal active transcription domain defined as mature SREBP (mSREBP) is released and translocates to the nucleus, where it binds to the promoters of its target genes and drives the expression of these genes (Brown et al., 1999)

1.2.2.2 Transcriptional regulation

Expression of the different isoforms of SREBP is regulated through different mechanisms. SREBP1a is expressed at low levels constitutively in the liver and other tissues in adults. On the other hand, SREBP1c and SREBP2 are

transcriptionally regulated via several mechanisms.

SREBP1c is regulated transcriptionally by the liver X-activated receptors (LXRs), and in response to insulin and glucagon. Nuclear LXRs generate heterodimers with retinoid X receptors and are present as two isoforms: LXRα and LXRβ. Sterol intermediates formed during cholesterol biosynthesis bind to these receptors and activate them (Janowski et al., 1999). SREBP1c has a LXR binding site within its promoter region and LXR agonists activate transcription of the *SREBP1*c gene. It has been demonstrated that LXR knock out mice have lower levels of SREBP1c and its target gene expression compared to wild type mice (Repa et al., 2000). In addition to LXRs, agonists of the peroxisome proliferator activated receptors (PPARs), another class of nuclear hormone receptors, also have been shown to enhance the activity of the SREBP1c promoter (Kliewer et al., 1997). Indeed, fatty acids and eicosanoids act as PPARs ligands to activate the expression of SREBP1c (Fernandez-Alvarez et al., 2011).

Promoting lipogenesis as part of the insulin response is mediated by several transcription factors. Forkhead box class-O transcription factor (FOXO) has been suggested as an important regulator of this response and the modulation of lipogenesis. FOXO transcription factors act downstream of AKT and play a role in the control of key metabolic processes. AKT phosphorylates FOXOs in the nucleus, and this phosphorylation inhibits the FOXOs transcriptional activity as well as protein stability and nuclear translocation (Hay, 2011). Constitutively active FOXO has been shown to decrease the basal expression of SREBP1c mRNA in liver, and liver specific FOXO knock-out mice display elevated SREBP1c mRNA levels. Moreover, FOXO-1 can bind to the promoter region of the *SREBF1* gene and interferes with the components of the transcriptional complex. Therefore, FOXO-1 repressed the expression of SREBP1c by disrupting the actions with other transcription factors such as Sp1 (Deng et al., 2012)

Sterols and fatty acids also regulate the transcriptional activity of SREBPs. Oleate, the MUFA (18:1) can contribute to the SREBP1 and SREBP2 transcriptional activity together with 25-hydroxychholesterol (Thewke et al., 1998). Likewise, other MUFAs antagonize the LXR and down-regulate SREBP1c

expression in rat hepatoma cells (Ou et al., 2001). In addition, PUFAs repress SREBP1-dependent gene transcription, while SREBP2 activity still remains intact (H. J. Kim et al., 2002).

1.2.2.3 Post-translational modification of SREBPs

Several post-translational modifications have been reported to affect either the stability of mSREBP or its transcriptional activity or both. Among these post-translational modifications, phosphorylation seems to be the major mechanism regulating the stability of SREBPs.

SREBP turnover has been shown to be regulated by the ubiquitin-proteasome system (Osborne et al., 2009). Likewise, SREBPs can be stabilised following treatment with proteasome inhibitors. Indeed, both SREBP1a and SREBP2 share PEST sequences that many other short-lived proteins contain and these sequences contribute to their rapid degradation (Hirano et al., 2001). In addition, the transcriptional activity of SREBPs affects its ubiquitination and degradation, as mutations in the transactivation or DNA binding domain lead to the stabilisation of the proteins (Shao et al., 2012). Therefore, transcription-dependent degradation of SREBPs provides a mechanism for the rapid turnover and tight control of the expression of genes responsible for cholesterol and fatty acid synthesis (Sundqvist et al., 2003). Later, it was shown that the F-box and WD repeat domain protein 7 (FBXW7), the substrate recognition subunit of the SCF^{FBXW7} E3–ubiquitin ligase complex, plays an important role in the degradation of SREBP1a and SREBP2. Phosphorylation of SREBPs by glycogen synthase kinase 3β (GSK3β) induces a recognition platform that mediates the binding of FBXW7. GSK3β phosphorylates SREBP1a at threonine 426 (T426) and serine 430 (S430) (T426/S430) leading to the formation of a CDC4 phosphodegron (CPD) (Punga et al., 2006). These sites correspond to S432 and S436 in SREBP2. FBXW7 then binds to these motifs and causes ubiquitinylation of SREBPs (SREBP1a and SREBP2). Any signaling event modulating GSK3 activity therefore affects the phosphorylation of the CPD motif, thereby attenuating the degradation by FBXW7 and leading to the accumulation of nuclear SREBP1 (Sundqvist et al.,

2005). In a later study, another phosphorylation site, S434, was identified in the C-terminal domain of mSREBP1a (S410 in SREBP1c) that can also be phosphorylated by GSK3β. This phosphorylation at S434 primes the phosphorylation of the CPD at T426/S430 by GSK3β (Bengoechea-Alonso et al., 2009).

SREBPs are also targets for extracellular signal-regulated kinase (ERK), thereby providing a link between metabolic and growth factor signaling. SREBP1a is phosphorylated by ERK1/2 at S117 *in vitro* and mutation of the phosphorylation site abolishes the transcriptional activity of SREBP1a in the presence of insulin *in vivo* (Roth et al., 2000). SREBP2 was also shown to be phosphorylated by mitogen activated protein kinases (MAPK) at S432 and S455 but this phosphorylation does not affect its transactivation potential (Kotzka et al., 2004).

In addition, proteolytic cleavage and processing of SREBP1c and SREBP2 is repressed by phosphorylation via AMPK. Under high glucose and insulin conditions, AMPK agonists were shown to inhibit proteolytic cleavage and nuclear translocation of SREBP1c in hepatocytes (J. Yang et al., 2009). Moreover, it was demonstrated that AMPK phosphorylates SREBP1c at S372 and this phosphorylation prevents its cleavage and represses the transcription of SREBP1c target genes (Y. Li et al., 2011).

Acetylation is another important post-translational modification that affects gene expression and metabolism. SREBPs are in contact with many cofactors; between those, CBP and p300 have histone acetyltransferase (HAT) activity. Histone acetylation triggers an open chromatin conformation, making promoters accessible to the transcriptional machinery. P300 also causes stabilisation of SREBP1a and SREBP2 via acetylation. SREBP1a gets acetylated on a specific lysine residue (K333) located in its core DNA-binding domain, and acetylation of this residue prevents SREBP1a from getting degraded (Giandomenico et al., 2003). Based on these findings, deacetylation was expected to decrease the stability of SREBPs and increase SREBP turnover. Indeed, a member of the class III NAD^+ - dependent family of protein deacetylase (SIRT1) can directly deacetylate SREBP1a and increases its ubiquitination and proteasomal degradation (Walker et al., 2010).

Moreover, the small ubiquitin-like modifier (SUMO) can also lead to the post-translational modification of SREBPs. Sumoylation of SREBPs inhibits their transcriptional activity by recruiting HDAC3 (Arito et al., 2008). SUMO-1 is a 101 amino acid protein with similar functions to ubiquitin (R. Sato, 2009). However, unlike ubiquitination, sumoylation does not require prior phosphorylation but rather competes with phosphorylation in response to growth stimuli.

1.2.3 SREBPs in cancer

As already outlined above, in adult humans, fatty acid biosynthesis only takes place in the liver, the adipose tissue and lactating breast (Menendez et al., 2007). Cancer cells display aberrant fatty acid and sterol biosynthesis in order to satisfy their metabolic demands. Several studies demonstrated that some cancer types rely on fatty acid and cholesterol biosynthesis and inhibition of these pathways generate a vulnerability in cancerous tissues by blocking cancer cell growth (Rohrig et al., 2016)

FASN was identified as a tumour antigen in aggressive breast cancer (Kuhajda et al., 1994). Later it was shown that *FASN* is overexpressed in many cancer types, such as breast, prostate, colorectal cancer (Menendez et al., 2007). Small molecule inhibitors, such as cerulenin, C75 and orlistat, have been demonstrated to induce apoptosis and reduce tumour growth in xenograft models, but the mechanism is not well understood. Likewise, initial strategies have been developed to inhibit FASN in preclinical cancer models, such as a breast cancer mouse model induced by HER2/neu expression, where inhibition of FASN caused chemoprevention (Alli et al., 2005). However, side effects leading to severe weight loss have been observed in response to FASN inhibition, suggesting that better strategies are needed (S. F. Jones et al., 2015). Moreover, *ACLY* and *ACC* are also overexpressed in many cancers, including hepatocellular carcinoma, and upregulation of *ACLY* has been correlated with decreased survival in glioblastoma (Beckner et al., 2010). In addition, these enzymes, which have roles in fatty acid biosynthesis, have been targeted experimentally. Silencing of *ACLY* blocked the cell growth both *in vitro* and *in vivo* (R. Lin et al., 2013). Likewise, the ACYL inhibitor SB-204990 has been shown to repress tumour growth of prostate and lung

xenografts (Shah et al., 2016),

Elevated levels of *SREBF1* expression were also found in many cancer types, including breast, ovarian and prostate cancer (Swinnen et al., 2006). In prostate cancer, elevated levels of *SREBF2* were correlated with expression of high levels of androgen receptor (AR), and this has been shown to induce proliferation, migration and invasion (Huang et al., 2012). Moreover, a subtype of glioblastoma which carries an activating mutation in epithelial growth factor receptor (EGFR) has high levels of *SREBF1* expression, and treatment with fatty acid synthesis inhibitors blocked xenograft tumour formation in this model (Guo et al., 2009). As a consequence of increased *de novo* fatty acid synthesis, there is accumulation of phospholipids containing saturated and monounsaturated fatty acids in cancer cells (Baenke et al., 2013). Also, *SCD1* is overexpressed in many cancer types such as colon, hepatocellular carcinoma (Yahagi et al., 2005). Several cancer types have been reported to rely on the expression of *SCD* for proliferation and survival, and inhibition of SCD results in regression of xenograft tumours, suggesting an anti-tumourigenic effect (Roongta et al., 2011). The decrease in the tumour growth was explained with induction of ER stress causing apoptosis (Ariyama et al., 2010). In addition, Griffiths et al demonstrated that inhibition of SREBP1 alone promoted the ER stress in glioblastoma and caused decrease in size of xenograft tumours (Griffiths et al., 2013; Williams et al., 2013), demonstrating the importance of a balance between the regulation of fatty acid biosynthesis and the control of desaturation of lipids in cancer (Peck et al., 2016)

As highly proliferative cancer cells need rapid membrane production, the mevalonate pathway and cholesterol biosynthesis are also elevated in tumour tissues (Mullen et al., 2016). Also, lipid rafts, which are necessary as signaling platforms, contain high local concentrations of cholesterol. Cholesterol synthesis was also shown to protect cancer cells from immune surveillance (H. Y. Li et al., 2003). In addition, cholesterol is the substrate for steroid hormone synthesis and elevation of this pathway could promote the initiation and progression of breast and prostate cancers (Ko et al., 2004). Statins inhibit HMGCR, the rate-limiting enzyme in the mevalonate pathway, have been used extensively in the treatment of hypercholesterolaemia patients and have been tested as an anti-cancer therapy in

breast and prostate cancer (Nielsen et al., 2013), (Kuoppala et al., 2008). In addition, combination therapies are currently developed to improve the efficacy of statin treatment in cancer patients. Indeed, a combination of lovastatin with thalidomide or dexamethasone has been shown to increase the overall survival in refractory multiple myeloma (Hus et al., 2011).

IPPs, which are the product of mevalonate pathway, have an important role in activating effector T cells that can kill cancer cells (reviewed in (Mullen et al., 2016)). Therefore, zoledronate has been developed, which leads to the accumulation of IPP by inhibiting the activity of FDFT. Zoledronate combined with interleukin-2 (IL-2) treatment led to the expansion of tumour infiltrating T cells and this effect resulted in an improved clinical outcome in breast cancer (Meraviglia et al., 2010) and prostate cancer (Dieli et al., 2007). As other mevalonate pathway metabolites, GGPP and FPP, have roles in the prenylation of oncoproteins such as RAS, inhibition of these enzymes has also been used as an anti-cancer strategy (Casey et al., 1996) Moreover, ubiquinone has been shown to have an anti-oxidant function in several diseases (Y. Wang et al., 2016) and its role in cancer treatment has not been well characterized.

1.3 The PI3K/AKT pathway

Phosphatidylinositol 3-kinases (PI3Ks) combine signals from growth factors, cytokines and other environmental cues and are important class of signaling proteins. Class I PI3Ks were discovered as oncoprotein-associated kinases that phosphorylate the 3'-OH group of the inositol lipids, PtdIns, PtdIns(4)P and PtdIns(4,5)P_2 , to form PtdIns(3,4,5)P_3 in response to growth factors (Sugimoto et al., 1984; Whitman et al., 1985) They are classified as 3 main groups (class I, class II and class III) and several subgroups. Class IA PI3Ks consist of heterodimers that include a p110 catalytic subunit (encoded by the *PIK3CA*, *PIK3CB* and *PIK3CD* genes) and a p85 regulatory subunit (Vanhaesebroeck et al., 2012). p85α has two SH2 domains that can bind to phosphorylated tyrosine residues on oncoproteins or growth factor receptors and an inter-SH2 domain that attaches to the p110 catalytic subunit (Vanhaesebroeck et al., 2012). In the resting state of the cells, the p85/p110

complex is already present to get activated by external cues. Autophosphorylation of receptor tyrosine kinases (RTK) promotes the recruitment of PI3Ks and the SH2-phosphotyrosine interaction removes the inhibition of p110 by p85 so that the catalytic subunit p110 can phosphorylate PtdIns(4,5) to PtdIns(3,4,5)P_3 thereby generating a lipid second messenger (Thorpe et al., 2015).

Several factors stimulate the PI3K activity and increase levels of PIP_3. One of the main downstream effectors of PI3K activity is the AKT kinase. *AKT*, the cellular homologue of the retroviral oncogene *v-AKT*, has three isoforms (AKT1, AKT2, AKT3) (Manning et al., 2007). AKT1 and AKT3 are important for embryonic and brain development, respectively. In addition, AKT1 and AKT2 have been identified as playing major roles in glucose homeostasis (Lu et al., 2012; Vivanco et al., 2002). After activation of PtdIns(3,4,5)P_3 by growth factors or other external signals, AKT is recruited to the PtdIns(3,4,5)P_3 via its PH-domain and activates an intracellular signaling cascade. AKT localizes at the plasma membrane where it is in close proximity to another kinase, the PH-domain containing protein kinase 1 (PDK1), leading to the phosphorylation of AKT at T308. However, full activation of AKT requires a second phosphorylation at S473 that is located in a hydrophobic region close to the carboxyl terminus (Scheid et al., 2001). Later it has been shown that mammalian target of rapamycin complex 2 (mTORC2) is responsible for this phosphorylation (Sarbassov et al., 2005). S473 phosphorylation also causes the translocation of AKT to the nucleus (Manning et al., 2007).

Activation of AKT promotes several downstream signaling events that regulate proliferation, protein synthesis and metabolism. AKT phosphorylates glycogen synthase 3 (GSK3) isoforms at an N-terminal serine residue (GSK3α-Ser21, GSK3β-Ser9) and this phosphorylation leads to the inactivation of GSK3 (Cross et al., 1995). Interestingly, phosphorylation of some proteins by GSK3 generates a phosphodegron motif , which is recognized by E3 ubiquitin ligases and promotes proteasomal degradation. This mechanism of regulation has been described for the c-MYC transcription factor and, as previously mentioned, for SREBPs. In addition, GSK3 inhibits the transcription factors NRF2 and (Robertson et al., 2018). In metabolic regulation, GSK3 phosphorylates glycogen synthase; the enzyme responsible for the last step in glycogen synthesis and this phosphorylation

inactivates glycogen synthase (Cohen et al., 2001). In addition to GSK3, other major downstream effectors of PI3K/AKT signaling are the FOXO transcription factors that play important roles in the adaptation to low insulin and IGF signaling (Webb et al., 2014). FOXO proteins are exported out of the nucleus when they get phosphorylated by AKT and this inhibits their transcriptional activity. As a consequence, the expression of FOXO targets is repressed, including factors that promote apoptosis (BIM, PUMA), cell cycle arrest (p21, p27) and metabolic changes (PEPCK-phosphoenolpyruvate carboxy kinase, G6PC-glucose 6-phosphatase) (van der Vos et al., 2011).

Aberrant activation of the PI3K/AKT pathway has been demonstrated in many cancer types. One of the main causes of this aberrant activation is the loss of the phosphatase and tensin homolog deleted on chromosome 10 (PTEN). PTEN acts as a phosphatase and dephoshorylates PIP_3, thereby counteracting the function of PI3K. Deletion of the *PTEN* locus or mutations leading to the loss of PTEN function have been identified in a wide variety of cancers (Fruman et al., 2017). In addition, mutations in the p110 and p85 subunits can lead to constitutively active AKT in several cancer types, including ovarian and cervical cancers (Thorpe et al., 2015). Moreover, AKT can also be hyperactivated by mutations of its PH-domain (Manning et al., 2017). Therefore, as there are many upstream and downstream mediators in the PI3K/AKT pathway, it is very important to understand the mechanism of its regulation in specific contexts and conditions in order to develop strategies for the targeting of this pathway for cancer therapy.

1.3.1 Role of PI3K/AKT pathway in metabolism

The PI3K/AKT pathway is a main mediator of insulin signaling. AKT has a major role in the metabolic adaptations in response to elevated blood glucose levels. Indeed, AKT2 knockout mice displayed insulin resistance and glucose intolerance and this phenotype was diminished by the deletion of FOXO (Cho et al., 2001). Active PI3K/AKT signaling leads to the translocation of GLUT4 to the plasma membrane (Fruman et al., 2017). Moreover, it promotes the expression of glycolytic enzymes by regulating HIF1a and supports the ‘Warburg effect’ as opposed to the effect of p53 (Robey et al., 2009). AKT also phosphorylates PPARG

coactivator 1 alpha (PGC-1α), a co-activator of FOXO, at S570 and thereby inhibits fatty acid oxidation and gluconeogenesis (Manning et al., 2007). Lastly, AKT has been shown to promote the activity of ACLY by direct phosphorylation (Berwick et al., 2002). Therefore, the PI3K/AKT signaling cascade plays many important roles in regulating glucose homeostasis and acts as a bridge between glucose signaling and lipid biosynthesis, depending on the cellular metabolic constraints and the presence of extracellular stimuli.

1.4 The mTOR complex

Initially, mTOR was identified as a serine/threonine protein kinase and a member of the PI3K-related kinase family (Saxton et al., 2017). The mTOR protein can be part of two different protein complexes; mTOR Complex 1 (mTORC1) and Complex 2 (mTORC2). The components of mTORC1 are mTOR, Raptor (Regulatory protein associated with mTOR) and mLST8 (mammalian lethal with Sec13 protein 8). Raptor regulates the subcellular localization of mTORC1. In contrast, mTORC2 contains mTOR, rapamycin-insensitive companion of mTOR (RICTOR) and the mammalian stress-activated MAPK-interacting protein 1 (mSIN1, also known as MAPKAP1) as subunits different than mTORC1 subunits (Dibble et al., 2015).

Activation of mTORC1 plays an important role in mediating the downstream effects of PI3K/AKT signaling in many cancer types (Saxton et al., 2017). Moreover, loss of tumour suppressors, such as p53 and LKB1, also leads to the aberrant activation of mTORC1 via affecting the activity of the tuberous sclerosis complex proteins, TSC1 and TSC2 (Feng et al., 2007). In addition, activation of AKT signaling can result in hyperactivation of mTORC2, which also has pro-proliferative functions such as increasing glucose uptake (Manning et al., 2007).

Importantly, mTORC1 gets activated via nutrient and growth factor signaling. As a result of aminoacid availability, mTORC1 moves to the lysosome and PI3K signaling activates AKT. AKT represses the activity of TSC1-TSC2

complex, which functions as a GTP-ase promoting protein (GAP) for the small GTPase Ras homolog mTORC1 binding (RHEB). Activated RHEB moves to the lysosome and binds to mTORC1 in order to activate it (Saxton et al., 2017). Cellular growth and proliferation are affected by mTORC1 and mTORC2, as they phosphorylate different metabolic enzymes and downstream effectors. mTORC1 affects cell growth by phosphorylating the ribosomal protein S6 kinase (S6K) at T389. S6K then activates many substrates including eIF4B, a positive regulator of the 5'cap binding eIF4F complex (Holz et al., 2005) to support mRNA translation initiation. The eIF4E binding protein (4EBP) is also phosphorylated by mTORC1 to promote translation. 4EBP then dissociates from eIF4E and 5'cap dependent translation can take place (Mossmann et al., 2018). Therefore, mTORC1 promotes general mRNA translation by affecting several downstream effectors (Hsieh et al., 2012).

1.4.1 Regulation of metabolism by mTOR

As mentioned before, glucose is a major nutrient source in most cancer types, and cancer cells display increased glucose uptake and metabolism to support their growth and proliferation. Moreover, cancer cells use glucose carbons for anabolic reactions to produce amino acids, lipids and nucleotides. Indeed, mTOR signaling has an important role in reprogramming anabolic reactions that cancer cells need for their growth and proliferation (Mossmann et al., 2018). Firstly, mTORC1 regulates glucose metabolism by upregulating the expression of *GLUT1* via inducing the translation of HIF1a and c-MYC (Buller et al., 2008). Hexokinase 2 translation is also increased in *PTEN*-deficient prostate cancer cells via AKT-mTORC1 axis and supports the glycolysis phenotype of this cancer type (L. Wang et al., 2014). Cancer cells also need nucleotides for the synthesis of DNA and RNA and nucleotides can be either synthesized de novo or formed via the salvage pathway. Ribose-5-phosphoribosyl-1-pyrophosphate (PRPP) is the key metabolite for the generation of pyrimidine and purine bases. PRPP is generated through the non-oxidative branch of the PPP from ribose-5-phosphate that is promoted by mTOR signaling, and mTORC1 activates the conversion of ribulose 5-phosphate to ribose 5-phosphate (Patra et al., 2014). In hepatocellular carcinoma, it has been demonstrated that mTORC1 induces flux through the PPP by increasing both

glycolysis and expression of *G6PD* thereby promoting the formation of ribose 5-phosphate (Evert et al., 2012). The trifunctional enzyme that initiates pyrimidine synthesis, carbamoyl phosphate synthetase 2, aspartate transcarbamylase and dihydroorotase (CAD), was shown to be a c-MYC transcriptional target (Miltenberger et al., 1995) and is also regulated by mTORC1. S6K has been suggested to phosphorylate CAD thereby inducing pyrimidine biosynthesis (Ben-Sahra et al., 2013). Moreover, the TCA cycle metabolite, aspartate, was reported as a regulator of mTORC1 activity and pyrimidine biosynthesis (Rabinovich et al., 2015).

Fatty acids can be taken up or synthesized de novo by cancer cells and mTOR signaling has an important role in regulating fatty acid metabolism. AKT signaling promotes SREBP1 activation by inducing mTORC1 (Porstmann et al., 2008). Moreover, both mTORC1 and mTORC2 have been reported to regulate the proteolytic cleavage of SREBP1 (Yecies et al., 2011) (Hagiwara et al., 2012; J. L. Owen et al., 2012). Nuclear entry of LPIN1, a negative regulator of SREBP1, is inhibited by mTORC1 in several cancer cell lines (Peterson et al., 2011). Moreover, the stability of the SREBP1 target genes, FASN, ACLY and SCD1, is increased through phosphorylation by mTORC1-S6K signaling (Duvel et al., 2010). mTORC2 promotes ACLY activation via phosphorylation and supports cell growth in breast cancer (Chen et al., 2016). In addition to fatty acid synthesis, mTOR signaling also regulates several enzymes in cholesterol biosynthesis. The mTORC1 phosphorylation target 4EBP1 has been shown to regulate SREBP2 activation by affecting its 5'cap-dependent translation (B. T. Wang et al., 2011).

In addition to the regulation by growth factors and amino acids, mTOR signaling also gets modulated in response to changes in cellular energy levels. In response to glucose deprivation, AMPK is activated and represses mTORC1 indirectly via phosphorylation of TSC2 or directly via phosphorylation of RAPTOR (Shaw et al., 2004). Unexpectedly, mTORC1 is repressed in cells without AMPK in response to glucose deprivation via interfering with the activity of Rag GTPases (Efeyan et al., 2013). Furthermore, mTORC1 is inhibited in response to hypoxia via AMPK activation but also via the action of the regulated in DNA damage and development 1 (REDD1) protein that activates the inhibitory action of TSC

(Brugarolas et al., 2004). Indeed, DNA damage induces p53 target genes (*PTEN, TSC2*) and this suppresses the mTORC1 activity by promoting TSC activity (Feng et al., 2007).

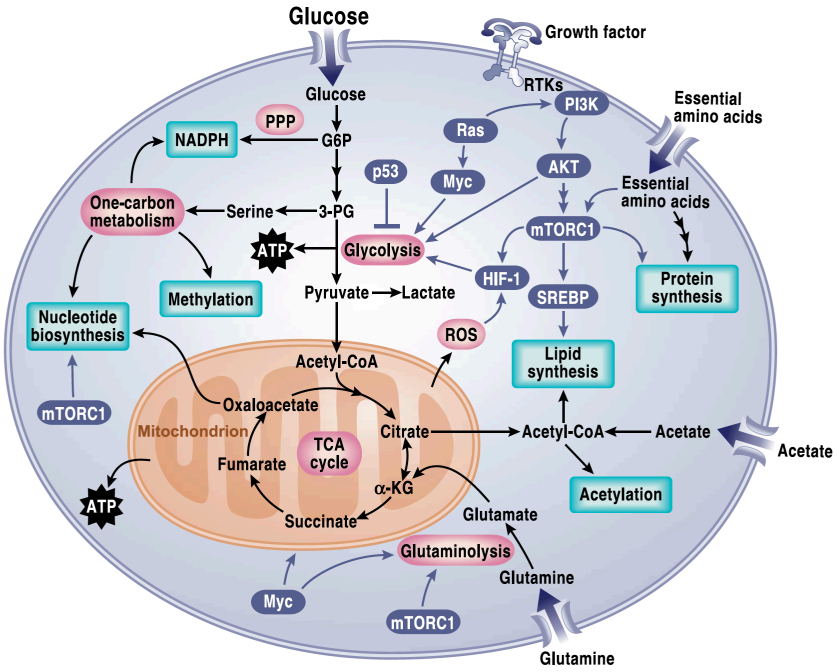

Figure 1.1: Regulation of cancer metabolism by different signalling pathways

Glucose and glutamine are the major nutrients for cancer cells. Tumour cells carry mutations that activate PI3K/AKT/mTOR signalling pathways, thereby promoting a robust anabolic program involving increased glycolytic flux and fatty acid synthesis through activation of hypoxia-inducible factor–1 (HIF1) and sterol regulatory element binding protein (SREBP), respectively. Moreover, oncogenes like Kras, which is frequently mutated in lung, colon, and pancreatic cancers, linked with the physiological functions of to promote tumourigenicity (DeBerardinis et al., 2016).

1.5 Tumour suppressor p53 *(TP53)*

TP53 was identified initially as a proto-oncogene in 1979. However, later it was demonstrated that deletion or mutations in the *TP53* locus lead to the formation of tumours (Finlay et al., 1989), (Eliyahu et al., 1989). *TP53* encodes for an important transcription factor, which is responsible for the expression of genes involved in cell cycle regulation, apoptosis and DNA repair (Park et al., 2016). Moreover, DNA damage, oncogene activation, nutrient and oxygen deprivation, induction of ribosomal and ER stress induce the levels of p53 protein (Soussi,

2007), (Vousden et al., 2007; Vousden et al., 2009), (Horn et al., 2007). The levels of p53 protein are controlled by mouse/human double minute 2 homolog (MDM2/HDM2) and MDM4 (or MDMX) (Marine et al., 2006), and MDM2 represses the expression of p53 response genes by governing the ubiquitinylation and degradation of the p53 protein (Kruse et al., 2009; Wade et al., 2010).

1.5.1 Post-translational regulation of P53

Tumour suppressor *TP53*, like other transcription factors, is subjected to many post-translational modifications. As mentioned before, p53 gets ubiquitinylated by MDM2 and degraded by the proteasome. The tumour suppressor ARF disrupts the MDM2-p53 interaction thereby stabilizing p53 (Lowe et al., 2003). MDMX was shown to be a negative regulator of MDM2, as MDM2 and MDMX form a complex with p53 on the promoters of specific p53 targets (Shadfan et al., 2012)

Different groups of kinases, such as ATM/ATR or CHK1/CHK2 can phosphorylate and modify the activity of p53. Upon DNA damage, these kinases phosphorylate p53 at S15 and S20 located at the N-terminus of the protein and interfere with the binding of MDM2, thereby stabilizing the p53 protein.

Acetylation of several lysine residues of p53 blocks the sites from ubiquitinylation and prevents p53 from getting degraded (Brooks et al., 2011). CBP/p300 acetylates the six C-terminal lysines of p53 (Gu et al., 1997). Ubiquitinylation is inhibited if p53 gets acetylated and there is a strong competition between acetylation and ubiquitinylation to maintain the stability of p53. Conversely, p53 can get deacetylated by histone deacetylase complexes (HDAC), such as HDAC1 and Sir2α/Sirt1 (Luo et al., 2001). Deacetylation of p53 attenuates the expression of p53 target genes, apoptosis, and growth arrest in response to DNA damage and oxidative stress (M. Li et al., 2002).

1.5.2 Canonical functions of p53

P53 is also known as the ‘guardian of the genome’ (D. Lane et al., 2010). During the acute stress response to DNA damage, p53 provides signals to facilitate transient cell cycle arrest and DNA repair and supports cell survival. However, in severe stress conditions, p53 triggers the induction of apoptosis or senescence by increasing the expression of several genes. Pro-apoptotic members of the BCL-2 family, BAX, PUMA and NOXA, have been shown to be p53 targets and they initiate cell death (Villunger et al., 2003). Moreover, senescence induction is mediated by p21 and p53 thus provides a barrier against cell transformation (Vousden et al., 2009).

As p53 is an important tumour suppressor, it is not surprising that at least 50% of all the human tumours carry genetic alterations leading to the inactivation of p53 (Freed-PastorPrives, 2012). Missense mutations are the most frequent of these alterations and are found in solid tumours, often associated with metastasis and invasive activity (Gasco et al., 2002). Most p53 mutations affect the DNA binding domain, resulting in reduced DNA association (Vegran et al., 2013). Mutant p53 cannot activate the expression of MDM2 and is therefore stabilized in many cancers (Muller et al., 2013).

1.5.3 Role of p53 in glucose metabolism

The influence of p53 on cancer metabolism is very complex and involves multiple nodes of regulation. To this end, many enzymes involved in glycolysis, oxidative phosphorylation, fatty acid and cholesterol synthesis are regulated via p53 through transcriptional and non-transcriptional mechanisms. The adaptation of cancer cells to nutrient and oxygen deprivation is another feature of p53 that controls the fitness of cancer cells in the metabolically compromised environments (Floter et al., 2017).

In addition to its role as a ‘guardian of genome’, p53 governs glucose metabolism in cancer cells and thereby opposes the ‘Warburg Effect’ (Kruiswijk et al., 2015). It generally promotes oxidative glucose metabolism while inhibiting

glycolysis. p53 inhibits the expression of the glucose transporters *GLUT1* and *GLUT4* via transcriptional regulation (Schwartzenberg-Bar-Yoseph, 2004). Moreover, it also inhibits expression of *GLUT3* by repressing the activity of IκB kinases α and β (IKKα/ β) and blocking the activation of nuclear factor kappa B1 (NF-κB) (Kawauchi et al., 2008). Likewise, p53 can bind to the promoter of *HK2* to repress its expression and also inhibits HK2 activity (Mathupala et al., 1997). Regulation of glucose transporters and HK2 points out the importance of G6P, metabolite that can enter glycolysis, but also the PPP and glycogen synthesis pathway. As mentioned above, G6P is converted to F6P, the substrate of PFK1. PFK1 is the rate-limiting enzyme in the glycolysis and it is regulated by p53 via different mechanisms (Floter et al., 2017). In response to DNA damage, p53 induces the expression of TIGAR and this inhibits PFK1 by decreasing F2,6BP levels. This mechanism prevents metabolites from glycolysis and promotes the flux to PPP for the production of ribose for nucleotide synthesis in response to DNA damage (Bensaad et al., 2006; J. Li et al., 2006). On the other hand, the expression of the related enzyme *PFKFB4* is repressed by p53. Ros et al demonstrated that p53 binds to the promoter of the *PFKFB4* gene and mediates transcriptional repression by promoting histone deacetylation (Ros, Floter, et al., 2017). Moreover, depletion of *PFKFB4* in p53 deficient colon cancer cells elevated F2,6BP levels and resulted in increased flux through glycolysis. At the same time, NADPH levels were decreased following *PFKFB4* depletion, and this led to the formation of ROS, loss of cell viability and reduced tumour growth (Ros, Flöter, et al., 2017).

In addition to allosteric regulation of glycolysis, metabolite entry into the PPP is also governed by the direct interaction of p53 with glucose-6-phosphate dehydrogenase (G6PD), the rate-limiting enzyme of the PPP. Wild type p53 inhibits the activity of this enzyme while mutant p53 lacks this ability, thereby promoting the flux of metabolites into the PPP (P. Jiang et al., 2011). Thus, p53 can have opposing effects in balancing the flux between glycolysis and PPP, and it exerts its influence depending on the level of stress and the metabolic demands of the cells.

To control the fate of pyruvate, p53 transcriptionally inhibits pyruvate

dehydrogenase kinase 2 (PDK2), which phosphorylates and represses PDH activity (Contractor et al., 2012). Thus, pyruvate can be converted into acetyl-CoA to enter the TCA cycle and, by this mechanism, p53 promotes oxidative glucose metabolism. In addition, p53 inhibits the expression of MCT1, thereby decreasing the conversion of pyruvate to lactate (Boidot et al., 2012).

Mitochondrial metabolism plays an important role in regulating the energy production of cancer cells. It has been demonstrated that p53 controls mitochondrial copy number and mitochondrial mass (Lebedeva et al., 2009). In addition, it supports oxidative phosphorylation via positive regulation of p53R2 (RRM2B), a subunit of ribonucleotide reductase (Bourdon et al., 2007). The expression of cytochrome c oxidase assembly 2 protein (SCO2), which promotes the formation of complex IV of the ETC {Matoba, 2006 #405; Kulawiec et al., 2009), and apoptosis-inducing factor (AIF), a mitochondrial flavoprotein required for complex I function (Stambolsky et al., 2006), are also transcriptionally promoted by p53, resulting in increased ATP generation by oxidative phosphorylation.

1.5.4 Regulation of lipid metabolism by p53

In addition to its role in controlling glucose metabolism, p53 also affects lipid metabolism via several mechanisms, resulting in the overall repression of fatty acid synthesis and increased fatty acid degradation (Feng et al., 2010). It affects AMPK, which phosphorylates ACC1 and ACC2, thereby repressing fatty acid biosynthesis (Feng et al., 2007). Deletion of p53 was also shown to elevate lipogenesis in adipocytes in a genetic model of obesity (ob/ob mice) by inducing the expression of SREBP1c (Yahagi et al., 2003). Interestingly, WT p53 inhibits lipid synthesis under glucose starvation by affecting the expression of *LPIN1*, a target of mTORC1 (Assaily et al., 2011). Freed-Pastor et al. demonstrated that mutant p53 binds to SREBP2 and induces the expression of SREBP2 target genes to promote the formation of GGPP for the prenylation of Rho-GTPases. Thereby, mutant p53 drives the loss of normal breast tissue architecture and promotes cell motility and invasion (Freed-Pastor, Mizuno, et al., 2012). Moreover, it has been shown that WT

p53 suppresses the mevalonate pathway by inhibiting the activation of SREBP2 via increasing the ATP binding cassette subfamily A member 1 (ABCA1), a cholesterol transporter gene. The same study also showed that inhibition of the mevalonate pathway limits the progression of p53 deficient hepatocellular carcinomas (Moon et al., 2018).

While p53 limits lipid synthesis, it also promotes fatty acid β-oxidation under nutrient deprivation by inducing AMPK (Buzzai et al., 2007). Also, p53 promotes the expression of genes that are responsible from mitochondrial oxidative metabolism by binding to PGC-1α, (C. Liu et al., 2011) and this interaction also induces fatty acid oxidation. P53 also induces CPT1C transcriptionally, both *in vivo* and *in vitro* (Sanchez-Macedo et al., 2013). Lastly, expression of pantothenate kinase-1 (PANK1), which governs the cellular amount of coenzyme A, was also shown to be increased by p53 (Zaugg et al., 2011).

As loss or mutation of p53 can cause resistance towards DNA damaging drugs in cancer, maintaining p53 function can be a useful strategy in cancer treatment (Khoo et al., 2014). Restoring the normal structure of the DNA-binding domain of mutant p53 by chemical compounds such as PRIMA-1 has been shown to repress the growth of p53 mutant tumours (Zache et al., 2008). Inhibition of MDM2 by chemical inhibitors (Nutlin) has also been tried as a strategy to stabilise and activate wild type p53, thus restoring its tumour suppressive function (Vassilev et al., 2004).

Under nutrient starvation, p53 deficient cells are unable to repress those biosynthetic processes that demand ATP. This causes further decrease of essential nutrients and the formation of ROS, which can lead to cell death. Therefore, it is crucial to assess the metabolic processes that function in a synthetically lethal manner with loss and mutation of p53. Moreover, targeting NADPH production could lead to the inhibition in macromolecule synthesis and decrease antioxidant production. Thus, targeting G6PD with a chemical inhibitor (RRx-001) is a strategy that has already been tested in clinical trials (Reid et al.,

2015). Lastly, targeting lipid metabolism could be a strategy in p53 deficient cancers, and a FASN inhibitor (TVP-2647) is currently tested in solid tumours (Rohrig et al., 2016). Importantly, statins could also be an effective strategy in p53 deficient or mutant tumours (Thurnher et al., 2012).

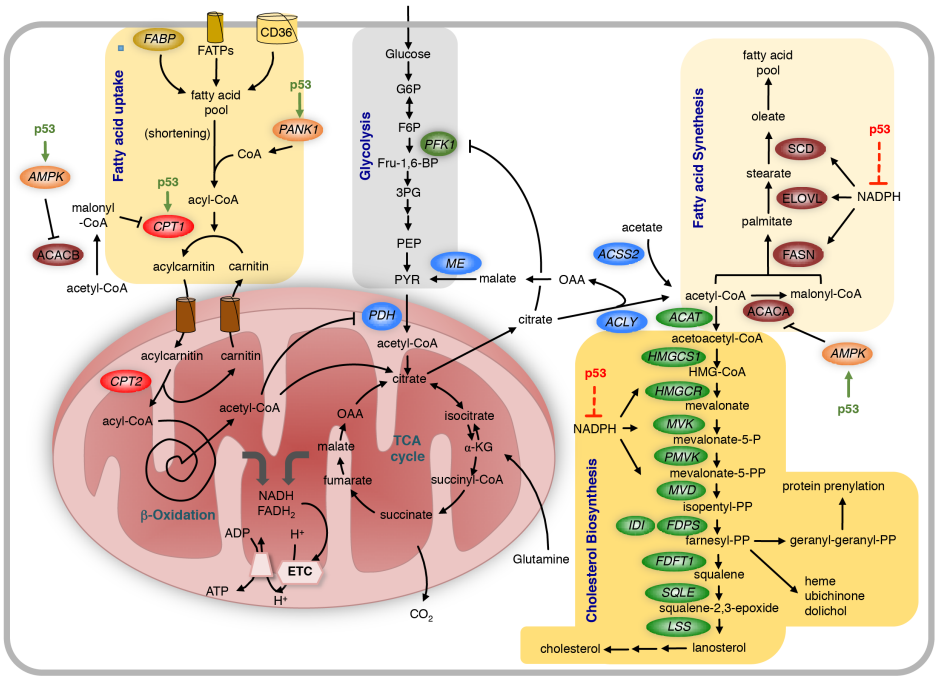

Figure 1.2: Regulation of lipid metabolism by p53

Fatty acids are taken up by the cells through receptor and non-receptor mediated transport. Unless prior shortening of very long chain fatty acids in peroxysomes is required, medium and short chain fatty acids are coupled to coenzyme A (CoA) in the cytoplasm and then transferred to carnitin by CPT1 for transport across the mitochondrial membrane. In the mitochondria, the acyl-chain is transferred back to CoA and then undergoes repeated shortening by the beta oxidation process. P53 promotes fatty acid metabolism by increasing the expression of CPT1C. p53 also activates AMPK, which phosphorylates and inhibits ACC, leading to reduced production of malonyl-CoA, thereby releasing the inhibition of CPT1. High levels of mitochondrial acetyl-CoA also block PDH and reduce the use of glucose-derived pyruvate in the TCA cycle. The TCA cycle also provides citrate, which is transported out of the mitochondria and is converted to acetyl-CoA and oxaloacetate (OAA) by ACLY. Another source of acetyl-CoA is the direct conversion of acetate to acetyl-CoA by ACSS2. Acetyl-CoA is the substrate for the synthesis of fatty acids and cholesterol. For fatty acid synthesis, acetyl-CoA is first converted to malonyl-CoA by ACC, and the two metabolites are then sequentially condensed by the multifunctional enzyme FASN to form the fatty acid palmitate. This is then further elongated and desaturated to contribute to the cellular fatty acid pool. For cholesterol biosynthesis,

acetyl-CoA is first converted to acetoacetyl-CoA, which enters the mevalonate pathway. In addition to cholesterol, this pathway produces multiple metabolic intermediates including farnesyl-pyrophsophate and geranyl-geranyl-phosphate, which are required for protein prenylation and the synthesis of heme, ubiquinone and dolichol. As fatty acid and cholesterol biosynthesis require large amounts of NADPH, reduction of NADPH levels by p53 reduces the overall activity of these biosynthetic reactions. fatty acid elongase (ELOVL), lanosterol synthase (LSS); pantothenate kinase-1 (PANK1) (Floter et al., 2017)

1.6 Hypoxia

Molecular oxygen (O_2) is important for many biological reactions, especially for oxidative mitochondrial metabolism that produces ATP with high efficiency. Because of uncontrolled proliferation, cancer cells often reside in an environment where fluctuating levels of nutrients, such as glucose and glutamine, and oxygen are present depending on the distance from blood vessels. Cancer cells that are further from the blood vessels often lack sufficient oxygen supply. The ambient oxygen percentage is 21% (150 mm Hg) and in normal tissues this percentage drops down to 2-9% (average 40 mm Hg). Conditions with less than 2% O_2 are defined as hypoxic, whereas less than 0.02% O_2 can be considered as severe hypoxia or anoxia (Bertout et al., 2008). Cells in the tumour microenvironment mostly face hypoxia and activate O_2 sensing pathways to cope with the hypoxia-related stress (Semenza, 2012). Moreover, it has been suggested that hypoxia generates a resistance in cancer cells as response to cytotoxic drugs and radiotherapy (Gorrini et al., 2013)

The hypoxia inducible transcription factor (HIF) controls the cellular adaptations to hypoxia and can promote the formation of new blood vessels. It is composed of a heterodimer, consisting of either HIF1a or HIF2a subunit (also known as endothelial PAS domain protein 1 (EPAS1)) and the HIF1β subunit (also known as aryl hydrocarbon receptor nuclear translocator 1, ARNT) (Denko, 2008). The von Hippel-Lindau (VHL) tumour suppressor protein is a component of a E3 ubiquitin ligase complex that also includes elongin B (TCEB2), elongin C (TCEB1), CUL2 and the ring box protein 1 (RBX1). VHL binds to the alpha subunit of HIF, leading to its ubiquitinylation and proteasomal degradation when

oxygen is present (normoxia). Two proline residues on the HIF alpha subunits are hydroxylated by the HIF prolyl hydroxylase (PHD) family of enzymes, and the VHL protein then recognizes these hydroxylated residues (Choudhry et al., 2018). In hypoxia, the prolyl hydroxylation reaction is inhibited and the HIF alpha subunits are stabilized and can move to the nucleus, where they bind to the constitutively expressed ARNT1. As mentioned for SREBPs, p300 and CBP serve as cofactors for the transcriptional activation by HIF. The HIF/ARNT complex binds to hypoxia response elements (HREs) and supports the expression of genes responsible from metabolic adaptation, survival, migration and angiogenesis (Eales et al., 2016). As there are two HIF alpha subunits with different expression profiles, different tumour types exhibit different hypoxia responses (Bertout et al., 2008). Indeed, HIF1a is ubiquitously expressed, while HIF2a expression differs between cell types and is more restricted (Eales et al., 2016)

Hypoxia and HIF activation can affect the expression, stability and function of several oncogenes and tumour suppressor proteins that have roles in cellular metabolism (Choudhry et al., 2018). It has been shown that p53 is activated by severe hypoxia due to DNA damage (Sermeus et al., 2011). Previously, it was shown that hypoxia-induced cell death is decreased in tumours that have lost the p53 tumour suppressor (Leszczynska et al., 2015). However, lack of oxygen can also generates a selective pressure for the cancer cells that requires adaptation to the metabolic stress in the tumour environment (Graeber et al., 1996). Interestingly, An *et al* suggested that physical interaction between p53 and HIF1a promotes p53 stabilisation (An et al., 1998). Moreover, it was also shown that HIF2a can interact with MYC:MAX heterodimers and promote c-MYC-induced transcriptional changes (Gordan et al., 2007). Thus, interactions between oxygen level adaptations and transcription factors that are regulating cell growth are key elements determining cell fate in the tumour microenvironment.

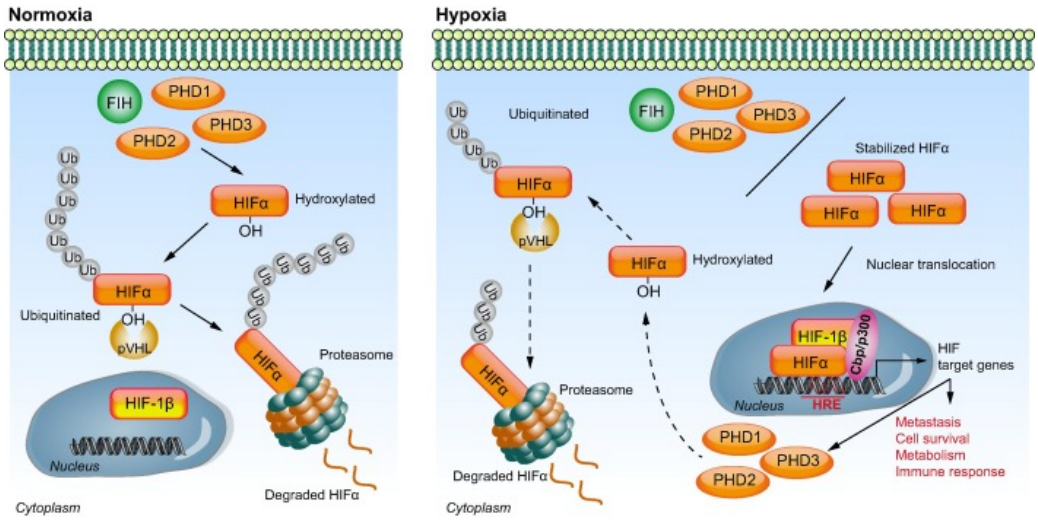

Figure 1.3: Oxygen dependent regulation of HIFs in cancer cells

Under normoxia, prolyl hydroxylases (PHDs) and factor inhibiting HIF (FIH) hydroxylate specific residues of HIF subunits. VHL recognizes the hydroxylated residues leading to its proteasomal degradation. Under hypoxia, activity of PHD and FIH is inhibited leading to the HIF translocation into nucleus where it binds to HREs in a complex with its coactivators, CBP and p300 and drives the expression of its target genes (Wilson et al., 2014).

1.6.1 Hypoxia and metabolism

As rapidly dividing cells rely on glycolysis even under normoxic conditions to generate NADPH, nucleotides, aminoacids, lipids and glycogen as well as ATP, aberrant stabilisation of HIFs in cancer can contribute to metabolic reprogramming and oncogene signaling to support the cell proliferation. HIF1a increases the expression of glucose transporters and enzymes responsible for glycolysis (Iyer et al., 1998; Semenza et al., 1996). HIF1 was reported to direct metabolites away from mitochondria by transactivating the gene *PDK1*, which is the kinase that phosphorylates and inhibits PDH and shunts pyruvate away from mitochondrial metabolism. This results in decreased ATP production and prevents ROS formation (J. W. Kim et al., 2006). In breast cancer, HIF1a dependent *PDK1* expression was shown to be a requirement for cancer cells to metastasize to the liver (Dupuy et al., 2015). However, there are other reports stating that mitochondrial ROS generated by the superoxide anions in hypoxic conditions contribute to the stabilisation of HIF1a (Guzy et al., 2005). In addition, *LDHA* and

MCT4 expression is directly regulated by HIF1a and this causes glucose-derived metabolites to be directed away from oxidative metabolism (Doherty et al., 2013).

In addition to p53, HIF was also demonstrated to be a transcriptional regulator of TIGAR, which functions as a fructose 2,6-bisphosphatase, and promotes its expression. In addition to repressing PFK1 activity through allosteric regulation, TIGAR also promotes the activity of HK2 and increased PPP flux (Cheung et al., 2012). HIF1a also regulates mitochondrial metabolism directly by inducing the change of the cytochrome c oxidase subunit COX4-1 to COX4-2, which helps transferring electrons to oxygen more efficiently under hypoxia, thereby decreasing ROS levels (Fukuda et al., 2007).

As hypoxia decreases the levels of glucose-derived acetyl-CoA entering into the TCA cycle, cancer cells develop a metabolic rewiring under these conditions to maintain the activity of the TCA cycle. Indeed, hypoxic cancer cells convert mitochondrial 2-oxoglutarate (also known as α-KG), that has been generated from glutamine, into citrate to form acetyl-CoA for the production of fatty acids and cholesterol, a phenomenon called ‘reductive carboxylation‘ (Metallo et al., 2011; Wise et al., 2011). Thus, hypoxic cells display high levels of glutamine uptake to compensate for the inhibition of glucose entry to the TCA cycle because of HIF stabilisation and inhibition of PDH. Hypoxia pushes cells towards metabolic reprogramming, where they switch from oxidative metabolism to reductive carboxylation by promoting the expression of the E1 subunit of 2-OG dehydrogenase (OGDH), mediated by HIF1a (R. C. Sun et al., 2014).

Interestingly, several studies showed that HIF stabilisation and activation is also regulated by metabolites of TCA cycle. For instance, mutations in *FH* or *SDH* that are frequent in hereditary leiomyomatosis and renal cell carcinoma (HLRCC) and hereditary paraganglioma– pheochomocytoma syndrome, respectively, lead to the accumulation of succinate and fumarate, two TCA cycle intermediates with oncometabolite function. In these tumours, accumulation of oncometabolites causes high HIF1□ levels and the expression of HIF target genes (Selak et al., 2005) (Isaacs et al., 2005) by inhibiting the catalytic activity of PHD

proteins (Koivunen et al., 2007). In addition, PHD hydroxylase levels get elevated in conditions where intracellular ascorbate is increased and this leads to HIF destabilisation and a less aggressive phenotype in colorectal cancers (Kuiper et al., 2014).

In hypoxic cells, extracellular acetate was shown to directly fuel the acetyl-CoA pool by the action of acetyl-CoA synthetase 2 (ACSS2) when the cells are under hypoxia to support lipid metabolism (Comerford et al., 2014; Mashimo et al., 2014) (Schug et al., 2015). Taken together, cancer cells reprogram their metabolism by several ways to replenish their acetyl-CoA pools under hypoxic conditions (Schug et al., 2016)

In cancer cells, the demand for lipids can be satisfied via de novo fatty acid and cholesterol synthesis, mostly from glucose derived carbon or by taking up the lipids especially under hypoxia. For this purpose, hydrolysing the lipids from circulating lipoprotein particles by lipoprotein lipase (LPL) and promoting fatty acid uptake by the activity of the CD36 transporter is very important for some cancer types to satisfy their demands for fatty acids and cholesterol under hypoxia (Kuemmerle et al., 2011).

When lipids are not available within the tumour microenvironment, cancer cells with highly activated mTOR signaling undergo apoptosis under hypoxic, nutrient-limited conditions. This is mediated by reduced activity of the SCD enzyme leading to the deregulation of desaturation (Young et al., 2013). Inhibition of this enzyme under hypoxia leads to the generation of ER stress and induction of a toxic unfolded protein response (UPR). Therefore, the ratio between saturated and unsaturated lipids is a determining factor for membrane homeostasis of the ER under hypoxia (Young et al., 2013). In addition, mild hypoxia causes to increase expression of *SCD1* and *scd2* in glioblastoma and in mice respectively (Lewis et al., 2015; J. Li et al., 2006). Interestingly, cells under hypoxia develop a mechanism to take up lysophosholipids containing mono-unsaturated fatty acids in order to bypass the need for fatty acid desaturation (Kamphorst et al., 2013). Lastly, it was reported that HIF1a promotes the expression of genes responsible for fatty acid uptake (FABP3, FABP7) and this causes an increase in lipid droplets under

hypoxic conditions in breast cancer and glioblastoma (Bensaad et al., 2014). Moreover, several reports have shown that *FASN* expression is increased through activation of AKT and SREBP1 in hypoxic regions of breast cancer xenografts (Furuta et al., 2008).

Interestingly, activation of HIF2□ represses fatty acid biosynthesis and β-oxidation in liver cells, whereas repression of HIF2□ increases fatty acid storage (Rankin et al., 2009). On the other hand, cancer cells in hypoxic conditions sustain certain level of β-oxidation by increasing the expression of CPT1C to survive under metabolic stress (Zaugg et al., 2011). In addition, in yeast it has been shown that cholesterol biosynthesis is repressed under hypoxic conditions and low levels of cholesterol activates the proteolytic processing of SRE1, the yeast homolog of mammalian SREBP, which acts as an oxygen sensor in yeast (Hughes et al., 2005). Taken together, cancer cells are flexible to reprogram their metabolism under metabolic stress by changing the expression of many genes encoding for key metabolic enzymes due to the regulatory functions of tumour suppressors and oncogenes.

1.7 Aims of the thesis

The progression of a tumour implies the acquisition of additional mutations, such that cancer cells survive and proliferate, despite adverse conditions. The inefficient vascularisation of solid tumors leads to the formation of oxygen and nutrient gradients throughout the tumour and this generates a tumour microenvironment. Tumour suppressor p53 has been demonstrated to play an important role in metabolic reprogramming. Therefore, the first aim of this thesis was to identify specific vulnerabilities that can be observed under metabolic stress with the effect of tumour suppressor p53. This was achieved by characterising multicellular tumor spheroids, which recreate the nutrient and oxygen gradients found in tumours, using RNA-SEQ and a metabolomics approach.

The second aim was to decipher metabolic liabilities depending on the p53 status in these metabolically compromised environments. This aim was accomplished by performing a pooled shRNA screen with a library consisting of several shRNAs targeting 5000 genes that are involved in signaling pathways.

2 MATERIALS

2.1 Cell lines and bacteria strains

2.1.1 Human cell lines

Cell lines were validated using STR analysis and routinely tested for mycoplasma contamination

HEK293T human embryonic kidney cell line (ATCC)
HCT116 human colon carcinoma cell line, wildtype ($p53^{+/+}$) or p53-deficient ($p53^{-/-}$) (B.Vogelstein)
HCT116 human colon carcinoma cell line wildtype ($p21^{+/+}$) or p21-deficient ($p21^{-/-}$) (M.Dobbelstein)

2.1.2 Mouse cell lines

Mouse small intestines were isolated from wild-type, *VillinCre*^{ER}*Apc*$^{fl/fl}$ or *VillinCre*^{ER}*Apc*$^{fl/fl}$*Kras*$^{G12D/+}$ mice (O.Sansom)

2.1.3 Bacteria strains

DH5α Escherichia coli, genotype F– Φ80lacZΔM15 Δ (lacZYAargF)
U169 recA1 endA1 hsdR17 (rK–,mK+) phoA supE44
λ– thi-1 gyrA96 relA1;
used for plasmid amplification

XL1 blue Escherichia coli, genotype recA1 endA1 gyrA96 thi-1hsdR17 supE44 relA1 lac [F′ proAB lacIqZΔM15 Tn10 (Tetr)];
used for plasmid amplification

2.2 Culture media and supplements

2.2.1 Cell culture media

Reconstituted media (#2) were sterile filtered with 0.45 µm, 250 ml vacuum filter immediately after preparation; all materials are from Sigma unless it is stated.

Table-2.1: Cell culture medium component

Name	**Use**	**Supplements**
DMEM (6546)	Cell lines propagation/infection	10% FBS 4 mM Glutamine 1% Penicillin/Streptomycin
DMEM (5030) dissolved in ddH_2O	Metabolic labeling Starvation experiment	3.7 g/l Sodium Bicarbonate 10% dialyzed FBS 4 mM Glutamine 1% Penicillin/Streptomycin
Freezing medium	Cell line storage	20% FBS 8% DMSO
Agilent Seahorse XF Base Medium	Oxygen Consumption Rate	100 mM Na pyruvate 200 mM Glutamine 2.5 M Glucose
Advanced DMEM/F-12 (Thermo Fisher)	Mouse organoids	EGF-recombinant human Recombinant murine Noggin (PeproTech) B-27 supplement minus vitamin A, N2, GlutaMAX (Thermo Fisher)

2.3 Bacterial Medium and Supplements

2.3.1 Culture media

Name Components and preparation

LB medium	10% (w/v) Bacto tryptone (Roth) 0.5% (w/v) yeast extract (Roth) 1% (w/v) NaCl (Roth) autoclaved immediately after preparation
LB agar	LB-medium with 1.2% (w/v) agar-agar (Roth) autoclaved, heated in a microwave oven, cooled down to 50°C; antibiotics were added the medium poured into 10 cm dishes

2.3.2 Antibiotics

All powder formulations were obtained from Roth. Stock solutions were prepared in ddH_2O and sterile filtered before use.

Ampicillin	100 µg/ml final concentration
Kanamycin	30 µg/ml final concentration
Chloramphenicol	25 µg/ml final concentration

2.4 Chemical & Reagents

All reagents were obtained from Sigma, unless otherwise indicated

Table-2.2: Chemicals and reagents

Name	Stock concentration	Final concentration
5-Bromouridine5′-triphosphate sodium salt	20 mM	20 µM
D-Glucose (U-^{13}C6, 99%) (Cambridge Isotope Laboratories,Inc)	1M in H2O stored at	22.5 mM
Lamivudine	1 mM in MeOH/ H_2O	0.1 µM
Etoposide	20 mM	20 µM
Rapamycin (LCLabs)	100 µM, in DMSO;	20 nM
CHIR99021	1 mM in DMSO	10 µM
SB216763	7.5 mM in DMSO	30 µM
Doxycycline hyclate	1 mg/ml in EtOH;	1 µg/ml
Puromycin (Invitrogen)	10 mg/ml	1 µg/ml

Hexadimethrine Bromide	8 mg/ml	8 µg/ml
Mevastatin (Biomol)	10 mM in EtOH	10 µM
(R)-Mevalonic acid lithium salt	1 M	0.5 mM
Hoechst 33258	5 mg/ml	1 µg/ml
Simvastain	10 mM in DMSO	10 µM
Zoledronic acid monohydrate	1 M	25 µM
YM-53601 (Biomol)	1 M	4 µM
Coenzyme Q9	1 mM	1 µM
Oligomycin (Merck)	6.3 mM	2 µM
FCCP	100 mM	0.5 µM
Antimycin A from Streptomyces sp.	100 mM	1 µM
Rotenone	100 mM	1 µM
Coenzyme Q10	1 mM	10 µM
NAC (N-Acetyl-L-cysteine)	1 M	5 mM
EmbryoMax Nucleosides (100x) (Merck)	100X	5X
Fluorouracil	1 mM	10 µM
Matrigel Matrix (BD BIOSCIENCE)	1 M	1 µM

2.5 Solutions and buffers

All solutions and buffers were prepared using ddH2O, unless otherwise indicated.

All solutions were stored at RT, unless otherwise specified.

All chemicals were purchased from Sigma and Roth.

Ammonium persulfate (10%)	5 g ammonium persulfate (APS) dissolved in 50 ml ddH_2O; aliquots stored at -20°C
Ampicillin stock solution	10 g ampicillin solubilized in 100 ml ddH_2O and sterile filtered; aliquots stored at -20°C
Crystal violet solution	0.1% (w/v) crystal violet 20% (v/v) ethanol
Deoxynucleotide triphosphate (dNTP) (10 mM)	50 µl each dNTP (100 mM) mixed with 300 µl ddH2O to 500 µl final volume

DNA loading buffer (6x)	10 mM EDTA, pH 8.0 0.2% (w/v) Orange G 40% (w/v) sucrose; stored at -20°C
Kanamycin stock solution	1 g kanamycin solubilized in 100 ml ddH_2O and sterile filtered; aliquots stored at -20°C
Miniprep lysis buffer	0.2 M NaOH 1% SDS
Miniprep neutralization buffer	3 M NaOAc pH 4.8
Miniprep resuspension buffer	1:1000 RNAse in TE buffer; stored at 4°C
Nuclear extraction Buffer C	10 mM HEPES/KOH pH 7.6 10 mM KCL 1.5 mM MgCl2 1 mM EDTA 1 mM EGTA 0.5 mM DTT Protease Inhibitor Cocktail and PhosStop Inhibitor
Nuclear extraction Buffer D	20 mM HEPES/KOH pH 7.6 0.5 M NaCl 1.5 mM MgCl2 1 mM EDTA, 1 mM EGTA, 25 % (v/v) glycerol Protease Inhibitor Cocktail and PhosStop Inhibitor
PBS 1x	137 mM NaCl 2.7 mM KCl 10.1 mM Na_2HPO_4 1.76 mM KH_2PO_4 autoclaved
Phenol-chloroform	25 ml phenol 24 ml chloroform 1 ml isoamyl alcohol prepare at least one day before using, stored at 4°C

Polybrene stock solution (4mg/ml)	200 mg dissolved in 50 ml H_2O sterile filtered with 0.2 µM syringe filter
Polyethylenimin (PEI)	450 µl PEI (10%, MW 25,000 g/mol, Sigma) 150 µl HCl (2 N), 49.5 ml ddH_2O
RIPA lysis buffer	50 mM HEPES, pH 7.9 140 mM NaCl 1 mM EDTA 1% Triton X-100 0.1% Na-deoxycholate 0.1% SDS; stored at 4°C;
Sample buffer (6 x)	1.2 g SDS pellet 6 mg bromphenol blue 4.7 ml 100% glycerol 1.2 ml 0.5 M Tris, pH 6.8 2.1 ml ddH_2O heated up, then dissolved 0.93 g DTT; aliquoted and frozen at -20°C
SDS running buffer (1X)	25 mM Tris base 250 mM glycine 0.1% (v/v) SDS
SDS separating gel	7.5 - 12.5% (v/v) acrylamide/bisacrylamide 375 mM Tris HCl pH 8.8 0.1% (w/v) SDS 0.1% (w/v) APS 0.1% (v/v) TEMED
SDS stacking gel	4% (v/v) acrylamide/bisacrylamide 125 mM Tris HCl pH 6.8 0.1% (w/v) SDS 0.1% (w/v) APS 0.1% (v/v) TEMED

Transfer buffer 10x	250 mM Tris base 1.5 M glycine
Transfer buffer 1x	prepared by diluting Transfer buffer 10x with 15% (v/v) methanol
TAE (50 x)	2 M Tris, pH 8.0 5.7% acetic acid 50 mM EDTA
TBS (20 x)	500 mM Tris base 2.8 M NaCl; adjusted to pH 7.4 with concentrated HCl
TBS-T	1 x TBS 0.2% Tween-20
TE	10 mM Tris, pH 7.4 1 mM EDTA, pH 8.0

2.6 Standards, enzymes and kits

2.6.1 Standards

DNA marker	Gene Ruler 1 kb Plus DNA ladder (Thermo Scientific)
Protein marker	PageRuler Prestained Protein Ladder (Thermo Scientific)
Protein marker	HiMark Prestained High molecular weight Standard (Life Technologies)

2.6.2 Enzymes

M-MLV Reverse Transcriptase	Promega

Phusion HF DNA polymerase	Thermo Scientific
RNase-free DNase	Qiagen
SYBR Green qPCR Master Mix	Thermo Scientific
T4 DNA ligase	NEB

2.6.3 Kits

Experion DNA 1K analysis kit	Bio-Rad
Experion RNA StdSense Analysis Kit	Bio-Rad
GeneJET Gel Extraction Kit	Thermo Scientific
RNeasy Mini Kit	Qiagen
NEBNext Poly (A) mRNA Magnetic Isolation Module	NEB
NEBNext Multiplex Oligos for Illumina (Index Primer 1-12)	NEB
PureLink HiPure Plasmid Maxiprep Kit	Invitrogen
QIAquick Gel Extraction Kit	Qiagen

2.7 Nucleic acids

2.7.1 Primers

Most of the oligos were synthetized by and obtained from Sigma. Several QPCR oligos were bought from Qiagen.

All oligos were synthetized at 0.025 μmole scale and purified by desalting (DST), unless otherwise indicated.

Each primer was resuspended in Ampuwa H2O to 100 μM and used at 10 μM final concentration, unless otherwise specified. Stock and diluted primers were stored at -20°C.

Table-2.3: Primers for shRNA cloning

Target	Forward sequence (5'-3')	Reverse sequence (5'-3')
SREBF2 #384	CCGGCCTGAGTTTCTC TCTCCTGAACTCGAGT TCAGGAGAGAGAAAC TCAGGTTTTT	AATTAAAAACCTGAG TTTCTCTCTCCTGAAC TCGAGTTCAGGAGAG AGAAACTCAGG
SREBF2 #385	CCGGCCTCAGATCATC AAGACAGATCTCGAG ATCTGTCTTGATGATC TGAGGTTTTT	AATTAAAAACCTCAG ATCATCAAGACAGAT CTCGAGATCTGTCTTG ATGATCTGAGG

Exon-exon spanning primers were designed with Primer 3, according to default parameters. Specificity of alignment was verified by nucleotide Blast alignment. Specific product amplification after qPCR was evaluated from the melting curve.

Table-2.4: Custom Primers for qPCR

Target	Forward sequence (5'-3')	Reverse sequence (5'-3')
Human *beta actin*	GCCTCGCCTTTGCCGAT	CGCGGCGATATCATCATCC
Human *CDKNA1*	TCACTGTCTTGTACCCTTGTGC	GGCGTTTGGAGTGGTAGAAA

Table-2.5: Ready Primers for qPCR

Target	Source	Identifier
Human *HMGCS1*	Quantitect	QT00055531
Human *MVD*	Quantitect	QT00044779
Human *HMGCR*	Quantitect	QT00004081
Human *DHCR7*	Quantitect	QT00074606
Human *FDFT1*	Quantitect	QT00092365
Human *SREBF2*	Quantitect	QT00052052

Table-2.6: Primers for shRNA screen

Oligo indexes	**(5'-3')**
decipherPCR_3_r_TGC	aatgatacggcgaccaccgagatctacacTGCctattctttcccctgcactgtacc*c
decipherPCR_3_r_GCT	aatgatacggcgaccaccgagatctacacGCTctattctttcccctgcactgtacc*c
decipherPCR_3_r_ACG	aatgatacggcgaccaccgagatctacacACGctattctttcccctgcactgtacc*c
decipherPCR_3_r_GTA	aatgatacggcgaccaccgagatctacacGTActattctttcccctgcactgtacc*c
decipherPCR_3_r_CAT	aatgatacggcgaccaccgagatctacacCATctattctttcccctgcactgtacc*c
decipherPCR_3_r_TAG	aatgatacggcgaccaccgagatctacacTAGctattctttcccctgcactgtacc*c
decipherPCR_3_r_ATC	aatgatacggcgaccaccgagatctacacATCctattctttcccctgcactgtacc*c
decipherPCR_3_r_TCA	aatgatacggcgaccaccgagatctacacTCActattctttcccctgcactgtacc*c
decipherPCR_3_r_GAC	aatgatacggcgaccaccgagatctacacGACctattctttcccctgcactgtacc*c
decipherPCR_3_r_CTG	aatgatacggcgaccaccgagatctacacCTGctattctttcccctgcactgtacc*c
decipherPCR_3_r_AGT	aatgatacggcgaccaccgagatctacacAGTctattctttcccctgcactgtacc*c
decipherPCR_3_r_ATG	*aatgatacggcgaccaccgagatctacac*ATGctattctttcccctgcactgtacc*c
decipherPCR_3_r_CGT	*aatgatacggcgaccaccgagatctacac*CGTctattctttcccctgcactgtacc*c
decipherPCR_3_r_GCA	*aatgatacggcgaccaccgagatctacac*GCActattctttcccctgcactgtacc*c
decipherPCR_3_r_TGA	*aatgatacggcgaccaccgagatctacac*TGActattctttcccctgcactgtacc*c
decipherPCR_3_r_CAG	*aatgatacggcgaccaccgagatctacac*CAGctattctttcccctgcactgtacc*c
decipherPCR_3_r_TAC	*aatgatacggcgaccaccgagatctacac*TACctattctttcccctgcactgtacc*c
decipherPCR_3_r_ACT	*aatgatacggcgaccaccgagatctacac*ACTctattctttcccctgcactgtacc*c
decipher_seq_read1_1	TCAGAGGTTCAGAGTTCTACAGTCCGAA
decipher_seq_index1_2	ATACGGCGACCACCGAGATCTACAC

2.7.2 Plasmids

All sequences cloned into the vectors refer to human sequences.

All constructs were verified by Sanger sequencing, which was carried out by LCG Genomics.

Table-2.7: Plasmids

psPAX.2	Addgene	Cat# 12260 D. Trono
pMD2.G	Addgene	Cat# 12259 D. Trono
Tet-pLKO-puro	Addgene	Cat#21915 D.Wiederschain
pRSI9-U6-(sh)-UbiC-TagRFP-2A-Puro (DECIPHER shRNA Expression Vector)	Addgene	Cat#28289 A.Chenchik
pGIPZ deltaEco GFP empty vector	N/A	from M.Eilers Lab
pGIPZ deltaEco GFP empty vector	N/A	from M.Eilers Lab

2.8 Antibodies

Table-2.8:Primary Antibodies

Target	Company	Order number	Use
Mouse monoclonal anti-p53 (DO-1)	Santa Cruz	Cat#sc-126 RRID: AB_628082	WB (1:1000)
Mouse FITC anti-BrdU, IgG1, kappa	Biozol/BioLegend	Clone: 3D4 Cat# BLD-364104	FACS
Rabbit monoclonal anti-Ki67 (SP6)	Thermo Fisher	RM-9106-S	IHC (1:250)
Rabbit polyclonal anti-HMGCS1	Abcam	Cat#Ab155787	WB (1:1000)
Mouse monoclonal anti-SREBP-2 (1D2)	Novus	Cat#NBP1-54446	WB (1:500)
Goat polyclonal-SREBP-2	R&D Systems	Cat#AF7119	WB (1:500)
Rabbit monoclonal anti-S6 ribosomal protein (5G10)	Cell Signaling	Cat#2217	WB (1:1000)
Mouse monoclonal anti-GSK3a (4G-1E)	Milipore	Cat#05-412	WB (1:1000)
Rabbit polyclonal anti-phospho-GSK3a/b (Ser21/9)	Cell Signaling	Cat#9331	WB (1:1000)
Rabbit polyclonal anti-phospho-S6 Ribosomal protein (Ser240/244)	Cell Signaling	Cat#2215	WB (1:1000)

Rabbit polyclonal anti-Histone H3	Abcam	Cat#ab1791	WB (1:1000)
Rabbit polyclonal anti-p21 (C-19)	Santa Cruz	Cat#sc-397	WB (1:1000)
Mouse monoclonal anti-beta-Actin (AC-15)	Sigma-Aldrich	Cat#A5441	WB (1:10000)
Mouse monoclonal anti-beta-Actin-Peroxidase (AC-15)	Sigma-Aldrich	Cat#A3854	WB (1:10000)
Mouse monoclonal anti-Vinculin (hVIN-1)	Sigma-Aldrich	Cat#V9131	WB (1:10000)

Table-2.9: Secondary Antibodies

IRDye® 800CW Donkey anti-Rabbit IgG (H + L)	LI-COR Biosciences GmbH	Cat# 926-32213	WB (1:5000)
IRDye® 800CW Donkey anti-Mouse IgG (H + L), Lot: C61116-02	LI-COR Biosciences GmbH	Cat#926-32212	WB (1:5000)
Biotinylated Anti-Rabbit IgG (H+L)	Vector Laboratories	Cat#BA-1000	IHC (1:1000)

2.9 Consumables

Consumables were purchased from the companies Eppendorf, Greiner, Nunc, Sarstedt and VWR and included disposable plastic items such as cell culture dishes, reaction tubes, cryotubes, syringes, cuvettes, pipettes.

2.10 Equipment and membranes

Automated Electrophoresis	Experion Automated Electrophoresis System (Bio-Rad)
Cell culture incubator	BBD 6220 (Heraeus)
Centrifuges	Avanti J-26 XP (Backman Coulter)
	Eppendorf 5417 R (Eppendorf) Eppendorf 5425 (Eppendorf) Eppendorf 5430 (Eppendorf) Galaxy MiniStar (VWR) Multifuge 1S-R (Heraeus)

Deep-sequencer	llumina GAIIx sequencer (Illumina) NextSeq 500 (Illumina)
Flow cytometer	BD FACS Canto II (BD Biosciences) BD FACS Aria III (BD Biosciences)
Heating block	Dry Bath System (Starlab) Thermomixer® comfort (Eppendorf
Immunoblot transfer chamber	Bio-Rad
Mass spectrometry	Q- Exactive mass spectrometer
Microscopes	Axiovert 40CFL (Zeiss) TCS SP5 (Leica)
PCR thermal cycler	C1000 Thermal cycler (Bio-Rad)
Photometer	Multiscan Ascent (Thermo Labsystems)
PVDF transfer membrane	Immobilon-P transfer membrane (Millipore)
Quantitative RT-PCR	StepOne plus (Applied Biosystem)
SDS-PAGE system	Minigel (Bio-Rad)
Strata® C18-E column	Phenomenex
Strata® SI-1 column	Phenomenex
Ultrasonifier	Digital Sonifier W-250 D (Branson)
Whatman filter paper	Gel Blotting Paper (Schleicher and Schuell)

2.11 Software and online programs

ApE plasmid editor	by M. Wayne Davis
BD FACSDiva v6.1.2	BD Biosciences
Bowtie v1.1.2	Langmead et al, 2009
EndNote X7	Clarivate Analytics
FlowJo v8.8.6	FlowJo, LLC

FreeStyle 1.4	Thermos Fisher
Illustrator, Photoshop, Acrobat	Adobe Inc.
Image J	by Wayne Rasband
Image Studio Lite Version 5.2.5	Licor
MSigDB v3.1	Subramanian et al, 2005
Prism7	GraphPad Software Inc.
R version v3.1.0 R samtools v1.16.0 EdgeR v3.6.2	R core team
Stepone software v2.3	Applied Biosystem
TraceFinder 4.1	Thermo Fisher

3 METHODS

3.1 Molecular biology methods

3.1.1 Transformation of competent cells with plasmid DNA and plasmid amplification

Chemically competent bacteria were thawed on ice and 90 µl were mixed with the plasmid DNA. The bacteria were incubated on ice for 30 min, followed by a heat shock for 30 sec at 42 °C. The reactions were shortly placed on ice for 2 min. 250 µl of pre-warmed LB medium were added and the mix was incubated for 1 hr at 37°C on a shaker. The mix was plated on pre-warmed LB-agar plate containing the appropriate antibiotic for selection. LB agar plates were incubated at 37°C over night.

3.1.2 Analytical preparation of plasmid-DNA from bacteria (Miniprep)

A bacteria overnight culture was transferred to a 1.5 ml tube and the rest was stored at 4°C. The bacteria were spun down for 5 min at RT and the culturing medium was completely removed. The bacteria pellet was re-suspended in 150 µl miniprep resuspension buffer, followed by the addition of 150 µl miniprep lysis buffer. The mix was inverted 5 times and incubated for 5 min at RT. Afterwards, 150 µl miniprep neutralization buffer were added to stop the reaction of lysis. The samples were spun down for 5 min at 4°C and the supernatant was transferred into a new 1.5 ml tube. 800 µl isopropanol were added and each sample was briefly vortexed and spun down for 30 min at 4°C. The supernatant was carefully removed, the pellets were washed with 500 µl 70 % EtOH and spun down for 10 min at 4°C. The supernatant was removed; the pellets were air-dried and re-suspended in 20-40 µl of TE buffer. The samples were stored at -20°C.

3.1.3 Preparative isolation of plasmid DNA (Maxiprep)

Two hundred ml overnight culture was processed according to the manufacturer's protocol (PureLink HiPure Plasmid Maxiprep Kit, Life Technologies). The purified plasmid DNA was solubilized in TE and adjusted to a concentration of 1 µg/µl.

3.1.4 Restriction analysis of DNA

Restriction endonucleases from Fermentas and New England Biolabs were used following the manufacturer's protocol, i.e. the recommended restriction buffers and enzyme amounts.

Analytical digestion was set up as follows:

0.5-1 µg DNA

0.5 µl restriction endonuclease (or 0.2 µl each, if two different enzymes were used)

2 µl 10x reaction buffer

up to 20 µl ddH2O

Preparative digestion was set up as follows:

5 µg DNA

2.5 µl restriction endonuclease (or 1 µl each, if two different enzymes were used)

5 µl 10x reaction buffer

up to 50 µl ddH2O

3.1.5 Gel electrophoretic separation of DNA fragments

Gels were prepared according to the expected size of the DNA fragments. The appropriate amount of agarose was boiled in TAE, briefly cooled down, supplemented with 0.4 µg/ml ethidium bromide and poured into a gel chamber with combs. The samples were mixed with DNA loading buffer and loaded into each well of the gel. A DNA ladder was loaded. The separation was performed at 120 V for 1 hr and the DNA fragments were visualized on a UV transilluminator.

3.1.6 Extraction and purification of DNA fragments and PCR products

The DNA fragment was cut out of the agarose gel and extracted with the gel extraction kit according to the manufacturer's protocol (GeneJET Gel Extraction Kit, Thermo Scientific).

3.1.7 Nucleic acid quantification

3.1.7.1 Nanodrop

DNA and RNA concentration was determined with the NanoDrop 1000, unless specifically indicated. The absorbance was measured at 260 nm. To assess the purity of the nuclei acid solution, the ratio of absorbance at 260 and 280 nm was determined.

A ratio of 1.8 for DNA and 2 for RNA indicate a pure preparation, i.e. without protein contaminants.

3.1.7.2 Bioanalyzer

RNA, which was used for library preparation for RNA-Sequencing, as well as the prepared DNA-libraries, were quantified with the Experion Automated Electrophoresis System (Bio-Rad) and Fragment Analyzer (Advanced Analytical), following the manufacturer's protocol.

3.1.8 Nucleic acid isolation

3.1.8.1 RNA isolation with TriFAST

Total RNA was isolated with peqGOLD TriFast (Peqlab), unless otherwise specified. Cells plated on a tissue culture dish or approximately 12 spheroids in a 1.5 ml tube were washed two times with PBS, lysed directly with 1 ml Trifast and monolayer cells were transferred into a 1.5 ml reaction tube. The mix was incubated for 5 min at RT. 200 µl chloroform was added and the suspension was vortexed for 30 s. The reactions were centrifuged for 15 min at 14,000 rpm, at 4 C°. The upper aqueous phase containing the RNA (c.ca 500 µl) was transferred into a new reaction tube. To precipitate the RNA, 500 µl isopropanol was added. The samples were incubated on ice for 15 min followed by centrifugation for 15 min at 14,000 rpm, at 4 C°. The supernatant was carefully discarded and the RNA pellet washed twice with 70% EtOH. The pellet was air-dried and solubilized in 50 µl RNAse free ddH2O. The RNA was stored at -80°C.

3.1.8.2 RNA isolation with the RNeasy Mini

RNA used for RNA-Sequencing (see 3.3.2), isolation was performed with the RNeasy Mini Kit and additional DNase I digestion according to manufacturer's protocol.

3.1.8.3 DNA isolation with phenol-chloroform

DNA used for shRNA screen library preparation. Cell suspension was lysed with a lysis buffer and 10% SDS from Maxi prep kit.One volume of phenol-chloroform-isoamyl alcohol solution was added to the mixture volume and vortexed for 30 sec. Samples were centrifuged for at 8,700 rpm for 30 min at RT and the upper phase containing the DNA was transferred to a new reaction tube. 4 ml isopropanol, 500 µl Na-acetate pH 5.2 and 30 µl Glyco blue were added to the mix. The samples were

briefly vortexed and incubated over night at RT. Afterwards, samples were centrifuged at 8,700 rpm for 30 min at 4°C. The DNA pellet was washed with 70% EtOH, air-dried and resuspended in TE buffer or ddH2O.

3.1.9 cDNA synthesis

In order to perform the quantitative reverse transcriptase PCR reaction (see 3.2.10), extracted total 2 µg RNA in a total volume of 7 µl water was reverse transcribed into complementary DNA (cDNA).

Reactions were set up as follows:

2 µg RNA

2.5 µl random hexanucleotide primers (2 µg/ml Stock, Roche)

1 µl DNAse 1

1 µl NAse buffer

1 µl dNTP (10 mM stock)

Mixture was incubated for 15 minutes at 37°C and 15 minutes at 70°C. Then, followings were added:

0.2 µl RiboLock RNase Inhibitor (40 U/µl, Invitrogen)

5x First strand reaction buffer (Promega)

1 µl M-MLV reverse transcriptase (200 U/µl, Promega)

up to 20 µl ddH2O

A reaction without M-MLV reverse transcriptase was included as used as negative control for the following quantitative reverse transcriptase PCR reaction.

The samples were incubated in a PCR thermal cycler as follows,

10 min 25°C

50 min 42°C

15 min 70°C

The cDNA was stored at -20°C.

3.1.10 Polymerase chain reaction (PCR)

3.1.10.1 PCR to amplify DNA

Custom primers (see *Table-2.6*) were used according to the purpose. Reactions were set up as follows:

10 ng DNA template
5 µl 5x Phusion High-Fidelity (HF) reaction buffer
1 µl dNTPs (10 mM Stock, Roth)
1µl forward primer (10 µM Stock)
1µl reverse primer (10 µM Stock)
1 µl Phusion HF DNA polymerase (2.5 U/ µl, Fermentas)
up to 50 µl nuclease-free H2O

The reaction was performed in a PCR thermal cycler as follows,

Segment	**Cycles**	**Temperature**	**Time**
Initial denaturation	1	95 °C	1 min
Denaturation	30	98 °C	15 sec
Annealing		55-62 °C	50 sec
Extension		72 °C	30 sec/kb
Final extension	1	72 °C	7 min

3.1.10.2 Quantitative real-time PCR (qPCR)

For a typical reaction, 100 ng cDNA from section 3.2.9 was used as a template for semi-quantitative PCR (RT-QPCR) analysis Reactions were set up as follows:
4 µl cDNA (see 3.2.9)
5 µl SYBRGreen Mix (Thermo Scientific)
1 µl forward + revers primer mix (10 µM Stock)

The reaction was performed in a quantitative RT-PCR machine as follows,

Segment	**Cycles**	**Temperature**	**Time**
Initial denaturation	1	50 °C	2 min
		95 °C	2 min
Denaturation	40	95 °C	3 sec
		60 °C	30 sec
		95 °C	15 sec

Melting curve	1	60 °C	1 min
		95 °C	15 sec

Each sample was analyzed in technical duplicate. Raw data were expressed as Ct (threshold cycle), i.e. the cycle in which the fluorescence is above the background.

For qPCR experiments, β-actin was used as housekeeping gene for internal normalization. qPCR data were analyzed according to the double Delta Ct method, i.e. the fold induction relative to a control was calculated.

First, the average Ct value was calculated.

The difference of Ct average between β-actin and the target gene was calculated per each condition (ΔCt).

The SD of the ΔCt was calculated: SD ΔCt = √ ($SD_{target\ gene}$^2+SD_{actin}^2).

The difference of ΔCt between the control and the treated sample was calculated (ΔΔCT). The relative expression (RE) per each condition was calculated (relative expression =2^- ΔΔCT).

The SD of the relative expression was calculated: SD RE = √ (($RE_{control}$ * ln (2))^2*$SD_{control}$^2);

or SD RE = √ (($RE_{treated}$ * ln (2))^2*$SD_{treated}$^2)

3.2 Cell biology methods

3.2.1 Cultivation of eukaryotic cell lines

HCT116 p53+/+, HCT116 p53-/- and HCT116 p21 +/+ and HCT116 p21-/- cell lines were obtained from B.Vogelstein (Johns Hopkins University, Baltimore) and M. Dobbelstein (Georg-August University, Göttingen). Human embryonic kidney (HEK) 293-T cells were obtained from M. Eilers (University of Würzburg, Würzburg). All cell lines were grown in a monolayer and maintained in DMEM media supplemented with 10% foetal bovine serum (FBS, Sigma), 4mM L-glutamine (Sigma) and 100units/ml penicillin/100µg/ml streptomycin (Sigma) and were cultivated in a cell incubator at 37°C in 5% CO2.

3.2.1.1 Cell passaging

Cells were passaged every two to three days, when they reached approximately 80% confluency. After medium removal, cells were washed twice with PBS and trypsinized to detach them from the cell culture dish. Once detached, serum-containing medium was added to the trypsin, in a ratio 4:1, in order to stop the enzymatic activity of the trypsin. The cells were collected into a 15 ml tube and centrifuged at 1500 rpm for 3 min. Supernatant was removed, the cell pellet re-suspended in the cell culture medium and a fraction of the cell suspension was plated on a new cell culture dish with fresh medium.

3.2.1.2 Cell freezing

Cells were harvested by trypsinization, as described above. After centrifugation, the cell pellet was re-suspended in the appropriate volume of freezing medium, e.g. 1 ml for cells collected from an 80% confluent 10 cm dish. Cell suspension was transferred to a cryotubes and immediately transferred into a freezing container filled with isopropanol and placed overnight at -80°C. Afterwards, cryotubes were transferred to storage boxes in liquid nitrogen tanks.

3.2.1.3 Cell thawing

Cryotubes were placed for few min in a water bath at 37°C. The cell suspension was transferred to a 15 ml falcon tube containing 5 ml fresh medium and centrifuged at 1500 rpm for 3 min. This step helped removing the DMSO present in the freezing medium. After centrifugation the supernatant was removed, the cell pellet re-suspended in 1 ml fresh culture medium and plated on a new cell culture dish with fresh medium. Thawed cells were passaged at least 2 times before performing experiments.

3.2.1.4 Culturing of the cells in hypoxic conditions

Cells cultured in hypoxia were incubated in a Don Whitley Hypoxia Workstation in 0.1-0.5% O2 and 5% CO2 at 37°C and 77% humidity. Dishes and plates containing cells were wrapped in aluminium foil to prevent evaporation of the media and to protect the cells from light.

3.2.1.5 Cell starvation

In order to perform starvation experiments, specific number of cells was plated, as described in 3.2.1.1. 24 hrs later cells were washed twice with PBS and the medium was changed to the reconstituted DMEM (D5030), lacking glucose, glutamine and FBS as indicated.

3.2.1.6 Culturing cells as multicellular tumour spheroids

Cells were passaged every two to three days, when they reached approximately 80% confluency. After medium removal, cells were washed twice with PBS and trypsinized to detach them from the cell culture dish. For individual spheroids 10000 cells were placed in each well in 96-well ultralow attachment plates (Corning® CORN7007). Spheroid formation was initiated by centrifugation at 850g for 10 min.
For the bulk spheroid formation, 3 million cells were put into spinner flasks with a 500 ml DMEM on the magnetic stirrer and grown. Culture media was changed every fourth day.

3.2.2 Cell transfection

3.2.2.1 Transfection by Polyethylenimine (PEI)

This method was used for lentiviral production (3.2.3). Cells were washed twice with PBS and medium was changed to transfection medium. In one 1.5 ml reaction tube 250 µl Opti-MEM (Gibco) were mixed with 24 µl PEI and incubated 5 min at RT; in a second 1.5 ml reaction tube 250 µl Opti-MEM were mixed with the appropriate amount of plasmid DNA. The reactions were mixed and incubated 20 min at RT. The mix was added drop-wise to the cells.

3.2.2.2 Transfection by Lipofectamine 2000

This method was used for lentiviral production (3.2.3). The amount of each reagent refers to a single well of a 24-well dish. Cells were washed twice with PBS and medium was changed to transfection medium. In one 1.5 ml reaction tube 25 µl Opti-MEM were mixed with 1.2 µl Lipofectamine 2000 (Invitrogen) and incubated 5 min at RT; in a second 1.5 ml reaction tube 25 µl Opti-MEM were mixed with 10 ng plasmid DNA. The reactions were mixed and incubated 20 min at RT. The mix was added dropwise to the cells.

3.2.3 Production of lentiviruses

Five million HEK293T cells were plated in 10 cm dish. After 24 hrs cells were transfected by PEI, using 8 µg lentiviral expression plasmid, 5 µg psPAX.2 plasmid and 1.25 µg pMD2.G. Cells were incubated in a biosafety level-2 (BSL-2) incubator and the following steps were performed in a BSL-2 environment. After 24 hrs transfection medium was replaced by 5 ml DMEM containing FBS and antibiotics. Viral sups were harvested for 3 times every 12 hrs, collected into a 15 ml falcon tube and stored at 4°C. After the last harvesting the viral sup was filtered using a 0.44 µm syringe-filter, aliquoted in cryotubes and stored at -80°C.

3.2.4 Cell infection with lentiviruses

One million HCT116 cells were plated in a 10 cm dish. The infections were performed in a BSL-2 environment after 24 hrs. The viral sups were thawed in a water bath at 37°C and 0.5 to 1 ml viral sup were used for each infection. Viral sups were mixed with 5 ml fresh medium and polybrene was added to a final concentration of 8 µg/ml. After 24 hrs the procedure was repeated. After 48 hrs from the first infection cells infected with Tet-pLKO-puro plasmids were selected with puromycin and cells infected with pRSI9 plasmids were sorted according to the highest RFP signal.

3.2.5 Crystal violet staining and quantification

Cells were fixed for 15 min with 3.7% formaldehyde, incubated for 1 hr with crystal violet solution, washed under tap water and air-dried. The color intensity was quantified by de-staining the cells with 10% w/v acetic acid solution. An aliquot of de-stained solution was diluted 1:4 with water and the absorbance at 550 nm was read with a microplate reader.

3.2.6 Cell Number Assay

For the determination of cell number, 5000 cells per well were cultivated in 96-well plates (Greiner, #655986) and fixed in 3.7% PFA for 10 min. After washing with PBS, cells were permeabilized with 0.2% Triton X-100/PBS and blocked in 3% BSA/PBS. After washing with PBS, nuclei were stained with 2.5 µg/ml Hoechst 33342 for 5 min. Images were acquired using the Operetta™ High Content Screening System (PerkinElmer) with the following settings: objective: 20 x WD; optical mode:

non-confocal; excitation: 50 %. Ten images per well were acquired and analysis was performed with the Harmony^{R} High Content Imaging and Analysis Software (Perkin Elmer).

3.2.7 Colour competition assays

250000 HCT116 p53 +/+ cells carrying pGIPZ deltaEco GFP vector and 7500000 HCT116 p53 -/- cells carrying pGIPZ deltaEco RFP vector was mixed and placed into spinner flasks. Fluorescence intensity was measured by using BD FACSCanto II every third day for 14 days.

3.2.8 BrdU Incorporation and Flow Cytometry Analysis FACS Analyses

Monolayer and spheroid cells were incubated with 20 µM 5-Bromo-2'-deoxyuridine (BrdU, Sigma) for 24 hr. Monolayer cells and spheroids were incubated with trypsin for 1 min or 10 min, respectively and collected together with supernatant in ice cold PBS. Cells were fixed in 80% EtOH over night at -20°C. Cells were washed with cold PBS and incubated in 2 M HCl with 0.5% Triton X-100 for 30 min at room temperature. Cell pellets were neutralized with $Na_2B_4O_7$. Pellets were incubated with anti-BrdU-FITC antibodies (Biozol) diluted in 100 µl 1% BSA, 0.5% Tween-20 in PBS for 30 min at room temperature in the dark. Cell were washed with PBS, resuspended in PBS with RNAse A (24 µg/ml) and propidium iodide (54 µM) and incubated for 30 min at 37°C. Analysis was performed on a BD FACSCanto II flow cytometer using BD FACSDIVA^{TM} software.

3.2.9 Immunohistochemistry

For immunohistochemical staining of spheroids grown *in vitro*, spheroids were collected with a cut 200 µl pipette tip and fixed in 3.7% PFA for 16 hrs at 4ºC. The spheroids were then centrifuged and washed with 70% EtOH for short-term storage. To facilitate handling and sectioning, spheroids were rehydrated in distilled water and transferred into liquid molten 2% agarose in a petri dish and then, when cooled, a small block of agarose containing the spheroids was isolated and paraffin processed. After embedding, serial 4 µm sections were cut onto positively charged slides and dried overnight at 37ºC. To remove paraffin, slides were incubated for 2 x 3 min in xylene, then for 2 x 3 min in 100%ethanol and rehydrated in 70% ethanol and distilled water. For antigen retrieval, slides were microwaved in 0.01 M sodium

citrate (pH=6) for 6 min (900W oven, on medium setting), and then cooled for 3 min. To block endogenous peroxidase activity slides were incubated for 10 min in 3% H_20_2/PBS. After brief washes in distilled water and PBS, slides were blocked in 1% BSA/PBS for 30 min before the primary antibody was applied. Primary antibodies were all diluted in 1% BSA/PBS and incubated overnight at 4ºC (dilutions are shown in *Table-2.8* and *2.9*). After primary incubation slides were washed 3 x 3 min in PBS and incubated in biotinylated goat anti rabbit IgG (1/2000 in 3%BSA) for 1 hr at RT. After 3 x 5 min PBS washes slides were incubated in Avidin-Biotin-Complex (Vector Labs) for 30 min washed again in PBS then developed with Diaminobenzidine (DAB). After washing in distilled water, slides were counterstained with haematoxylin, washed in tap water, dehydrated, cleared and finally mounted in DPX mountant. As positive controls, different tissues were the protein of interest is expressed, were used. Moreover, secondary antibody only stain as negative control was performed on some tissue samples to check for unspecific binding.

3.2.10 TUNEL staining

For TUNEL staining (In Situ Cell Death Detection Kit, Fluorescein, Sigma) , sections were heated in citrate buffer (pH 6.0) in a 900W oven, on medium setting for 2 min. slides were blocked in 1% BSA/PBS for 30 min before TUNEL reaction was carried out for 1 hour according to manufacturer's instructions and counterstained with Hoechst (Sigma).

3.2.11 Organoid Culture

Mouse small intestines were isolated from wild-type, *VillinCre*^{ER}*Apc*$^{fl/fl}$ or *VillinCre*^{ER}*Apc*$^{fl/fl}$*Kras*$^{G12D/+}$ mice sacrificed three days post-induction with tamoxifen, opened longitudinally and washed with PBS. Crypts were isolated as previously described (T. Sato et al., 2011). Isolated crypts were mixed with 20 µl of Matrigel (BD Bioscience), plated in 24-well plates in Advanced DMEM/F12 (Thermo Fisher) supplemented with 1% penicillin-streptomycin, 10 mM HEPES, 2 mM glutamine, N2 (Thermo Fisher) , B27 (Thermo Fisher), 100 ng/ml Noggin and 50 ng/ml EGF (both from Peprotech). Growth factors were added every two days.

3.3 Next-Generation Sequencing

3.3.1 shRNA screen

3.3.1.1 Viral transduction and cell sampling

Lentivirus was generated with Decipher lentiviral library module-I library as described in 3.2.3 and transduced into HCT116 cells using conditions that predominantly resulted in a single stable shRNA integration per cell (MOI of <0.3). To this end, a total of 10^8 cells were infected and selected for three days using 1 μg/ml puromycin in four biological replicates (n=3). At each passage three million cells were maintained to preserve library representation throughout the experiment. Cells were either cultured as monolayer or as spheroids in the spinner flasks representing seven to ten population doublings.

3.3.1.2 shRNA recovery and sequencing library preparation

Cells were harvested, genomic DNA was isolated and purified by phenol-chloroform extraction and ethanol precipitation (see section 3.1.8.3). The shRNA sequences were recovered from the genomic DNA of each sample in two subsequent amplification steps. First, multiple parallel PCRs were done using a standard PCR reaction mixture (see section 3.1.10.1) with 100 μg genomic DNA and a custom primer pair (listed in *Table 2.6*). PCR products from the first amplification step were gel purified (see section 3.1.6) and used as template for the subsequent PCR. The final library was amplified using custom primers (*Table 2.6*) that added barcodes for multiplexing and adaptors suitable for next generation sequencing. This second PCR was done according to protocol as in section 3.1.10.1 with 12 denaturation/ annealing/ extension cycles. Libraries were size-selected by excision from an agarose gel followed by gel extraction with the GeneJET Gel Extraction Kit (3.1.6). The Experion system (3.1.7.2) was used for sizing and quantification. The libraries were sequenced on a NextSeq 500 (Illumina) platform with a custom sequencing primer (listed in *Table 2.6*) generating more than 450,000 reads per sample. Bioinformatics analysis of the data is described in section 3.3.1.3.

3.3.1.3 shRNA screen data analysis

Reads of recovered guide-stem sequences were aligned to a reference file containing oligo sequences of all 27500 shRNAs included in the library using Bowtie v0.12.8 (Langmead, 2010). The total number of library-specific reads was used for normalization of reads per shRNA between different samples. Only shRNAs represented by >0.01 % of all normalized reads in the initial untreated population were included in the primary analysis. Fold changes (FC) of shRNA abundance between time point zero (T_0) and at the end of the screen after 14 days (T_{end}) were generated by calculation a ratio of the means of the normalized reads of all three replicates. Z-scores were calculated for each log2FC based on this ratio. shRNAs with z-scores <(-2) (implicating a depletion of more than 2 standard deviations below the mean of T_0) were defined as "scoring" shRNAs. A gene was defined as a "hit" in the screen if more than 2 oligonucleotides displayed z-scores <(-2).

3.3.2 RNA Sequencing

3.3.2.1 Library preparation

The experiment was performed in triplicate per each condition. RNA for RNA-seq was extracted using the RNeasy Mini kit. The RNA was eluted using 40 µl RNAase-free H2O. The samples were kept in ice and the RNA concentration was measured using a standard sense chip for Bioanalyzer (see 3.1.7.2). One µg/µl RNA per each condition was used for library preparation. The library was prepared using the NEBNext Ultra RNA library prep kit for Illumina and the NEBNext Multiplex Oligos for Illumina (Dual Index Primers Set 1), according to the manufacturer´s instructions. H2O was used as negative control to check the purity of the preparation. The amplification by PCR was performed for 12 cycles and the PCR products were purified using the Agencourt AMPure XP beads. The quality of the purified DNA was verified on the Bioanalyzer (see 3.1.7.2) before performing the sequencing, using the Illumina GAIIx sequencer. All samples were mixed at equimolar concentration of 50 nM.

3.3.2.2 RNA-Sequencing data analysis

RNA-seq data analysis was performed by Susanne Walz. The main steps are described. Base calling was performed with Illumina's CASAVA software and overall sequencing quality was tested using the FastQC script. Reads were aligned to

the human genome (hg19) with TopHat2 (D. Kim et al., 2013) Bowtie v0.12.8 (Langmead, 2010) using default parameters. Mapped reads per gene (EnsEMBL GRCh37, release 74) were counted using the "summarizeOverlaps" function in the GenomicAlignments R package, non-expressed genes were removed (mean read count per gene over all samples >1) and TMM normalized with EdgeR. Gene set enrichment analyses (Subramanian et al., 2005) were performed with the C2 and Hallmark collection from the MSigDB v5.2 (Liberzon et al., 2011) with default parameters and 1000 permutations. Principle component analysis (PCA) was performed with the prcomp function from R after centering sequencing depth-normalized expression values of all expressed genes (n=20,434).

3.4 Biochemical methods

3.4.1 Preparation of whole cell protein extracts

Cells were washed with ice cold PBS, harvest by scraping with ice cold PBS (1 ml/10 cm tissue culture dish) (100 µl for 12 spheroids) and collected into a 1.5 ml tube. Cells were centrifuged at 1,500 rpm, for 5 min, at 4°C. Samples were kept on ice for the whole procedure. The cell pellet was resuspended in RIPA lysis buffer, containing proteinase and phosphatase inhibitors, using a 10:1 ratio (e.g. 1 ml RIPA buffer for 100 µl pellet). Samples were incubated on ice for 30 min. Afterwards, samples were centrifuged at 14,000 rpm, for 15min, at 4°C and cleared lysates were transferred to a new pre-chilled 1.5 ml tube. Lysates were stored at -80°C. Alternatively, samples were directly prepared for SDS-PAGE (see 3.3.6).

3.4.2 Nuclear fractionation of cells

The following protocol is based on that originally described by Wang and colleagues for the nuclear fractionation of mature SREBP proteins (Wang et al., 1994) and has been adapted to ensure optimal enrichment of nuclear proteins from HCT116 cells (Porstmann et al., 2008). HCT116 cells from two 15 cm dishes were washed once in ice cold PBS, scraped into 1 mL ice cold PBS containing Protease Inhibitor Cocktail and PhosStop Phosphatase Inhibitor Cocktail (Roche) and transferred to 15 mL falcon tubes (on ice). Cells were centrifuged for 5 minutes at 650 x g at 4°C and transferred to fresh 1.5 mL microcentrifuge tubes in 1 mL ice cold PBS containing the inhibitor

cocktails described above. Cells were centrifuged again at 855 x g for 5 minutes at 4°C and all PBS was removed. The cell pellets were resuspended in 3 volumes of Buffer C (10 mM HEPES/KOH pH 7.6, 10 mM KCL, 1.5 mM MgCl2, 1 mM EDTA, 1 mM EGTA, 0.5 mM DTT, Protease Inhibitor Cocktail and PhosStop Inhibitor Cocktail) and swelled on ice for 10 minutes. The cells were disrupted by trituration 15 times with a 23G needle and the lysate was centrifuged at 855 x g for 10 minutes. The supernatant (containing the membrane and cytoplasmic fractions) was transferred to a fresh 1.5 mL microcentrifuge tube and centrifuged for another 5 minutes at 855 x g at 4°C to remove any nuclei. The cleared supernatant fraction was then snap frozen on dry ice and stored at -80°C.

To continue nuclear lysis, the pelleted nuclei were washed twice in 200 µL Buffer C and centrifuged at 855 x g at 4°C for 5 minutes between washes. Nuclei were centrifuged again for 3 minutes at 855 x g and any remaining Buffer C was removed using a gel-loading tip. The pelleted nuclei were then re-suspended in one volume of Buffer D (20 mM HEPES/KOH pH 7.6, 0.5 M NaCl, 1.5 mM MgCl2, 1 mM EDTA, 1 mM EGTA, 25 % (v/v) glycerol, Protease Inhibitor Cocktail and PhosStop) and incubated on ice for 30 minutes with occasional votexing. The nuclear lysates were cleared by centrifugation at 16,000 x g for 10 minutes at 4°C, transferred to a fresh, cold 1.5 mL microcentrifuge tube, snap frozen on dry ice and stored at -80°C.

3.4.3 Bicinchoninic acid assay (BCA) assay

As second way to determine the protein concentration of protein lysates, the bicinchoninic acid (BCA) assay was applied. A BCA solution mix was prepared consisting of 49 parts of BCA buffer A and 1 part BCA buffer B. 4 µl sample or lysis buffer (as a blank) were mixed with 200 µl of BCA solution mix, incubated for 20 min at 37 °C and absorbance was measured at 550 nm and protein concentrations were determined using a BSA standard curve.

3.4.4 SDS Polyacrylamide gel electrophoresis (SDS-PAGE)

The appropriate amount of sample buffer 6x was added to the protein lysates, samples were boiled at 95°C for 5 min and spun down. An equal amount of proteins was loaded into the gel pockets using a 50 µl glass syringe (Hamilton). The PageRuler Pre-Stained Protein Ladder (Thermo Scientific) was used as a molecular weight

marker. SDS polyacrylamide gels were used for separating the proteins according to their molecular weight. The electrophoresis was performed using SDS-PAGE chambers (Biorad) filled with 1x SDS running buffer at 80-120 V.

3.4.5 Immunoblot

After separating protein lysates by SDS-PAGE, proteins were transferred onto a PVDF membrane. The PVDF membrane was activated by incubation in methanol for 30 sec, followed by 2 min in H2O. The membrane was equilibrated in the transfer buffer 1x before proceeding to the immunoblot assembly. The immunoblot sandwich was assembled in transfer buffer as follows: starting from the black side of the cassette (i.e. towards the negative charged site of the immunoblot chamber), 1 sponge layer, 2 Whatman filter paper layers, the gel, the membrane, 2 Whatman filter paper layers, 1 sponge layer, ending with the red site of the cassette (i.e. towards the positive charged site of the immunoblot chamber). During the preparation, the immunoblot sandwich was inspected for the absence of air bubbles. The cassette was placed into the tank, which was filled with transfer buffer 1x. The transfer was carried out at 4°C, at 300 mA for 2 hrs. Afterwards, the membrane was briefly washed in TBS-T and incubated in blocking solution (LI-COR) for 1 hr at RT under constant shaking. BSA blocking solution was used only for subsequent detection of phosphorylated proteins. After blocking, the membrane was incubated with the primary antibody at 4°C over night. On the next day, the membrane was washed 3 times for 10 min with 1x TBS-T and incubated for 1 hr with the secondary antibody (diluted 1:5000 in blocking solution) followed by additional 5 washing steps of 5 min each with TBS-T. Fluorescent signals were detected with a LI-COR Odyssey Infrared scanner and quantified using Image Studio Lite Version 5.2.5 (LI-COR).

3.5 Metabolic Assays

3.5.1 Stable Isotope Labelling

For monolayer culture, HCT116 cells ($1x10^6$) were seeded in 6-well plates (for polar metabolites) or ($2.5x10^6$) in 10 cm plates (for cholesterol and ubiquinone) and cultured in normal growth medium for 16 hr. For spheroid culture, 12-16 spheroids per replicate sample were initiated and grown for 12 days, during which medium was

replaced every three days. For glucose labelling, cells or spheroids were washed with PBS and medium was replaced with either complete medium or glucose-free medium with 25 mM [$U^{13}C$] glucose (Cambridge Isotope Laboratories). Cells were incubated for the indicated times.

3.5.2 Extraction and Liquid Chromatography-Mass Spectrometry of polar metabolites

Cells were washed with cold 154 mM ammonium acetate, snap frozen in liquid nitrogen and scraped off after addition of 0.5 ml ice-cold extraction buffer consisting of 0.1 µM lamivudine (Sigma) in MeOH/H_2O (80/20, v/v). The resulting suspension was transferred to a reaction vial, mixed vigorously and centrifuged (2 min 16,000*g*). Supernatants were transferred to a Strata® C18-E column (Phenomenex) which has been conditioned with 1 ml of CH_3CN and 1 ml of MeOH/H_2O (80/20, v/v). The eluate was taken to dryness in a SpeedVac and dissolved in 50 µl of a mixture of CH_3CN and 5 mM NH_4OAc (25/75, v/v). Samples were diluted 1:2 with CH_3CN and 5 µl of each sample was applied to a HILIC column (Acclaim Mixed-Mode HILIC-1, 3µm, 2.1*150 mm). Metabolites were separated at 30°C by LC using a DIONEX Ultimate 3000 UPLC system and the following solvents: Solvent A consisting of 5 mM NH_4OAc in CH_3CN/H_2O (5/95, v/v) and solvent B consisting of 5 mM NH_4OAc in CH_3CN/H_2O (95/5, v/v). A linear gradient starting at 100% solvent B decreasing to 50% solvent B over 6 min was applied followed by 15 min constant elution with 40% solvent B.

3.5.3 Extraction and Liquid Chromatography-Mass Spectrometry of Cholesterol and Ubiquinone

Cells were washed with cold 154 mM ammonium acetate, snap frozen in liquid nitrogen and scraped off after addition of 0.4 ml ice-cold MeOH/H_2O (80/20, v/v) containing 1 µM CoQ9 (Sigma). The resulting suspension was transferred to a reaction vial, mixed vigorously and centrifuged (2 min 16,000*g*). Supernatants were extracted twice with 0.4 ml of hexane each. The combined extracts were collected and taken to dryness under a stream of nitrogen gas at 35°C. The residues were redissolved in 150 µl of hexane and transferred to Strata® SI-1 columns (Phenomenex). Undesired compounds were washed out with 750 µl hexane and 500 ml hexane/acetic acid ethyl ether (18/1, v/v). Ubiquinones and some cholesterol were

eluted with 0.5 ml hexane/acetic acid ethylester (9/1, v/v). Complete elution of Cholesterol was accomplished applying another 0.5 ml hexane/acetic acid ethylester (9/1, v/v). Eluates were taken to dryness under a stream of nitrogen gas at 35°C. The resulting residues were dissolved in 50 µl iPrOH. For LC/MS analysis of ubiquinones, 5 µl of each sample was applied to a C8 column (Acclaim RSLC C8 column, 2.2 µm particles, 50 × 2.1 mm, Thermo Scientific, Bremen, Germany) (at 40°C). Ubiquinones were eluted isocratically with 5 mM NH_4OAc in CH_3CN/H_2O (95/5, v/v) for 30 minutes at a flow rate of 350 µl/min. The eluent was directed to the ESI source of the QE-MS from 15 min to 29 min after sample injection. For cholesterol measurements, both cholesterol-containing fractions were combined and also separated on the C8 column with mobile phase buffer A consisting of 0.1% formic acid in CH_3CN/H_2O (10/90, v/v), and solvent B consisting of 0.1% formic acid in CH_3CN/H_2O (90/10, v/v). After application of 5 µl sample (at 40°C), the LC gradient program was 20% solvent B for 2 min, followed by a linear increase to 100% solvent B within 5 min, then maintaining 100% solvent B for 12 min. The flow rate was maintained at 350 µl/min. The eluent was directed to the ESI source of the QE-MS from 7.0 min to 13.0 min after sample injection. Exactive mass spectrometer) applying the following scan and HESI source parameters: Scan Ranges: For polar metabolites: 810 - 950 m/z (alternating positive and negative mode), for ubiquinones: 810 - 950 m/z (positive mode) and for cholesterol: 365 - 400 m/z (positive mode). Resolution: 70,000, AGC-Target: 1E6, Maximum Injection Time: 200 ms. Sheath gas: 30, auxiliary gas: 10, sweep gas: 3, Aux Gas Heater temperature: 120 °C. Spray voltage: 2.5 kV, Capillary temperature: 320 °C, S-lens RF level: 55.0. Signal determination and quantitation was performed using TraceFinder™ Software Version 4.1 (Thermo Fisher)

3.5.4 Measurements of extracellular flux

To determine cellular bioenergetics of the two main metabolic processes: mitochondrial respiration (OCR) and extracellular acidification (ECAR) simultaneously in HCT116 monolayer cultures, a XF96e Extracellular Flux Analyser (Seahorse Biosciences, North Billerica, MA, USA) for 96-well plates was used. A flux analyser kit consisted of a dual-analyte sensor XFe96 cartridge plate and a XFe96-well microplate. Briefly, cells were plated in a volume of 80µl per well of a XFe96-well microplate in their normal medium conditions 24 hrs prior to the experiment. The XFe96 flux cartridge plate includes a hydrogen and oxygen sensor

that needed calibration for at least 6 hrs in the XFe96 flux analyser. On the day of the experiment, the injection ports of the XFe96 flux assay cartridge plate were loaded with different metabolite solutions (pH7.4). The cartridge plate was then loaded into the flux analyser. The cells were then rinsed once with assay medium pH 7.4 before cultured in 200 µl assay medium. The cells were incubated for 25 min before plate was loaded onto the analyser. The standard protocol included three readings of 3 min each per treatment. Between each reading there was a 3 min waiting time. The values were normalised to protein content of the cells. For spheroids, prior to analysis, they were washed twice in complete growth media and transferred directly into XFe96 Spheroid Microplates containing 160 µl of Seahorse XF Assay Medium supplemented with 25 mM D-glucose and 10 mM sodium pyruvate at pH 7.4. Plates were incubated in a CO_2 free incubator for 1 hr. Oxygen consumption rates (OCR) were determined using an XF96^e Extracellular Flux Analyzer (Software Version 1.4) (Agilent). During the experiment, 2 µM Oligomycin (Merck-Milipore), 0.5 µM FCCP (Sigma) and 1 µM Rotenone/Antimycin A (Sigma) were injected to determine ATP-coupled, maximal and mitochondrial dependent basal OCR. OCRs were normalized to spheroid area.

3.6 Statistical analysis

Data are usually presented as mean or median values and the error bars represent either the standard deviation (SD) or standard error of the mean (SEM) as described in the figure legend. The quantitative data are depicted using GraphPad Prism 7.0 (GraphPad software). All experiments have been preformed at least twice independently from each other with multiple replicates for each experiment or otherwise indicated. The p-values were obtained by using a two-tailed paired/unpaired student t-test. P-values smaller than 0.05 were considered to be statistically significant.

4 RESULTS

4.1 Identification of metabolic features of cancer cells in metabolically compromised environments

Cancer cells reprogram their metabolism in order to fulfil their demands for macromolecules, which are essential for proliferation. They also need to change their metabolisms to survive under the metabolically compromised conditions of the tumour microenvironment. Oncogenes and tumour suppressors play important roles in remodelling tumour metabolism. For instance, the PI3K/AKT pathway is essential for regulating growth and proliferation and it has a role in governing lipid and amino acid metabolism via mTOR (Manning et al., 2017). In addition, the tumour suppressor p53 has been recognised as an essential part of in cell transformation, tumour progression and in cancer metabolism (Humpton et al., 2016).

Colorectal cancer (CRC) is the most widespread malignant gastrointestinal cancer type. Although recent studies have shown that its incidence rates have gone down in recent years, 14% of the men and 9% of the women in the USA were reported to suffer from this disease in the last years (Siegel et al., 2016). The current treatments for CRC include surgery, chemotherapy and targeted therapies. However, there is still need for new potential therapeutic targets and prognostic markers.

As mentioned above, the tumour microenvironment pushes cancer cells to adapt their metabolisms in order to survive under unfavourable conditions. As tumours increase in size and outgrow the existing vascular network, cancer cells are subjected to gradients of nutrients, oxygen and pH. As a result of these microenvironmental adjustments, tumour cells located far from the nearest blood vessel have to adapt their metabolism in order to continue proliferating under reduced nutrient and oxygen provision. In addition, poorly vascularised tumour areas are also protected from the delivery of anti-cancer drugs, resulting in treatment resistance and

relapse. Therefore, targeting this population of cells is very important for cancer therapy

Cancer cells exposed to classical cell culture conditions are not restricted by the availability of basic nutrients. They have access to high concentrations of glucose and glutamine provided by the culture medium. However, in tumours, access of cells to these nutrients is frequently impaired due to the distance to the closest blood vessel.

4.1.1 Assessing the effects of oxygen and nutrient deprivation on cells in monolayer

HCT116 cells were obtained that are either wild type for p53 (p53+/+) or an isogenic derivative, in which p53 was removed by homologous recombination (p53-/-)(Bunz et al., 1998). For both cell types, p53 levels were assessed under basal levels and in the presence of etoposide, a commonly used chemotherapeutic agent. As a result, levels of the p53 target gene p21 were induced under the condition where DNA damage occurs (Fig 4.1A).

In order to observe whether lack of nutrients has an effect on the viability of colon cancer cells, HCT116 cells were cultured in different conditions in monolayer cultures. Culture medium with 2.5 g/L glucose was used without FBS to test the effect of serum and without glutamine to check the effect of glutamine and same for the glucose. HCT116 p53 isogenic cells were cultured at 80% confluency in these conditions for 24 hrs. Since hypoxia is another important factor of the tumour microenvironment, cells were incubated in the presence of 0.5% O_2 (hypoxia) and 20% O_2 (normoxia) for 24 hrs. To check the effect of nutrient starvation, serum deprivation and oxygen limitation, crystal violet (CV) staining was performed and quantified. Under normoxia, reduced cell viability was observed in the absence of serum, glucose and glutamine (Fig 4.1C) although p53 deficient cells were less affected by the absence of serum, suggesting that these cells can continue to proliferate in the absence of serum-derived factors. The effect of glutamine deficiency

was similar in both wild type and p53 deficient cells. This is in contrast to resistance of wild type HCT116 cells to glutamine deprivation reported by Tajan *et al*. (Tajan et al., 2018). Moreover, glucose deprivation affected p53 deficient cells more severely than p53 wild type cells. This is consistent with previous findings showing that activation of AMPK induced p53 dependent metabolic arrest but not cell death (R. G. Jones et al., 2005). Moreover, p53 deficient cells seem to be less resistant to hypoxic conditions and serum deprivation, as seen in Fig 4.1C. Taken together, these experiments show that p53 isogenic cells undergo different metabolic reprogramming and are affected severely under conditions where several nutrients and oxygen are lacking.

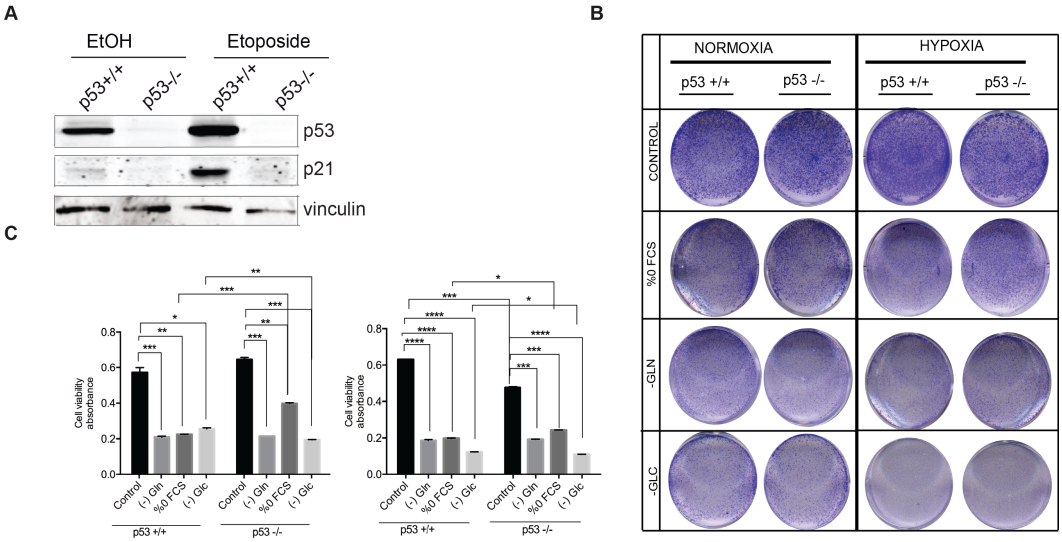

Figure 4.1: Serum, glutamine and glucose starvation reduces cell viability both in normoxic and hypoxic conditions

A) HCT116 p53+/+ and p53-/- cells were cultured as monolayers and treated with 20 µM etoposide for 24 hrs. Cells were lysed and protein extracts were analysed for expression of p53 and p21.
B) CV staining of HCT116 cells cultured either in complete medium or in nutrient and serum deprived conditions both in normoxia and hypoxia for 24 hrs.
C) Quantification of the CV staining shown in B. Left graph represents the cells cultured in normoxia and right graph represents cells in hypoxia (0.5% O2). Values represent mean ± SEM (n=3 independent biological replicates). p values were calculated using two tailed student t-test. (**** $p<0.0001$; *** $p<0.001$; ** $p<0.01$; * $p<0.05$)

4.1.2 Characterization of HCT116 tumour spheroids

In order to mimic a tumour-like environment *in vitro*, multicellular tumour spheroids (SPH) were generated by using ultra-low attachment 96-well plates. Spheroids were grown for 14 days in complete medium. To compare the proliferation between cells cultured in monolayer and as spheroids, BrdU labelling was performed for 24 hrs. This analysis showed that spheroid culture decreases cell proliferation by more than 60% compared to monolayer cultures and the reduction was similar in both genotypes (Fig 4.2A). In order to further characterise the properties of cells cultured in this condition, spheroids were grown for 15 days, fixed, paraffin embedded and cut into serial sections, which were then stained for markers of cell proliferation (Ki67) and apoptosis (TUNEL). Spheroids formed by p53+/+ cells displayed a ring of proliferating cells on the outside of the spheroid. In contrast, spheroids show Ki67 positive cells throughout the diameter of the spheroid (Fig. 4.2B). Moreover, TUNEL staining for apoptotic cells revealed that cell death is observed in the core of the p53+/+ spheroids, whereas p53-/- cells show no evidence of apoptotic cells (Fig. 4.2B). These results indicated that p53+/+ cells are more vulnerable to the deficiency of nutrients and oxygen available within the spheroid core. In contrast, cells lacking p53 are protected from apoptosis under metabolically compromised environments.

In order to determine the effect of hypoxia, H1F1a protein amounts were analysed for spheroid and monolayer cultures under normal (20% O_2) or severely hypoxic (0.5% O_2) conditions. HIF1a protein was observed only in monolayer cells exposed to severe hypoxia, demonstrating that the oxygen levels in spheroid cultures are higher than 0.5% suggesting only a mildly hypoxic environment (Fig. 4.3A). Moreover, there was no difference in the induction of HIF1a between p53 wild type and deficient cells. Although it has been shown that p53 suppresses HIF1a (Yeung et al., 2008), the mechanism of this regulation is not well-defined.

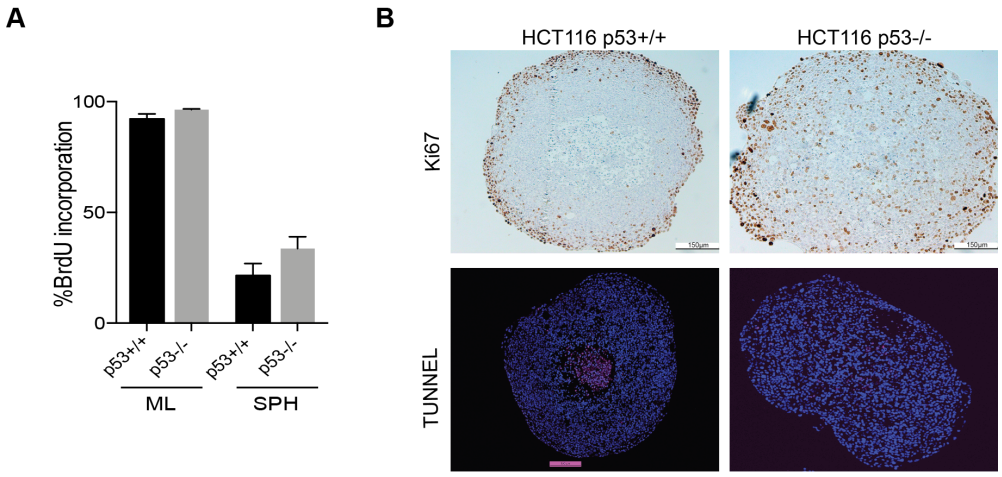

Figure 4.2: HCT116 spheroids display reduced proliferation compared with monolayer cultures

A) HCT116 p53+/+ and p53-/- cells were cultured as monolayers for 48 hrs or as multi-layered tumour spheroids on ultra-low attachment plates for 14 days. Cells were incubated with BrdU for 24 hrs and BrdU incorporation was determined by FACS.
B) HCT116 p53+/+ and p53-/- cells were cultured as spheroids for 14 days, fixed and embedded in paraffin. Histological sections were analysed for expression of the proliferation marker Ki67 and for cell death by TUNEL. Representative images are shown.

In addition, spheroids from both genotypes were treated with pimonidazole to detect regions of hypoxia. Pimonidazole forms adducts with thiol groups in proteins, peptides and amino acids, which are increased when oxygen is absent. As expected, pimonidazole staining was observed in the spheroid sections. Interestingly, p53+/+ sections displayed a ring of hypoxia between the core and the outside of the spheroids. In contrast, p53-/- spheroid sections revealed an intense hypoxia staining mostly in the inner parts of the spheroid (Fig 4.3B). Taken together, mild hypoxia seems to be induced in the spheroid conditions and this is more pronounced in the core of p53 deficient spheroids. It is possible that the fact that p53 deficient cells continue to proliferate induces a larger region of hypoxia in the centre of the spheroid.

After having evaluated the levels of hypoxia in the spheroids, metabolic assays were performed to determine whether spheroids are dependent on respiration

or glycolysis. To assess the effect of spheroid culture on oxygen consumption and lactate export, the extracellular acidification rate (ECAR) and the oxygen consumption rate (OCR) were measured in p53+/+ and p53-/- spheroids formed after 15 days of spheroid growth. Interestingly, p53-/- spheroids showed increased oxygen consumption rates compared to p53+/+ cells (Fig 4.3C). This might be related to the homogenous proliferation pattern in p53 deficient cells under metabolically compromised conditions. In contrast, p53-/- spheroids displayed slightly higher ECAR levels compared to p53+/+ cells, which could be related to HIF1a activation under metabolic stress, but this difference was not significant.

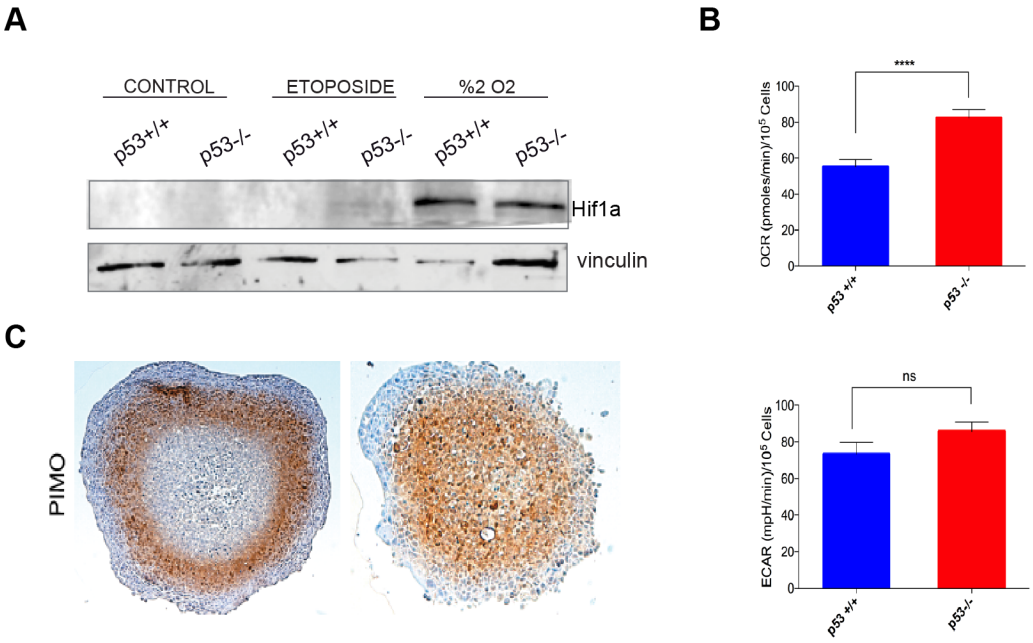

Figure 4.3: HCT116 multicellular spheroids show p53 specific differences in hypoxia and metabolic activity

A) Cells cultured in normoxia (20% O_2) and hypoxia (0.5% O_2) for 24 hrs or grown as spheroids for 15 days. HIF1a levels were detected in whole cell extracts by Western blot.

B) HCT116 p53+/+ and p53-/- cells were cultured as spheroids for 14 days, fixed and embedded in paraffin. Histological sections were analysed for hypoxia by pimanidazole detection. Representative images are shown.

C) Oxygen consumption rate (OCR) and extracellular acidification rate (ECAR) measured using the Seahorse Bioanalyzer in p53+/+ and p53-/- spheroids grown for 15 days. Mean basal respiration and glycolysis levels were calculated from 48 replicate spheroids. Error bars represent SEM. (**** $p<0.0001$).

4.1.3 Identification of gene expression differences between HCT116 p53+/+ and p53-/- cells cultured as monolayer, spheroids or subcutaneous xenograft tumours

Having confirmed that there are differences between p53 wild type and deficient HCT116 cells cultured as monolayer and tumour spheroids; RNA-SEQ was performed to obtain a global transcription profile of cells cultured in the different conditions. For this purpose, RNA was isolated from HCT116 isogenic cells cultured as monolayers, as spheroids for 15 days or grown as subcutaneous tumours in immunocompromised mice. Archival tumour material was obtained from a previous study (Ros, Floter, et al., 2017). Sequencing was performed for biologically independent triplicate samples and data were analysed by Susanne Walz (Bioinformatics Core Unit of the Comprehensive Cancer Centre Mainfranken). Firstly, principal component analysis (PCA) was performed in order to compare how the different conditions relate to each other. PCA is a statistical tool that is used to visualise the likelihood of similarity in different populations. Different components (PC1, PC2 etc.) determine the level of variance. Thus, PCA performed with the normalised read counts of all samples showed that the replicates from each condition accurately grouped together. Interestingly, tumour samples clustered close to the spheroid samples, particularly in PC1, which accounts for 80% of the variance (Fig 4.4A). These results show that global gene expression in cells grown as spheroids has similar characteristics to those observed in tumours.

In addition, gene set enrichment analysis (GSEA) was performed in order to obtain insight into different gene expression signatures induced by the different culture conditions. GSEA is a statistical approach designed to rank pre-designed gene lists according to the strength of association with a specific condition (Subramanian et al., 2005). The molecular signature database C2, which contains 4729 curated gene sets, and the HALLMARK database, which contains 50 gene sets associated with crucial biological processes (Liberzon et al., 2015), were used for this analysis. Normalised enrichment scores (NES) and false discovery rates (FDR) q-values were used to define the significance of a given gene set. NES shows the ranking of a certain gene set in a whole ranking list. The higher the absolute NES, the more genes in a given gene set are differentially expressed between two conditions.

FDR q-values smaller than 0.25 were considered to indicate a significant enrichment (Hochberg et al., 1990).

As a result of the GSEA, both p53+/+ and p53-/- cells showed very strongly enriched proliferation of associated gene signatures in monolayers compared to spheroid cultures or tumours (Fig 4.4B and C). In addition, hypoxia related signatures were strongly increased in spheroids, irrespective of p53 status (Fig 4.4B). Strong enrichment of the hypoxia signature was also observed in tumours as well as in spheroids compared to monolayer cultures (Fig 4.4C).

Overall, these results demonstrate that the spheroid condition recapitulates some of the features that are also found in tumours and thus represents a suitable *in vitro* model to study cancer cells in a tumour-like environment.

In order to gain more insight into the p53 effects, gene expression data from the isogenic cell lines in the different culture conditions were compared by GSEA. Interferon signalling signatures were enriched in p53+/+ cells compared to p53-/- cells in all conditions (Fig. 4.5A). In contrast, p53 targets associated signatures were only enriched in p53+/+ cells cultured as monolayer (Fig 4.5A). Surprisingly, "HORTON_SREBF_TARGETS" and "REACTOME_CHOLESTEROL_BIOSYNTHESIS" gene signatures were enriched in p53-/- spheroids and tumours compared to their p53+/+ counterparts (Fig 4.5B). This finding suggests that loss of p53 function increased the expression of genes involved in cholesterol biosynthesis, in particular under the conditions of a tumour-like environment.

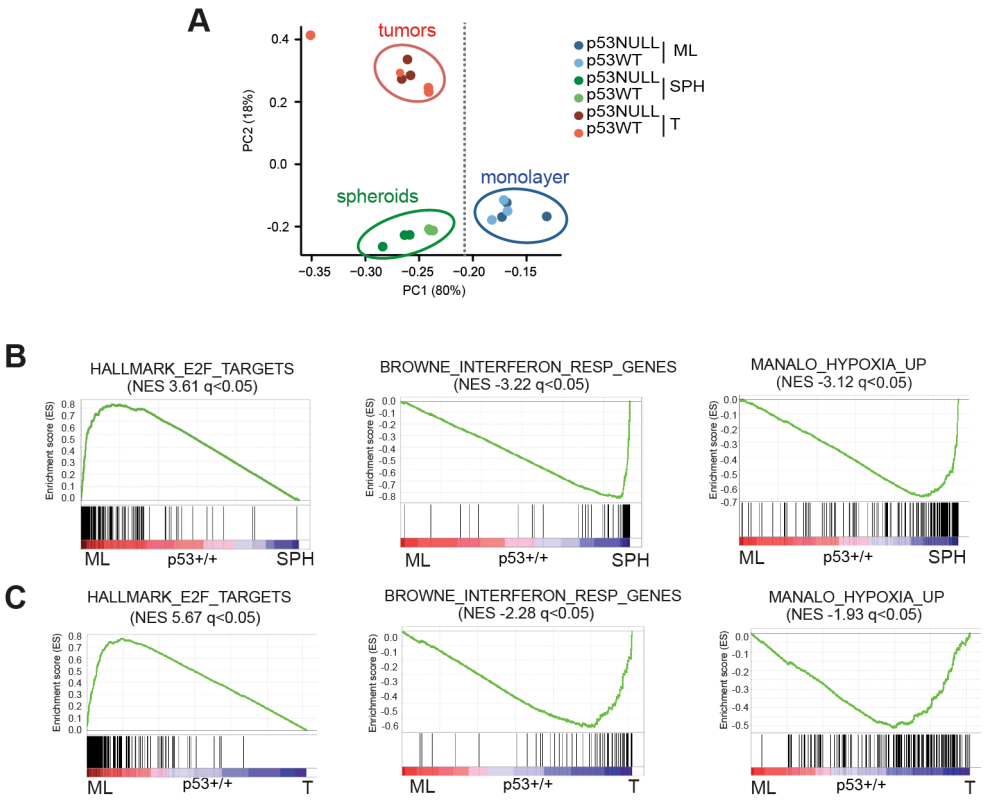

D

Condition	ML vs. SPH		ML vs. T	
Genotype	p53+/+	p53-/-	p53+/+	p53-/-
HALLMARK_E2F_TARGETS	3.61	3.05	5.67	5.67
BROWNE_INTERFERON_RESPONSE_GENES	-3.22	-3.47	-2.28	-2.28
MANALO_HYPOXIA_UP	-3.12	-3.32	-1.93	-1.93

Figure 4.4: Spheroids recapitulate tumour features *in vitro*

A) RNA from HCT116 p53+/+ and p53-/- cells grown either as monolayers (ML), as spheroids (SPH) or as subcutaneous tumours in immunocompromised mice (T) was analysed by RNA-SEQ. PCA was performed on normalised read counts and principal component 1 (PC1) and PC2 are displayed. Each replicate sample is represented by a single dot.

B) Gene set enrichment analysis (GSEA) comparing monolayer (ML) and spheroid (SPH) cultures of HCT116 p53+/+ cells was performed. Enrichment plots for HALLMARK_E2F_TARGETS (Liberzon et al., 2011), BROWNE_INTERFERON_RESPONSE_GENES (Browne et al., 2001) and MANALO_HYPOXIA_UP (Manalo et al., 2005) are shown.

C) Enrichment plots for the same gene sets comparing monolayer cultures (ML) and tumours (T) of HCT116 p53+/+ cells.

D) Table showing the gene sets mentioned above regulated both in p53+/+ and p53-/- ML, SPH and T conditions

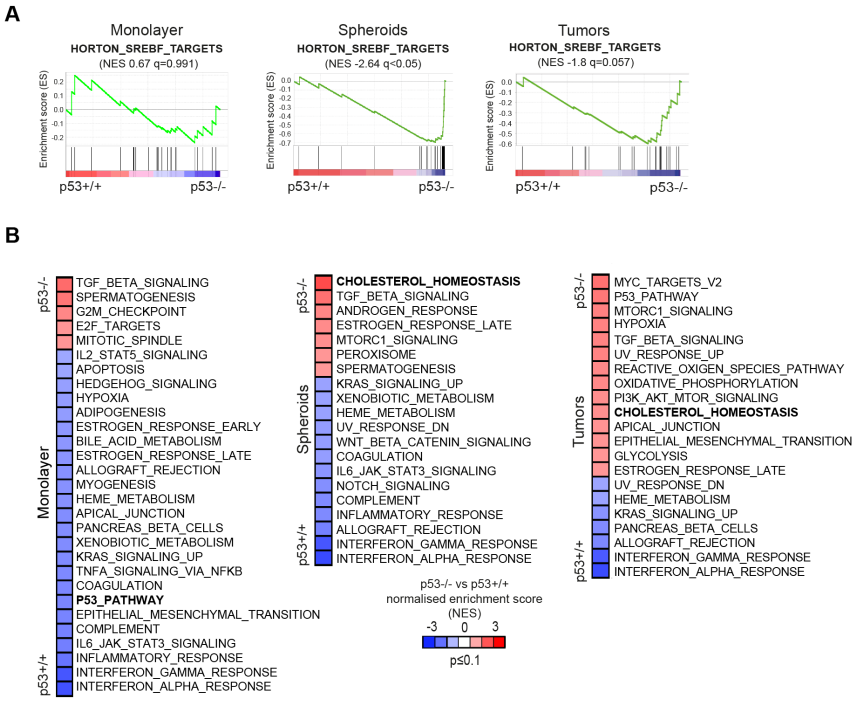

Figure 4.5: Loss of p53 induces enzymes of the mevalonate pathway only in spheroids and tumours

A) Heat maps showing the normalised enrichment scores (NES) of a gene set enrichment analysis (GSEA) comparing RNA-SEQ data from HCT116 p53+/+ and p53-/- cells cultured as monolayer or spheroids cultures or grown as xenograft tumours (Ros, Floter, et al., 2017). Gene sets were from the MSigDB Hallmark collection (Liberzon et al., 2015).
B) Enrichment plots for HORTON_SREBF_TARGETS (Horton et al., 2003) for HCT116 p53+/+ and p53-/- cells cultured as monolayer or spheroid culture or as xenograft tumours.

Following RNA-SEQ analyses, QPCR results, which were performed to validate global expression analysis, revealed similar results. Both in wild type p53 and p53 deficient spheroids and tumours individual hypoxia target genes the vascular endothelial growth factor A (*VEGFA*), lactate dehydrogenase A (*LDHA*) and pyruvate dehydrogenase 1 (*PDHK*) were upregulated (Fig 4.6A and B), confirming the RNA-SEQ results. Interestingly, expression of the canonical HIF target *LDHA* was different between p53 WT and p53 deficient spheroids (Fig 4.6A), leading to the question

whether *LDHA* expression is regulated independent of hypoxia. Indeed, *LDHA* was identified as a miR-34 target in breast cancer (X. Xiao et al., 2016). miR-34 was described as a bona fide p53 target and p53 induces its expression in many cancer types to prevent tumour progression (Okada et al., 2014). Therefore, the decrease in the expression of *LDHA* in the wild type spheroids could be explained via p53-induced, miR-34 dependent inhibition.

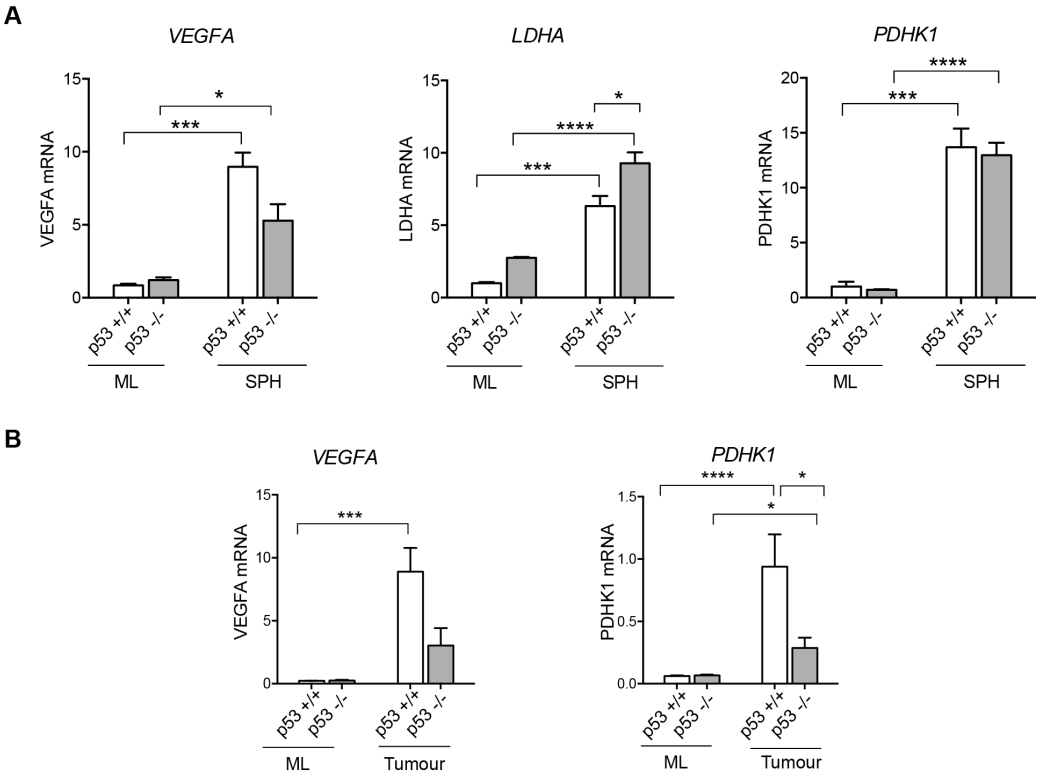

Figure 4.6: Hypoxia target genes are upregulated in tumour spheroids and tumours.

A) Expression of *VEGFA, LDHA and PDHK1* genes was determined in RNA from monolayer cultures (ML) or from cells grown as spheroids (SPH) and normalized to β-actin. Values represent mean ± SEM (n=3, each biological replicate in technical duplicates). p-values were calculated using unpaired two tailed student t-test. ($p<0.0001$, **** ; $p<0.001$, ***; $p<0.01$, **; $p<0.05$, *).

B) Expression of *VEGFA, LDHA and PDHK1* in RNA from monolayer cultures (ML) or tumours was determined and normalized to β-actin. Values represent mean ± SEM (n=3, each biological replicate in technical duplicates). p-values were calculated using unpaired two tailed student t-test. ($p<0.0001$, **** ; $p<0.001$, ***; $p<0.01$, **; $p<0.05$, *).

Comparison of gene expression differences according to the p53 status in spheroids and tumours revealed the upregulation of cholesterol biosynthesis in p53 deficient condition. Expression of genes involved in cholesterol biosynthesis is regulated by the transcription factor SREBP2. Therefore, expression of SREBP2 and its targets was investigated in order to validate the results observed in the RNA-SEQ experiment.

The mevalonate pathway is an important process that uses acetyl-CoA, NADPH and ATP for the generation of isoprenoids and sterols and expression of the enzymes of this pathway is driven by SREBP2. First, three molecules of acetyl-CoA get condensed to form HMG-CoA by the enzyme HMGCS1. HMG-CoA is then reduced to mevalonate by the rate-limiting enzyme HMGCR. In the following reactions, the enzymes MVD and FDFT1 generate IPP and FPP that are important for protein prenylation and the formation of other important metabolites. After several additional steps, cholesterol is formed by the DHCR7 enzyme (reviewed in (Mullen et al., 2016)) (Fig 4.7).

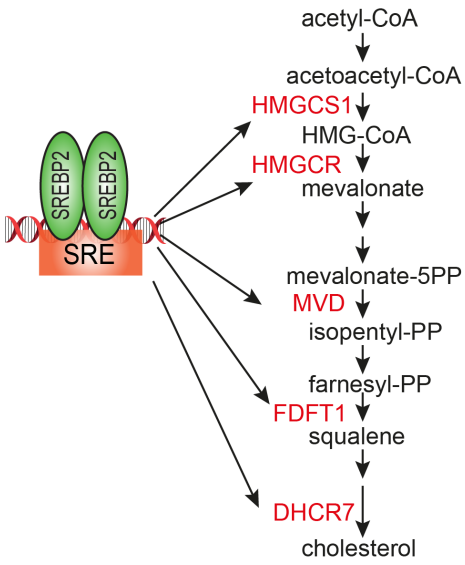

Figure 4.7: Schematic representation of the cholesterol biosynthesis pathway

To this end, expression of the genes in the mevalonate pathway was investigated. Expression of *HMGCR*, the rate-limiting enzyme, *HMGCS1*, *MVD* and *FDFT1* was overall increased in spheroid condition compared to monolayer (Fig.

4.8). Induction of SREBP2 targets in spheroid cultures might be due to the hypoxia as it was shown that cholesterol biosynthesis could function as a sensor for the oxygen levels in yeast (Hughes et al., 2005). Moreover, it is possible that deprivation of serum-derived sterols could contribute to increased expression of SREBP2 target genes in this condition.

Recently, p53 has been established as a transcription factor which inhibits SREBP in certain conditions (Moon et al., 2018) consistent with the data shown here. However, in contrast to the findings reported in the study by Moon *et al*., p53-dependent differences in the expression of SREBP2 target genes was not present in monolayer cultures (Fig 4.1A). This could suggest that under monolayer culture conditions p53 is not sufficiently active to block the activation of SREBP2 targets. However, in p53 deficient spheroids expression of SREBP2 targets was significantly upregulated (Fig. 4.8), suggesting an inhibitory effect of p53 under these conditions.

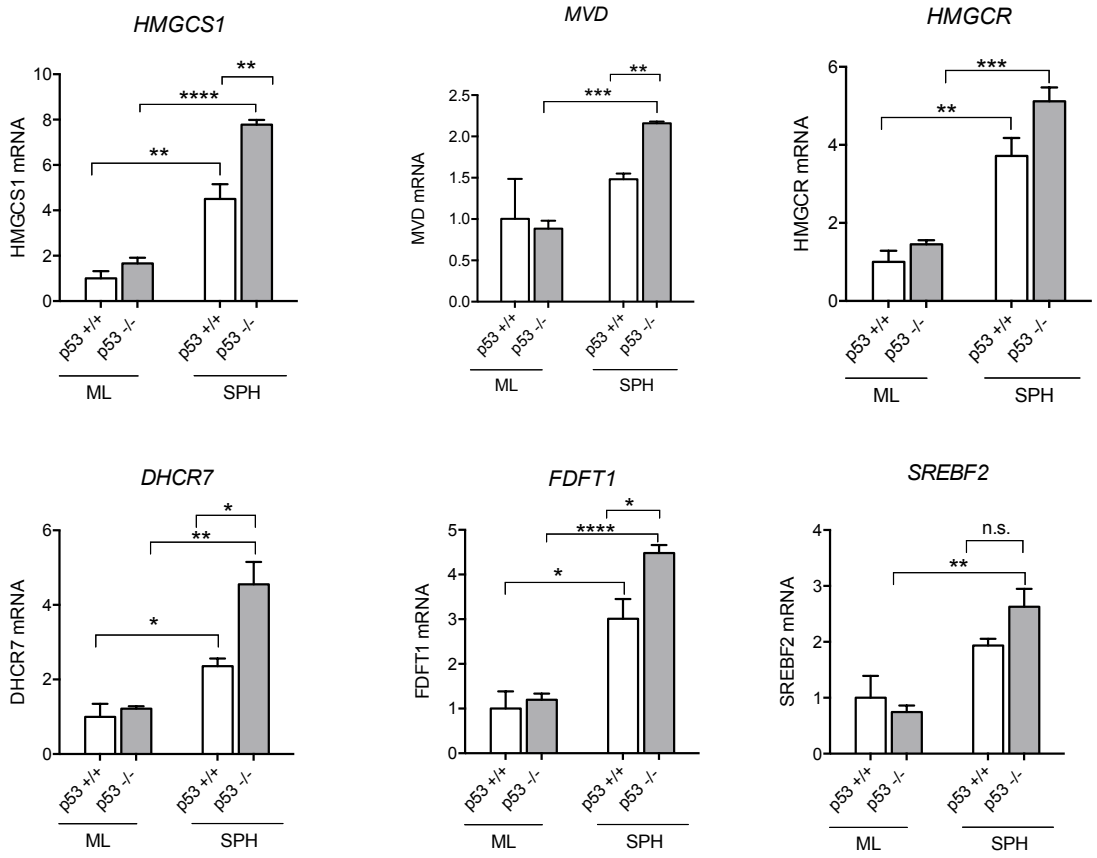

Figure 4.8: Increased expression of cholesterol biosynthesis genes in p53 deficient spheroids

HCT116 p53+/+ and HCT116 p53-/- cells were cultured as monolayer (ML) for 48 hrs or as tumour spheroids (SPH) for 15 days. Expression of several SREBP2 targets was determined and normalised to β-actin. Values represent mean ± SEM (n=3, each biological replicate in technical duplicates). p-values were calculated using unpaired two tailed student t-test. ($p<0.0001$, **** ; $p<0.001$, ***; $p<0.01$, **; $p<0.05$, *).

Taken together, by using spheroids as a model, it was revealed that p53 exerts an inhibitory effect on the expression of SREBP2 target genes. This could indicate a tumour specific metabolic vulnerability of p53 deficient cells that depends on the tumour microenvironment.

4.1.4 Identification of detailed metabolic features of HCT 116 p53+/+ and HCT 116 p53-/- cells cultured as monolayer and spheroids

Transcriptomic analyses revealed the specific features of tumour spheroids, such as hypoxia and reduced proliferation (Fig 4.4A). In addition, comparison of p53 isogenic cells in different culture conditions demonstrated that p53 deficient spheroids increased the expression of genes that are involved in cholesterol biosynthesis. Therefore, further analyses were performed to investigate the activity of metabolic pathways in the different culture conditions.

In order to gain insight into the metabolic alterations between the monolayer and spheroid cultures, stable isotope tracing experiments were performed using [U^{13}C] glucose. By using stable isotope tracing, which was performed in a dynamic manner as a time course, the contribution of glucose carbons to different metabolic pathways was identified. Both mass isotopomer distribution (MID) and levels of individual isotopologues were determined. MID analysis provides information about the metabolite contribution to the pathway and it is independent of the metabolite levels (Buescher et al., 2015). This analysis helps to understand the fractional contribution of the nutrient to specific pathways as cancer cells can be fed by different metabolites such as glucose, glutamine and acetate. In both conditions, steady state labelling for pyruvate and lactate was already reached after 2 hrs (Fig 4.9), indicating that the contribution of glucose to pyruvate and lactate is similar in monolayer and spheroid cultures.

Interestingly, fractional labelling to alanine, glutamate and other TCA cycle metabolites reached a steady state more rapidly in spheroids than monolayers suggesting additional carbon contribution in spheroids. However, labelling was overall not affected by p53 status as labelling patterns were similar between p53 wild type and p53 deficient cells (Fig 4.9A and B).

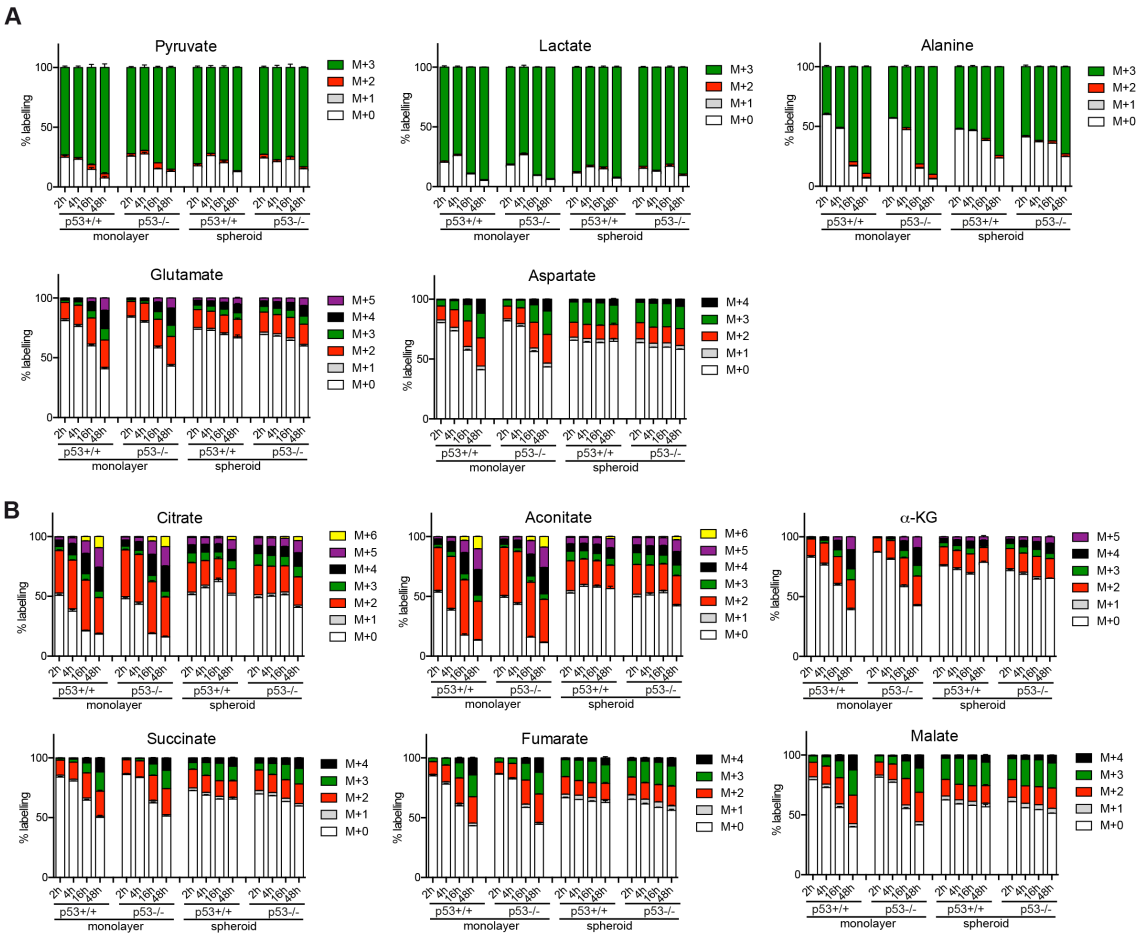

Figure 4.9: Reprogramming of glucose metabolism in spheroid cultures

HCT116 p53+/+ and p53-/- cells were cultured as monolayer (ML) for 24 hrs or as spheroids (SPH) for 14 days and used for stable isotope tracing analysis. After incubation with [U^{13}C] glucose for 48, 16, 4 or 2 hours, cells were extracted and metabolites were analysed by LC-MS. Values represent mean ± SEM (n=3 independent biological replicates).

A) % labelling for pyruvate, lactate, alanine, gluatamate, aspartate was shown

B) % labelling for TCA cycle metabolites was shown.

Moreover, the abundance of lactate was increased in both p53+/+ and p53-/- spheroids, suggesting the induction of glycolytic mechanism (Fig 4.10B). Indeed, this increase in lactate levels was also consistent with the induction of hypoxia gene signatures found by GSEA.

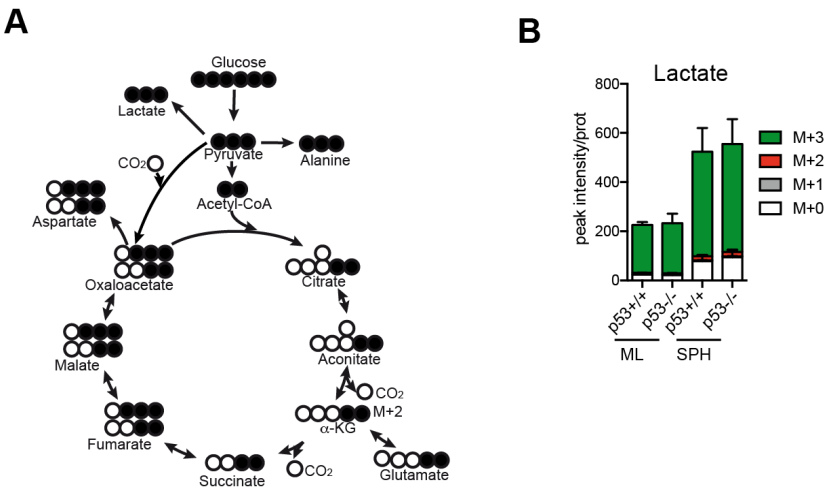

Figure 4.10: Spheroid cultures promote 'glycolytic phenotype'

A) Diagram showing the labelling of TCA cycle metabolites from [U^{13}C] glucose
B) HCT116 p53+/+ and p53-/- cells were cultured as monolayer (ML) or spheroid (SPH) cultures and stable isotope tracing analysis was performed. After 16 hours of incubation with [U^{13}C] glucose, cells were extracted and metabolites were analysed by LC-MS. Values represent mean ± SEM (n=3 independent biological replicates)

Interestingly, pyruvate dependent anaplerosis was observed in both p53 wild type and p53 deficient cultures. As seen from Fig 4.10A, pyruvate is usually converted to acetyl-CoA and contributes to the m+2 fraction of citrate and other TCA cycle metabolites. During anaplerosis, pyruvate can enter the TCA cycle by the conversion to oxaloacetate via pyruvate carboxylase enzyme and this leads to the formation of m+3 fractions in the TCA cycle intermediates. A relative increase in m+3 over m+2 isotopologues can be attributed to the activity of pyruvate dependent anaplerosis (Buescher et al., 2015). Indeed, higher m+3/m+2 ratios for aspartate and malate detected in spheroid cultures compared to monolayers indicate the presence of pyruvate dependent anaplerosis, which are the metabolic consequences of a hypoxic environment (Fig 4.11).

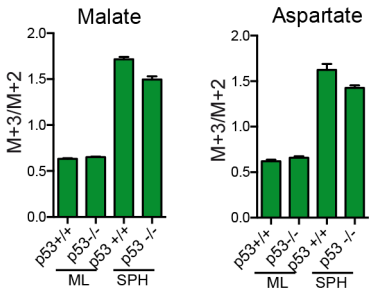

Figure 4.11: Spheroid cultures show pyruvate dependent anaplerosis
HCT116 p53+/+ and p53-/- cells were cultured as monolayer (ML) or spheroid (SPH) cultures and stable isotope tracing analysis was performed. After 16 hours of incubation with [U^{13}C] glucose, cells were extracted and metabolites were analysed by LC-MS. Ratios of M+3 and M+2 isotopologues for malate and aspartate are shown. Values represent mean ± SEM (n=3 independent biological replicates)

Furthermore, analysis for the p53 specific differences revealed that levels of aspartate are higher only in p53 wild type spheroids (Fig.4.12A). Aspartate has been demonstrated to be very important for cell proliferation because it provides essential carbon atoms for pyrimidine biosynthesis (Sullivan et al., 2015). Indeed, incorporation of glucose carbons into UMP was overall lower in spheroid cultures compared to monolayers, most likely representing reduced proliferation. However, this reduction was less pronounced in p53 deficient cells (Fig. 4.12B). This result suggests that p53 deficient cells maintain higher levels of pyrimidine nucleotide biosynthesis under spheroid culture conditions compared to their p53 wild type counterparts. As pyrimidine synthesis also requires aspartate, this results in a reduced accumulation of this metabolite in p53 deficient cells.

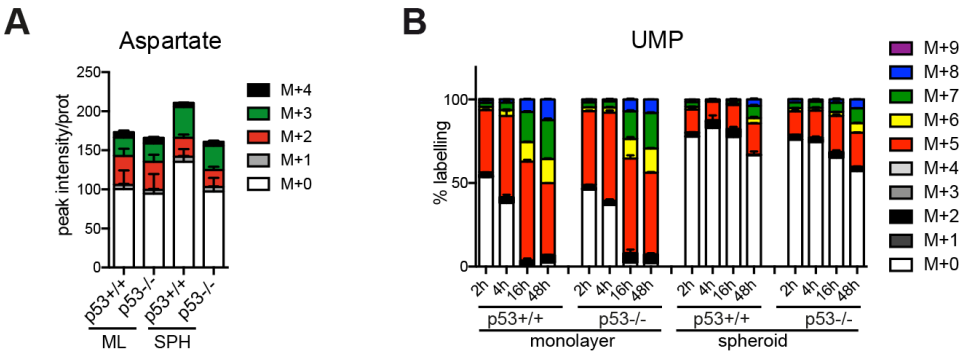

Figure 4.12: Glucose labelling to UMP is higher in p53 deficient spheroids

A) HCT116 p53+/+ and p53-/- cells were cultured as monolayer (ML) or spheroid (SPH) cultures and stable isotope tracing analysis was performed. After 16 hours of incubation with [$U^{13}C$] glucose, cells were extracted and metabolites were analysed by LC-MS. Relative peak intensities of aspartate was shown. Values represent mean ± SEM (n=3 independent biological replicates)
B) Incubation with [$U^{13}C$] glucose for 48, 16, 4 or 2 hours, cells were extracted and metabolites were analysed by LC-MS. % labelling for UMP was shown.

Taken together, spheroids undergo metabolic reprogramming in order to survive under hypoxia with reduced glucose oxidation, enhanced lactate production and increase TCA cycle anaplerosis. Moreover, while these adaptations were observed in cells with both genotypes only aspartate showed reduction in p53 deficient spheroids to support pyrimidine biosynthesis.

4.2 Regulation of SREBP2 and cholesterol metabolism by p53

Metabolic reprogramming takes place in cancer cells for the tumour formation. During this transformation, elevated levels of de novo lipid synthesis were identified as an important feature of tumour cells (Menendez et al., 2007). While enhanced lipid synthesis in cancer is established, the mechanisms and consequences of this deregulation are not fully understood (Rohrig et al., 2016) Especially, the regulation of sterol synthesis in colorectal cancer is not well studied.

SREBP2 is a transcription factor that is responsible for the expression of genes involved in cholesterol biosynthesis (Osborne et al., 2009). Activation and

stability of SREBPs are tightly regulated by the availability of the sterol levels and other signalling events (Shao et al., 2012) (Osborne et al., 2009). SREBPs are synthesized as inactive precursors bound to the ER membrane where they are associated to SCAP. Under conditions where sterol levels are low, the SREBP/SCAP complex translocates to the Golgi where SREBP is proteolytically cleaved and the N-terminal half of the protein is released, which then translocates to nucleus to drive the expression of target genes by binding to SRE (Goldstein et al., 2006; Horton, 2002).

Several reports demonstrated that the activity of SREBPs is needed for cancer cell proliferation. For instance, activation of SREBP1 was shown to be necessary for the growth of xenograft models of glioblastoma multiforme that carry EGFR mutations (Guo et al., 2009). Moreover, activation of SREBP as a result of PI3K/mTORC1 signalling was demonstrated as an important factor for the growth and proliferation in breast cancer (Ricoult et al., 2016). p53 has been identified as a negative regulator of SREBP and lipogenesis in mice from a genetic model of obesity (ob/ob) in a fed state (Yahagi et al., 2003). In addition, mutant p53 was shown to bind to SREBP2 to drive the expression of genes that have roles in mevalonate pathway to disrupt breast tissue architecture (Freed-Pastor, Mizuno, et al., 2012). Moreover, a recent paper demonstrated that wild type p53 correlates with the inhibition of mevalonate pathway in hepatocellular carcinoma (Moon et al., 2018). However, the exact mechanism of how wild type p53 regulates SREBP2 in cancer is not well defined.

4.2.1 Evaluation of SREBP2 levels in monolayer and spheroid cultures

The results described in section 4.1.3 showed that the SREBP2 targets are upregulated in spheroid cultures compared to monolayers and were most abundant in p53 deficient spheroids. However, expression of *SREBF2* mRNA itself was similar between p53 isogenic spheroids (see Fig. 4.8), suggesting a post transcriptional mechanism of regulation for SREBP2. Therefore, levels of mature SREBP2 and SREBP targets were investigated at the protein level. As Fig 4.13 demonstrates, levels of mature SREBP2 protein were increased in p53 deficient cells, especially in spheroids.

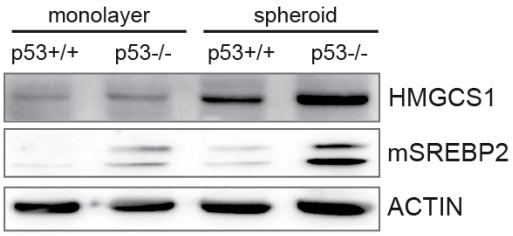

Figure 4.13: Loss of p53 promotes formation of mature SREBP2 and expression of HMGCS1 protein in spheroids

Western blots showing expression of HMGCS1 and mature SREBP2 in HCT116 p53+/+ or p53-/- cells grown as monolayer or spheroid cultures. Actin is shown as loading control.

As SREBP gets processed at low sterol levels (Brown et al., 1997) experiments were performed in medium containing 1% FCS, a serum concentration at which sterol levels should not be sufficient to block SREBP activation, in order to check how SREBP2 is regulated in monolayer cultures. For this, mRNA expression of SREBP2 target genes in p53+/+ and p53-/- cells treated with 10% and 1% FCS for 24 hrs were analysed by qPCR. Interestingly, expression of *HMGCS1* and *HMGCR* was induced in p53 deficient cells by low serum condition (Fig 4.14A). In contrast, low serum was not able to increase expression of these proteins in p53 wild type cells, suggesting an inhibitory effect of p53 on SREBP2 activation.

Nuclear fractionation was performed to enrich the mature form of SREBP2 from cells cultured either in 10% or 1% FBS for 24 hrs. Nuclear SREBP2 is subjected to multiple phosphorylation (Sundqvist et al., 2003) making the protein appear as multiple bands. It can be concluded that there is a moderate upregulation of mature SREBP2 in nuclear fractions of p53 deficient cells incubated with 1% FBS (Fig 4.14B), confirming the results of the qPCR analysis. In contrast, p53 wild type cells did not increase levels of mature SREBP2 when cultured in low serum (Fig 4.14B), indicating that sterol levels affect the mature SREBP levels in monolayer cultures only in p53 deficient cells. Consistent with these findings, it can be speculated that cells in spheroid cultures are exposed to low sterols levels and this induced the formation of mature SREBP when p53 is absent. Conversely, the presence of p53 inhibits the formation of mature SREBP2 under metabolic stress, thereby blocking the expression of SREBP2 target genes.

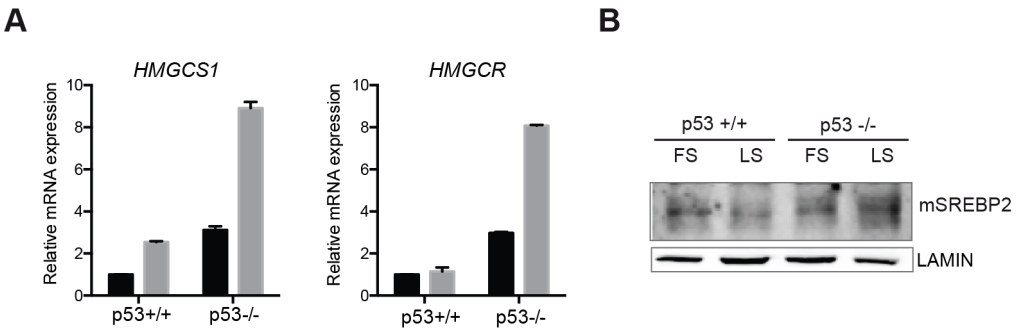

Figure 4.14: Loss of p53 promotes activation of SREBP2 by sterol deprivation in monolayer cells

A) Expression of *HMGCS1* and *HMGCR* mRNA in HCT116 p53+/+ and p53-/- cells cultured as monolayers either in full medium (FS) or in lipid-reduced medium (LS, 1% FCS) for 24 hours.
B) Western blot of nuclear extracts from HCT116 p53+/+ and p53-/- cells cultured as monolayers either in full medium (FS) or lipid-reduced medium (LS) for 24 hours. mSREBP2 was detected in the upper blot with lamin as a loading control.

4.2.2 Establishing cell lines expressing shRNAs targeting SREBP2 and effects of SREBP2 silencing

In order to gain more insight into the mechanism by which p53 regulates SREBP2, p53 isogenic cell lines were generated stably expressing short-hairpin RNA interference (shRNA) constructs targeting *SREBF2*. First, the knock-down efficiency of two different shRNA sequences was established and it was confirmed that SREBP2 levels were downregulated by at least 70% in p53 deficient cells by both sequences (Fig 4.15A). Sequence #484 also efficiently reduced *SREBF2* expression in p53 wild type cells, while the results for sequence #485 were inconclusive in these cells (Fig 4.15A). Moreover, silencing of SREBP2 using this approach did not alter levels of *SREBF1* expression (Fig 4.15A), confirming the specificity of the constructs.

Spheroids were generated from these cell lines and knock-down of *SREBF2* was induced for 72 hrs. Investigation of HMGCS protein levels revealed that HMGCS1 levels were higher in p53 deficient spheroids compared to the p53+/+ confirming that p53 inhibits SREBP2 and its target gene expression under metabolic stress (Fig 4.15B). Moreover, *SREBF2* silencing only decreased HMGCS1 levels in

spheroids from p53 deficient cells. In contrast, the basal level of HMGCS1 in p53+/+ cells was not affected by *SREBF2* knock-down-down (Fig 4.15B). These results suggest that p53 dependent regulation of mevalonate pathway genes is mediated through SREBP2.

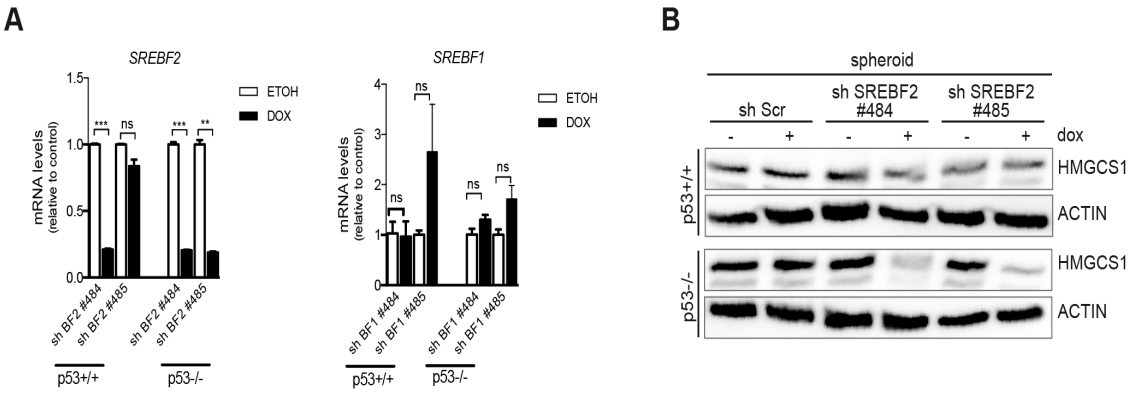

Figure 4.15: Loss of p53 activates HMGCS1 via SREBP2

A) HCT116 p53+/+ and p53-/- cells expressing doxycycline-inducible shRNA sequences targeting *SREBF2* (sequence #484 and #485) were cultured in monolayer cultures and treated with 1 µg/ml doxycycline (DOX) for 72 hours. Expression of *SREBF2* and *SREBF1* was determined. Values represent mean ± SEM (n=2, each biological replicate in technical duplicates).
B) HCT116 p53+/+ and p53-/- cells expressing doxycycline-inducible shRNA sequences targeting *SREBF2* (sequence #84 and #85) were cultured as spheroids and treated with 1 µg/ml DOX for 72 hours. Expression of *HMGCS1* was determined by western blotting. Actin is shown as loading control.

4.2.3 Mechanism of SREBP2 regulation by p53

Several mechanisms were suggested for the post-translational regulation of SREBPs by oncogenic signalling pathways. Increased processing and nuclear accumulation of SREBP1 can be promoted via the AKT/mTORC1 pathway (Duvel et al., 2010). In addition, stability of SREBPs is controlled by glycogen synthase kinase 3 (GSK3). GSK3 dependent phosphorylation of SREBPs lead to their recognition and ubiquitination by a FBXW7-containing ubiquitin ligase complex (Sundqvist et al., 2005) and the activity of GSK3 can be controlled by inactivating phosphorylation by AKT (Manning et al., 2017). In order to reveal the mechanism by which SREBP2 is regulated by p53 in different culture conditions, the activation status of several

signalling pathways was investigated in cells cultured in monolayer and spheroid conditions.

Interestingly, phosphorylation of ribosomal S6 protein was prominently observed especially in spheroid cultures both in p53 wild type and p53 deficient spheroids (Fig 4.16A). In addition, western blot analyses revealed increased phosphorylation of GSK3 in p53 deficient spheroids (Fig 4.16B), consistent with an inactivation of its activity. This could explain the presence of more mature SREBP2 in p53 deficient spheroids, as inactive GSK3 cannot phosphorylate SREBP2, leading to its accumulation in the nucleus.

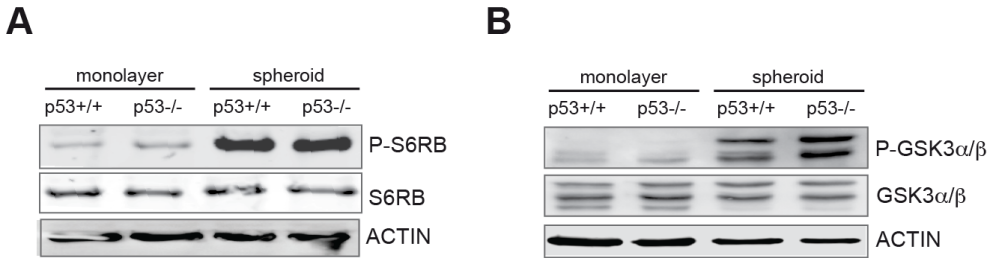

Figure 4.16: Spheroids induce phosphorylation of S6RB and GSK3

A) Western blots showing levels of phosphorylated ribosomal protein S6 (P-S6RB) and total ribosomal protein S6 expression (S6RB) in HCT116 p53+/+ or p53-/- cells grown as monolayer or spheroids. Actin is shown as loading control
B) Western blots showing phosphorylation on GSK3a/b (serine 21/9) and total GSK3a/b protein expression in HCT116 p53+/+ or p53-/- cells grown as monolayer or spheroid cultures. Actin is shown as loading control.

To confirm the involvement of GSK3 in the regulation of SREPB2 by p53, spheroids were treated with different GSK3 inhibitors. First, the effect of GSK3 inhibition of HMGCS1 protein levels was determined in spheroids treated with the inhibitors for 24 hrs. Interestingly, HMGCS1 levels in p53 deficient spheroids treated with GSK3 inhibitors were increased to the same levels as those observed in p53 wild type spheroids without inhibitor (Fig 4.17A), suggesting that SREBP2 might be regulated via GSK3. In addition, expression of *HMGCS1* and *HMGCR* was increased after GSK3 inhibition for 72 hrs in p53 wild type spheroids confirming the previous results and suggesting that GSK3 regulates SREBP2 stability (Fig 4.17B).

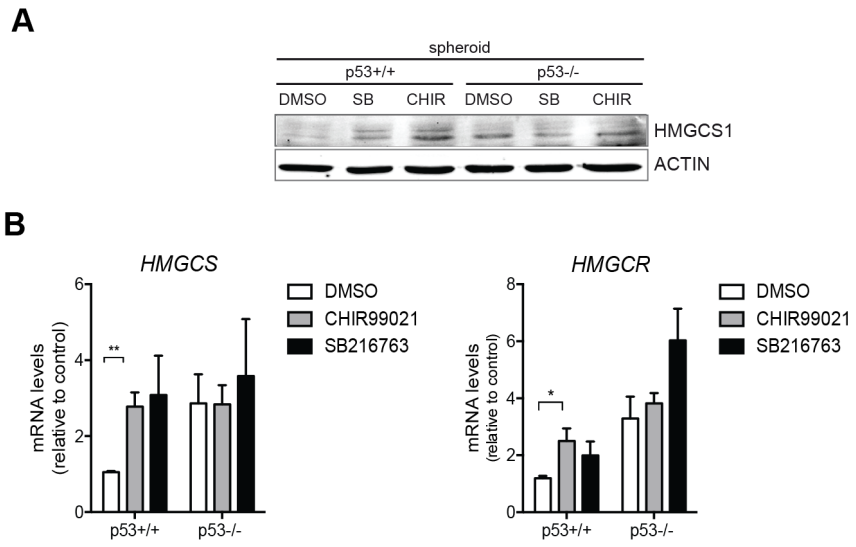

Figure 4.17: GSK3 regulates the stability of SREBP2

A) HCT116 p53+/+ or p53-/- cells were grown as spheroids and treated with 30 μM of SB216763 (SB) or 10 μM of CHIR99021 (CHIR) for 24 hours. Levels of HMGCS1 protein expression were determined by western blotting. Actin is shown as loading control

B) Expression of *HMGCS1* mRNA in HCT116 p53+/+ or p53-/- cells grown as spheroids and treated with 10 μM of CHIR99021 (CHIR) for 72 hours. Values represent mean ± SEM (n=3, each biological replicate in technical duplicates). p-values were calculated using unpaired two tailed student t-test. ($p<0.01$, **; $p<0.05$, *).

As high levels of S6RB were observed in both p53 wild type and p53 deficient spheroids, it was reasoned that mTORC1 might also play a role in the regulation of SREBP2 by p53. Thereby, rapamycin, a specific mTORC1 inhibitor, was used to treat both p53 wild type and p53 deficient spheroids for 72 hrs. As a result, *HMGCS1* and *HMGCR* levels were decreased strongly in p53 deficient spheroids (Fig 4.18), suggesting that mTORC1 activity is required for the activation of SREBP2 in p53 deficient cells.

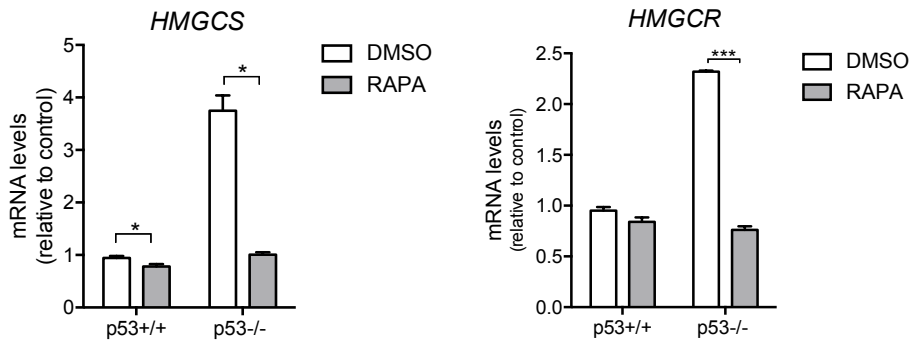

Figure 4.18: mTORC1 regulates the activity of SREBP2

Effect of rapamycin on *HMGCS1* and *HMGCR* expression in spheroid cultures of HCT116 p53+/+ or p53-/- cells. Values represent mean ± SEM (n=2 each biological replicate in technical duplicates). p-values were calculated using unpaired two tailed student t-test. ($p<0.001$, ***; $p<0.05$, *)

4.2.4 Metabolic characterisation of cholesterol pathway

Cholesterol biosynthesis has been shown to play a role in many metabolic processes and the production of mevalonate from acetyl-CoA with NADPH and ATP was demonstrated as a rate-limiting step in the cholesterol pathway (Mullen et al., 2016). After having shown that cholesterol biosynthesis is transcriptionally regulated by the transcription factor SREBP2, levels of metabolites that play a role in the cholesterol biosynthesis were determined. Stable isotope labelled glucose was traced into acetyl-CoA in both monolayer and spheroid condition of p53 isogenic cells. As seen in Fig 4.19A, steady state levels of labelled acetyl-CoA were reached in monolayer cultures already after 16 hrs. In contrast, steady state was not reached even after 48 hrs in spheroid cultures, suggesting that low PDH activity in the hypoxic environment reduces the efficiency of acetyl-CoA production from glucose

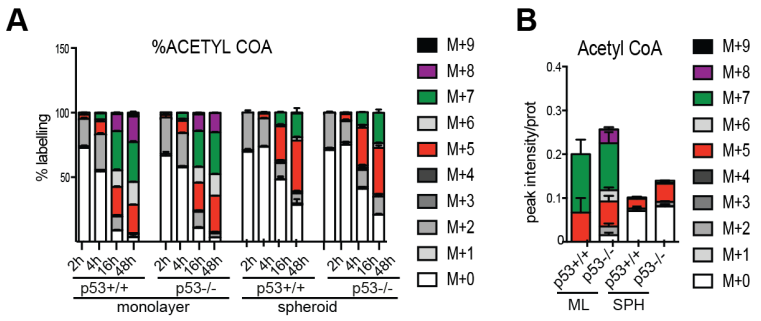

Figure 4.19: Metabolic characterization of HCT116 cells in monolayer and spheroids reveals differences in acetyl-CoA labelling

A) HCT116 p53+/+ and p53-/- cells were cultured as ML for 24 hrs or as SPH for 14 days and used for stable isotope tracing analysis. After incubation with [$U^{13}C$] glucose for 48, 16, 4 or 2 hours, cells were extracted and metabolites were analysed by LC-MS. Values represent mean ± SEM (n=3 independent biological replicates)
B) Relative peak intensities for acetyl-CoA at 16 hrs.

In order to gain more insight into the metabolic activity of the mevalonate pathway, labelled glucose was traced into mevalonate, cholesterol and CoQ10 in spheroids and relative peak intensities of different isotope fractions were calculated. Relative peak intensities of mevalonate labelled from glucose were increased in p53 deficient spheroids (Fig 4.20B) and this difference was observed across all mevalonate isotopologue fractions (Fig 4.20C), suggesting that mevalonate production is higher in these cells. Interestingly, the distribution of the different isotopologues for cholesterol showed significant changes between cells from the two genotypes. The fraction of labelled cholesterol isotopologues was higher in wild type p53 spheroids compared with those in p53 deficient cultures (Fig 4.20D). Surprisingly, most labelled fractions of CoQ10 isotopologues were higher in the p53 deficient compared to wild type spheroids (Fig 4.20E). This pattern of labelling was opposite to that of cholesterol, leading to a conclusion that p53 deficient cells reprogram their metabolism to favour the production of CoQ10 instead of cholesterol under metabolically compromised conditions.

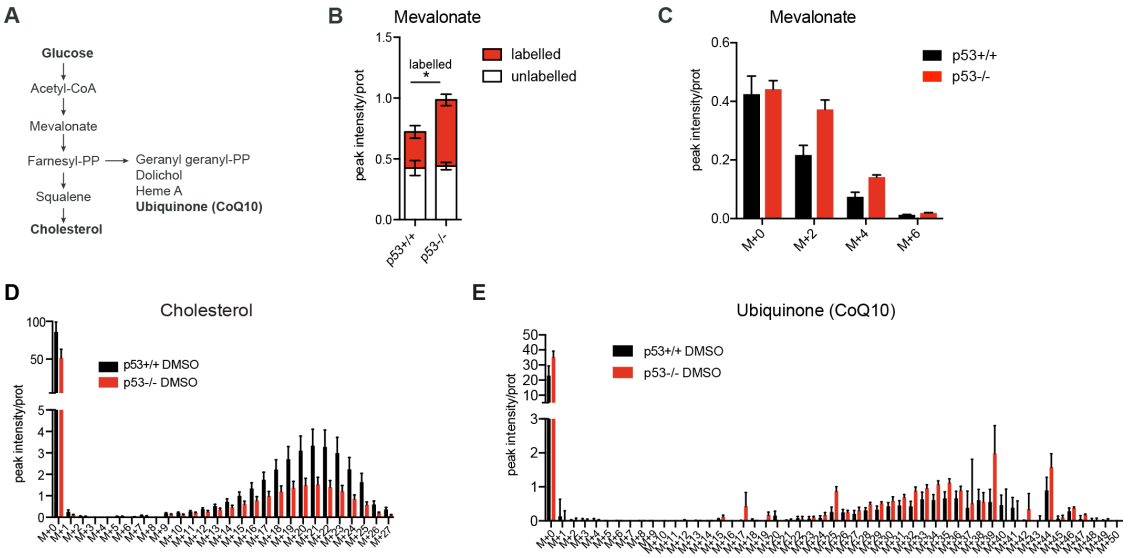

Figure 4.20: Loss of p53 results in metabolic rewiring of the mevalonate pathway

A) Schematic representation of cholesterol pathway.
B) HCT116 p53+/+ or p53-/- cells were grown as spheroids and labelled with [U^{13}C] glucose for 16 hrs before cells were extracted and analysed for mevalonate levels. Values represent mean ± SEM (n=3 independent biological replicates). p-values were calculated using unpaired two tailed student t-test. ($p<0.05$, *).
C) Relative peak intensities of mevalonate isotopologues.
D) HCT116 p53+/+ or p53-/- cells were grown as spheroids and labelled with [U^{13}C] glucose for 72 hrs before cells were extracted and analysed for the abundance of cholesterol isotopologues.
E) Relative peak intensities of individual labelled fractions for CoQ10.

Taken together, this analysis showed that cholesterol levels are higher in p53 WT spheroids, which might be necessary for production of membranes. In contrast, p53 deficient spheroids display higher levels of glucose-dependent CoQ10 synthesis, indicating that rewiring of the mevalonate pathway could support important metabolic functions in these cells under nutrient and oxygen restricted environment, which will be discussed in the next chapter.

4.3 Effects of mevalonate pathway inhibition

In the result shown so far, induction of cholesterol biosynthesis in p53 deficient cells in metabolically compromised environment has been demonstrated. Likewise, different rewiring of the mevalonate pathway in spheroids was observed. Cholesterol levels were higher in wild type p53 spheroids whereas CoQ10 levels were more abundant in p53 deficient spheroids. As shown previously, oncogenic signalling plays a role in regulating the mevalonate pathway for cell survival and growth. Thus, the mevalonate pathway can be suggested as a potential vulnerability that can be targeted as therapeutic strategy. Statins are commonly used drugs that block the activity of HMGCR, the rate-limiting enzyme of this pathway.

4.3.1 Effect of inhibition of mevalonate pathway in monolayer cultures

To investigate the effect of drugs that inhibit the activity of the mevalonate pathway, monolayer cultures were treated with statins. To this end, first, metabolomic analyses were performed to determine the effects of statins on cholesterol and CoQ10 levels in monolayer cultures. Interestingly, p53 deficient cells seem to have more cholesterol in contrast to the spheroid condition although this difference failed to reach significance. Moreover, CoQ10 levels were restored in p53 deficient cells suggesting the absence of metabolic reprogramming in monolayers. Cholesterol and CoQ10 levels were found to be blocked by the statins in the monolayer cultures (Fig 4.21) suggesting the complete inhibition of the mevalonate pathway.

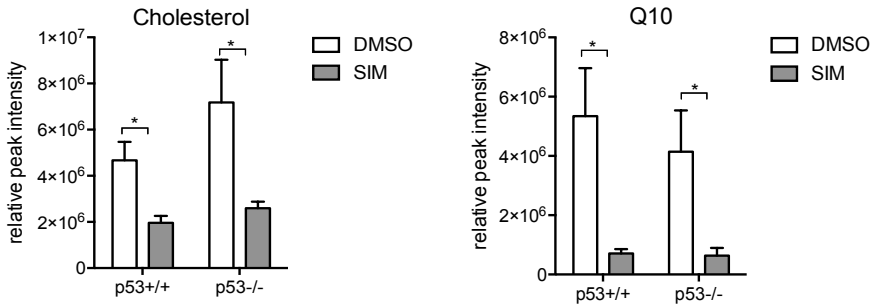

Figure 4.21: Simvastatin blocks the mevalonate pathway metabolites in monolayer cultures

HCT116 p53+/+ and p53-/- cells were cultured as ML for 24 hrs and treated with 10 μM simvastatin for 48 hrs. Cholesterol and CoQ10 levels were analysed by LC-MS. Values represent mean ± SEM (n=3 independent biological replicates). p-values were calculated using unpaired two tailed student t-test. ($p<0.05$, *)

CoQ10 acts as an electron carrier that transfers electrons from respiration complex I to respiration complex III (Y. Wang et al., 2016). Since statins decreased the levels of CoQ10, their effect on respiration was investigated. For this purpose, metabolic assays measuring the oxygen consumption rate (OCR) were performed either in basal state or after sequential addition of oligomycin, FCCP and antimycin/rotenone in order to determine mitochondrial function. In p53 WT cells, simvastatin reduced both basal and maximal OCR, but this was not restored by mevalonate addition (Fig 4.22 left graph). In p53 deficient cells, simvastatin addition also caused a reduction in basal and maximal OCR and this was further enhanced in the presence of mevalonate (Fig 4.22 right graph). This result either suggests that mevalonate addition does not restore CoQ10 synthesis in monolayer cells or that the reduction in respiration in the presence of statins is caused by a mechanism not related to CoQ10. The further inhibition of respiration by mevalonate addition in p53 deficient cells could be related to oxygen usage by enhanced cholesterol synthesis as shown before in yeast (Hughes et al., 2005), which is more active in these cells suggesting that mevalonate pathway acts as an oxygen sensor.

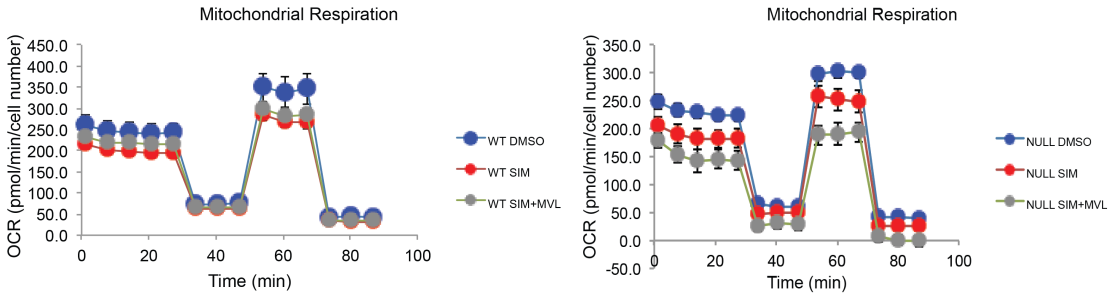

Figure 4.22: Inhibition of mevalonate pathway inhibits mitochondrial respiration

HCT116 p53+/+ (LEFT) or p53-/- cells (RIGHT) were grown as monolayers for 24 hrs and treated with solvent (DMSO), 10 µM simvastatin (SIM) or either alone or in the presence of 0.5 mM mevalonate for 24 hrs. Oxygen consumption rates (OCR) were determined using the Seahorse Bioanalyzer. Oligomycin (oligo), FCCP and rotenone/antimycin A (R/A) were added to determine ATP-dependent, maximal and basal respiration. Values represent mean±SEM of the 8 technical replicates (n=2)

Next, the effect of statins on the colon cancer cell viability was investigated as statins were shown to kill cancer cells (Wong et al., 2002). Initially, three different statins (mevastatin, simvastatin, cerivastatin) were used to inhibit HMGCR, the rate-limiting enzyme of the mevalonate pathway. Different doses of statins had significant effects on both p53 WT and p53 deficient monolayer cell viability (Fig 4.23A, B and C). Moreover, loss of cell viability was rescued with the addition of mevalonate, showing the specificity of the inhibitory effect of the compounds. As CoQ10 levels showed changes after statin treatment, exogenous CoQ10 effect on the cell viability was investigated. However, addition of CoQ10 was not able to rescue viability in the presence of mevastatin and simvastatin (Fig 4.23A and B) suggesting that CoQ10 is not the rate-limiting factor in monolayer cultures.

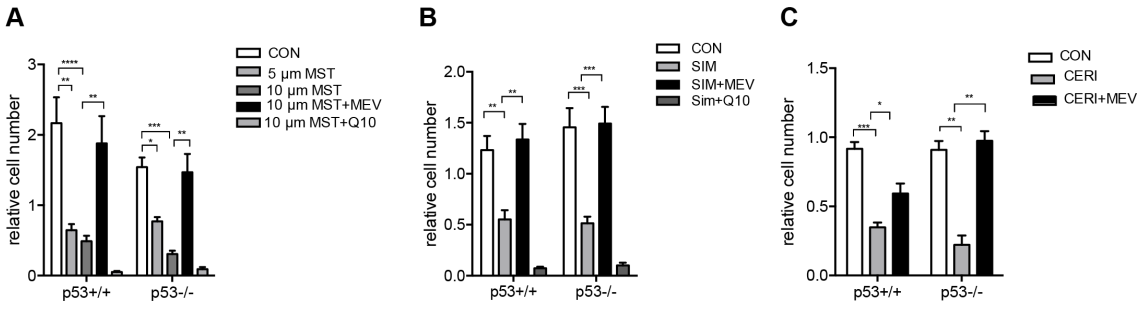

Figure 4.23: Inhibition of mevalonate pathway is detrimental for cells cultured in monolayer

A) Monolayers of HCT116 p53+/+ or p53-/- cells were treated with the indicated concentrations of mevastatin (MST) alone or in combination with 0.5 mM mevalonate or 10 µM CoQ10 for 48 hours. Cell numbers were determined by DAPI staining and automated counting. Values represent mean ± SEM (n=3 independent biological replicates). p-values were calculated using unpaired two tailed student t-test. ($p<0.0001$, **** ; $p<0.001$, ***; $p<0.01$, **; $p<0.05$, *)
B) Monolayers of HCT116 p53+/+ or p53-/- cells were treated with 10 µM simvastatin (SIM) alone or in combination with 0.5 mM mevalonate or 10 µM CoQ10 for 48 hours.
C) Monolayers of HCT116 p53+/+ or p53-/- cells were treated with 10 µM cerivastatin (CERI) alone or in combination with 0.5 mM mevalonate for 48 hours.

In addition, the effect of inhibitors, which target the downstream reactions of mevalonate pathway, such as YM-53601 and zoledronic acid, were investigated. YM-53601 is a squalene synthetase inhibitor and zoledronic acid has been used as a farnesyl diphosphate synthase inhibitor and doses of these drugs were chosen in a range that they affected the proliferation of cancer cells in other studies(Freed-Pastor, Mizuno, et al., 2012; Sorrentino et al., 2014). Cell viability was reduced dramatically after zoledronic acid treatment with two different doses (Fig 4.24B), suggesting the importance of the FDPS enzyme for cell survival. In contrast, the YM-53601 effect on cell viability was mild both in p53 WT and p53 deficient cells cultured in monolayer (Fig 4.24C), confirming the essentiality of mevalonate pathway upstream of FDPS. Moreover, as expected, cell death could not be rescued with the addition of mevalonate after YM-53601 and zoledronic acid treatment.

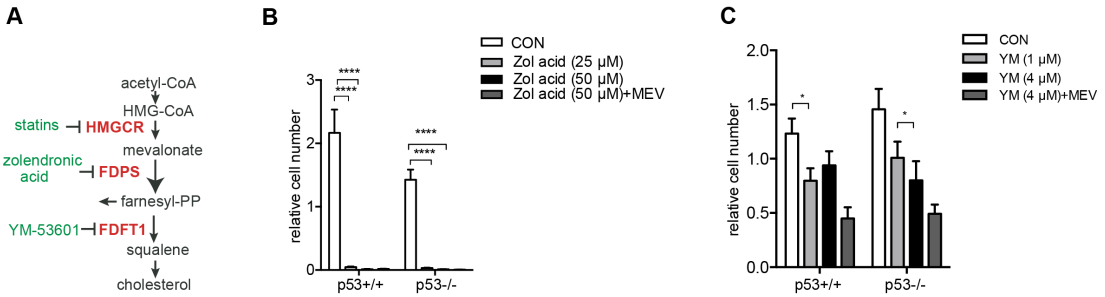

Figure 4.24: Inhibition of mevalonate pathway with zoledronic acid reduces cell viability in monolayer cultures

A) Schematic representation of mevalonate pathway.
B) Monolayers of HCT116 p53+/+ or p53-/- cells were treated with the indicated concentrations of zoledronic acid (Zol acid) either alone or in combination with 0.5 mM mevalonate for 48 hrs. Cell numbers were determined by DAPI staining. Values represent mean ± SEM (n=3 independent biological replicate). p-values were calculated using unpaired two tailed student t-test. ($p<0.0001$, ****)
C) Monolayers of HCT116 p53+/+ or p53-/- cells were treated with the indicated concentrations of YM-53601 (YM) either alone or in combination with 0.5 mM mevalonate for 48 hrs. Cell numbers were determined by DAPI staining. Values represent mean ± SEM (n=3 independent biological replicate). p-values were calculated using unpaired two tailed student t-test. ($p<0.05$, *)

In order to reveal the mechanism of reduction in the cell number induced by statins, mRNA and protein levels of several candidate genes were investigated. For this purpose, induction of SREBP targets expression levels was evaluated. Expression of *FASN* was upregulated with the addition of simvastatin to monolayer cultures in both cell lines (Fig 4.25), suggesting an increase in SREBP activity due to reduced cholesterol levels relieving the feedback inhibition. However, because of the high variation for expression of *SCD, ACSS2* in p53 wild type cells, results have been found inconclusive and needed further validation.

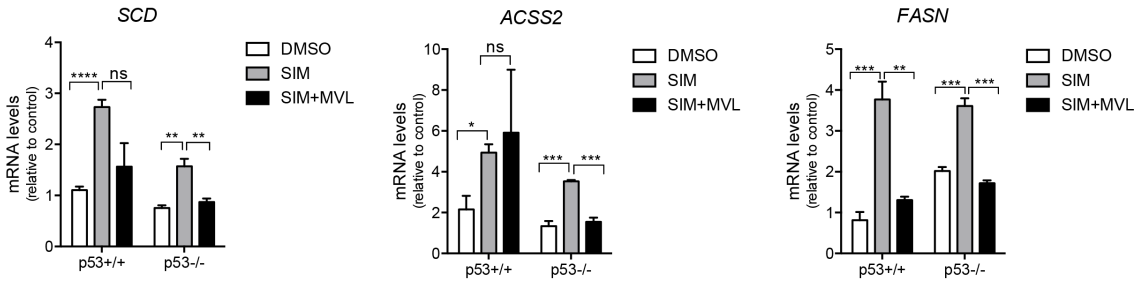

Figure 4.25: Inhibition of mevalonate pathway induces SREBP target genes in monolayer cultures

HCT116 p53+/+ and HCT116 p53-/- cells cultured as monolayer for 24 hrs and treated with 10 μM simvastatin (SIM) either alone or in the presence of 0.5 mM mevalonate for 48 hrs. Expression of *SCD*, *FASN* and *ACSS2* mRNA was determined and normalized to β-actin. Values represent mean ± SEM (n=3, independent biological replicates in technical duplicates). P-values were calculated using unpaired two tailed student t-test. ($p<0.0001$, **** ; $p<0.001$, ***; $p<0.01$, **; $p<0.05$, *).

MYC has been shown to be related to the proliferation and growth (Ji et al., 2011). Loss of MYC has been demonstrated to affect the growth and proliferation programs in many cancer types (Zanet et al., 2005), (Sansom et al., 2007). Stability of MYC was identified to be regulated via phosphorylation of S62 and T58 by MAPK/ERK and GSK3β respectively (Gregory et al., 2003; Yeh et al., 2004). Moreover, inhibition of mevalonate pathway was demonstrated to affect MYC phosphorylation and MYC levels in hepatocellular carcinoma (Cao et al., 2011). Therefore, protein levels of MYC and p-MYC were checked. As a result, MYC and p-MYC levels were restored (Fig 4.26). These results might suggest the decrease in cell number after statin treatment is not dependent on MYC under these conditions suggesting a different mechanism. Another explanation could be that there could be another factor keeping MYC levels the same, which requires further investigation.

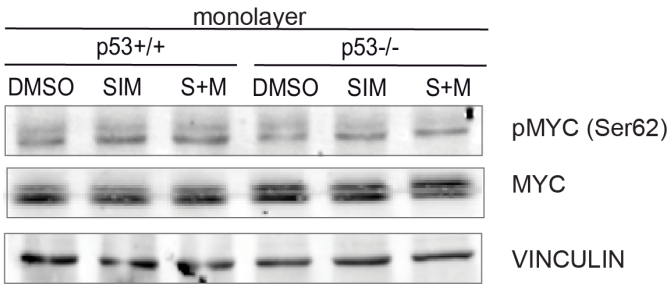

Figure 4.26: Cell death induced by statins suggested to be independent of MYC induction in monolayers

Western blots showing levels of phosphorylated MYC at S62 (P-MYC), MYC in HCT116 p53+/+ or p53-/- cells grown as monolayer and treated with 10 μM simvastatin (SIM) either alone or in the presence of 0.5 mM mevalonate for 48 hrs. Actin is shown as loading control.

Taken together, it can be concluded that inhibition of the mevalonate pathway results in low levels of cholesterol and CoQ10 leading to inhibition in cell respiration in both p53 wild type and p53 deficient cells cultured in monolayer. In addition statins block viability of both p53 WT and p53 deficient cells cultured in monolayer and decrease in cell viability is not dependent on MYC levels. Moreover, from the observation that CoQ10 does not restore cell viability and the mild effect of YM-53601 on the cell number, it can be concluded that CoQ10 is not required for the cell survival in monolayer cultures.

4.3.2 Effect of inhibition of mevalonate pathway in metabolically compromised environments

Having investigated the effect of statins in monolayer culture, spheroids were also used to see their effect on cell viability under metabolically compromised environment. For this purpose, control or statin treated spheroids were fixed, paraffin embedded and sectioned into thin slices. dUTP nick end labelling (TUNEL) staining (used to detect double-strand DNA breaks associated with the induction of apoptosis) and counterstaining with Hoechst was performed. Following mevastatin treatment, p53 deficient cells displayed evidence of apoptosis restricted to the centre of the

spheroids. In contrast, p53 WT cells were fully resistant to the statin treatment, as no apoptosis could be detected in the centre of the spheroids (Fig 4.27A). Cell death was rescued by the addition of mevalonate in p53 deficient spheroids, confirming the specific effect of mevastatin. Quantification of TUNEL positive cells revealed a significant effect of statins causing death of p53 deficient cells under metabolically compromised environment, which was rescued by mevalonate (Fig 4.27B).

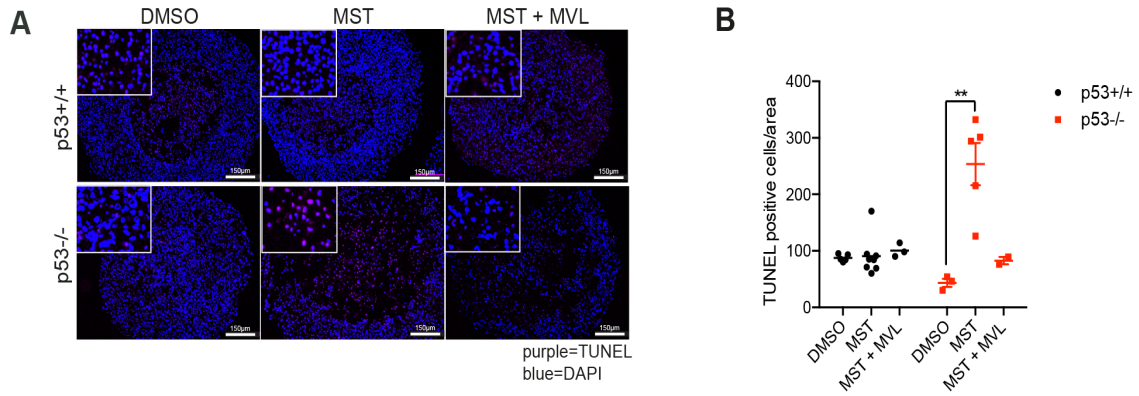

Figure 4.27: The mevalonate pathway is essential for the survival of p53 deficient cell under metabolically compromised environment

A) HCT116 p53+/+ or p53-/- cells were grown as spheroids and treated with 10 µM mevastatin (MST) or solvent (DMSO) either alone or in combination with 0.5 mM mevalonate (MVL) for 72 hours. Spheroids were fixed and histological sections were analyzed for the presence of apoptotic cells by TUNEL staining. Images show representative results.
B) Quantitation of data shown in A. Values represent mean ± SEM of at least 3 spheroids analysed per condition. p-values were calculated using unpaired two tailed student t-test. ($p<0.01$, **)

In order to reveal the mechanism why p53 deficient cells were affected by statins in the metabolically compromised environment, an RNA-SEQ experiment was performed. For this purpose, HCT116 p53+/+ and HCT116 p53-/- spheroids were treated with DMSO, simvastatin or simvastatin with mevalonate for the rescue. Data analysis using either hierarchical clustering of normalised read counts or GSEA analysis showed that in both types of spheroids simvastatin treatment led to the induction of the SREBP target gene signature, which was prevented by co-treatment with mevalonate (Fig 4.28A and B). This is most likely caused by reduced feedback

inhibition caused by the lower sterol levels. However, induction of SREBP targets was less pronounced in p53 deficient spheroids as these genes were already expressed at higher levels in untreated cells (Fig 4.28A).

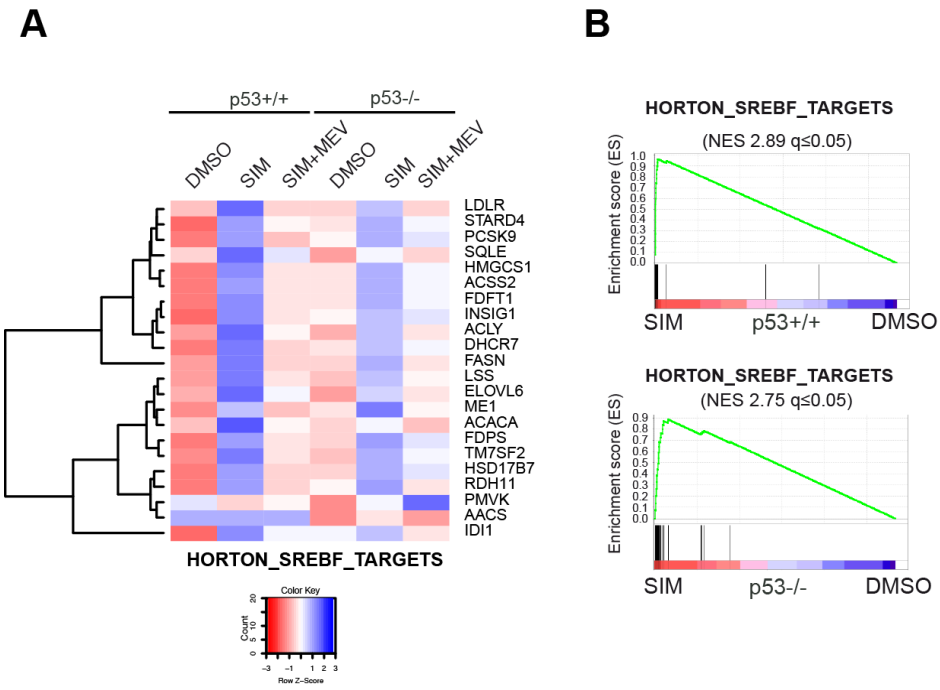

Figure 4.28: SREBP target genes are induced after statin treatment

A) HCT116 p53+/+ or p53-/- cells were grown as spheroids and treated with 10 µM simvastatin (SIM) or solvent (DMSO) either alone or in the presence of 0.5 mM mevalonate for 72 hrs. RNA was extracted and analysed by RNA-SEQ. Heatmap of genes from the HORTON_SREBF_TARGETS signature across all samples.
B) Enrichment plots for the comparison between simvastatin treated and control samples for genes from the HORTON_SREBF_TARGETS signature (Horton et al., 2003) are shown

Interestingly, treatment with simvastatin also strongly reduced expression of genes associated with cell cycle (CHANG_CYCLING_GENES) and Hallmark targets of the MYC transcription factor (H_MYC_TARGETS_V1) (Fig 4.29A and B). Both signatures are highly expressed in proliferating cells indicating that statins reduce cell proliferation. In addition, genes functionally associated with ribosomes were also down regulated in response to statin treatment and this was more pronounced in p53 deficient spheroids. Ribosome biogenesis is strongly associated with a primordial gene expression signature controlled by MYC (Ji et al., 2011).

Together, these results confirm the importance of the mevalonate pathway for cell proliferation (Shamma et al., 2009) and also suggest a link between this metabolic process and the control of MYC activity. As expected, changes in expression of ribosomal genes caused by simvastatin were rescued by the addition of mevalonate (Fig 4.29C), emphasizing the specificity of the simvastatin.

In addition, mTOR signalling has been identified to be strongly linked to MYC to regulate cell proliferation and growth (West et al., 1998) (Holz et al., 2005). In addition, the stability of MYC is controlled by phosphorylation at S62 (Yeh et al., 2004), while mTORC1 mediates the induction of protein synthesis through phosphorylation of S6RB at S244 (Manning et al., 2007). Phosphorylation on MYC at S62 and S6RB at S240 and S244 was checked in both cell types in monolayer and spheroid condition. Overall, there was an increase in the ratio of phosphorylated to total protein for both MYC and S6RB in spheroid cultures of both genotypes. However, phosphorylation levels were not affected by statin treatment (Fig 4.29D).

Moreover, comparison between statin treated p53 WT and p53 deficient spheroids revealed additional gene signatures. Interestingly, the NFE2L2 target gene signature was induced by simvastatin treatment in spheroids form both genotypes (Fig 4.30A). However, a direct comparison of simvastatin treated p53 WT and p53 deficient spheroids revealed a stronger induction in p53 deficient cells (Fig 4.30B). NFE2L2 (also known as NRF2) is a transcription factor that has been shown to regulate the antioxidant pathway in cancer cells (Singh et al., 2008). Therefore, it can be concluded that statins induce the formation of reactive oxygen species (ROS), particularly in p53 deficient cells cultured under a metabolically compromised environment, and this could lead to reduced viability of these cells.

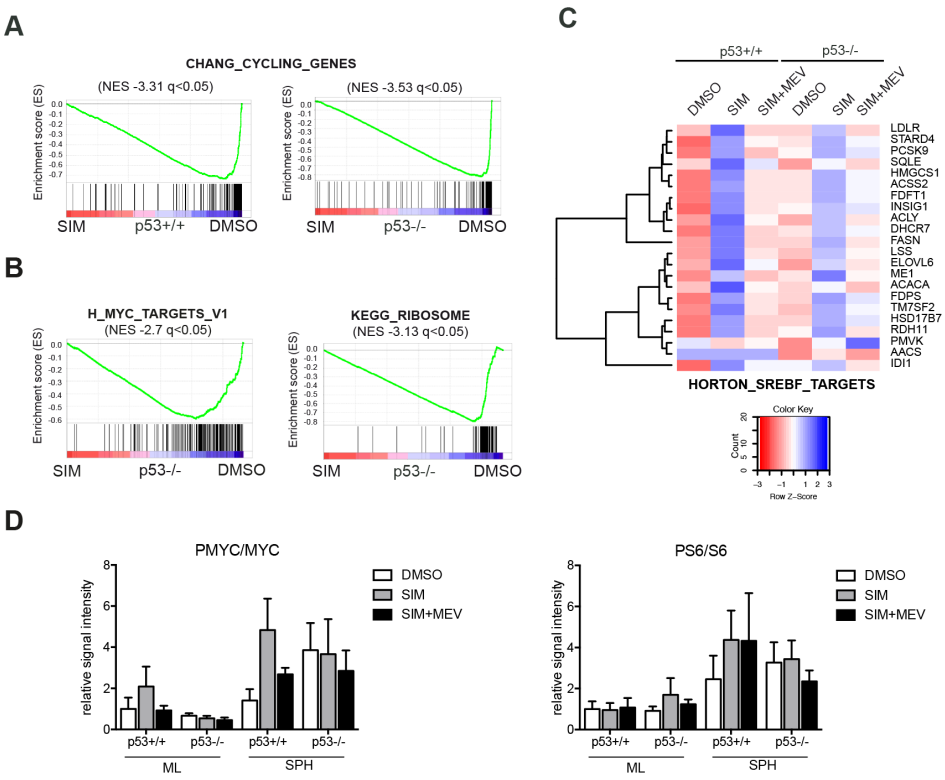

Figure 4.29: Inhibition of mevalonate pathway blocks proliferation

A) Enrichment plots for the signature CHANG_CYCLING_GENES (Chang et al., 2004) in DMSO and simvastatin treated HCT116 p53+/+ and p53-/- cells.
B) Enrichment plots for the signature HALLMARK_MYC_TARGETS_V1 and KEGG_RIBOSOME in DMSO and simvastatin treated HCT116 p53-/- cells.
C) Heatmap of genes from the KEGG_RIBOSOME signature across all samples.
D) Expression of pMYC/MYC and pS6RB/S6RB protein ratio was determined by western blotting. Vinculin is shown as loading control

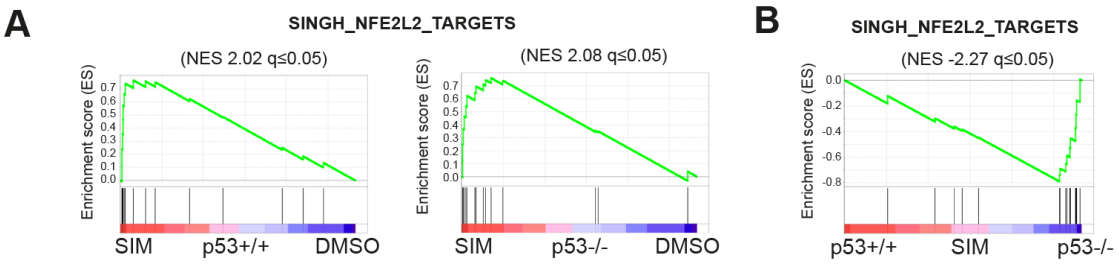

Figure 4.30: Inhibition of mevalonate promotes antioxidant response

A) Enrichment plots for the signature SINGH_NFE2L2_TARGETS (Singh et al., 2008) in DMSO and simvastatin treated HCT116 p53+/+ and p53-/- spheroids.
B) Enrichment plots for the signature SINGH_NFE2L2_TARGETS (Singh et al., 2008) in simvastatin treated HCT116 p53+/+ and p53-/- spheroids

After having checked the global expression profile after statin treatment in the spheroids, individual genes expressing SREBP targets and protein levels of stress and apoptosis markers were further investigated to reveal the mechanism by which p53 deficient cells are sensitized to statins. SREBP targets were upregulated on protein and mRNA level in response to statin treatment in both p53 WT and deficient cells, consistent with the previous results. Expression of *DDIT3* (also known as CHOP) was checked as a marker for endoplasmic reticulum (ER) stress and this gene was only upregulated in p53 deficient cells, which was rescued by mevalonate addition (Fig 4.31A). This suggests that statin treatment causes ER stress induction selectively in p53 deficient spheroids. Moreover, induction of p53 and p21 was investigated. Expression of p53 protein in p53 WT cells was unaffected by statin treatment. In contrast, p21 protein was induced in both cell lines (Fig 4.31B), suggesting that statin treatment induced p21 expression independent of p53. To sum up, in order to provide an explanation for the selective killing of p53 deficient cells by statins, CHOP induction could be suggested since a strong upregulation in the mRNA levels were observed only in p53 deficient cells.

In order to determine whether p21 is involved in the induction of apoptosis in p53 deficient spheroids, simvastatin treatment was performed for shorter (24 hrs) and longer (72 hrs) times and mRNA expression of p21 (*CDKN1A*) was determined. At the shorter time point, p21 was induced only in p53 WT spheroids (Fig 4.32A). However, after 72 hrs, p21 was also induced in p53 deficient cells, suggesting a p53-independent mechanism of p21 induction by mevalonate pathway inhibition. In addition, analysis of protein levels demonstrates that induction of p21 protein was observed in both genotypes. Finally, induction of apoptosis by simvastatin treatment was also analysed in p21 deficient spheroids. Here, statin treatment did not induce apoptosis, indicated by the absence of TUNEL positive cells in the center of the spheroids (Fig 4.32C), suggesting a p21 independent mechanism. Together, these results demonstrate that the induction of apoptosis by mevalonate pathway inhibition in p53 deficient spheroids is independent of p21.

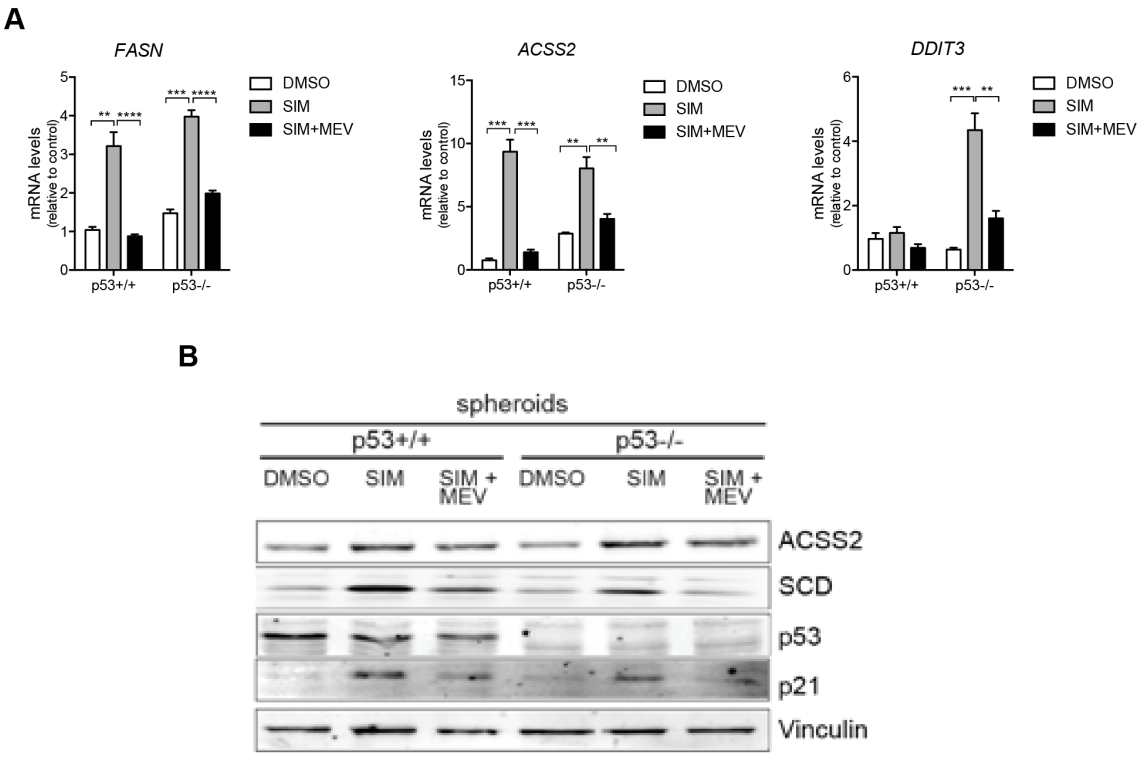

Figure 4.31: Simvastatin treatment induces expression of several targets

A) HCT116 p53+/+ or p53-/- cells were grown as spheroids and treated with 10 μM simvastatin (SIM) or solvent (DMSO) either alone or in combination with 0.5 mM mevalonate (MEV) for 72 hours. Expression of *FASN, ACSS2* and *DDIT3* mRNA was determined and normalized to β-actin. Values represent mean ± SEM (n=3, each biological replicate in technical duplicates). p-values were calculated using unpaired two tailed student t-test. ($p<0.0001$, **** ; $p<0.001$, ***; $p<0.01$, **)

B) Western blots showing levels of ACSS2, SCD, p53 and p21. Vinculin was used as loading control.

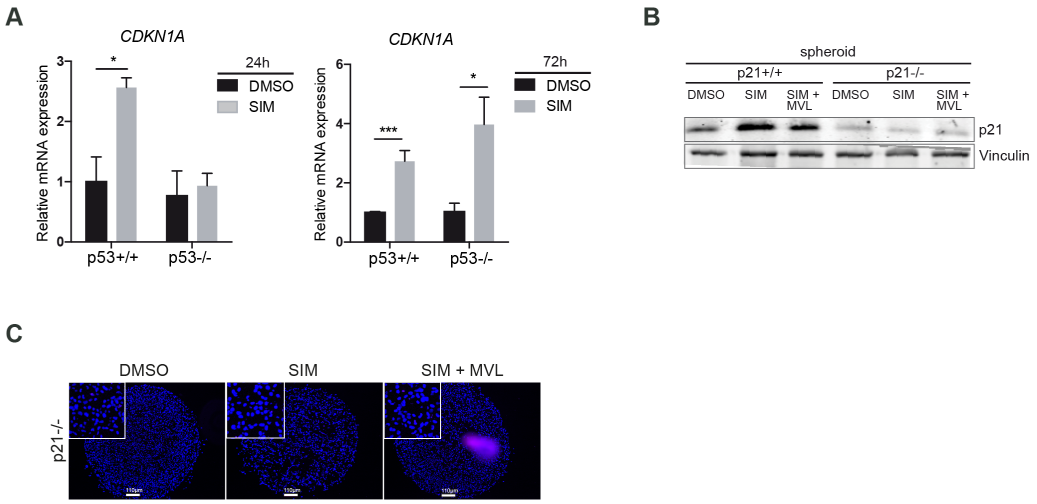

Figure 4.32: Cell death in p53 deficient spheroids is independent of p21 induction

A) HCT116 p53+/+ and p53-/- cells grown as spheroids were treated with 10 µM simvastatin (SIM) or solvent (DMSO) for 24 or 72 hrs. Expression of *CDKN1A* mRNA was determined by qPCR. Values represent mean ± SEM (n=3, each biological replicate in technical duplicates). p-values were calculated using unpaired two tailed student t-test. ($p<0.0001$, **** ; $p<0.001$, ***; $p<0.01$, **; $p<0.05$, *).
B) HCT116 p21+/+ or p21-/- cells were grown as spheroids and treated with 10 µM simvastatin (SIM) or solvent (DMSO) either alone or in combination with 0.5mM mevalonate (MVL) for 72 hours. Expression of p21 protein was determined by western blotting. Vinculin is shown as loading control.
C) HCT116 p21-/- cells were grown as spheroids and treated with 10 µM simvastatin (SIM) or solvent (DMSO) either alone or in combination with 0.5 mM mevalonate for 72 hrs. Spheroids were fixed and histological sections were analysed for the presence of apoptotic cells by TUNEL staining. Images show representative results.

After having determined how statins affected the expression levels of enzymes in the cholesterol pathway, the statin effect to the activity of the cholesterol pathway under metabolic stress was investigated. For this purpose, [U^{13}C] labelled glucose was traced into cholesterol and CoQ10. As described previously, both the labelled and unlabelled fraction of cholesterol were higher in p53 wild type spheroids (Fig 4.34A). In both conditions, treatment with simvastatin diminished the labelled fractions and all stable isotope-containing isotopologues fractions, confirming that simvastatin completely blocks de novo cholesterol synthesis (Fig 4.33A). Levels of CoQ10 were higher in p53 deficient spheroids suggesting p53-dependent metabolic

reprogramming under metabolic stress. However, statin treatment also completely reduced the labelled fraction of CoQ10, and, importantly, also reduced the overall amount of this metabolite (Fig 4.33B).

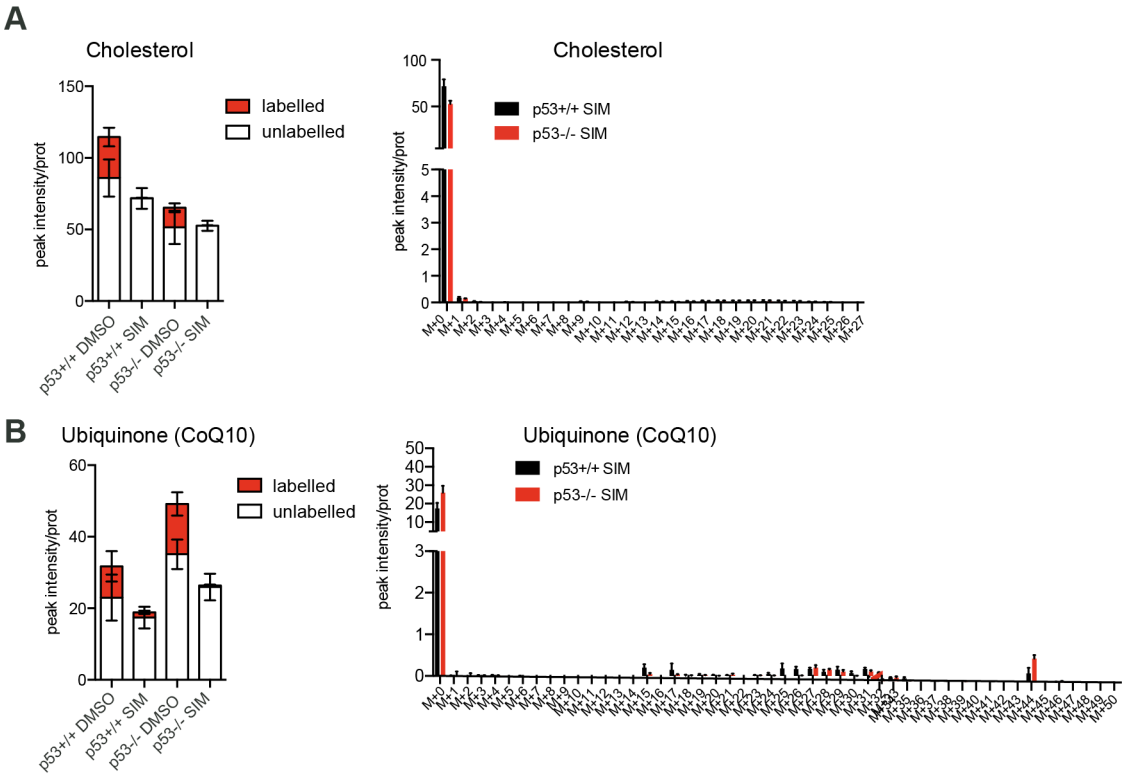

Figure 4.33: Inhibition of mevalonate pathway blocks cholesterol and CoQ10 production under metabolic stress

HCT116 p53+/+ or p53-/- cells were grown as spheroids and treated with 10 µM simvastatin (SIM) or solvent (DMSO) for 72 hrs. For the last 16 hours, cells were labelled with [U^{13}C] glucose before cells were extracted and metabolites were analysed by LC-MS. Values represent mean ± SEM (n=3, independent biological replicates). p-values were calculated using unpaired two tailed student t-test. ($p<0.0001$, **** ; $p<0.001$, ***; $p<0.01$, **; $p<0.05$, *)
A) Relative peak intensities of labelled and unlabelled fractions as well as individual isotopologues for cholesterol.
B) Relative peak intensities of labelled and unlabelled fractions as well as individual isotopologues for ubiquinone (CoQ10).

After having observed that statins decrease CoQ10 levels in cells exposed to metabolically compromised environments, the role of CoQ10 was further investigated. Firstly, its role in the electron transport chain (ETC) and TCA cycle was

analysed. For this purpose, metabolic assays to check OCR of spheroids in the presence of simvastatin and mevalonate rescue were performed. Basal OCR of p53 WT spheroids was not affected by the presence of simvastatin, while the maximal respiration after addition of oligomycin and FCCP was slightly reduced (Fig 4.34). In contrast, in p53 deficient spheroids, basal OCR was substantially decreased in the presence of statins and was fully restored by addition of mevalonate. In conclusion, although depletion of CoQ10 levels was observed in both p53 WT and p53 deficient spheroids, the effect of this depletion on respiration was restricted to p53 deficient spheroids.

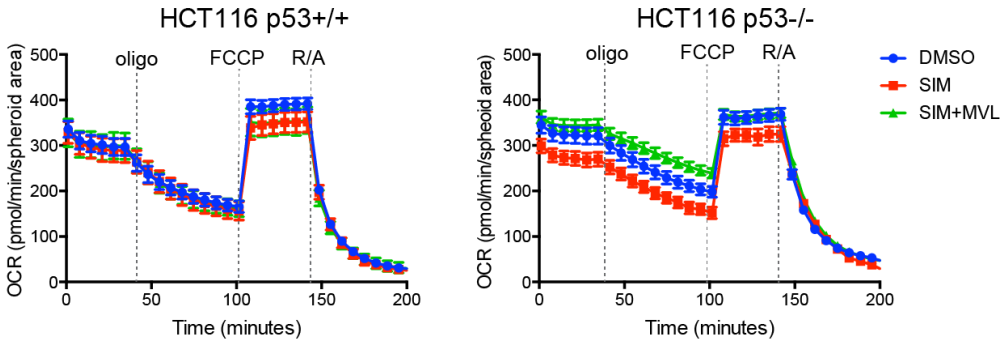

Figure 4.34: Inhibition of mevalonate pathway affects cellular respiration in spheroids

HCT116 p53+/+ or p53-/- cells were grown as spheroids and treated with 10 µM simvastatin (SIM) or solvent (DMSO) either alone or in the presence of 0.5 mM mevalonate for 72 hr. Oxygen consumption rates (OCR) were determined using the Seahorse Bioanalyzer. Oligomycin (oligo), FCCP and rotenone/antimycin A (R/A) were added sequentially to determine basal, ATP-dependent and maximal respiration, respectively, as well as proton leak. Values represent mean ± SEM of 16 technical replicates.

Within the respiratory chain, CoQ10 is responsible for the transfer of electrons from complex I and complex II to complex III (Fig 4.35A). This allows the oxidation of NADH to NAD^+ by complex I and thus provides cofactors for the enzymes of the TCA cycle. Moreover, the conversion of succinate to fumarate by complex II requires the conversion of CoQ10 to $CoQH_2$ (Y. Wang et al., 2016). Therefore, inhibition of CoQ10 production was hypothesized to affect TCA cycle metabolites. For this purpose, [$U^{13}C$] glucose was traced into TCA cycle metabolites in control and simvastatin treated conditions. As expected, both labelled and

unlabelled fractions of several TCA cycle metabolites were reduced following statin treatment (Fig 4.35B). Moreover, levels of aspartate, which is produced from oxaloacetate, were also reduced by statin treatment (Fig 4.35C).

Ubiquinone also functions as an electron acceptor for the rate-limiting enzyme in the pyrimidine biosynthesis pathway, dehydroorotate dehydrogenase (DHODH) (Laredj et al., 2014). Most importantly, UMP levels were dramatically decreased in the presence of simvastatin and this was more pronounced in p53 deficient spheroids (Fig 4.35D). Thus, inhibition of CoQ10 synthesis by mevalonate pathway inhibition could also result in reduced UMP synthesis.

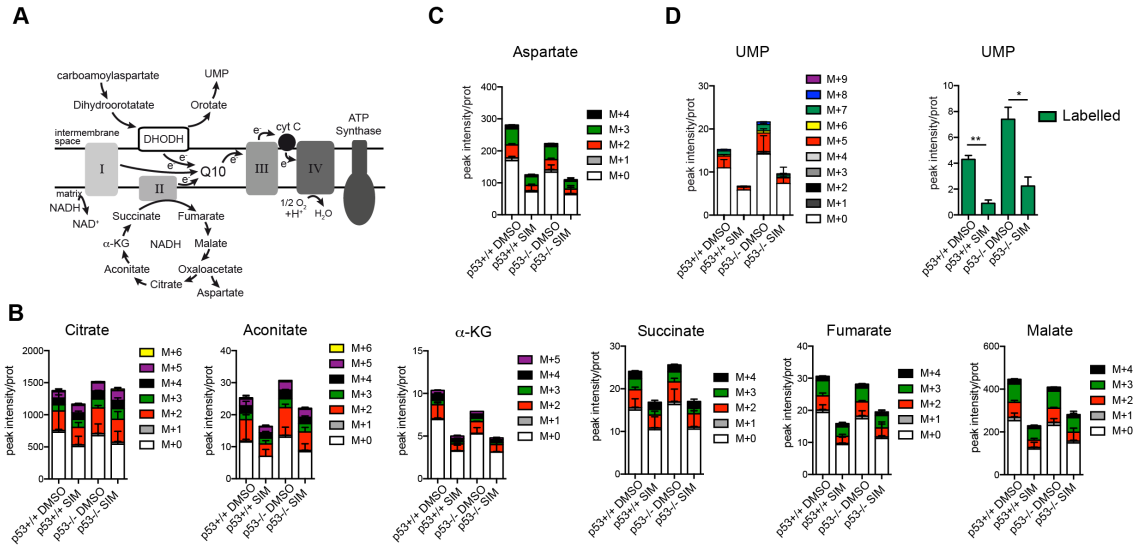

Figure 4.35: Inhibition of mevalonate pathway decreased levels of TCA cycle metabolites and precursors for pyrimidine nucleotide biosynthesis

A) Diagram showing the role of ubiquinone (CoQ10) in electron transport within the mitochondrial electron transport chain (ETC) and the conversion of dihydroorotate to orotate during pyrimidine biosynthesis.
B) HCT116 p53+/+ or p53-/- cells were grown as spheroids and treated with 10 μM simvastatin (SIM) or solvent (DMSO) for 72 hrs. For the last 16 hours, cells were labelled with [U^{13}C] glucose before cells were extracted and TCA cycle metabolite levels were analysed by LC-MS.
C) Aspartate levels were analysed by LC-MS
D) UMP levels were analysed by LC-MS. Values represent mean ± SEM (n=3, independent biological replicates). p-values were calculated using unpaired two tailed student t-test. ($p<0.01$, **; $p<0.05$, *)

Altogether these results revealed the importance of the effect of statins on CoQ10 production. In the case of statin treatment where CoQ10 synthesis was inhibited, reduction of TCA cycle intermediates and respiration was observed in the p53 deficient cells under metabolically compromised environment. In addition, inhibition of CoQ10 synthesis decreased levels of UMP production in spheroids, emphasizing the importance of CoQ10 in pyrimidine synthesis.

To understand the role of CoQ10 production in supporting cell viability under metabolic stress, spheroids were treated with simvastatin either alone or in combination with exogenous CoQ10 or nucleosides, since CoQ10 also affects the production of pyrimidines. To investigate the possibility that inhibition of the electron transport chain causes oxidative stress, N-acetyl-cysteine (NAC) rescue was also performed. As a result of the TUNEL staining, statin-induced cell death in p53 deficient spheroids was rescued by the addition of either CoQ10, NAC or nucleosides (Fig 4.36B and C), suggesting the depletion of CoQ10 as a metabolic vulnerability in p53 deficient cells. Although the decrease in UMP and CoQ10 was observed in both cell lines, simvastatin treatment led to the formation of ROS due to the inhibition of ETC and respiration in p53 deficient spheroids. Indeed, this was also consistent with the transcriptomic analysis, as the NFE2L2 gene set was specifically enriched in simvastatin treated p53 deficient compared to p53 WT spheroids.

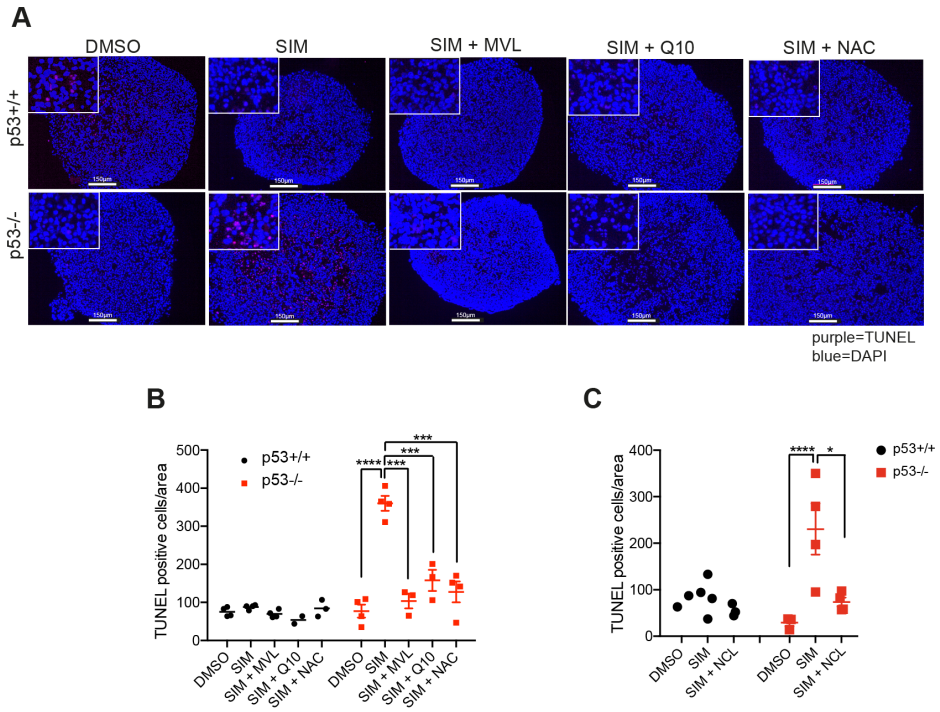

Figure 4.36: Cell death caused by inhibition of mevalonate pathway activity can be rescued with exogenous CoQ10, NAC and nucleosides

A) HCT116 p53+/+ or p53-/- cells were grown as spheroids and treated with 10 µM simvastatin (SIM) or solvent (DMSO) either alone or in combination with 10 µM ubiquinone (CoQ10) or 5 mM N-acetyl-cysteine (NAC) for 72 hours. Spheroids were fixed and histological sections were analysed for the presence of apoptotic cells by TUNEL staining. Images show representative results.
B) Quantitation of data shown in A. Values represent mean ± SEM and at least 3 spheroids analysed per condition. p-values were calculated using unpaired two tailed student t-test. ($p<0.0001$, **** ; $p<0.001$, ***; $p<0.01$, **; $p<0.05$, *)
C) Quantitation of data generated with HCT116 p53+/+ or p53-/- cells were grown as spheroids and treated with solvent (DMSO) or 10 µM simvastatin (SIM) either alone or in combination with nucleosides (150 µM each of cytidine, guanosine, adenosine, uridine and 50 µM of thymidine) for 72 hours.

Next, levels of polar metabolites were investigated after the simvastatin treatment with mevalonate or CoQ10 addition. Consistent with the previous data, all TCA cycle metabolite levels were decreased with the addition of simvastatin. Mevalonate addition restored levels of most TCA cycle metabolites to the level of control cells. Interestingly, CoQ10 addition increased the levels even above those seen in control samples (Fig 4.37A), suggesting that CoQ10 is rate-limiting for TCA

cycle activity. This was particularly obvious for aspartate (Fig 4.37B). Likewise, UMP levels were affected to the same degree as TCA cycle metabolites and could be restored by either mevalonate or CoQ10 addition (Fig 4.37B), confirming a metabolic coupling between mevalonate pathway and pyrimidine biosynthesis. Therefore, it can be concluded that CoQ10 supports cell survival in p53 deficient spheroids by maintaining TCA flux and allowing the production of pyrimidines.

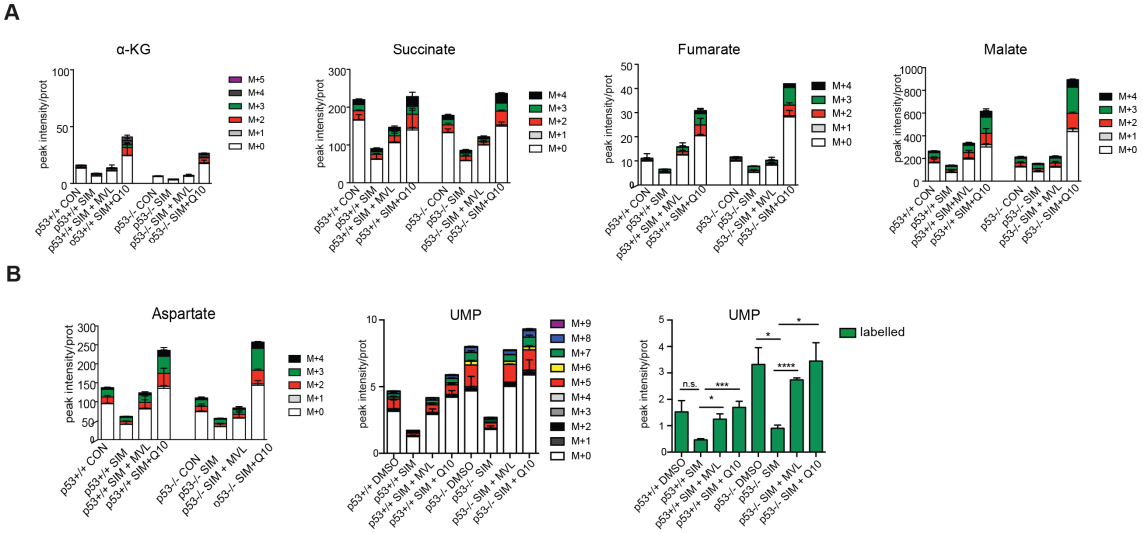

Figure 4.37: Mevalonate pathway activity is essential for pyrimidine nucleotide biosynthesis

A) HCT116 p53+/+ or p53-/- cells were grown as spheroids and treated with 10 µM simvastatin (SIM) or solvent (DMSO) and either with 0.5 mM mevalonate or 10 µM Q10 for 72 hrs. For the last 16 hours, cells were labelled with [U^{13}C] glucose before cells were extracted and TCA cycle metabolite levels were analysed by LC-MS. Values represent mean ± SEM (n=3, each biological replicate)
B) Relative peak intensities of aspartate and UMP isotopologues and labelled UMP fractions. p-values were calculated using unpaired two tailed student t-test. ($p<0.0001$, **** ; $p<0.001$, ***; $p<0.05$, *)

The chemotherapeutic 5-fluoro-uracil (5-FU) is a commonly prescribed anti-metabolite drug for the treatment of colorectal cancer and it has been demonstrated that it inhibits thymidylate synthase (TYMS) (Longley et al., 2003). The conversion of deoxy-UMP to dTMP was shown to be inhibited by 5-FU and the drug is a potent inhibitor of DNA and RNA synthesis, thereby causing DNA damage and cell death (Longley et al., 2002). Having shown that UMP synthesis is blocked by

the addition of statins, it was hypothesised that 5-FU and statins could synergise in affecting the viability of colon cancer cells in spheroid culture. For this purpose, p53 WT and deficient spheroids were treated with simvastatin and 5-FU for 72 hrs. Interestingly, p53 WT cells were largely resistant to single treatment with either 5-FU or simvastatin under the metabolically compromised environment. However, 5-FU treatment sensitised these cells to simvastatin treatment as a significant induction of apoptosis was observed in cells treated with a combination of both drugs (Fig 4.38). In contrast, in p53 deficient spheroids, cell death was already induced by simvastatin treatment alone and no synergy with 5-FU was observed. It is possible that DNA damage caused by 5-FU treatment increases the need for pyrimidine nucleotides in p53 WT cells, as p53 is required for the coordination of DNA repair (Sengupta et al., 2005). This renders p53 WT cells highly dependent on CoQ10 availability and sensitises them to mevalonate pathway inhibition. Taken together, these results suggest that 5-FU and statins could be a better strategy for targeting p53 WT colon cancer cells under metabolically compromised environment.

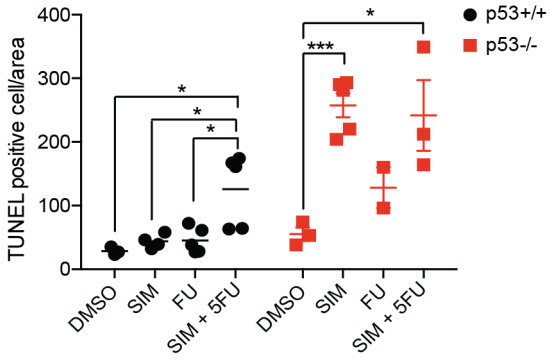

Figure 4.38: 5-FU combined with statins lead to death of p53 wild type cells under metabolic stress

Quantitation of data generated in HCT116 p53+/+ or p53-/- cells were grown as spheroids and treated with solvent (DMSO), 10 µM simvastatin (SIM), 10 µM 5-fluorouracil (5-FU) or a combination of the two for 72 hours. Spheroids were analysed by TUNEL staining. Values represent mean ± SEM and at least 3 spheroids analysed per condition. p values were calculated using unpaired two tailed student t-test. ($p<0.001$, ***; $p<0.05$, *)

4.3.3 Effect of inhibition of mevalonate pathway in mouse organoids

Colon cancer organoids have been established as organotypic disease models ex vivo (T. Sato et al., 2009). For this purpose, intestinal epithelial cells were used from mice carrying conditional alleles of *apc*, *p53* or mutant *Kras* (V12D) and expressing the Lgr5-EGFP-IRES-creERT2 transgene (T. Sato et al., 2011), which had been treated with tamoxifen to induce recombination. Due to their stem cell features, these cells grow as tumour spheres in organoid media with addition of growth factors such as R-spondin (for WNT signaling), epidermal growth factor (EGF) (for intestinal growth) and Noggin (for the expansion of crypt numbers) {Sato, 2009 #734. After several passages and growing several generations of tumour spheres, organoids were treated with simvastatin for 48 hrs and cultures were photographed and total sphere area per microscopic field was determined. Interestingly, $apc^{-/-}$ organoids were not affected by simvastatin treatment (Fig 4.39A, upper panel and Fig 4.39B) consistent with the results obtained in spheroid cultures. In contrast, sphere size of $apc^{-/-}$; *p53-/-*, $apc^{-/-}$; *p53-/-* and $apc^{-/-}$ $Kras^{V12D}$ organoids was substantially decreased following simvastatin treatment (Fig 4.39A, middle and lower panel and Fig 4.39B). Mevalonate was able to rescue the reduction in organoid size, confirming the specificity of the inhibitor. As the experiments described earlier showed that the mevalonate pathway is important for CoQ10 production and pyrimidine biosynthesis in tumour spheroids, organoid growth defect was tried to be rescued by the addition of exogenous ubiquinone or nucleosides. Indeed, reduction in organoid growth was restored by the addition of either ubiquinone or nucleoside mixture (Fig 4.39C and D), suggesting the general importance of the mevalonate pathway for providing metabolites for pyrimidine biosynthesis in cancer cells.

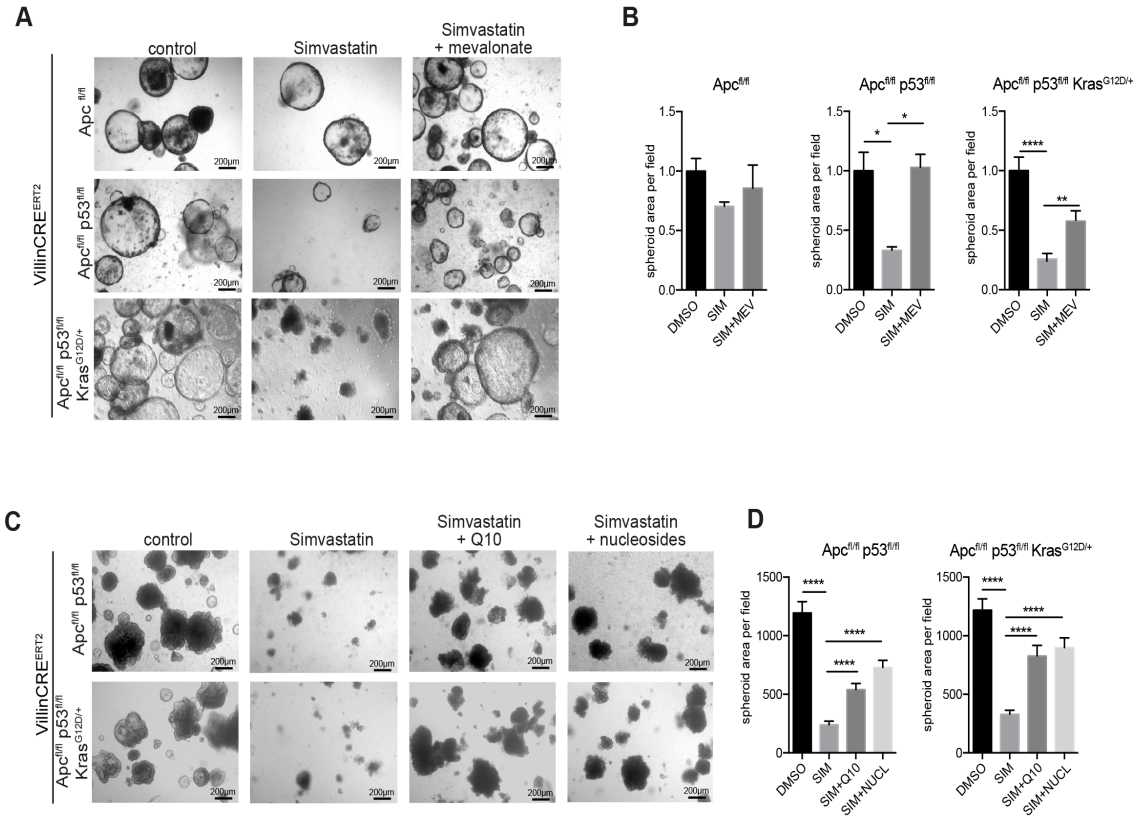

Figure 4.39: Simvastatin reduces growth of p53 deficient tumor organoids

A) Primary mouse intestinal cells derived from Villin CRE-ERT2; $Apc^{fl/fl}$, Villin CRE-ERT2; $Apc^{fl/fl}$;$p53^{fl/fl}$ or Villin CRE-ERT2;$Apc^{fl/fl}$;$p53^{fl/fl}$;$Kras^{G12D}$ animals were treated with tamoxifen *in vitro* and used to generate organoid cultures. Organoids were treated with 10 µM simvastatin (SIM) either alone or in combination with 0.5 mM mevalonate (MEV) for 48 hrs. Images show organoids in a microscopic field representative for each condition.

B) Quantitation of data shown in (A). Values represent mean ± SEM and at least 3 spheroids analysed per condition. p-values were calculated using unpaired two tailed student t-test. ($p<0.0001$, **** ; $p<0.001$, ***; $p<0.01$, **; $p<0.05$, *)

C) $Apc^{fl/fl}$;$p53^{fl/fl}$ or $Apc^{fl/fl}$;$p53^{fl/fl}$;$Kras^{G12D}$ organoids were treated with 10 µM simvastatin either alone or in combination with 10 µM ubiquinone (CoQ10) or nucleosides (150 µM each of cytidine, guanosine, adenosine, uridine and 50µM of thymidine) for 48 hrs.

D) Quantitation of data shown in (C). Values represent mean ± SEM and at least 3 spheroids analysed per condition. p-values were calculated using unpaired two tailed student t-test. ($p<0.0001$, **** ; $p<0.001$, ***; $p<0.01$, **; $p<0.05$, *)

Taken together, p53 deficient mouse organoids also displayed sensitivity towards simvastatin treatment, thereby replicating the findings from the tumour spheroids. In addition, growth defects induced by statins could be rescued via the addition of CoQ10 or nucleosides. This indicates the requirement of CoQ10 for pyrimidine biosynthesis, as seen in spheroids.

In conclusion, the results reported here have shown that the mevalonate pathway is induced in the p53 deficient cells. Statins were demonstrated to selectively kill p53 deficient cells under the metabolically compromised environments present in spheroid cultures and in tumour organoids. Reduction in CoQ10 resulted in the decrease of oxygen consumption rates and defective electron transport chain and most likely caused the formation of ROS. In addition, decreased levels of CoQ10 subsequently affected the production of UMP, which was more pronounced in p53 deficient cells, leading to cell death. Therefore, production of CoQ10 by the mevalonate pathway is essential for the viability of p53 deficient cancer cells under metabolically compromised environments.

4.4 Global approach to decipher p53 dependent vulnerabilities in metabolically compromised environments

Functional genetic screens were developed in recent years to identify novel genes, targets and pathways connected to a specific phenotype. RNAi and CRISPR/Cas9 systems are able to selectively perturb gene activity in cultured cells. Functional genetic screens are most frequently used in two formats: using arrayed or pooled libraries. For the pooled approach, large collections of shRNAs are pooled and used to transduce cells (Sims et al., 2011). After application of a selection condition, specific depletion of individual shRNAs can be revealed using next-generation sequencing.

To find the p53 selective vulnerabilities in colon cancer cells, a pooled shRNA screen was performed by using p53 isogenic cell lines cultured as monolayers or spheroids. For this purpose, the Decipher shRNA library focused on pathway targets (Module 1) consisting of 27500 individual shRNAs targeting 5000 genes was

used https://www.cellecta.com/resources. Before starting the screen, several setup experiments were performed in order to define optimal conditions for library representation and gene depletion.

As HCT116 p53+/+ and p53-/- cells were used for the screen, it was important to establish whether cells show a proliferation difference due to the presence or absence of p53. Doubling times for both cell lines were calculated according to the following equation:

$$\textit{Doubling time} = \frac{T\,(\ln 2)}{\ln (Xe/Xb)}$$

Xb: cell number at time point 0
Xe: cell number at the end of the experiment
T: time in any unit

where Xb is the number of cells at time point 0, Xe is the number of cells at the end of the experiment and *T* is time in any units.

Doubling times for monolayer cultures in full medium were determined to be 20 hrs for p53+/+ and 22 hrs for p53-/- cells. This experiments showed that there was no major difference in the proliferation between the HCT116 p53 isogenic cells.

In order to expose cells to metabolic stress, the shRNA screen was planned to be performed using spheroid cultures. Due to the size of the library, the 96-well spheroid generation method could not be used. Instead, spheroids were generated in bulk cultures using spinner flasks, in which cell aggregation is induced by slow stirring of the culture with a magnetic stirrer. Culture medium was changed every third day. During a three day culture, spheroid formation could be observed and these expanded further over 7 days to reach sizes similar to those of spheroids generated in 96-well plates.

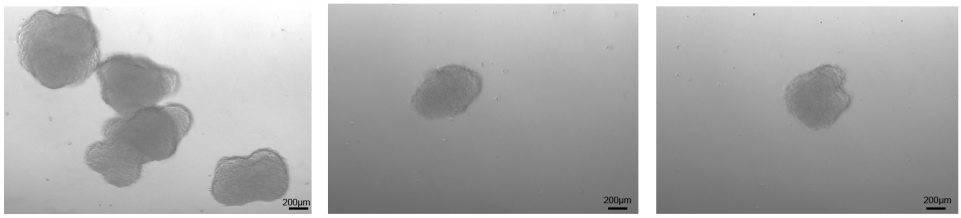

Figure 4.40: HCT116 p53+/+ cells are able to generate spheroids in spinner flasks

1 million of HCT116 p53+/+ cells were put into spinner flasks and cultured for 7 days. Representative pictures were shown from random spheroids.

In addition to calculating the doubling times for monolayer cultures, doubling times in spinner flasks were also calculated for spheroids cultured over 14 days to be 48 hrs for both genotypes (Fig 4.41A).

In order to confirm the efficient selection of cells after knock-down of an essential gene in spinner flask cultures, depletion of PFKFB4 was investigated. Depletion of PFKFB4 has been demonstrated to induce cell death in p53 deficient colon cancer cells (Ros, Floter, et al., 2017). Therefore, p53 deficient HCT116 cells carrying a non-targeting shRNA construct were co-transfected with pGIPZ deltaEco GFP plasmid. The same cell line expressing an shRNA targeting PFKFB4 was co-transfected with a pGIPZ deltaEco RFP plasmid. 75% positive RFP positive cells were mixed with 25% and placed into spinner flask cultures to form spheroids. Fluorescence intensity for GFP and RFP was analysed at different time points over 14 days using FACS. Surprisingly, the ratio of RFP to GFP positive cells was initially increased. However, at later time points this ratio was decreased abruptly (Fig 4.41B), leading to the conclusion that knock-down of PFKFB resulted in the efficient depletion of RFP positive cells from the culture. This supported the feasibility of the screening approach and confirmed that shRNA-mediated gene silencing exerts its effect in the metabolically compromised environments generated by spheroid culture using the spinner flasks method.

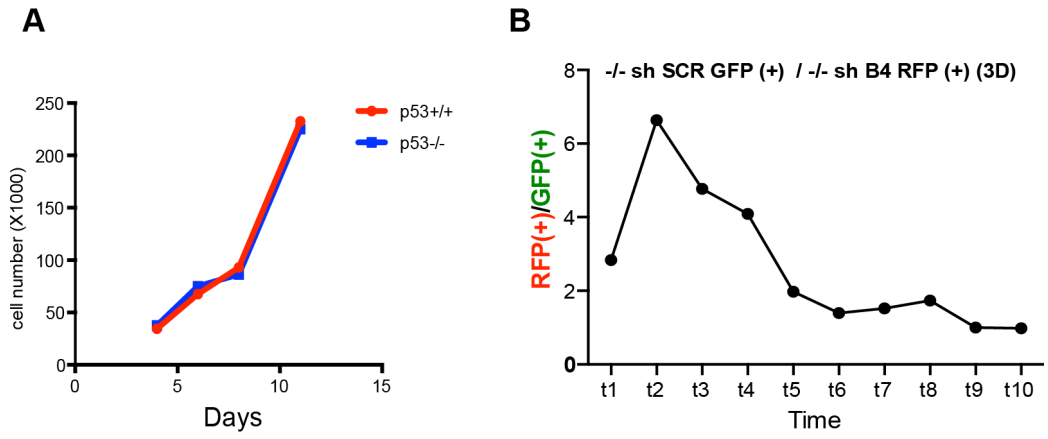

Figure 4.41: Spheroids form in the spinner flasks have same proliferation pattern

A) HCT116 p53+/+ and p53-/- cells were seeded at a density of 45.000 cells per 10 ml and grown in spinner flasks for 14 days. Doubling times were calculated according to the formula stated above

B) HCT116 p53-/- shSCR cells transduced with a GFP expression plasmid and HCT116 -/- shPFKFB4 cells transduced with an RFP expression plasmid were mixed and placed into spinner flasks and grown for 14 days. Every third day, samples for FACS analysis were taken and the ratio of RFP to GFP positive cells was evaluated.

After having set up the virus titre and infection conditions and establishing doubling times both in monolayer and spheroid culture, the shRNA screen was performed. For this purpose, HCT116 p53+/+ and p53-/- cells were infected with virus at an (multiplicity of infection) MOI of 0.3 in monolayer culture to assure each cell was infected at least once and selected with puromycin for 72 hours. After this time, 3 million cells were collected from both cell types and archived as time point zero (T_0). From the remaining cell population, 30 million cells per replicate were placed either in monolayer cultures or in spinner flasks to form spheroids for 14 days. In monolayer culture condition, cells were split several times and always 30 million cells were kept in culture. In the spinner flask culture, medium was changed every 3 days and cells were maintained throughout the curation of the experiment. At the end of 14 days (T_{end}), 30 million cells were collected and frozen from each condition. Genomic DNA was extracted and serial PCR reactions were performed in order to amplify the barcodes of the library prior to sequencing (Fig 4.42). For the analysis of the screen, z-scores were calculated from the normalised read counts of

the barcodes for each T_{end} condition compared to T_0. Genes were considered as potential hits when at least two shRNA sequences showed a z-score smaller than -2.

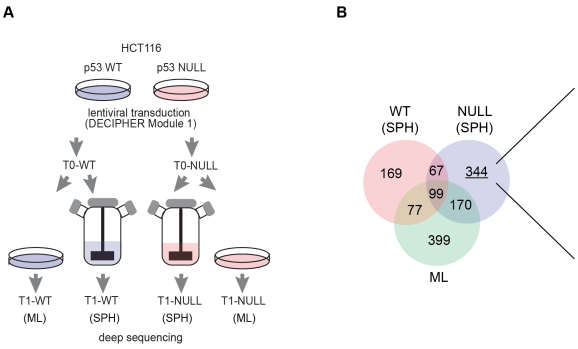

SYMBOL	NAME	# oligos	med Z-score
PSMA1	Proteasome Subunit Alpha 1	4	-14.9
RAN	RAN, Member RAS Oncogene Family	4	-15.1
PSMD6	Proteasome 26S Subunit, Non-ATPase 6	4	-9.9
TUBA1C	Tubulin Alpha 1c	4	-10.5
SNRPN	Small Nuclear Ribonucleoprotein Polypeptide N	3	-10.5
RPL30	Ribosomal Protein L30	3	-12.9
HDAC1	Histone Deacetylase 1	2	-9.2
MEF2D	Myocyte Enhancer Factor 2D	2	-6.4
ASCC3L1	Small Nuclear Ribonucleoprotein U5 Subunit 200	2	-8.5
SPTLC1	Serine Palmitoyltransferase Long Chain Base Subunit 1	2	-7.9
RUNX1	Runt Related Transcription Factor 1	2	-3.4
SNRPA1	Small Nuclear Ribonucleoprotein Polypeptide A	2	-7.4
INPP4A	Inositol Polyphosphate-4-Phosphatase Type I A	2	-5.1
RETN	Resistin	2	-5.7
CLTA	Clathrin	2	-4.6
CDK4	Cyclin Dependent Kinase 4	2	-5.2

Figure 4.42: shRNA screen identifies vulnerabilities of p53 deficient colon cancer cells exposed to metabolic stress

A) shRNA screen with lentiviral library (Decipher, Module 1) was performed in monolayer and bulk spheroid culture conditions. Screen scheme representing the time point (T_0) after the selection of infected cells and time point (T_{end}) after 14 days of culture under monolayer or spheroid condition. z-score was calculated based on T_0 in different culture conditions

B) Individual shRNA sequences depleted with a z-score ≤2 in p53+/+ (WT) or p53-/- (NULL) cells in spheroid cultures (SPH) were compared to those depleted in monolayers (ML) of either genotype. 344 sequences specific to p53-/- spheroids were selected. Genes with more than two sequences showing a z-score ≤-2 were selected. Table representing the list of selected genes showing the number of sequences and median z-scores.

shRNA sequences with a z-score lower than -2 only in spheroids from p53 deficient cells were selected. These 344 oligos were mapped to 16 genes for which at least two independent sequences were found. Among the selected genes, the top hit was RAN, a member in RAS oncogene family. In addition, several subunits of the proteasome and several ribosomal proteins were found as potenatial hits specific to p53 deficient spheroids.

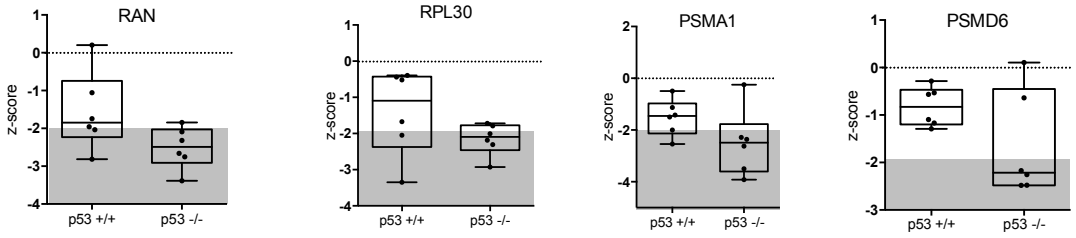

Figure 4.43: Ras family member, proteasome subunits and ribosomal proteins are identified as vulnerabilities in p53 deficient spheroids

Representative plots of z-scores of individual shRNA sequences in p53 wild type and p53 deficient spheroids for selected genes.

Interestingly, the group of proteasomal subunits scored prominently in p53 deficient tumour spheroids. It has been previously shown that mTORC1 requires proteasomal degradation of cellular proteins to maintain high intracellular amino acid levels and to perform quality control of newly synthesised proteins (Y. Zhang et al., 2014). Therefore, increased proteasomal activity serves as an adaptive response to increased protein synthesis in the cell. Based on these findings, it could be hypothesized that depletion of proteasomal subunits impairs the ability of p53 deficient cancer cells to maintain their amino acid pool for cell growth, resulting in reduced proliferation or selective cell death. This would be exacerbated by conditions of high mTORC1 activity. As the results described in section 4.2.3 demonstrated that phosphorylation of the ribosomal protein S6RB was increased in spheroid cultures indicating enhanced mTORC1 activity, depletion of proteasomal subunits could be particularly detrimental under these conditions.

RPL30 and other ribosomal proteins were also detected as potential targets in the p53 deficient spheroids. These factors are important regulators of protein biosynthesis and depletion of these components might therefore have an effect on growth and proliferation in the spheroids. In addition, depletion of these genes can cause nucleolar stress due to dysregulated ribosomal biogenesis, leading to cell death. In p53 WT spheroids, induction of cell death in response to nucleolar stress could be prevented by the canonical functions of p53 (Deisenroth et al., 2010). However, p53 deficient cells would not be able to adequately respond to the depletion of these

genes, resulting in excess nucleolar stress leading to cell death. Further experiments are needed to establish the exact function of the identified factors in supporting cell survival in p53 deficient cancer cells exposed to metabolic stress.

In conclusion, shRNA screening has been used to detect selective vulnerabilities of cancer cells in a metabolically compromised environment compared to the cells cultured in conventional monolayer cultures. Several candidate hits were identified that are specific to p53 deficient cancer cells. However, these hits need to be validated for further analysis.

5 DISCUSSION

5.1 HCT116 colon cells show different vulnerabilities under metabolic stress

5.1.1 Nutrient and oxygen starvation in monolayer affects viability of colon cancer cells

Carcinogenesis has been defined as a multistep process that includes alterations in signalling pathways, resulting in mutations that favour aberrant proliferation, which is an essential part of cancer development and progression (Feitelson et al., 2015). Due to their high metabolic activity, cancer cells are subject to gradients of nutrients and oxygen depending on their distance from the blood vessels. The diffusion limit of oxygen in tumours was reported to be between 100 and 200 μm (Eales et al., 2016). Thereby, in the tumour microenvironment, cancer cells residing near blood vessels are exposed to environments rich in nutrients and oxygen. In contrast, cells further from the blood vessels are deprived of nutrients and oxygen. Indeed, cancer cells reprogram their metabolism according to their demands for the production of energy and their biosynthetic needs under conditions of limited oxygen and nutrient availability. Many cancer cells support aerobic glycolysis, defined as the fermentation of glucose and produce lactate, even in the presence of oxygen, a phenomenon called the 'Warburg effect'. Although this phenotype is less energy effective, cancer cells favour aerobic glycolysis in order to obtain macromolecules for their biosynthetic needs. Reprogramming of metabolism in cancer cells depends on the respective biosynthetic needs of the cancer cells, the context of the tissue microenvironment, and activation of oncogenes and loss of tumour suppressors.

The combination of loss of tumour suppressor function with hypoxia and nutrient deprivation are important conditions that cancer cells experience in tumours. Therefore, determining the viability of p53 isogenic colon cancer cells under deprivation of several nutrients, such as serum, glucose and glutamine under

normoxia and hypoxia, is important to understand tumour suppressor function in the context of the microenvironment. This analysis showed that the metabolic stress resulted from the depletion of important nutrients and oxygen causes a decrease in cell viability. Moreover, the absence of the tumour suppressor p53 affects the survival of colon cancer cells under these conditions.

Glutamine is the most prominent amino acid in the serum and its levels are often diminished in several cancers (Kamphorst et al., 2015). Moreover, p53 was shown to induce the levels of the SLC1A3 aspartate/glutamate transporter to compensate for the effect of glutamine deprivation by maintaining glutamate uptake and nucleotide synthesis in the cells (Tajan et al., 2018). However, HCT116 cells express very low levels of this transporter (data obtained from RNA-SEQ, not shown) and are therefore vulnerable to the depletion of glutamine to the same extent in normoxia and hypoxia. Several reports have demonstrated the effect of serum deprivation on cancer cell viability via the modulation of different signalling pathways (Ackerman et al., 2018; Young et al., 2013). Moreover, decreased glucose levels led to the activation of AMPK and phosphorylation of p53 at S15, thereby blocking cell proliferation (R. G. Jones et al., 2005).

The results of the first part of this thesis demonstrated that p53 isogenic colon cancer cells displayed different vulnerabilities, thus confirming the role of p53 in protecting against nutrient deprivation. In addition, p53 deficient cells showed more sensitivity towards a lack of oxygen, emphasizing the role of p53 in the hypoxia response.

The exact role of p53 in the regulation of hypoxic responses is still not fully understood in the literature (Humpton et al., 2016). As a consensus, severe hypoxia was identified to induce apoptosis in cancer cells by upregulating p21 and also many other stress related responses (Carmeliet et al., 1998). Hypoxia generally induces p53; however, this response might depend on the cellular context, as in some cases hypoxia has no impact on p53 (Sermeus et al., 2011). There are reports suggesting that the secondary effects of hypoxia, such as the induction of acidosis and DNA damage, are sufficient to induce p53 (Choudhry et al., 2018). Interestingly, the results described in section 4.1.1 of this thesis show that p53 deficient colon cancer

cells tend to be more sensitive to the lack of oxygen. Indeed, p53 can act as a guardian for cells with elevated levels of ROS caused by severe hypoxia by inducing antioxidant mechanisms. In contrast, ROS leads to cell death in p53 deficient cells because of the lack of these antioxidant mechanisms (Bensaad et al., 2009). Taken together, it was established that HCT116 wild type and p53 deficient colon cancer cells are both vulnerable to glutamine deprivation, whereas p53 exerts a protective effect during lack of oxygen, serum and glucose, suggesting the importance of p53 in the context of the microenvironment. Therefore, more detailed analyses were conducted to reveal the vulnerabilities of p53 isogenic colon cancer cells in tumour spheroids that are representative models of the oxygen and nutrient gradients found in tumours.

5.1.2 Spheroid cultures recapitulate important tumour features *in vitro*

In order to mimic the metabolically deprived tumour microenvironment *in vitro*, multicellular tumour spheroids were used in this study. Spheroids are frequently used as *in vitro* models of cancer and make use of the ability of cancer cells to aggregate into large structures that contain nutrient and oxygen gradients (R. M. Sutherland, 1986). Since tumour cells need energy and nutrients for growth, cell proliferation is limited to areas in close vicinity to the vascular network. Therefore, tumour spheroids are good models of the tumour microenvironment as they represent proliferation gradients according to the oxygen and nutrients levels (Pampaloni et al., 2007).

Results that were obtained in this study revealed that proliferation was regulated differentially under metabolically compromised environments and in monolayers. Indeed, cells cultured as spheroids displayed overall slower proliferation compared to the monolayer cultures. Moreover, histological analysis revealed different proliferation patterns between p53 wild type and p53 deficient spheroids. Spheroids formed by p53 WT cells had a ring of proliferating cells at the outer part where nutrients and oxygen are readily available, whereas p53 deficient cells displayed a homogenous proliferation pattern throughout the spheroid, even within the core. This suggests that loss of p53 provides a growth advantage to cells under metabolic stress. Indeed, p53 WT cells at the core of the spheroids, where there is

lack of nutrient and oxygen, displayed cell death up to a certain level. In contrast, spheroids formed by p53 deficient cells did not show any signs of apoptosis. Interestingly, the same cells cultured as monolayer and placed under hypoxia and low levels of nutrients displayed reduced cell viability, suggesting that the severity of metabolic stress in this condition might not be reached in spheroids. Moreover, cell-cell contact in the spheroid condition might provide a survival signal specifically to p53 deficient cells by inducing different signalling pathways (Balzer et al., 2012). In addition, pimonidazole which stains the adducts of thiol groups in proteins when oxygen is absent, stained the region between outer and inner core in the p53 WT spheroids, whereas p53 deficient spheroids were stained homogenously (Fig 4.3B), except for the outer layer which has access to ambient oxygen. However, ECAR levels that measure the conversion of glucose to lactate were similar between p53 WT and deficient spheroids, suggesting the overall induction of glycolysis due to lack of oxygen is quite similar in both genotypes.

One possible explanation for the depletion of proliferation in spheroids could be due to the induction of hypoxia. Unexpectedly, spheroid culture did not lead to the induction of HIF1a whereas monolayer cells cultured at 0.5% oxygen showed clear accumulation of HIF1a (Fig 4.3A), demonstrating the hypoxia level in the spheroids was less severe. Indeed, Jiang *et al* identified the oxygen concentration where HIF1a gets activated to be 0.5% and that this activation gradually decreases with increasing concentration of oxygen in the environment (B. H. Jiang et al., 1996).

Overall, these analyses suggested that spheroids can be used as a suitable *in vitro* model to mimic important aspects of the tumour phenotype as they displayed more similarities with the tumours in contrast to cells cultured in monolayer.

Global transcriptome analysis that was performed to compare monolayers, spheroid cultures and xenograft tumours supported the findings mentioned above with a clear hypoxia signature induced only in spheroids and tumours. Moreover, the comparison of p53 WT and p53 deficient cells cultured as monolayers revealed the induction of p53 targets in p53 WT cells. However, when the same comparison was performed in spheroids and tumours, canonical p53 targets were not higher expressed in p53 WT cells. As part of its canonical function, the

tumour suppressor p53 is activated by DNA damage and metabolic stress and induces DNA repair, cell cycle arrest and apoptosis (Vousden et al., 2007). Moreover, p53 also regulates different aspects of metabolism by inhibiting the Warburg phenotype and by promoting mitochondrial metabolism and oxidative phosphorylation (Floter et al., 2017). However, no clear gene expression signatures associated with glycolysis or mitochondrial metabolism were identified as differentially regulated in these experiments.

Most importantly, inflammatory signatures were strongly associated with p53 WT cells in all conditions (Fig 4.5B). Previously, it was shown that p53 activates NF-κB signalling by transcriptionally inducing the IFN regulatory factor 9 (IRF 9) in mouse embryonic fibroblasts (MEFs) and in HCT116 colon cancer cells after viral infection and *in vivo* (Munoz-Fontela et al., 2008). Similarly, another study demonstrated $p19^{ARF}$ as an inhibitory factor for interferon beta production in cancer cells, and showed that p53 deficient cells display elevated levels of $p19^{ARF}$, confirming the suppression of inflammation signalling by loss of p53 (Forys et al., 2014). Moreover, p53 has been described as a target of IFN α / β, and IFN α / β helps to promote the anti-proliferative response of p53 triggered by metabolic stress and DNA damage (Takaoka et al., 2003). Overall, these signatures might be observed due to the canonical function of p53. However, additional work is required to understand the mechanism of p53 induction.

In addition to the regulation of inflammation by p53, several reports have demonstrated that hypoxia induces the expression of inflammatory genes and there is cross-talk between HIF signalling and nuclear factor-kappa B (NF-κB) (Bertout et al., 2008). NF-κB is a well-known transcription factor that gets activated by several cellular stresses, including hypoxia, and is known as a regulator of an anti-apoptotic and inflammatory response mediated by Janus kinase 1 (JAK1) and signal transducer and activator of transcription (STAT) proteins (Yoon et al., 2010). The canonical induction of NF-κB might be due to the need for protecting cells from the metabolic stress caused by hypoxia and nutrient deprivation. However, as part of its non-canonical activity, activated NF-κB also induces transcription of *HIF1A* mRNA and the *HIF1A* promoter has a binding site for NF-κB (Taylor, 2008). Interestingly,

HIF1a also functions as a transcriptional regulator of NF-κB, as overexpression of HIF-1a in mouse keratinocytes promotes NF-κB target genes causing an inflammatory stimulus (Scortegagna et al., 2008). Therefore, in spheroids and tumours, the induction of the inflammation and hypoxia signatures might suggest cross talk between HIF1a and NF-κB. Moreover, ROS was reported to promote NF-κB by inducing upstream kinases, such as inhibitor of kappa B kinase (IKK) and c-Jun N-Terminal kinase (JNK), suggesting that production of ROS in cells exposed to metabolic stress also promotes the expression of NF-κB target genes to promote survival under unfavourable conditions.

Taken together, global expression analyses revealed that spheroids can recapitulate the tumour features *in vitro* by showing hypoxia as a prominent gene signature that was observed both in spheroids and tumours, whereas increased proliferation was the determining gene signature in monolayer cultures. In addition, hypoxia could be an additional factor to enhance the inflammatory phenotype that was observed also in spheroids and tumours. However, additional work is needed to reveal the exact mechanism of the induction of these inflammatory signatures by p53.

5.1.3 HCT116 cells undergo metabolic reprogramming under spheroid conditions

Analysis of the metabolic reactions that are performed by using stable isotope labelled metabolites is one of the most commonly used methods to assess the metabolic rewiring in cells and organisms. Metabolomics analysis performed as a time course in colon cancer cells cultured as monolayers and spheroids revealed results consistent with the hypoxia gene signature that was obtained in the global transcriptome analysis.

Most importantly, as glucose and glutamine are the most commonly used fuels for the TCA cycle (C. Yang et al., 2014), stable isotope labelling can be used to reveal the relative contribution of different nutrients to TCA cycle metabolites. The isotopologue distribution for glutamate and aspartate in monolayer cultures after glucose labelling suggested that glutamine might contribute to their isotopologue

distribution (Fig 4.9A). Glutamine can enter the TCA cycle in two different ways: it can either be converted to glutamate and then to a-KG by glutamate dehydrogenase and with subsequent oxidative reactions of the TCA cycle to oxaloacetate, or it can be reductively converted to isocitrate by isocitrate dehydrogenase and to citrate (reductive carboxylation), which is enhanced in hypoxia (Metallo et al., 2011; Wise et al., 2011). However, stable isotope tracing experiments using labelled glutamine are needed to demonstrate the contribution of glutamine to colon cancer cell metabolism in monolayer cultures.

Another striking finding from the metabolomics analysis was the rapid generation of m+3 isotopologues of succinate, fumarate and malate in spheroids. This indicates that glucose-derived pyruvate enters the TCA cycle via the activity of pyruvate carboxylase. Moreover, the ratio of the m+3 isotopologue of aspartate, derived from this anaplerotic reaction, to its m+2 isotopologue, derived from PDH driven TCA cycle, was induced in spheroids, confirming the enhanced relative activity of pyruvate carboxylase in spheroid cultures. Hypoxia has been shown to inhibit PDH activity (Golias et al., 2016) and to promote pyruvate-dependent anaplerosis (Christen et al., 2016). Indeed, pyruvate carboxylase is induced under hypoxia and pyruvate-dependent anaplerosis has been observed under hypoxic conditions (O. E. Owen et al., 2002). Along those lines, Christen *et al* demonstrated that breast cancer cells proliferating as lung metastases displayed metabolic rewiring and induced pyruvate carboxylase activity to adapt to the lung microenvironment (Christen et al., 2016), suggesting the importance of pyruvate-dependent anaplerosis. In addition, pyruvate-dependent anaplerosis was reported as a compensation mechanism of glutamine addicted cells for their survival under glutamine depleted conditions (Cheng et al., 2011). Moreover, pyruvate carboxylation can function as an alternative program to generate aspartate for cells that carry SDH mutations, leading to a truncated TCA cycle (Cardaci et al., 2015).

In addition, it was observed that aspartate levels were slightly reduced in p53 deficient spheroids (Fig 4.12A). A likely explanation for this observation is that p53 deficient spheroids use more aspartate for pyrimidine (UMP) synthesis compared to their wild type counterparts. This was also confirmed by higher levels of glucose-derived labelling of UMP observed in p53 deficient cells. Aspartate is a non-essential

amino acid and important for the synthesis of the ring of pyrimidine nucleobases as it provides three carbon atoms, derived from either glutamine or glucose, to the UMP molecule (A. N. Lane et al., 2015). Interestingly, the contribution of glucose carbons to UMP was overall reduced in spheroids. Based on this observation, it can be concluded that overall proliferation is reduced in spheroids, as also shown by further analyses, and thus requires lower activity of nucleotide biosynthesis pathways. However, p53 deficient spheroids upregulate pyrimidine biosynthesis and have to reprogram their metabolism so that aspartate can be used for UMP synthesis. Therefore, aspartate might be the limiting factor for the growth and proliferation of p53 deficient cells under metabolic stress.

Taken together, the experimental setup used here provides a clear way to reveal the metabolic rewiring in complex systems and helps to understand the contribution of different fuels that cells need under specific conditions. Using this method, it could be demonstrated that spheroids undergo a specific metabolic reprogramming caused by hypoxia in order to generate metabolites for the cell survival and proliferation under metabolic stress.

5.1.4 p53 inhibits cholesterol synthesis under metabolically compromised environments

Interestingly, p53 deficient spheroids and tumours upregulated gene signatures associated with cholesterol biosynthesis and SREBP targets. Most importantly, these gene signatures were not present in the p53 deficient cells cultured in monolayer. Although the HORTON_SREBF target gene signature includes several *SREBF1* targets, such as *FASN, ACC and ACLY*, the mostly strongly upregulated genes are those controlled by SREBP2. Previously, Yahagi *et al* demonstrated that p53 represses the expression of SREBP1 targets in ob/ob mice (Yahagi et al., 2003). Moreover, mutant p53 was shown to associate with promoters via SREBP2 transcription factors, either directly or via the p53 interacting partners NF-Y and SP1, and to promote the expression of the genes related to the mevalonate pathway (Freed-Pastor, Mizuno, et al., 2012). Through this mechanism, mutant p53 affects the mammary acinar morphology and promoted breast cancer progression via regulating the mevalonate pathway (Freed-Pastor, Mizuno, et al., 2012). Conversely, wild type

p53 has been demonstrated to exert its tumour suppressive functions by repressing the mevalonate pathway (Moon et al., 2018). Binding of SREBP2 to the promoters of its target genes was increased in p53 deficient cells and p53 was shown to induce the expression of the ATP-binding cassette 1 (ABCA1) transporter to prevent the maturation of SREBP2 both *in vitro* and *in vivo* (Moon et al., 2018). In summary, repression of the mevalonate pathway provides additional mechanistic explanation of how p53 reprograms metabolism in cancer cells and acts as a tumour suppressor. In addition, the induction of gene sets associated with the cholesterol biosynthesis seems to be strongly dependent on the microenvironment and the inhibitory function of p53.

One possible explanation why SREBP2 targets were not significantly induced in p53 deficient cells cultured in monolayer could be that p53 is not activated in monolayer conditions, possibly due to the lack of oxidative stress. Indeed, Moon *et al* showed the inhibitory effect of p53 on SREBP2 activation was increased by Nutlin, a chemical that is used as a p53 activator (Moon et al., 2018). Conditions inducing metabolic and/or oxidative stress, such as spheroid cultures or tumours, activate p53 and allow it to exert its tumour suppressive functions by inhibiting the expression of SREBP2 targets. Interestingly, the expression of SREBP2 targets was already increased in wild type spheroid cultures, leading to the hypothesis that SREBP might act as a hypoxia sensor. In fact, Lewis *et al* demonstrated that the expression of SREBP1 target genes was induced under hypoxia (Lewis et al., 2015). In addition, the yeast SREBP homologue, SRE, was shown to upregulate the expression of cholesterol pathway genes in response to reduced oxygen levels, suggesting SRE-mediated oxygen sensing (Hughes et al., 2005). Although this has not yet been shown in mammalian systems, the induction of SREBP2 targets in hypoxia could be an indication of an oxygen sensing feature of SREBP regulation. Moreover, the loss of p53 further increased the expression of SREBP2 targets leading to the conclusion that active p53 inhibits SREBP2 under metabolically compromised environments.

5.2 Regulation of cholesterol biosynthesis genes in monolayer and spheroid cultures

Expression of the genes that play role in cholesterol biosynthesis is mainly driven by the transcription factor SREBP2 (Horton et al., 2002b). As mentioned previously, SREBPs get proteolytically cleaved when sterol levels are low and the N-terminal domain translocates to the nucleus and drives the expression of SREBP target genes (Brown et al., 1997). Indeed, expression of *HMGCS1* and *HMGCR* was induced under low serum conditions, especially in p53 deficient cells. Having observed the inhibitory effect of p53 on the expression of SREBP2 target genes, but not on the expression levels of *SREBF2* itself, suggests that SREBP2 could be regulated post-transcriptionally. Indeed, mSREBP2 levels were upregulated in the nuclear fraction of p53 deficient cells under low serum.

It was previously demonstrated in hepatic chromatin, that SREBP1 and SREBP2 binding profiles show 12% overlap at DNA binding sites associated with lipid metabolism genes (Jeon et al., 2012). In this project, the results proved that silencing of SREBP2 abolished the induction of HMGCS1 and HMGCR in p53 deficient cells, suggesting that SREBP2 is responsible for the increased expression of mevalonate pathway genes in p53 deficient spheroids cultures.

Taken together, these results demonstrated that spheroid culture and low serum both induce the levels of mature SREBP2. This is further enhanced by the loss of p53 function. Based on these results, finding the mechanism as to how SREBP2 is regulated under these conditions was the next focus of the study.

5.2.1 SREBP2 is regulated via GSK3 and mTORC1

It has been demonstrated previously that AKT dependent activation of SREBP requires mTORC1 (Porstmann et al., 2008) and lipogenesis in the liver occurs through SREBP1 depending on mTORC1 (Yecies et al., 2011). The molecular mechanism as to how mTORC1 activates SREBP2 is not fully understood but it is

likely that downstream targets of the mTORC1 pathway are involved. Several groups have shown that mTORC1 can induce SREBP processing through the mTORC1 regulated protein kinase S6K (X. Liu et al., 2012; J. L. Owen et al., 2012; B. T. Wang et al., 2011). Thereby, investigating mTORC1 activity could give important insight into the mechanism by which SREBP2 is regulated in spheroids.

Interestingly, S6RB, a direct phosphorylation target of S6K, was strongly phosphorylated in spheroids, confirming higher mTORC1 activity. This is unexpected, considering the fact that spheroids are models for limited nutrients and oxygen. One possible explanation for this observation could be the lack of TSC1/2 in the spheroid conditions, indeed gene expression analysis showed downregulation of TSC2 expression in spheroids (data not shown). Although p53 has been shown to inhibit mTORC1 (Budanov et al., 2008), this inhibitory effect cannot be exerted in TSC deficient cells, explaining the high S6K activity in spheroids.

Furthermore, the inhibition of mTORC1 via rapamycin treatment downregulated the expression of SREBP2 targets in spheroids. These findings are consistent with the report by Peterson et al., showing the inhibition of mTORC1 represses levels of mature SREBP2 in NIH3T3 cells by controlling the nuclear entry of LPIN1 (phosphatidic acid phosphatase), which binds to mature SREBPs leading to their sequestration to the nuclear lamina. This keeps the transcription factors away from the promoters of their target genes (Peterson et al., 2011). In addition, Ricoult *et al* have identified mTORC1 and S6K as a regulator of both SREBP1 and SREBP2 in breast epithelial cells with active K-Ras and PI3K (Ricoult et al., 2016).

As described previously, phosphorylation by GSK3 promotes SREBPs for proteasomal degradation (Sundqvist et al., 2005). Importantly, it was shown that phosphorylation of GSK3 leads to the inhibition of its kinase activity (Cohen et al., 2001). The results in this study have demonstrated that p53 deficient spheroids display elevated levels of phosphorylated GSK3. One possible explanation could be that induction of hypoxia in the spheroids increases the phosphorylation of GSK3. Indeed, it was shown that hypoxia promotes the activating phosphorylation of AKT (at S473) leading to phosphorylation and the inhibition of GSK3 (Beitner-Johnson et al., 2001). However, AKT phosphorylation was not investigated in this study. Also,

constitutively active S6K was shown to phosphorylate GSK3 (H. H. Zhang et al., 2006), which could further contribute to the high phosphorylation levels of GSK3 in spheroids.

Based on these observations, it can be concluded that inhibition of GSK3 activity via phosphorylation leads to the stabilization and accumulation of mature SREBP2 in p53 deficient cells cultured in spheroid culture. Interestingly, the inhibition of GSK3 by SB-216753 and CHIR99021 compounds led to the restoration of HMGCS1 expression, both at mRNA and protein level, in wild type p53, suggesting that GSK3 regulates the stability of SREBP2 in spheroids. Taken together, it can be concluded that loss of p53 induces the expression of SREBP2 targets under metabolic stress and this can be explained by the regulation of SREBP2 via mTORC1 and GSK3, leading to changes in both its activity and stability.

5.2.2 Metabolic rewiring in the cholesterol pathway under spheroid condition

Metabolic characterization of the cholesterol pathway also revealed interesting results. The mevalonate pathway starts with the condensation of three molecules of acetyl-CoA to form HMG-CoA. To monitor the activity of the mevalonate pathway, stable isotope labelled glucose was traced into acetyl-CoA over different time points. In addition, as cholesterol synthesis provides several metabolites that are essential for cell survival (Mullen et al., 2016), stable isotope labelled glucose was traced into mevalonate, cholesterol and CoQ10, and individual isotopologues were evaluated to reveal how this pathway is metabolically reprogrammed in spheroids.

Interestingly, the contribution of glucose carbons to cholesterol synthesis and the total levels of cholesterol were lower in p53 deficient spheroids compared to their wild type counterparts. In contrast, labelling into CoQ10 was much higher in p53 deficient spheroids, suggesting a metabolic rewiring of the cholesterol pathway in p53 deficient spheroids. Nevertheless, both in spheroids from p53 WT and p53 deficient cells the peaks for the isotopic fractions were located in similar places. Kamphorst *et al* showed that the pattern of isotopologues of metabolites that use acetyl-CoA as a carbon donor displays a binomial distribution as a representation of the percentage of

the labelled cytosolic acetyl-CoA pool. Increase in acetyl-CoA labelling was reported to shift the distribution peak to the right as more labelled precursors are incorporated (Kamphorst et al., 2014). Based on these findings, it can be concluded that the percentage of glucose-derived labelling in the acetyl-CoA pool was similar in both cell types.

Taken together, stable isotope labelling revealed the metabolic rewiring between p53 wild type and p53 deficient spheroids. Although, mevalonate levels were higher in p53 deficient spheroids, cholesterol levels have not reflected this difference. In contrast, p53 wild type spheroids displayed high cholesterol levels; whereas p53 deficient spheroids had high CoQ10 levels suggesting the request for CoQ10 in other metabolic reactions which will be discussed in the next chapter.

5.3 Inhibition of the mevalonate pathway has different affects on cancer cells under different culture conditions

Statins, a class of cholesterol-lowering drugs, are widely used substances that inhibit the rate-limiting enzyme in the mevalonate pathway (HMGCR) via competitive inhibition (Agarwal et al., 1999). As they are structural analogues of HMG-CoA, they represent a high affinity for binding to the active site of the HMGCR enzyme and completely suppress *de novo* cholesterol synthesis. Moreover, statins promote the clearance of cholesterol from blood via enhancing the expression of LDLR (Istvan et al., 2001). Besides their mode of action as cholesterol-lowering drugs, it has been demonstrated that a subset of patients benefit from anticancer statin therapy (Sassano et al., 2008) and different statins inhibit the growth of colorectal cell lines *in vitro* (Agarwal et al., 1999; J. C. Liu et al., 2016; Sehdev et al., 2014). For instance, atorvastatin combined with celecoxib (a selective COX-2 inhibitor) was reported to repress intestinal tumourigenesis in APC^{min} mice whereas atorvastatin alone displayed only mild effects on the reduction of tumourigenesis (Swamy et al., 2006). However, most clinical trials investigating the efficacy of statins were inconclusive, mainly because of dosage problems (Lochhead et al., 2013). Moreover, the exact mechanism by which statins exert their effect on cell viability in tumours is not well-known.

5.3.1 Statins have detrimental effects on cancer cells cultured in monolayer

When investigating the effect of simvastatin on mevalonate pathway activity in monolayer cells, it could be implied that the drug efficiently diminished both CoQ10 and cholesterol levels. However, comparison of the basal levels of these metabolites showed no clear differences between p53 WT and deficient cells, suggesting that the p53 dependent metabolic rewiring of the mevalonate pathway is absent in monolayer cultures.

Moreover, when oxygen consumption rates were investigated, simvastatin alone resulted in a small reduction of OCR both in wild type p53 and p53 deficient cells. The addition of mevalonate was unable to restore respiration, suggesting that the respiration defect in monolayer cultures was caused by another mechanism.

Based on the findings in the literature, the effect of different types of statins (type-1 and type-2) on cell viability was investigated. Both type-1 statins (simvastatin and mevastatin with a decalin ring structure) and type-2 statin that are fully synthetic (cerivastatin) strongly decreased cell viability in monolayer cultures. Importantly, while mevalonate was able to rescue the cell viability, this was not observed for CoQ10, suggesting that CoQ10 production is not essential for cell viability in monolayer cultures.

5.3.2 Inhibition of the mevalonate pathway induces apoptosis selectively in p53 deficient spheroids

After having observed the effects of statins in monolayer cells, their effects on cell survival in spheroids was analysed revealeing that the viability of p53 wild type cells was not affected by statin treatment. In contrast, p53 deficient cells in the centre of the spheroids displayed evidence of apoptotic cell death, suggesting the selective vulnerability of these cells under conditions of oxygen and nutrient starvation also present in the tumour microenvironment.

Transcriptomic analysis revealed the upregulation of gene signatures associated with the SREBP 'Hallmark Cholesterol homeostasis' and 'Horton SREBP Targets' in the presence of simvastatin both in p53 wild type and p53 deficient spheroids. This is likely caused by alleviating the feedback inhibition due to reduced cholesterol levels (Brown et al., 1997).

Furthermore, statins downregulated the 'Chang cycling', 'KEGG Ribosome' and 'MYC targets' gene sets, which are all associated with proliferation, both in wild type p53 and p53 deficient cells (Fig 4.29A). Canonical MYC targets and genes encoding ribosomal proteins have been shown to be among the most actively transcribed genes (Ji et al., 2011; C. Y. Lin et al., 2012), indicating that statins might inhibit global gene expression due to reduced availability of ribonucleotides. MYC has previously been demonstrated to be a proliferation inducing transcription factor in the intestine for the adenomatous polyposis coli tumour suppressor protein (APC) (Sansom et al., 2007). Similar to other E-box transcription factors, MYC is phosphorylated by the MAPK/ERK pathway at S62, leading to its stabilisation, while subsequent phosphorylation on T58 by GSK3 targets the protein for proteasomal degradation once S62 is dephosphorylated (Yeh et al., 2004). Interestingly, Myant *et al* demonstrated that S62 phosphorylation of MYC is necessary for progenitor cell proliferation and intestinal regeneration upon DNA damage (Myant et al., 2015). Moreover, mutations in these phosphorylation sites were reported to promote tumourigenesis in many cell types.

In the light of this data, the inhibition of MYC function could be one potential mechanism by which statins reduce cancer cell viability. Interestingly, spheroid cultures displayed overall higher S62 phosphorylation levels of MYC compared to monolayer cultures that are highly proliferative (Fig 4.29D), indicating higher stability of the protein. A potential explanation for this paradoxical result could be that MYC functions as a regulator for the cellular redox balance in spheroid cultures. MYC binds to the promoters of γ-glutamyl-cysteine (γ-GCS), the rate-limiting enzyme catalyzing GSH biosynthesis and S62 phosphorylation is essential for c-MYC recruitment. Thus, MYC activates a glutathione mediated survival pathway to support resistance to oxidative stress (Benassi et al., 2006). Indeed,

increased levels of oxidative stress caused by hypoxia and insufficient nutrient might induce S62 phosphorylation of MYC in spheroids. Moreover, spheroid cultures expressed an additional form of MYC, which is derived from an upstream start codon and associated with culture at high density (Hann et al., 1992). However, the exact function of this isoform of MYC is not fully established.

Although statins reduced the expression of gene signatures associated with MYC function, levels of MYC protein and S62 phosphorylation of MYC were unchanged in the presence of statins. This suggests that statins do not repress MYC *per se*, but that the reduction in expression of its target genes is caused by reduced availability of nucleotides. Indeed, MYC has been suggested as a sensor of cellular nucleotide provision (Dejure et al., 2017).

Interestingly, gene sets associated with the proliferation are downregulated both in the p53 WT and p53 deficient spheroids, cell death was only observed in p53 deficient spheroids under statin treatment. This might be explained by other stress responses that lead to the activation of the protective mechanisms associated with p53 function. In the absence of p53, cells are unable to engage in these programmes and undergo apoptosis. Indeed, gene sets associated with the stress response 'SINGH NFE2L2 TARGETS' were significantly upregulated in simvastatin treated p53 deficient spheroids (Fig 4.30), suggesting the presence of oxidative stress. The Nuclear Factor, Erythroid 2 Like 2 (NRF2) is the transcription factor responsible for the expression of detoxifying enzymes and antioxidant stress proteins in response to oxidative stress by binding to the antioxidant response element (ARE) (Gorrini et al., 2013). In the absence of oxidative stress, Kelch Like ECH Associated Protein 1 (KEAP1) contributes to the rapid turnover of NRF2 by promoting its proteasomal degradation (Kobayashi et al., 2004). Statins have been reported to induce NRF2 and heme oxygenase (*HMOX1*) expression in colon cancer via the PI3K and ERK pathways (Jang, Hong, Kim, et al., 2016). However, it is not clear how statins induce NRF2 and how HMOX1 activation could contribute to cell death in colon cancer.

One possible explanation to cell death could be via induction of p21. Maddocks *et al* demonstrated the induction of a p21 dependent cell cycle arrest as a protective mechanism against oxidative stress in p53 wild type cells after serine

starvation (Maddocks et al., 2013). However, it was reported that statins exert their effects by acting as HDAC inhibitors and increasing histone acetylation especially of the promoter region of the p21 gene (*CDKN1A*). This inhibition was shown to be independent of p53, as p53 levels were restored (Y. C. Lin et al., 2008). Here, the induction of p21 was observed in both cell lines after statin treatment for 72 hours (Fig 4.32A), suggesting a p53 independent regulation.

Importantly, simvastatin treatment diminished the *de novo* synthesis and overall levels of both cholesterol and CoQ10. The importance of CoQ10 in the ETC provides a clear connection to its role in controlling the production of ROS. In addition, CoQ10 was identified as an important metabolite for other metabolic reactions (Hernandez-Camacho et al., 2018), its role and how reduction in the CoQ10 levels after statins influence cell death in spheroids will be discussed in the next sections.

Taken together, the results discussed in this section provide evidence for the selective sensitivity of p53 deficient colon cancer cells to statins under metabolic stress. Inhibition of the mevalonate pathway led to decreased levels of metabolites causing the induction of SREBP target genes. In addition, gene signatures associated with oxidative stress were strongly induced in p53 deficient cancer cells treated with statins, suggesting a selective metabolic vulnerability of these cells in metabolically compromised environments.

5.3.3 CoQ10 is essential for respiration, electron transport chain and pyrimidine biosynthesis

CoQ10 is produced via *de novo* synthesis from intermediates of the mevalonate pathway and has many functions in mammalian cells (Y. Wang et al., 2016). The main function of CoQ10 is to transfer electrons in the mitochondrial inner membrane to complex III and it can be found in three different redox states: fully oxidised (ubiquinone), partially reduced (ubisemiquinone) and fully reduced (ubiquinol). CoQ10 can be converted to different redox states via the electron transfer chain (Lenaz et al., 1997). NADH–ubiquinone reductase (complex I) reduces

ubiquinone to ubiquinol, while oxidising NADH to NAD^+. Moreover, the succinate dehydrogenase complex (complex II) provides electrons to ubiquinone through $FADH_2$, thereby connecting the TCA cycle metabolites succinate and fumarate to CoQ10. Moreover, CoQ10 was demonstrated to contribute to the assembly and stability of complex III and this assembly helps the recycling of CoQ10 (Cramer et al., 2011).

Partially reduced CoQ10 (ubisemiquinone) reacts with oxygen, resulting in the formation of superoxide in the ETC. Superoxide formation causes the generation of ROS in the mitochondria (Lambert et al., 2004). In addition, reverse electron transport (RET) was shown to transfer electrons from succinate to complex II and CoQ10 and subsequently to complex I, which reduces NAD^+ to NADH (Murphy, 2009). This limits the availability of NAD^+ as a cofactor for TCA cycle enzymes and blocks the production of important metabolic intermediates. Taken together, these processes show that CoQ10 is important for mitochondrial energy production and has antioxidant properties in its reduced form (Y. Wang et al., 2016).

Indeed, the inhibition of the mevalonate pathway via statins led to decreased levels of succinate and fumarate, most likely due to defects in CoQ10 synthesis. Moreover, metabolic assays to measure the oxygen consumption rates in spheroids demonstrated that statins reduced both basal and maximum respiration only in p53 deficient spheroids. This effect could be rescued by mevalonate addition (Fig 4.34), suggesting that the mevalonate pathway provides important metabolites for respiration under metabolic stress.

Although these findings initially seem inconsistent with the fact that spheroids are hypoxic, they clearly indicate that cells in spheroid culture still rely on respiration. Indeed, there are reports demonstrating the importance of mitochondrial metabolism in spheroids and tumours. Previous papers showed the vulnerability of cancer cells to OXPHOS inhibitors in spheroid conditions as cells, particularly those in the center, underwent apoptosis when respiration was suppressed (X. Zhang et al., 2014). Similarly, statins were used in combination with OXPHOS inhibitors to induce death of quiescent cells in spheroids of colon cancer cells. In fact, this paper showed that the mevalonate pathway is upregulated in situations when OXPHOS is repressed,

suggesting that the mevalonate pathway supports oxidative phosphorylation under metabolic stress (Senkowski et al., 2016).

Overall, these findings demonstrate that statins block respiration and sensitise p53 deficient cancer cells to apoptosis in the core of the spheroid, suggesting the importance of oxidative metabolism in cells exposed to combined deprivation of nutrients and oxygen.

In addition, it can be suggested that the metabolic rewiring of p53 deficient cells in spheroids to increase the production of CoQ10 is essential for ETC functions. Moreover, ROS production due to the metabolic stress could be scavenged via increased levels of CoQ10 acting as an antioxidant (Stockwell et al., 2017). Indeed, CoQ10 was able to restore viability of p53 deficient cancer cells in the presence of statins, confirming that production of this metabolite by the mevalonate pathway is essential for cell survival under these conditions.

Moreover, simvastatin induced cell death was rescued by the addition of N-acetyl cysteine (NAC), a commonly used anti-oxidant (Fig 4.36A and B), highlighting the importance of CoQ10 to prevent ROS production in the ETC. Consistent with this rescue after statin treatment observed here, Qi *et al* demonstrated that simvastatin leads to the induction of ROS by interfering with the antioxidant mechanisms, including superoxide dismutase (SOD) and catalase (CAT) in a murine colon cancer cell line (Qi et al., 2010). Thus, measuring ROS levels could be an additional approach to further understand the mechanism of cell death of p53 deficient cells treated with statins.

Taken together, the results from this section demonstrates that the rescue of the statin induced cell death by the addition of NAC could emphasize the role of CoQ10 in balancing the ROS levels most likely because of its role in ETC.

Interestingly, stable isotope tracing revealed that statin treatment reduces total cellular UMP levels. Moreover, the fractions of UMP labelled from glucose were dramatically decreased, suggesting a connection between CoQ10 and pyrimidine biosynthesis. Pyrimidines can be synthesised via two different mechanisms; either via

de novo synthesis from precursors derived from the cellular intermediate metabolism or via the salvage pathway. The enzymes CAD, DHODH and UMP synthase are necessary enzymes for *de novo* synthesis of pyrimidines. CAD and UMP synthase are located outside the mitochondria; whereas DHODH is localized at the inner mitochondrial membrane (Evans et al., 2004). DHODH oxidises dihydroorotate to orotate and electrons are transferred directly by CoQ10 which is very important for the pyrimidine biosynthesis (M. E. Jones, 1980). Interestingly, it has been demonstrated that DHODH-driven pyrimidine biosynthesis rather than ATP production represents the essential mitochondrial function for tumorigenesis (Bajzikova et al., 2018).

Despite the fact that spheroids exhibited low proliferation rates, they could be dependent on pyrimidines for ribosome biogenesis. mTORC1 was demonstrated as the main mediator of cell growth by coordinating ribosome biogenesis and nucleotide synthesis (Valvezan et al., 2017). Indeed, spheroids displayed active mTORC1 signalling, as the phosphorylation of the S6K target S6RB was induced. In addition, GSEA revealed the downregulation of gene signatures associated with the ribosome when the mevalonate pathway was inhibited in spheroids (Fig 4.29B and C). It could be suggested that spheroids require pyrimidines for the maintenance of ribosomal biogenesis and the mevalonate pathway provides an important cofactor for their synthesis. Inhibition of the mevalonate pathway thus suppresses ribosome biogenesis and leads to cell death, potentially via the induction of ribosomal stress (T. H. Kim et al., 2014).

In addition to rescuing cell survival, exogenous CoQ10 addition restored levels of TCA cycle metabolite in statin treated cells. Most importantly, the decrease in UMP levels was also rescued by adding either mevalonate or CoQ10 after statin treatment. Given the fact that UMP levels were already higher in p53 deficient spheroids even without statin treatment, the importance of metabolic rewiring to increase the production of CoQ10 and promote pyrimidine biosynthesis following the loss of p53 is further emphasised. Moreover, the addition of a nucleoside mixture was also able to rescue cell death induced by statin treatment (Fig 4.36C, right graph), suggesting that nucleotides are indeed essential for survival of p53 deficient cancer cells under spheroid conditions.

Taken together, these data provides evidence that CoQ10 is important for the ETC in mitochondria and for preventing oxidative stress under hypoxia and nutrient deprivation. Moreover, induction of the mevalonate pathway is essential to support pyrimidine biosynthesis especially in p53 deficient cancer cells under metabolic stress. Thus, inhibition of the mevalonate pathway leads to low levels of UMP, inhibition of electron transport and possibly causes the induction of oxidative stress that limits cell viability.

Based on these findings, combining 5-fluorouracil (5-FU) and statins for possible therapy was considered. 5-FU, an analogue of uracil with a fluorine atom at the C_5 position, is a commonly used drug for the treatment of colorectal cancer (Grem, 2000). It is a heterocyclic aromatic organic compound, which has a similar structure to uracil and it can be incorporated into RNA and DNA, leading to DNA and RNA damage and interference with nucleoside metabolism (Rutman et al., 1954). In mammals, 5-FU can be converted to fluorodeoxyuridine monophosphate (FdUMP) that forms a complex with thymidylate synthase (*TS*) and represses the formation of deoxythymidine monophosphate (dTMP) (Parker et al., 1990), leading to cell death due to the lack of thymine (N. Zhang et al., 2008).

In addition, 5-FU was combined with simvastatin to treat spheroids formed by p53 WT and p53 deficient spheroids. Interestingly, 5-FU treatment alone was not able to induce apoptosis in p53 WT spheroids. This is not surprising, as it was shown previously that overexpression of p53 is associated with drug resistance towards 5-FU (J. T. Liang et al., 2002). It seems likely that the activation of p53 under conditions of metabolic stress leads to the resistance to cell death induced by 5-FU. However, this resistance could be overcome with the combined treatment with statins. Indeed, treatment with 5-FU together with simvastatin increased cell death in wild type p53 spheroids (Fig 4.38). Combined therapy of 5-FU with statins was previously successfully in killing colon cancer cell lines that were resistant to the anti-tumour agent irinotecan (Jang, Hong, Jang, et al., 2016). However, the literature is still lacking conclusive studies of statins in combination with 5-FU.

Taken together, these results reveal a novel role of the mevalonate pathway in providing CoQ10 to maintain electron transport for respiration and pyrimidine biosynthesis under conditions of metabolic stress. The results also suggest that combining mevalonate pathway inhibitors with 5-FU for the treatment of colorectal cancer.

5.3.4 Inhibition of the mevalonate pathway leads to cell death in p53 deficient mouse organoids

The small intestine epithelium is ordered into structures called crypts and villi and displays a large capacity for self-renewal (Bjerknes et al., 2006). Newly generated intestinal epithelial cells from the bottom of the crypts sequentially move along its axis to ultimately die via apoptosis at the tips of the villi over a 5 day turnover time. Sato *et al* established the culture system called intestinal organoid culture to maintain the crypt physiology under cell culture conditions with the help of several growth factors (T. Sato et al., 2009). Deletion of *APC*, a commonly mutated tumour suppressor gene in colorectal cancer, from intestinal epithelial cells leads to the formation of tumour spheres under organoid culture conditions (T. Sato et al., 2011).

Similar to the tumour spheroids, colon organoids displayed increased sensitivity of p53 deficient cells towards simvastatin treatment (Fig 4.39A, middle panel and B). In contrast, wild type p53 organoids were largely unaffected by statin treatment (Fig 4.39A, upper panel and B). Moreover, addition of nucleosides or CoQ10 rescued the viability of the organoids, suggesting that the mevalonate pathway provides CoQ10 for pyrimidine synthesis in cancer cells. Indeed, it has been shown that LGR5+ stem cells in the intestinal organoids are highly dependent on mitochondrial metabolism (Rodriguez-Colman et al., 2017) and are enriched for gene signatures associated with purine and pyrimidine metabolism (Lindeboom et al., 2018).

5.4 shRNA screen identified novel metabolic liabilities of p53 deficient cells in metabolically compromised environments

Functional genomic approaches are useful tools to determine specific dependencies of cells in a high-throughput manner. Firstly, RNAi screens using short interfering RNA oligonucleotides were used as common tools and later their utility was expanded by configuration of stem loop structures called short-hairpin RNAs (shRNAs) (Brummelkamp et al., 2003; Sims et al., 2011). shRNAs can be continuously expressed from Pol III promoters and they can be introduced into target cells using retroviral and lentiviral vectors (McManus et al., 2002). Availability of shRNA-based libraries has promoted high-throughput screens in mammalian cells. The concept of pooled shRNA screen is based on generating large pools of cells that carry a distinct shRNA sequence. Using this method, genes required for specific cellular states can be inferred by quantifying the changes between the representation of shRNAs in the starting population of cells with that of cells at the end of the experiment, *i.e.* after the selective pressure has been applied. Cells carrying a specific shRNA targeting a gene whose repression is essential for a specific phenotype are diluted from the pool of cells. Conversely, cells carrying shRNAs that target genes that inhibit a particular phenotype can accumulate in the cellular pool. As a result, in pooled screens, each cell carrying an shRNA is barcoded by a specific sequence so that the frequency of the shRNA sequences within a population and its differential depletion can be calculated. Pooled screens can be applied both *in vivo* and *in vitro* to identify genes that are responsible from the development, growth, and survival of normal or cancer cells.

For this purpose, a lentiviral shRNA library targeting signalling pathway genes was used, which was obtained through the DECIPHER Open Source RNAi Screening project (http://www.decipherproject.net/). This library targets 5,043 human genes and consists of 27,500 shRNA sequences (5 or 6 shRNA sequences per gene). As mentioned previously, each shRNA is tagged with a unique barcode sequence, which allowed its identification for analysis.

As the purpose of the screen was to identify metabolic dependencies under metabolic stress, spheroid cultures were used. Hits were detected according to the cut off (z-scores < -2) and shRNAs whose depletion was significant and specific to p53 deficient spheroids were taken into consideration. Among those genes, proteasomal subunits and ribosomal genes were the most significant ones (Fig 4.42B).

5.4.1 Proteasomal subunits and ribosome proteins are important for the survival of p53 deficient cells under metabolic stress

Regulated proteasomal degradation is very important to maintain the function of intracellular proteins, to check protein quality and to adjust regulatory processes. The ubiquitin-proteasome system is essential for the intracellular protein degradation machinery in the cells. The proteasome Subunit Alpha 1 (PSMA1) and PSMD6 are components of the core 20S and 26S proteasome subunits respectively (Narayanaswamy et al., 2014). Proteasome biogenesis is regulated transcriptionally via the erythroid-derived 2-related factor 1 (NRF1) signalling pathway (Radhakrishnan et al., 2010). Moreover, promoters of the genes coding for proteasomal subunits often include antioxidant response elements (ARE) and targeting these subunits triggers oxidative stress in these cells (Steffen et al., 2010). In addition, it has been established that mTORC1 activation promotes the expression of mRNAs coding for proteasomal subunits (Y. Zhang et al., 2015). As previously described, NRF1 inhibition suppresses mTORC1 dependent expression of proteasomal genes, suggesting that NRF1 is a downstream target of mTORC1. Indeed, SREBP1 was shown to regulate the expression of *NRF*1 downstream of mTORC1, and increased mTORC1 activity with the accompanying protein synthesis can be controlled via proteasomal activity, which is important for the prevention ER stress (Y. Zhang et al., 2014). Therefore, depleting proteasome subunits could generate a selective vulnerability in p53 deficient cancer cells under metabolic stress, potentially because of the high mTORC1 activity that was observed in this condition.

In addition to proteasomal subunits, several ribosomal proteins were also identified as hits whose depletion caused cell death in p53 deficient spheroids. Ribosome biogenesis is a highly regulated process involving all 3 classes of RNA polymerase to adjust the balance between ribosomal RNA (rRNA) transcription and

the processing of ribosomal proteins. rRNA is transcribed from rDNA gene clusters and is further processed and modified in the nucleolus. Perturbations in ribosome biogenesis generate imbalances and nucleolar stress, leading to the activation of p53 (Deisenroth et al., 2010). Depletion of ribosomal proteins also results in nucleolar stress and p53 was reported to be required to counteract this stress (Deisenroth et al., 2011). Changes in cellular energy status caused by reduced nutrient availability might have an impact on the demand for producing new ribosomes. Moreover, mTORC1 has a major role in regulating ribosome biogenesis by affecting Pol-I, Pol-II and Pol-III dependent transcription (Mayer et al., 2006) (Hannan et al., 2003). Therefore, it is important to keep ribosomal biogenesis and nutrient availability in balance to avoid nucleolar stress.

It is likely that the depletion of ribosomal subunits causes nucleolar stress under conditions of oxygen and nutrient deprivation. The lack of p53 could then cause the accumulation of damaged ribosomal proteins, further exacerbating the stress and leading to cell death. While this is an interesting hypothesis, the hits of the shRNA screen have to be validated. In addition, specific assays must be performed to establish the individual functions of the genes identified by the screen, before the importance of these pathways can be revealed.

6 CONCLUDING REMARKS AND OUTLOOK

After Otto Warburg's discovery in 1920s stating cancer cells perform glucose fermentation even in the presence of oxygen, the cancer metabolism field experienced a recent resurgence. During the last 20 years, findings describing how oncogenes, such as MYC, RAS, PI3K/AKT/mTOR, and tumour suppressors, such as p53 and VHL, regulate metabolic enzymes contribute to the understanding of how metabolic rewiring occurs in cancer cells. As cancer cells rapidly proliferate in a tumour microenvironment as consequence of constitutive activation of oncogenic signals, they get susceptible towards the depletion of nutrients and oxygen in the tumour microenvironment. Cancer cells then have to reprogram their metabolism in order to satisfy their biosynthetic and energy demands, for example by upregulation of nucleotide synthesis, glycolysis and de novo fatty acid and cholesterol synthesis under these conditions. As the tumour suppressor p53 contributes to the regulation of cancer metabolism, the effects of metabolically compromised environments on p53 wild type and deficient cancer cells were investigated in this study. Representation of nutrient and oxygen gradients was generated *in vitro* by using tumour spheroids. Using transcriptomic and metabolic analysis, spheroids were characterized and it was found that they recapitulate important features of tumours, including induction of hypoxia and reduced proliferation. In addition, p53 was found to inhibit cholesterol synthesis in cells cultured as spheroids and tumours but not in monolayers.

The transcription factors SREBP1 and SREBP2 are master regulators of lipid metabolism, controlling the expression of enzymes responsible for fatty acid and cholesterol synthesis. Here it was found that p53 blocks the expression of SREBP2 target genes in spheroids through a mechanism dependent on GSK3. Moreover, mature SREBP2 levels were identified as regulated by mTORC1 in spheroid cultures.

Metabolic characterization of the mevalonate pathway revealed metabolic rewiring that occurs in p53 deficient spheroids to induce the production of CoQ10, whereas p53 wild type spheroids used the mevalonate pathway mainly for the production of cholesterol. In contrast, p53 dependent rewiring was not observed in

cells cultured in monolayer suggesting the induction in CoQ10 production as a specific metabolic phenomenan in spheroid cultures.

Inhibition of the mevalonate pathway decreases cell viability in monolayer cultures of both p53 WT and p53 deficient cells. Interestingly, p53 wild type cells in spheroids did not induce cell death after statin treatment, whereas p53 deficient cells displayed a specific vulnerability in the center of the spheroids. Moreover, these results were reproducible in tumour organoids and cell survival could be restored with mevalonate, CoQ10 and the antioxidant NAC. Statins reduced levels of CoQ10 synthesis and TCA cycle metabolites, suggesting that this vulnerability is mediated by the generation of ROS that could be rescued by the addition of CoQ10 and NAC. In addition, inhibition of the mevalonate pathway led to decrease in respiration in p53 deficient spheroids, emphasizing the importance of CoQ10 synthesis under metabolic stress.

Interestingly, statin treatment lowered cellular UMP levels, suggesting a connection between the mevalonate pathway and pyrimidine biosynthesis via CoQ10 that acts as an electron acceptor for the dihydroorotate dehydrogenase enzyme. Addition of CoQ10 restored UMP levels after statin treatment. Moreover, exogenous nucleosides rescued cell death in spheroids and organoids after statin treatment. Additionally, combined therapy of statins with 5-FU, a commonly used drug in colon cancer, was able to sensitize p53 wild type cells cultured as spheroids, suggesting a possible mechanistic explanation for combining these drugs for the treatment for the colon cancer.

Taken together, in this thesis it was demonstrated that p53 inhibits SREBP2 in cancer cells exposed to metabolic stress. P53 deficient cells upregulate the mevalonate pathway for the production of CoQ10, thereby maintaining its essential electron transfer function for mitochondrial respiration and UMP synthesis. Inhibition of the mevalonate pathway selectively killed p53 deficient cancer cells in the center of the spheroids and blocked respiration and TCA cycle activity, leading to the formation of ROS and cell death. In addition, the decrease in CoQ10 levels after statin treatment resulted in the block of UMP synthesis, thereby revealing an

additional mechanism of cell death caused by mevalonate pathway inhibitors and suggesting combined therapy with 5-FU as an anti-cancer strategy.

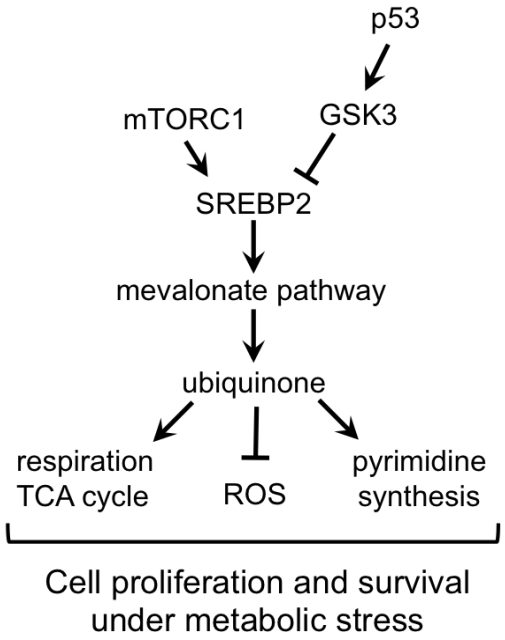

Figure 6.1: Proposed model showing the regulation of SREBP2 in the spheroids

Tumour suppressor p53 leads to the inhibition of the transcription factor SREBP2 by activating GSK3 under metabolic stress formed by spheroids. Moreover, spheroid cultures increase the activity of the mTORC1/S6-kinase pathway, which is crucial for SREBP activation. Thereby, loss of p53 leads to the induction of enzymes of the mevalonate pathway via activation of the transcription factor SREBP2, resulting in a metabolic rewiring that supports the generation of ubiquinone (coenzyme Q10) which is important for the nucleotide biosynthesis, ETC and inhibition of ROS for the cell survival under metabolic stress.

Although statins and 5-FU were shown to be used for colon cancer in clinical trials, studies were inconclusive so far. Therefore, it is important to reveal the mechanism of action of statins in different tumour types. However, it is important to confirm the effect of statins *in vivo,* in mouse models of cancer that where there are limited levels of oxygen and nutrients, recapitulating the representation of the tumour microenvironment.

In the second part of the study, several selective vulnerabilities were identified that led to the death of p53 deficient cells under metabolicslly compromised

environments by global shRNA screening. Several ribosomal proteins and proteasomal subunits were identified as hits whose depletion leads to cell death only in p53 deficient cells under metabolic stress. However, further validation is needed to understand how these proteins affect the viability and these cells. Further analyses will lead to important findings to understand specific vulnerabilities in cancer cells that could be translated into cancer therapy.

7 BIBLIOGRAPHY

Ackerman, D., Tumanov, S., Qiu, B., Michalopoulou, E., Spata, M., Azzam, A., . . . Kamphorst, J. J. (2018). Triglycerides Promote Lipid Homeostasis during Hypoxic Stress by Balancing Fatty Acid Saturation. *Cell Rep, 24*(10), 2596-2605 e2595. doi:10.1016/j.celrep.2018.08.015

Adam, J., Hatipoglu, E., O'Flaherty, L., Ternette, N., Sahgal, N., Lockstone, H., . . . Pollard, P. J. (2011). Renal cyst formation in Fh1-deficient mice is independent of the Hif/Phd pathway: roles for fumarate in KEAP1 succination and Nrf2 signaling. *Cancer Cell, 20*(4), 524-537. doi:10.1016/j.ccr.2011.09.006

Agarwal, B., Bhendwal, S., Halmos, B., Moss, S. F., Ramey, W. G., & Holt, P. R. (1999). Lovastatin augments apoptosis induced by chemotherapeutic agents in colon cancer cells. *Clin Cancer Res, 5*(8), 2223-2229.

Alli, P. M., Pinn, M. L., Jaffee, E. M., McFadden, J. M., & Kuhajda, F. P. (2005). Fatty acid synthase inhibitors are chemopreventive for mammary cancer in neu-N transgenic mice. *Oncogene, 24*(1), 39-46. doi:10.1038/sj.onc.1208174

An, W. G., Kanekal, M., Simon, M. C., Maltepe, E., Blagosklonny, M. V., & Neckers, L. M. (1998). Stabilization of wild-type p53 by hypoxia-inducible factor 1alpha. *Nature, 392*(6674), 405-408. doi:10.1038/32925

Arito, M., Horiba, T., Hachimura, S., Inoue, J., & Sato, R. (2008). Growth factor-induced phosphorylation of sterol regulatory element-binding proteins inhibits sumoylation, thereby stimulating the expression of their target genes, low density lipoprotein uptake, and lipid synthesis. *J Biol Chem, 283*(22), 15224-15231. doi:10.1074/jbc.M800910200

Ariyama, H., Kono, N., Matsuda, S., Inoue, T., & Arai, H. (2010). Decrease in membrane phospholipid unsaturation induces unfolded protein response. *J Biol Chem, 285*(29), 22027-22035. doi:10.1074/jbc.M110.126870

Assaily, W., Rubinger, D. A., Wheaton, K., Lin, Y., Ma, W., Xuan, W., . . . Benchimol, S. (2011). ROS-mediated p53 induction of Lpin1 regulates fatty acid oxidation in response to nutritional stress. *Mol Cell, 44*(3), 491-501. doi:10.1016/j.molcel.2011.08.038

Baenke, F., Peck, B., Miess, H., & Schulze, A. (2013). Hooked on fat: the role of lipid synthesis in cancer metabolism and tumour development. *Dis Model Mech, 6*(6), 1353-1363. doi:10.1242/dmm.011338

Bajzikova, M., Kovarova, J., Coelho, A. R., Boukalova, S., Oh, S., Rohlenova, K., . . . Neuzil, J. (2018). Reactivation of Dihydroorotate Dehydrogenase-Driven Pyrimidine Biosynthesis Restores Tumor Growth of Respiration-Deficient Cancer Cells. *Cell Metab*. doi:10.1016/j.cmet.2018.10.014

Balzer, E. M., & Konstantopoulos, K. (2012). Intercellular adhesion: mechanisms for growth and metastasis of epithelial cancers. *Wiley Interdiscip Rev Syst Biol Med, 4*(2), 171-181. doi:10.1002/wsbm.160

Beckner, M. E., Fellows-Mayle, W., Zhang, Z., Agostino, N. R., Kant, J. A., Day, B. W., & Pollack, I. F. (2010). Identification of ATP citrate lyase as a positive regulator of glycolytic function in glioblastomas. *Int J Cancer, 126*(10), 2282-2295. doi:10.1002/ijc.24918

Beitner-Johnson, D., Rust, R. T., Hsieh, T. C., & Millhorn, D. E. (2001). Hypoxia activates Akt and induces phosphorylation of GSK-3 in PC12 cells. *Cell Signal, 13*(1), 23-27.

Ben-Sahra, I., Howell, J. J., Asara, J. M., & Manning, B. D. (2013). Stimulation of de novo pyrimidine synthesis by growth signaling through mTOR and S6K1. *Science, 339*(6125), 1323-1328. doi:10.1126/science.1228792

Benassi, B., Fanciulli, M., Fiorentino, F., Porrello, A., Chiorino, G., Loda, M., . . . Biroccio, A. (2006). c-Myc phosphorylation is required for cellular response to oxidative stress. *Mol Cell, 21*(4), 509-519. doi:10.1016/j.molcel.2006.01.009

Bengoechea-Alonso, M. T., & Ericsson, J. (2009). A phosphorylation cascade controls the degradation of active SREBP1. *J Biol Chem, 284*(9), 5885-5895. doi:10.1074/jbc.M807906200

Bensaad, K., Cheung, E. C., & Vousden, K. H. (2009). Modulation of intracellular ROS levels by TIGAR controls autophagy. *EMBO J, 28*(19), 3015-3026. doi:10.1038/emboj.2009.242

Bensaad, K., Favaro, E., Lewis, C. A., Peck, B., Lord, S., Collins, J. M., . . . Harris, A. L. (2014). Fatty acid uptake and lipid storage induced by HIF-1alpha contribute to cell growth and survival after hypoxia-reoxygenation. *Cell Rep, 9*(1), 349-365. doi:10.1016/j.celrep.2014.08.056

Bensaad, K., Tsuruta, A., Selak, M. A., Vidal, M. N., Nakano, K., Bartrons, R., . . . Vousden, K. H. (2006). TIGAR, a p53-inducible regulator of glycolysis and apoptosis. *Cell, 126*(1), 107-120. doi:10.1016/j.cell.2006.05.036

Bertout, J. A., Patel, S. A., & Simon, M. C. (2008). The impact of O2 availability on human cancer. *Nat Rev Cancer, 8*(12), 967-975. doi:10.1038/nrc2540

Berwick, D. C., Hers, I., Heesom, K. J., Moule, S. K., & Tavare, J. M. (2002). The identification of ATP-citrate lyase as a protein kinase B (Akt) substrate in primary adipocytes. *J Biol Chem, 277*(37), 33895-33900. doi:10.1074/jbc.M204681200

Bjerknes, M., & Cheng, H. (2006). Intestinal epithelial stem cells and progenitors. *Methods Enzymol, 419*, 337-383. doi:10.1016/S0076-6879(06)19014-X

Boidot, R., Vegran, F., Meulle, A., Le Breton, A., Dessy, C., Sonveaux, P., . . . Feron, O. (2012). Regulation of monocarboxylate transporter MCT1 expression by p53 mediates inward and outward lactate fluxes in tumors. *Cancer Res, 72*(4), 939-948. doi:10.1158/0008-5472.CAN-11-2474

Bourdon, A., Minai, L., Serre, V., Jais, J. P., Sarzi, E., Aubert, S., . . . Rotig, A. (2007). Mutation of RRM2B, encoding p53-controlled ribonucleotide reductase (p53R2), causes severe mitochondrial DNA depletion. *Nat Genet, 39*(6), 776-780. doi:10.1038/ng2040

Briggs, M. R., Yokoyama, C., Wang, X., Brown, M. S., & Goldstein, J. L. (1993). Nuclear protein that binds sterol regulatory element of low density lipoprotein receptor promoter. I. Identification of the protein and delineation of its target nucleotide sequence. *J Biol Chem, 268*(19), 14490-14496.

Brooks, C. L., & Gu, W. (2011). p53 regulation by ubiquitin. *FEBS Lett, 585*(18), 2803-2809. doi:10.1016/j.febslet.2011.05.022

Brown, M. S., & Goldstein, J. L. (1997). The SREBP pathway: regulation of cholesterol metabolism by proteolysis of a membrane-bound transcription factor. *Cell, 89*(3), 331-340.

Brown, M. S., & Goldstein, J. L. (1999). A proteolytic pathway that controls the cholesterol content of membranes, cells, and blood. *Proc Natl Acad Sci U S A, 96*(20), 11041-11048.

Browne, E. P., Wing, B., Coleman, D., & Shenk, T. (2001). Altered cellular mRNA levels in human cytomegalovirus-infected fibroblasts: viral block to the accumulation of antiviral mRNAs. *J Virol, 75*(24), 12319-12330. doi:10.1128/JVI.75.24.12319-12330.2001

Brugarolas, J., Lei, K., Hurley, R. L., Manning, B. D., Reiling, J. H., Hafen, E., . . . Kaelin, W. G., Jr. (2004). Regulation of mTOR function in response to hypoxia by REDD1 and the TSC1/TSC2 tumor suppressor complex. *Genes Dev, 18*(23), 2893-2904. doi:10.1101/gad.1256804

Brummelkamp, T. R., & Bernards, R. (2003). New tools for functional mammalian cancer genetics. *Nat Rev Cancer, 3*(10), 781-789. doi:10.1038/nrc1191

Budanov, A. V., & Karin, M. (2008). p53 target genes sestrin1 and sestrin2 connect genotoxic stress and mTOR signaling. *Cell, 134*(3), 451-460. doi:10.1016/j.cell.2008.06.028

Buescher, J. M., Antoniewicz, M. R., Boros, L. G., Burgess, S. C., Brunengraber, H., Clish, C. B., . . . Fendt, S. M. (2015). A roadmap for interpreting (13)C metabolite labeling patterns from cells. *Curr Opin Biotechnol, 34*, 189-201. doi:10.1016/j.copbio.2015.02.003

Buller, C. L., Loberg, R. D., Fan, M. H., Zhu, Q., Park, J. L., Vesely, E., . . . Brosius, F. C., 3rd. (2008). A GSK-3/TSC2/mTOR pathway regulates glucose uptake and GLUT1 glucose transporter expression. *Am J Physiol Cell Physiol, 295*(3), C836-843. doi:10.1152/ajpcell.00554.2007

Bunz, F., Dutriaux, A., Lengauer, C., Waldman, T., Zhou, S., Brown, J. P., . . . Vogelstein, B. (1998). Requirement for p53 and p21 to sustain G2 arrest after DNA damage. *Science, 282*(5393), 1497-1501.

Busk, M., Horsman, M. R., Kristjansen, P. E., van der Kogel, A. J., Bussink, J., & Overgaard, J. (2008). Aerobic glycolysis in cancers: implications for the usability of oxygen-responsive genes and fluorodeoxyglucose-PET as markers of tissue hypoxia. *Int J Cancer, 122*(12), 2726-2734. doi:10.1002/ijc.23449

Buzzai, M., Jones, R. G., Amaravadi, R. K., Lum, J. J., DeBerardinis, R. J., Zhao, F., . . . Thompson, C. B. (2007). Systemic treatment with the antidiabetic drug metformin selectively impairs p53-deficient tumor cell growth. *Cancer Res, 67*(14), 6745-6752. doi:10.1158/0008-5472.CAN-06-4447

Cao, Z., Fan-Minogue, H., Bellovin, D. I., Yevtodiyenko, A., Arzeno, J., Yang, Q., . . . Felsher, D. W. (2011). MYC phosphorylation, activation, and tumorigenic potential in hepatocellular carcinoma are regulated by HMG-CoA reductase. *Cancer Res, 71*(6), 2286-2297. doi:10.1158/0008-5472.CAN-10-3367

Cardaci, S., Zheng, L., MacKay, G., van den Broek, N. J., MacKenzie, E. D., Nixon, C., . . . Gottlieb, E. (2015). Pyruvate carboxylation enables growth of SDH-deficient cells by supporting aspartate biosynthesis. *Nat Cell Biol, 17*(10), 1317-1326. doi:10.1038/ncb3233

Carmeliet, P., Dor, Y., Herbert, J. M., Fukumura, D., Brusselmans, K., Dewerchin, M., . . . Keshert, E. (1998). Role of HIF-1alpha in hypoxia-mediated apoptosis, cell proliferation and tumour angiogenesis. *Nature, 394*(6692), 485-490. doi:10.1038/28867

Casey, P. J., & Seabra, M. C. (1996). Protein prenyltransferases. *J Biol Chem, 271*(10), 5289-5292.

Chang, H. Y., Sneddon, J. B., Alizadeh, A. A., Sood, R., West, R. B., Montgomery, K., . . . Brown, P. O. (2004). Gene expression signature of fibroblast serum response predicts human cancer progression: similarities between tumors and wounds. *PLoS Biol, 2*(2), E7. doi:10.1371/journal.pbio.0020007

Chen, Y., Qian, J., He, Q., Zhao, H., Toral-Barza, L., Shi, C., . . . Yu, K. (2016). mTOR complex-2 stimulates acetyl-CoA and de novo lipogenesis through ATP citrate lyase in HER2/PIK3CA-hyperactive breast cancer. *Oncotarget, 7*(18), 25224-25240. doi:10.18632/oncotarget.8279

Cheng, T., Sudderth, J., Yang, C., Mullen, A. R., Jin, E. S., Mates, J. M., & DeBerardinis, R. J. (2011). Pyruvate carboxylase is required for glutamine-independent growth of tumor cells. *Proc Natl Acad Sci U S A, 108*(21), 8674-8679. doi:10.1073/pnas.1016627108

Cheung, E. C., Ludwig, R. L., & Vousden, K. H. (2012). Mitochondrial localization of TIGAR under hypoxia stimulates HK2 and lowers ROS and cell death. *Proc Natl Acad Sci U S A, 109*(50), 20491-20496. doi:10.1073/pnas.1206530109

Cho, H., Mu, J., Kim, J. K., Thorvaldsen, J. L., Chu, Q., Crenshaw, E. B., 3rd, . . . Birnbaum, M. J. (2001). Insulin resistance and a diabetes mellitus-like syndrome in mice lacking the protein kinase Akt2 (PKB beta). *Science, 292*(5522), 1728-1731. doi:10.1126/science.292.5522.1728

Choudhry, H., & Harris, A. L. (2018). Advances in Hypoxia-Inducible Factor Biology. *Cell Metab, 27*(2), 281-298. doi:10.1016/j.cmet.2017.10.005

Christen, S., Lorendeau, D., Schmieder, R., Broekaert, D., Metzger, K., Veys, K., . . . Fendt, S. M. (2016). Breast Cancer-Derived Lung Metastases Show Increased Pyruvate Carboxylase-Dependent Anaplerosis. *Cell Rep, 17*(3), 837-848. doi:10.1016/j.celrep.2016.09.042

Cohen, P., & Frame, S. (2001). The renaissance of GSK3. *Nat Rev Mol Cell Biol, 2*(10), 769-776. doi:10.1038/35096075

Comerford, S. A., Huang, Z., Du, X., Wang, Y., Cai, L., Witkiewicz, A. K., . . . Tu, B. P. (2014). Acetate dependence of tumors. *Cell, 159*(7), 1591-1602. doi:10.1016/j.cell.2014.11.020

Contractor, T., & Harris, C. R. (2012). p53 negatively regulates transcription of the pyruvate dehydrogenase kinase Pdk2. *Cancer Res, 72*(2), 560-567. doi:10.1158/0008-5472.CAN-11-1215

Cramer, W. A., Hasan, S. S., & Yamashita, E. (2011). The Q cycle of cytochrome bc complexes: a structure perspective. *Biochim Biophys Acta, 1807*(7), 788-802. doi:10.1016/j.bbabio.2011.02.006

Crane, F. L., Hatefi, Y., Lester, R. L., & Widmer, C. (1957). Isolation of a quinone from beef heart mitochondria. *Biochim Biophys Acta, 25*(1), 220-221.

Cross, D. A., Alessi, D. R., Cohen, P., Andjelkovich, M., & Hemmings, B. A. (1995). Inhibition of glycogen synthase kinase-3 by insulin mediated by protein kinase B. *Nature, 378*(6559), 785-789. doi:10.1038/378785a0

Currie, E., Schulze, A., Zechner, R., Walther, T. C., & Farese, R. V., Jr. (2013). Cellular fatty acid metabolism and cancer. *Cell Metab, 18*(2), 153-161. doi:10.1016/j.cmet.2013.05.017

DeBerardinis, R. J., & Chandel, N. S. (2016). Fundamentals of cancer metabolism. *Sci Adv, 2*(5), e1600200. doi:10.1126/sciadv.1600200

Deisenroth, C., & Zhang, Y. (2010). Ribosome biogenesis surveillance: probing the ribosomal protein-Mdm2-p53 pathway. *Oncogene, 29*(30), 4253-4260. doi:10.1038/onc.2010.189

Deisenroth, C., & Zhang, Y. (2011). The Ribosomal Protein-Mdm2-p53 Pathway and Energy Metabolism: Bridging the Gap between Feast and Famine. *Genes Cancer, 2*(4), 392-403. doi:10.1177/1947601911409737

Dejure, F. R., Royla, N., Herold, S., Kalb, J., Walz, S., Ade, C. P., . . . Eilers, M. (2017). The MYC mRNA 3'-UTR couples RNA polymerase II function to glutamine and ribonucleotide levels. *EMBO J, 36*(13), 1854-1868. doi:10.15252/embj.201796662

Deng, X., Zhang, W., I, O. S., Williams, J. B., Dong, Q., Park, E. A., . . . Elam, M. B. (2012). FoxO1 inhibits sterol regulatory element-binding protein-1c (SREBP-1c) gene expression via transcription factors Sp1 and SREBP-1c. *J Biol Chem, 287*(24), 20132-20143. doi:10.1074/jbc.M112.347211

Denko, N. C. (2008). Hypoxia, HIF1 and glucose metabolism in the solid tumour. *Nat Rev Cancer, 8*(9), 705-713. doi:10.1038/nrc2468

Dibble, C. C., & Cantley, L. C. (2015). Regulation of mTORC1 by PI3K signaling. *Trends Cell Biol, 25*(9), 545-555. doi:10.1016/j.tcb.2015.06.002

Dieli, F., Vermijlen, D., Fulfaro, F., Caccamo, N., Meraviglia, S., Cicero, G., . . . Hayday, A. C. (2007). Targeting human {gamma}delta} T cells with zoledronate and interleukin-2 for immunotherapy of hormone-refractory prostate cancer. *Cancer Res, 67*(15), 7450-7457. doi:10.1158/0008-5472.CAN-07-0199

Doherty, J. R., & Cleveland, J. L. (2013). Targeting lactate metabolism for cancer therapeutics. *J Clin Invest, 123*(9), 3685-3692. doi:10.1172/JCI69741

Dupuy, F., Tabaries, S., Andrzejewski, S., Dong, Z., Blagih, J., Annis, M. G., . . . Siegel, P. M. (2015). PDK1-Dependent Metabolic Reprogramming Dictates Metastatic Potential in Breast Cancer. *Cell Metab, 22*(4), 577-589. doi:10.1016/j.cmet.2015.08.007

Duvel, K., Yecies, J. L., Menon, S., Raman, P., Lipovsky, A. I., Souza, A. L., . . . Manning, B. D. (2010). Activation of a metabolic gene regulatory network downstream of mTOR complex 1. *Mol Cell, 39*(2), 171-183. doi:10.1016/j.molcel.2010.06.022

Eales, K. L., Hollinshead, K. E., & Tennant, D. A. (2016). Hypoxia and metabolic adaptation of cancer cells. *Oncogenesis, 5*, e190. doi:10.1038/oncsis.2015.50

Efeyan, A., & Sabatini, D. M. (2013). Nutrients and growth factors in mTORC1 activation. *Biochem Soc Trans, 41*(4), 902-905. doi:10.1042/BST20130063

Eliyahu, D., Michalovitz, D., Eliyahu, S., Pinhasi-Kimhi, O., & Oren, M. (1989). Wild-type p53 can inhibit oncogene-mediated focus formation. *Proc Natl Acad Sci U S A, 86*(22), 8763-8767.

Ernster, L., & Dallner, G. (1995). Biochemical, physiological and medical aspects of ubiquinone function. *Biochim Biophys Acta, 1271*(1), 195-204.

Evans, D. R., & Guy, H. I. (2004). Mammalian pyrimidine biosynthesis: fresh insights into an ancient pathway. *J Biol Chem, 279*(32), 33035-33038. doi:10.1074/jbc.R400007200

Evert, M., Calvisi, D. F., Evert, K., De Murtas, V., Gasparetti, G., Mattu, S., . . . Dombrowski, F. (2012). V-AKT murine thymoma viral oncogene homolog/mammalian target of rapamycin activation induces a module of metabolic changes contributing to growth in insulin-induced hepatocarcinogenesis. *Hepatology, 55*(5), 1473-1484. doi:10.1002/hep.25600

Farese, R. V., Jr., & Walther, T. C. (2009). Lipid droplets finally get a little R-E-S-P-E-C-T. *Cell, 139*(5), 855-860. doi:10.1016/j.cell.2009.11.005

Feitelson, M. A., Arzumanyan, A., Kulathinal, R. J., Blain, S. W., Holcombe, R. F., Mahajna, J., . . . Nowsheen, S. (2015). Sustained proliferation in cancer: Mechanisms and novel therapeutic targets. *Semin Cancer Biol, 35 Suppl*, S25-S54. doi:10.1016/j.semcancer.2015.02.006

Feng, Z., Hu, W., de Stanchina, E., Teresky, A. K., Jin, S., Lowe, S., & Levine, A. J. (2007). The regulation of AMPK beta1, TSC2, and PTEN expression by p53: stress, cell and tissue specificity, and the role of these gene products in modulating the IGF-1-AKT-mTOR pathways. *Cancer Res, 67*(7), 3043-3053. doi:10.1158/0008-5472.CAN-06-4149

Feng, Z., & Levine, A. J. (2010). The regulation of energy metabolism and the IGF-1/mTOR pathways by the p53 protein. *Trends Cell Biol, 20*(7), 427-434. doi:10.1016/j.tcb.2010.03.004

Fernandez-Alvarez, A., Alvarez, M. S., Gonzalez, R., Cucarella, C., Muntane, J., & Casado, M. (2011). Human SREBP1c expression in liver is directly regulated by peroxisome proliferator-activated receptor alpha (PPARalpha). *J Biol Chem, 286*(24), 21466-21477. doi:10.1074/jbc.M110.209973

Finlay, C. A., Hinds, P. W., & Levine, A. J. (1989). The p53 proto-oncogene can act as a suppressor of transformation. *Cell, 57*(7), 1083-1093.

Floter, J., Kaymak, I., & Schulze, A. (2017). Regulation of Metabolic Activity by p53. *Metabolites, 7*(2). doi:10.3390/metabo7020021

Forys, J. T., Kuzmicki, C. E., Saporita, A. J., Winkeler, C. L., Maggi, L. B., Jr., & Weber, J. D. (2014). ARF and p53 coordinate tumor suppression of an oncogenic IFN-beta-STAT1-ISG15 signaling axis. *Cell Rep, 7*(2), 514-526. doi:10.1016/j.celrep.2014.03.026

Freed-Pastor, W. A., Mizuno, H., Zhao, X., Langerod, A., Moon, S. H., Rodriguez-Barrueco, R., . . . Prives, C. (2012). Mutant p53 disrupts mammary tissue architecture via the mevalonate pathway. *Cell, 148*(1-2), 244-258. doi:10.1016/j.cell.2011.12.017

Freed-Pastor, W. A., & Prives, C. (2012). Mutant p53: one name, many proteins. *Genes Dev, 26*(12), 1268-1286. doi:10.1101/gad.190678.112

Frezza, C., & Gottlieb, E. (2009). Mitochondria in cancer: not just innocent bystanders. *Semin Cancer Biol, 19*(1), 4-11. doi:10.1016/j.semcancer.2008.11.008

Fruman, D. A., Chiu, H., Hopkins, B. D., Bagrodia, S., Cantley, L. C., & Abraham, R. T. (2017). The PI3K Pathway in Human Disease. *Cell, 170*(4), 605-635. doi:10.1016/j.cell.2017.07.029

Fukuda, R., Zhang, H., Kim, J. W., Shimoda, L., Dang, C. V., & Semenza, G. L. (2007). HIF-1 regulates cytochrome oxidase subunits to optimize efficiency of respiration in hypoxic cells. *Cell, 129*(1), 111-122. doi:10.1016/j.cell.2007.01.047

Furuta, E., Pai, S. K., Zhan, R., Bandyopadhyay, S., Watabe, M., Mo, Y. Y., . . . Watabe, K. (2008). Fatty acid synthase gene is up-regulated by hypoxia via activation of Akt and sterol regulatory element binding protein-1. *Cancer Res, 68*(4), 1003-1011. doi:10.1158/0008-5472.CAN-07-2489

Galdieri, L., & Vancura, A. (2012). Acetyl-CoA carboxylase regulates global histone acetylation. *J Biol Chem, 287*(28), 23865-23876. doi:10.1074/jbc.M112.380519

Gallamini, A., Zwarthoed, C., & Borra, A. (2014). Positron Emission Tomography (PET) in Oncology. *Cancers (Basel), 6*(4), 1821-1889. doi:10.3390/cancers6041821

Gasco, M., Shami, S., & Crook, T. (2002). The p53 pathway in breast cancer. *Breast Cancer Res, 4*(2), 70-76.

Gaude, E., & Frezza, C. (2014). Defects in mitochondrial metabolism and cancer. *Cancer Metab, 2*, 10. doi:10.1186/2049-3002-2-10

Giandomenico, V., Simonsson, M., Gronroos, E., & Ericsson, J. (2003). Coactivator-dependent acetylation stabilizes members of the SREBP family of transcription factors. *Mol Cell Biol, 23*(7), 2587-2599.

Goldstein, J. L., DeBose-Boyd, R. A., & Brown, M. S. (2006). Protein sensors for membrane sterols. *Cell, 124*(1), 35-46. doi:10.1016/j.cell.2005.12.022

Golias, T., Papandreou, I., Sun, R., Kumar, B., Brown, N. V., Swanson, B. J., . . . Denko, N. C. (2016). Hypoxic repression of pyruvate dehydrogenase activity is necessary for metabolic reprogramming and growth of model tumours. *Sci Rep, 6*, 31146. doi:10.1038/srep31146

Gong, Y., Lee, J. N., Lee, P. C., Goldstein, J. L., Brown, M. S., & Ye, J. (2006). Sterol-regulated ubiquitination and degradation of Insig-1 creates a convergent mechanism for feedback control of cholesterol synthesis and uptake. *Cell Metab, 3*(1), 15-24. doi:10.1016/j.cmet.2005.11.014

Gordan, J. D., Bertout, J. A., Hu, C. J., Diehl, J. A., & Simon, M. C. (2007). HIF-2alpha promotes hypoxic cell proliferation by enhancing c-myc transcriptional activity. *Cancer Cell, 11*(4), 335-347. doi:10.1016/j.ccr.2007.02.006

Gorrini, C., Harris, I. S., & Mak, T. W. (2013). Modulation of oxidative stress as an anticancer strategy. *Nat Rev Drug Discov, 12*(12), 931-947. doi:10.1038/nrd4002

Graeber, T. G., Osmanian, C., Jacks, T., Housman, D. E., Koch, C. J., Lowe, S. W., & Giaccia, A. J. (1996). Hypoxia-mediated selection of cells with diminished apoptotic potential in solid tumours. *Nature, 379*(6560), 88-91. doi:10.1038/379088a0

Gregory, M. A., Qi, Y., & Hann, S. R. (2003). Phosphorylation by glycogen synthase kinase-3 controls c-myc proteolysis and subnuclear localization. *J Biol Chem, 278*(51), 51606-51612. doi:10.1074/jbc.M310722200

Grem, J. L. (2000). 5-Fluorouracil: forty-plus and still ticking. A review of its preclinical and clinical development. *Invest New Drugs, 18*(4), 299-313.

Griffiths, B., Lewis, C. A., Bensaad, K., Ros, S., Zhang, Q., Ferber, E. C., . . . Schulze, A. (2013). Sterol regulatory element binding protein-dependent regulation of lipid synthesis supports cell survival and tumor growth. *Cancer Metab, 1*(1), 3. doi:10.1186/2049-3002-1-3

Gu, W., & Roeder, R. G. (1997). Activation of p53 sequence-specific DNA binding by acetylation of the p53 C-terminal domain. *Cell, 90*(4), 595-606.

Guo, D., Prins, R. M., Dang, J., Kuga, D., Iwanami, A., Soto, H., . . . Mischel, P. S. (2009). EGFR signaling through an Akt-SREBP-1-dependent, rapamycin-resistant pathway sensitizes glioblastomas to antilipogenic therapy. *Sci Signal, 2*(101), ra82. doi:10.1126/scisignal.2000446

Guzy, R. D., Hoyos, B., Robin, E., Chen, H., Liu, L., Mansfield, K. D., . . . Schumacker, P. T. (2005). Mitochondrial complex III is required for hypoxia-induced ROS production and cellular oxygen sensing. *Cell Metab, 1*(6), 401-408. doi:10.1016/j.cmet.2005.05.001

Hagiwara, A., Cornu, M., Cybulski, N., Polak, P., Betz, C., Trapani, F., . . . Hall, M. N. (2012). Hepatic mTORC2 activates glycolysis and lipogenesis through Akt, glucokinase, and SREBP1c. *Cell Metab, 15*(5), 725-738. doi:10.1016/j.cmet.2012.03.015

Halestrap, A. P., & Meredith, D. (2004). The SLC16 gene family-from monocarboxylate transporters (MCTs) to aromatic amino acid transporters and beyond. *Pflugers Arch, 447*(5), 619-628. doi:10.1007/s00424-003-1067-2

Han, J., Li, E., Chen, L., Zhang, Y., Wei, F., Liu, J., . . . Wang, Y. (2015). The CREB coactivator CRTC2 controls hepatic lipid metabolism by regulating SREBP1. *Nature, 524*(7564), 243-246. doi:10.1038/nature14557

Hanahan, D., & Weinberg, R. A. (2011). Hallmarks of cancer: the next generation. *Cell, 144*(5), 646-674. doi:10.1016/j.cell.2011.02.013

Hann, S. R., Sloan-Brown, K., & Spotts, G. D. (1992). Translational activation of the non-AUG-initiated c-myc 1 protein at high cell densities due to methionine deprivation. *Genes Dev, 6*(7), 1229-1240.

Hannan, K. M., Brandenburger, Y., Jenkins, A., Sharkey, K., Cavanaugh, A., Rothblum, L., . . . Hannan, R. D. (2003). mTOR-dependent regulation of ribosomal gene transcription requires S6K1 and is mediated by phosphorylation of the carboxy-terminal activation domain of the nucleolar transcription factor UBF. *Mol Cell Biol, 23*(23), 8862-8877.

Hay, N. (2011). Interplay between FOXO, TOR, and Akt. *Biochim Biophys Acta, 1813*(11), 1965-1970. doi:10.1016/j.bbamcr.2011.03.013

Hay, N. (2016). Reprogramming glucose metabolism in cancer: can it be exploited for cancer therapy? *Nat Rev Cancer, 16*(10), 635-649. doi:10.1038/nrc.2016.77

Hernandez-Camacho, J. D., Bernier, M., Lopez-Lluch, G., & Navas, P. (2018). Coenzyme Q10 Supplementation in Aging and Disease. *Front Physiol, 9*, 44. doi:10.3389/fphys.2018.00044

Hers, H. G., & Van Schaftingen, E. (1982). Fructose 2,6-bisphosphate 2 years after its discovery. *Biochem J, 206*(1), 1-12.

Herzig, S., Raemy, E., Montessuit, S., Veuthey, J. L., Zamboni, N., Westermann, B., . . . Martinou, J. C. (2012). Identification and functional expression of the mitochondrial pyruvate carrier. *Science, 337*(6090), 93-96. doi:10.1126/science.1218530

Hirano, Y., Yoshida, M., Shimizu, M., & Sato, R. (2001). Direct demonstration of rapid degradation of nuclear sterol regulatory element-binding proteins by the ubiquitin-proteasome pathway. *J Biol Chem, 276*(39), 36431-36437. doi:10.1074/jbc.M105200200

Hitosugi, T., Fan, J., Chung, T. W., Lythgoe, K., Wang, X., Xie, J., . . . Chen, J. (2011). Tyrosine phosphorylation of mitochondrial pyruvate dehydrogenase kinase 1 is important for cancer metabolism. *Mol Cell, 44*(6), 864-877. doi:10.1016/j.molcel.2011.10.015

Hochberg, Y., & Benjamini, Y. (1990). More powerful procedures for multiple significance testing. *Stat Med, 9*(7), 811-818.

Holz, M. K., Ballif, B. A., Gygi, S. P., & Blenis, J. (2005). mTOR and S6K1 mediate assembly of the translation preinitiation complex through dynamic protein interchange and ordered phosphorylation events. *Cell, 123*(4), 569-580. doi:10.1016/j.cell.2005.10.024

Horn, H. F., & Vousden, K. H. (2007). Coping with stress: multiple ways to activate p53. *Oncogene, 26*(9), 1306-1316. doi:10.1038/sj.onc.1210263

Horton, J. D. (2002). Sterol regulatory element-binding proteins: transcriptional activators of lipid synthesis. *Biochem Soc Trans, 30*(Pt 6), 1091-1095. doi:10.1042/

Horton, J. D., Goldstein, J. L., & Brown, M. S. (2002a). SREBPs: activators of the complete program of cholesterol and fatty acid synthesis in the liver. *J Clin Invest, 109*(9), 1125-1131. doi:10.1172/JCI15593

Horton, J. D., Goldstein, J. L., & Brown, M. S. (2002b). SREBPs: transcriptional mediators of lipid homeostasis. *Cold Spring Harb Symp Quant Biol, 67*, 491-498.

Horton, J. D., Shah, N. A., Warrington, J. A., Anderson, N. N., Park, S. W., Brown, M. S., & Goldstein, J. L. (2003). Combined analysis of oligonucleotide microarray data from transgenic and knockout mice identifies direct SREBP target genes. *Proc Natl Acad Sci U S A, 100*(21), 12027-12032.

Hsieh, A. C., Liu, Y., Edlind, M. P., Ingolia, N. T., Janes, M. R., Sher, A., . . . Ruggero, D. (2012). The translational landscape of mTOR signalling steers cancer initiation and metastasis. *Nature, 485*(7396), 55-61. doi:10.1038/nature10912

Hua, X., Wu, J., Goldstein, J. L., Brown, M. S., & Hobbs, H. H. (1995). Structure of the human gene encoding sterol regulatory element binding protein-1 (SREBF1) and localization of SREBF1 and SREBF2 to chromosomes 17p11.2 and 22q13. *Genomics, 25*(3), 667-673.

Hua, X., Yokoyama, C., Wu, J., Briggs, M. R., Brown, M. S., Goldstein, J. L., & Wang, X. (1993). SREBP-2, a second basic-helix-loop-helix-leucine zipper protein that stimulates transcription by binding to a sterol regulatory element. *Proc Natl Acad Sci U S A, 90*(24), 11603-11607.

Huang, W. C., Li, X., Liu, J., Lin, J., & Chung, L. W. (2012). Activation of androgen receptor, lipogenesis, and oxidative stress converged by SREBP-1 is responsible for regulating growth and progression of prostate cancer cells. *Mol Cancer Res, 10*(1), 133-142. doi:10.1158/1541-7786.MCR-11-0206

Hughes, A. L., Todd, B. L., & Espenshade, P. J. (2005). SREBP pathway responds to sterols and functions as an oxygen sensor in fission yeast. *Cell, 120*(6), 831-842. doi:10.1016/j.cell.2005.01.012

Humpton, T. J., & Vousden, K. H. (2016). Regulation of Cellular Metabolism and Hypoxia by p53. *Cold Spring Harb Perspect Med, 6*(7). doi:10.1101/cshperspect.a026146

Hus, M., Grzasko, N., Szostek, M., Pluta, A., Helbig, G., Woszczyk, D., . . . Dmoszynska, A. (2011). Thalidomide, dexamethasone and lovastatin with autologous stem cell transplantation as a salvage immunomodulatory therapy in patients with relapsed and refractory multiple myeloma. *Ann Hematol, 90*(10), 1161-1166. doi:10.1007/s00277-011-1276-2

Im, S. S., Yousef, L., Blaschitz, C., Liu, J. Z., Edwards, R. A., Young, S. G., . . . Osborne, T. F. (2011). Linking lipid metabolism to the innate immune response in macrophages through sterol regulatory element binding protein-1a. *Cell Metab, 13*(5), 540-549. doi:10.1016/j.cmet.2011.04.001

Isaacs, J. S., Jung, Y. J., Mole, D. R., Lee, S., Torres-Cabala, C., Chung, Y. L., . . . Neckers, L. (2005). HIF overexpression correlates with biallelic loss of fumarate hydratase in renal cancer: novel role of fumarate in regulation of HIF stability. *Cancer Cell, 8*(2), 143-153. doi:10.1016/j.ccr.2005.06.017

Israelsen, W. J., Dayton, T. L., Davidson, S. M., Fiske, B. P., Hosios, A. M., Bellinger, G., . . . Vander Heiden, M. G. (2013). PKM2 isoform-specific deletion reveals a differential requirement for pyruvate kinase in tumor cells. *Cell, 155*(2), 397-409. doi:10.1016/j.cell.2013.09.025

Istvan, E. S., & Deisenhofer, J. (2001). Structural mechanism for statin inhibition of HMG-CoA reductase. *Science, 292*(5519), 1160-1164. doi:10.1126/science.1059344

Iyer, N. V., Kotch, L. E., Agani, F., Leung, S. W., Laughner, E., Wenger, R. H., . . . Semenza, G. L. (1998). Cellular and developmental control of O2 homeostasis by hypoxia-inducible factor 1 alpha. *Genes Dev, 12*(2), 149-162.

Jang, H. J., Hong, E. M., Jang, J., Choi, J. E., Park, S. W., Byun, H. W., . . . Lee, J. (2016). Synergistic Effects of Simvastatin and Irinotecan against Colon Cancer Cells with or without Irinotecan Resistance. *Gastroenterol Res Pract, 2016*, 7891374. doi:10.1155/2016/7891374

Jang, H. J., Hong, E. M., Kim, M., Kim, J. H., Jang, J., Park, S. W., . . . Lee, J. (2016). Simvastatin induces heme oxygenase-1 via NF-E2-related factor 2 (Nrf2) activation through ERK and PI3K/Akt pathway in colon cancer. *Oncotarget, 7*(29), 46219-46229. doi:10.18632/oncotarget.10078

Janowski, B. A., Grogan, M. J., Jones, S. A., Wisely, G. B., Kliewer, S. A., Corey, E. J., & Mangelsdorf, D. J. (1999). Structural requirements of ligands for the oxysterol liver X receptors LXRalpha and LXRbeta. *Proc Natl Acad Sci U S A, 96*(1), 266-271.

Jenkins, C. M., Yang, J., Sims, H. F., & Gross, R. W. (2011). Reversible high affinity inhibition of phosphofructokinase-1 by acyl-CoA: a mechanism integrating glycolytic flux with lipid metabolism. *J Biol Chem, 286*(14), 11937-11950. doi:10.1074/jbc.M110.203661

Jeon, T. I., & Osborne, T. F. (2012). SREBPs: metabolic integrators in physiology and metabolism. *Trends Endocrinol Metab, 23*(2), 65-72. doi:10.1016/j.tem.2011.10.004

Ji, H., Wu, G., Zhan, X., Nolan, A., Koh, C., De Marzo, A., . . . Zeller, K. I. (2011). Cell-type independent MYC target genes reveal a primordial signature involved in biomass accumulation. *PLoS One, 6*(10), e26057. doi:10.1371/journal.pone.0026057

Jiang, B. H., Semenza, G. L., Bauer, C., & Marti, H. H. (1996). Hypoxia-inducible factor 1 levels vary exponentially over a physiologically relevant range of O2 tension. *Am J Physiol, 271*(4 Pt 1), C1172-1180. doi:10.1152/ajpcell.1996.271.4.C1172

Jiang, P., Du, W., Mancuso, A., Wellen, K. E., & Yang, X. (2013). Reciprocal regulation of p53 and malic enzymes modulates metabolism and senescence. *Nature, 493*(7434), 689-693. doi:10.1038/nature11776

Jiang, P., Du, W., Wang, X., Mancuso, A., Gao, X., Wu, M., & Yang, X. (2011). p53 regulates biosynthesis through direct inactivation of glucose-6-phosphate dehydrogenase. *Nat Cell Biol, 13*(3), 310-316. doi:10.1038/ncb2172

Jones, M. E. (1980). Pyrimidine nucleotide biosynthesis in animals: genes, enzymes, and regulation of UMP biosynthesis. *Annu Rev Biochem, 49*, 253-279. doi:10.1146/annurev.bi.49.070180.001345

Jones, R. G., Plas, D. R., Kubek, S., Buzzai, M., Mu, J., Xu, Y., . . . Thompson, C. B. (2005). AMP-activated protein kinase induces a p53-dependent metabolic checkpoint. *Mol Cell, 18*(3), 283-293. doi:10.1016/j.molcel.2005.03.027

Jones, S. F., & Infante, J. R. (2015). Molecular Pathways: Fatty Acid Synthase. *Clin Cancer Res, 21*(24), 5434-5438. doi:10.1158/1078-0432.CCR-15-0126

Kallin, A., Johannessen, L. E., Cani, P. D., Marbehant, C. Y., Essaghir, A., Foufelle, F., . . . Demoulin, J. B. (2007). SREBP-1 regulates the expression of heme

oxygenase 1 and the phosphatidylinositol-3 kinase regulatory subunit p55 gamma. *J Lipid Res, 48*(7), 1628-1636. doi:10.1194/jlr.M700136-JLR200

Kamphorst, J. J., Chung, M. K., Fan, J., & Rabinowitz, J. D. (2014). Quantitative analysis of acetyl-CoA production in hypoxic cancer cells reveals substantial contribution from acetate. *Cancer Metab, 2*, 23. doi:10.1186/2049-3002-2-23

Kamphorst, J. J., Cross, J. R., Fan, J., de Stanchina, E., Mathew, R., White, E. P., . . . Rabinowitz, J. D. (2013). Hypoxic and Ras-transformed cells support growth by scavenging unsaturated fatty acids from lysophospholipids. *Proc Natl Acad Sci U S A, 110*(22), 8882-8887. doi:10.1073/pnas.1307237110

Kamphorst, J. J., Nofal, M., Commisso, C., Hackett, S. R., Lu, W., Grabocka, E., . . . Rabinowitz, J. D. (2015). Human pancreatic cancer tumors are nutrient poor and tumor cells actively scavenge extracellular protein. *Cancer Res, 75*(3), 544-553. doi:10.1158/0008-5472.CAN-14-2211

Kawauchi, K., Araki, K., Tobiume, K., & Tanaka, N. (2008). p53 regulates glucose metabolism through an IKK-NF-kappaB pathway and inhibits cell transformation. *Nat Cell Biol, 10*(5), 611-618. doi:10.1038/ncb1724

Kerscher, S. J., Okun, J. G., & Brandt, U. (1999). A single external enzyme confers alternative NADH:ubiquinone oxidoreductase activity in Yarrowia lipolytica. *J Cell Sci, 112 (Pt 14)*, 2347-2354.

Khoo, K. H., Verma, C. S., & Lane, D. P. (2014). Drugging the p53 pathway: understanding the route to clinical efficacy. *Nat Rev Drug Discov, 13*(3), 217-236. doi:10.1038/nrd4236

Kim, D., Pertea, G., Trapnell, C., Pimentel, H., Kelley, R., & Salzberg, S. L. (2013). TopHat2: accurate alignment of transcriptomes in the presence of insertions, deletions and gene fusions. *Genome Biol, 14*(4), R36. doi:10.1186/gb-2013-14-4-r36

Kim, H. J., Miyazaki, M., & Ntambi, J. M. (2002). Dietary cholesterol opposes PUFA-mediated repression of the stearoyl-CoA desaturase-1 gene by SREBP-1 independent mechanism. *J Lipid Res, 43*(10), 1750-1757.

Kim, J. B., Spotts, G. D., Halvorsen, Y. D., Shih, H. M., Ellenberger, T., Towle, H. C., & Spiegelman, B. M. (1995). Dual DNA binding specificity of ADD1/SREBP1 controlled by a single amino acid in the basic helix-loop-helix domain. *Mol Cell Biol, 15*(5), 2582-2588.

Kim, J. W., Tchernyshyov, I., Semenza, G. L., & Dang, C. V. (2006). HIF-1-mediated expression of pyruvate dehydrogenase kinase: a metabolic switch required for cellular adaptation to hypoxia. *Cell Metab, 3*(3), 177-185. doi:10.1016/j.cmet.2006.02.002

Kim, T. H., Leslie, P., & Zhang, Y. (2014). Ribosomal proteins as unrevealed caretakers for cellular stress and genomic instability. *Oncotarget, 5*(4), 860-871. doi:10.18632/oncotarget.1784

Kliewer, S. A., Sundseth, S. S., Jones, S. A., Brown, P. J., Wisely, G. B., Koble, C. S., . . . Lehmann, J. M. (1997). Fatty acids and eicosanoids regulate gene expression through direct interactions with peroxisome proliferator-activated receptors alpha and gamma. *Proc Natl Acad Sci U S A, 94*(9), 4318-4323.

Kluckova, K., Bezawork-Geleta, A., Rohlena, J., Dong, L., & Neuzil, J. (2013). Mitochondrial complex II, a novel target for anti-cancer agents. *Biochim Biophys Acta, 1827*(5), 552-564. doi:10.1016/j.bbabio.2012.10.015

Ko, Y. J., & Balk, S. P. (2004). Targeting steroid hormone receptor pathways in the treatment of hormone dependent cancers. *Curr Pharm Biotechnol, 5*(5), 459-470.

Kobayashi, A., Kang, M. I., Okawa, H., Ohtsuji, M., Zenke, Y., Chiba, T., . . . Yamamoto, M. (2004). Oxidative stress sensor Keap1 functions as an adaptor for Cul3-based E3 ligase to regulate proteasomal degradation of Nrf2. *Mol Cell Biol, 24*(16), 7130-7139. doi:10.1128/MCB.24.16.7130-7139.2004

Koivunen, P., Hirsila, M., Remes, A. M., Hassinen, I. E., Kivirikko, K. I., & Myllyharju, J. (2007). Inhibition of hypoxia-inducible factor (HIF) hydroxylases by citric acid cycle intermediates: possible links between cell metabolism and stabilization of HIF. *J Biol Chem, 282*(7), 4524-4532. doi:10.1074/jbc.M610415200

Kotzka, J., Lehr, S., Roth, G., Avci, H., Knebel, B., & Muller-Wieland, D. (2004). Insulin-activated Erk-mitogen-activated protein kinases phosphorylate sterol regulatory element-binding Protein-2 at serine residues 432 and 455 in vivo. *J Biol Chem, 279*(21), 22404-22411. doi:10.1074/jbc.M401198200

Kruiswijk, F., Labuschagne, C. F., & Vousden, K. H. (2015). p53 in survival, death and metabolic health: a lifeguard with a licence to kill. *Nat Rev Mol Cell Biol, 16*(7), 393-405. doi:10.1038/nrm4007

Kruse, J. P., & Gu, W. (2009). Modes of p53 regulation. *Cell, 137*(4), 609-622. doi:10.1016/j.cell.2009.04.050

Kuemmerle, N. B., Rysman, E., Lombardo, P. S., Flanagan, A. J., Lipe, B. C., Wells, W. A., . . . Kinlaw, W. B. (2011). Lipoprotein lipase links dietary fat to solid tumor cell proliferation. *Mol Cancer Ther, 10*(3), 427-436. doi:10.1158/1535-7163.MCT-10-0802

Kuhajda, F. P., Jenner, K., Wood, F. D., Hennigar, R. A., Jacobs, L. B., Dick, J. D., & Pasternack, G. R. (1994). Fatty acid synthesis: a potential selective target for antineoplastic therapy. *Proc Natl Acad Sci U S A, 91*(14), 6379-6383.

Kuiper, C., Dachs, G. U., Munn, D., Currie, M. J., Robinson, B. A., Pearson, J. F., & Vissers, M. C. (2014). Increased Tumor Ascorbate is Associated with Extended Disease-Free Survival and Decreased Hypoxia-Inducible Factor-1 Activation in Human Colorectal Cancer. *Front Oncol, 4*, 10. doi:10.3389/fonc.2014.00010

Kulawiec, M., Ayyasamy, V., & Singh, K. K. (2009). p53 regulates mtDNA copy number and mitocheckpoint pathway. *J Carcinog, 8*, 8. doi:10.4103/1477-3163.50893

Kuoppala, J., Lamminpaa, A., & Pukkala, E. (2008). Statins and cancer: A systematic review and meta-analysis. *Eur J Cancer, 44*(15), 2122-2132. doi:10.1016/j.ejca.2008.06.025

Lambert, A. J., & Brand, M. D. (2004). Inhibitors of the quinone-binding site allow rapid superoxide production from mitochondrial NADH:ubiquinone oxidoreductase (complex I). *J Biol Chem, 279*(38), 39414-39420. doi:10.1074/jbc.M406576200

Lane, A. N., & Fan, T. W. (2015). Regulation of mammalian nucleotide metabolism and biosynthesis. *Nucleic Acids Res, 43*(4), 2466-2485. doi:10.1093/nar/gkv047

Lane, D., & Levine, A. (2010). p53 Research: the past thirty years and the next thirty years. *Cold Spring Harb Perspect Biol, 2*(12), a000893. doi:10.1101/cshperspect.a000893

Langmead, B. (2010). Aligning short sequencing reads with Bowtie. *Curr Protoc Bioinformatics, Chapter 11*, Unit 11 17. doi:10.1002/0471250953.bi1107s32

Laredj, L. N., Licitra, F., & Puccio, H. M. (2014). The molecular genetics of coenzyme Q biosynthesis in health and disease. *Biochimie, 100*, 78-87. doi:10.1016/j.biochi.2013.12.006

Lebedeva, M. A., Eaton, J. S., & Shadel, G. S. (2009). Loss of p53 causes mitochondrial DNA depletion and altered mitochondrial reactive oxygen species homeostasis. *Biochim Biophys Acta, 1787*(5), 328-334. doi:10.1016/j.bbabio.2009.01.004

Lenaz, G., Parenti Castelli, G., Fato, D'Aurelio, M., Bovina, C., Formiggini, G., . . . Rauchova, H. (1997). Coenzyme Q deficiency in mitochondria: kinetic saturation versus physical saturation. *Mol Aspects Med, 18 Suppl*, S25-31.

Leszczynska, K. B., Foskolou, I. P., Abraham, A. G., Anbalagan, S., Tellier, C., Haider, S., . . . Hammond, E. M. (2015). Hypoxia-induced p53 modulates both apoptosis and radiosensitivity via AKT. *J Clin Invest, 125*(6), 2385-2398. doi:10.1172/JCI80402

Lewis, C. A., Brault, C., Peck, B., Bensaad, K., Griffiths, B., Mitter, R., . . . Schulze, A. (2015). SREBP maintains lipid biosynthesis and viability of cancer cells under lipid- and oxygen-deprived conditions and defines a gene signature associated with poor survival in glioblastoma multiforme. *Oncogene, 34*(40), 5128-5140. doi:10.1038/onc.2014.439

Li, H. Y., Appelbaum, F. R., Willman, C. L., Zager, R. A., & Banker, D. E. (2003). Cholesterol-modulating agents kill acute myeloid leukemia cells and sensitize them to therapeutics by blocking adaptive cholesterol responses. *Blood, 101*(9), 3628-3634. doi:10.1182/blood-2002-07-2283

Li, J., Bosch-Marce, M., Nanayakkara, A., Savransky, V., Fried, S. K., Semenza, G. L., & Polotsky, V. Y. (2006). Altered metabolic responses to intermittent hypoxia in mice with partial deficiency of hypoxia-inducible factor-1alpha. *Physiol Genomics, 25*(3), 450-457. doi:10.1152/physiolgenomics.00293.2005

Li, M., Luo, J., Brooks, C. L., & Gu, W. (2002). Acetylation of p53 inhibits its ubiquitination by Mdm2. *J Biol Chem, 277*(52), 50607-50611. doi:10.1074/jbc.C200578200

Li, Y., Xu, S., Mihaylova, M. M., Zheng, B., Hou, X., Jiang, B., . . . Zang, M. (2011). AMPK phosphorylates and inhibits SREBP activity to attenuate hepatic steatosis and atherosclerosis in diet-induced insulin-resistant mice. *Cell Metab, 13*(4), 376-388. doi:10.1016/j.cmet.2011.03.009

Liang, G., Yang, J., Horton, J. D., Hammer, R. E., Goldstein, J. L., & Brown, M. S. (2002). Diminished hepatic response to fasting/refeeding and liver X receptor agonists in mice with selective deficiency of sterol regulatory element-binding protein-1c. *J Biol Chem, 277*(11), 9520-9528. doi:10.1074/jbc.M111421200

Liang, J. T., Huang, K. C., Cheng, Y. M., Hsu, H. C., Cheng, A. L., Hsu, C. H., . . . Chang, K. J. (2002). P53 overexpression predicts poor chemosensitivity to high-dose 5-fluorouracil plus leucovorin chemotherapy for stage IV colorectal cancers after palliative bowel resection. *Int J Cancer, 97*(4), 451-457.

Liberzon, A., Birger, C., Thorvaldsdottir, H., Ghandi, M., Mesirov, J. P., & Tamayo, P. (2015). The Molecular Signatures Database (MSigDB) hallmark gene set collection. *Cell Syst, 1*(6), 417-425. doi:10.1016/j.cels.2015.12.004

Liberzon, A., Subramanian, A., Pinchback, R., Thorvaldsdottir, H., Tamayo, P., & Mesirov, J. P. (2011). Molecular signatures database (MSigDB) 3.0. *Bioinformatics, 27*(12), 1739-1740. doi:10.1093/bioinformatics/btr260

Lin, C. Y., Loven, J., Rahl, P. B., Paranal, R. M., Burge, C. B., Bradner, J. E., . . . Young, R. A. (2012). Transcriptional amplification in tumor cells with elevated c-Myc. *Cell, 151*(1), 56-67. doi:10.1016/j.cell.2012.08.026

Lin, R., Tao, R., Gao, X., Li, T., Zhou, X., Guan, K. L., . . . Lei, Q. Y. (2013). Acetylation stabilizes ATP-citrate lyase to promote lipid biosynthesis and tumor growth. *Mol Cell, 51*(4), 506-518. doi:10.1016/j.molcel.2013.07.002

Lin, Y. C., Lin, J. H., Chou, C. W., Chang, Y. F., Yeh, S. H., & Chen, C. C. (2008). Statins increase p21 through inhibition of histone deacetylase activity and release of promoter-associated HDAC1/2. *Cancer Res, 68*(7), 2375-2383. doi:10.1158/0008-5472.CAN-07-5807

Lindeboom, R. G., van Voorthuijsen, L., Oost, K. C., Rodriguez-Colman, M. J., Luna-Velez, M. V., Furlan, C., . . . Vermeulen, M. (2018). Integrative multi-omics analysis of intestinal organoid differentiation. *Mol Syst Biol, 14*(6), e8227. doi:10.15252/msb.20188227

Liu, C., & Lin, J. D. (2011). PGC-1 coactivators in the control of energy metabolism. *Acta Biochim Biophys Sin (Shanghai), 43*(4), 248-257. doi:10.1093/abbs/gmr007

Liu, J. C., Hao, W. R., Hsu, Y. P., Sung, L. C., Kao, P. F., Lin, C. F., . . . Wu, S. Y. (2016). Statins dose-dependently exert a significant chemopreventive effect on colon cancer in patients with chronic obstructive pulmonary disease: A population-based cohort study. *Oncotarget, 7*(40), 65270-65283. doi:10.18632/oncotarget.11263

Liu, X., Yuan, H., Niu, Y., Niu, W., & Fu, L. (2012). The role of AMPK/mTOR/S6K1 signaling axis in mediating the physiological process of exercise-induced insulin sensitization in skeletal muscle of C57BL/6 mice. *Biochim Biophys Acta, 1822*(11), 1716-1726. doi:10.1016/j.bbadis.2012.07.008

Lochhead, P., & Chan, A. T. (2013). Statins and colorectal cancer. *Clin Gastroenterol Hepatol, 11*(2), 109-118; quiz e113-104. doi:10.1016/j.cgh.2012.08.037

Longley, D. B., Boyer, J., Allen, W. L., Latif, T., Ferguson, P. R., Maxwell, P. J., . . . Johnston, P. G. (2002). The role of thymidylate synthase induction in modulating p53-regulated gene expression in response to 5-fluorouracil and antifolates. *Cancer Res, 62*(9), 2644-2649.

Longley, D. B., Harkin, D. P., & Johnston, P. G. (2003). 5-fluorouracil: mechanisms of action and clinical strategies. *Nat Rev Cancer, 3*(5), 330-338. doi:10.1038/nrc1074

Lowe, S. W., & Sherr, C. J. (2003). Tumor suppression by Ink4a-Arf: progress and puzzles. *Curr Opin Genet Dev, 13*(1), 77-83.

Lu, M., Wan, M., Leavens, K. F., Chu, Q., Monks, B. R., Fernandez, S., . . . Birnbaum, M. J. (2012). Insulin regulates liver metabolism in vivo in the absence of hepatic Akt and Foxo1. *Nat Med, 18*(3), 388-395. doi:10.1038/nm.2686

Lunt, S. Y., & Vander Heiden, M. G. (2011). Aerobic glycolysis: meeting the metabolic requirements of cell proliferation. *Annu Rev Cell Dev Biol, 27*, 441-464. doi:10.1146/annurev-cellbio-092910-154237

Luo, J., Nikolaev, A. Y., Imai, S., Chen, D., Su, F., Shiloh, A., . . . Gu, W. (2001). Negative control of p53 by Sir2alpha promotes cell survival under stress. *Cell, 107*(2), 137-148.

Maddocks, O. D., Berkers, C. R., Mason, S. M., Zheng, L., Blyth, K., Gottlieb, E., & Vousden, K. H. (2013). Serine starvation induces stress and p53-dependent

metabolic remodelling in cancer cells. *Nature, 493*(7433), 542-546. doi:10.1038/nature11743

Manalo, D. J., Rowan, A., Lavoie, T., Natarajan, L., Kelly, B. D., Ye, S. Q., . . . Semenza, G. L. (2005). Transcriptional regulation of vascular endothelial cell responses to hypoxia by HIF-1. *Blood, 105*(2), 659-669. doi:10.1182/blood-2004-07-2958

Manning, B. D., & Cantley, L. C. (2007). AKT/PKB Signaling: Navigating Downstream. *Cell, 129*(7), 1261-1274.

Manning, B. D., & Toker, A. (2017). AKT/PKB Signaling: Navigating the Network. *Cell, 169*(3), 381-405. doi:10.1016/j.cell.2017.04.001

Marchiq, I., & Pouyssegur, J. (2016). Hypoxia, cancer metabolism and the therapeutic benefit of targeting lactate/H(+) symporters. *J Mol Med (Berl), 94*(2), 155-171. doi:10.1007/s00109-015-1307-x

Marine, J. C., Francoz, S., Maetens, M., Wahl, G., Toledo, F., & Lozano, G. (2006). Keeping p53 in check: essential and synergistic functions of Mdm2 and Mdm4. *Cell Death Differ, 13*(6), 927-934. doi:10.1038/sj.cdd.4401912

Martinez-Reyes, I., & Chandel, N. S. (2018). Acetyl-CoA-directed gene transcription in cancer cells. *Genes Dev, 32*(7-8), 463-465. doi:10.1101/gad.315168.118

Mashimo, T., Pichumani, K., Vemireddy, V., Hatanpaa, K. J., Singh, D. K., Sirasanagandla, S., . . . Bachoo, R. M. (2014). Acetate is a bioenergetic substrate for human glioblastoma and brain metastases. *Cell, 159*(7), 1603-1614. doi:10.1016/j.cell.2014.11.025

Mathupala, S. P., Heese, C., & Pedersen, P. L. (1997). Glucose catabolism in cancer cells. The type II hexokinase promoter contains functionally active response elements for the tumor suppressor p53. *J Biol Chem, 272*(36), 22776-22780. doi:10.1074/jbc.272.36.22776

Mayer, C., & Grummt, I. (2006). Ribosome biogenesis and cell growth: mTOR coordinates transcription by all three classes of nuclear RNA polymerases. *Oncogene, 25*(48), 6384-6391. doi:10.1038/sj.onc.1209883

McCleland, M. L., Adler, A. S., Shang, Y., Hunsaker, T., Truong, T., Peterson, D., . . . Firestein, R. (2012). An integrated genomic screen identifies LDHB as an essential gene for triple-negative breast cancer. *Cancer Res, 72*(22), 5812-5823. doi:10.1158/0008-5472.CAN-12-1098

McDonnell, E., Crown, S. B., Fox, D. B., Kitir, B., Ilkayeva, O. R., Olsen, C. A., . . . Hirschey, M. D. (2016). Lipids Reprogram Metabolism to Become a Major Carbon Source for Histone Acetylation. *Cell Rep, 17*(6), 1463-1472. doi:10.1016/j.celrep.2016.10.012

McManus, M. T., Petersen, C. P., Haines, B. B., Chen, J., & Sharp, P. A. (2002). Gene silencing using micro-RNA designed hairpins. *RNA, 8*(6), 842-850.

Menendez, J. A., & Lupu, R. (2007). Fatty acid synthase and the lipogenic phenotype in cancer pathogenesis. *Nat Rev Cancer, 7*(10), 763-777. doi:10.1038/nrc2222

Meraviglia, S., Eberl, M., Vermijlen, D., Todaro, M., Buccheri, S., Cicero, G., . . . Hayday, A. C. (2010). In vivo manipulation of Vgamma9Vdelta2 T cells with zoledronate and low-dose interleukin-2 for immunotherapy of advanced breast cancer patients. *Clin Exp Immunol, 161*(2), 290-297. doi:10.1111/j.1365-2249.2010.04167.x

Metallo, C. M., Gameiro, P. A., Bell, E. L., Mattaini, K. R., Yang, J., Hiller, K., . . . Stephanopoulos, G. (2011). Reductive glutamine metabolism by IDH1 mediates lipogenesis under hypoxia. *Nature, 481*(7381), 380-384. doi:10.1038/nature10602

Miltenberger, R. J., Sukow, K. A., & Farnham, P. J. (1995). An E-box-mediated increase in cad transcription at the G1/S-phase boundary is suppressed by inhibitory c-Myc mutants. *Mol Cell Biol, 15*(5), 2527-2535.

Minchenko, O. H., Ochiai, A., Opentanova, I. L., Ogura, T., Minchenko, D. O., Caro, J., . . . Esumi, H. (2005). Overexpression of 6-phosphofructo-2-kinase/fructose-2,6-bisphosphatase-4 in the human breast and colon malignant tumors. *Biochimie, 87*(11), 1005-1010. doi:10.1016/j.biochi.2005.04.007

Moon, S. H., Huang, C. H., Houlihan, S. L., Regunath, K., Freed-Pastor, W. A., Morris, J. P. t., . . . Prives, C. (2018). p53 Represses the Mevalonate Pathway to Mediate Tumor Suppression. *Cell*. doi:10.1016/j.cell.2018.11.011

Mor, I., Cheung, E. C., & Vousden, K. H. (2011). Control of glycolysis through regulation of PFK1: old friends and recent additions. *Cold Spring Harb Symp Quant Biol, 76*, 211-216. doi:10.1101/sqb.2011.76.010868

Mossmann, D., Park, S., & Hall, M. N. (2018). mTOR signalling and cellular metabolism are mutual determinants in cancer. *Nat Rev Cancer, 18*(12), 744-757. doi:10.1038/s41568-018-0074-8

Mullen, P. J., Yu, R., Longo, J., Archer, M. C., & Penn, L. Z. (2016). The interplay between cell signalling and the mevalonate pathway in cancer. *Nat Rev Cancer, 16*(11), 718-731. doi:10.1038/nrc.2016.76

Muller, P. A., & Vousden, K. H. (2013). p53 mutations in cancer. *Nat Cell Biol, 15*(1), 2-8. doi:10.1038/ncb2641

Munoz-Fontela, C., Macip, S., Martinez-Sobrido, L., Brown, L., Ashour, J., Garcia-Sastre, A., . . . Aaronson, S. A. (2008). Transcriptional role of p53 in interferon-mediated antiviral immunity. *J Exp Med, 205*(8), 1929-1938. doi:10.1084/jem.20080383

Murphy, M. P. (2009). How mitochondria produce reactive oxygen species. *Biochem J, 417*(1), 1-13. doi:10.1042/BJ20081386

Myant, K., Qiao, X., Halonen, T., Come, C., Laine, A., Janghorban, M., . . . Westermarck, J. (2015). Serine 62-Phosphorylated MYC Associates with Nuclear Lamins and Its Regulation by CIP2A Is Essential for Regenerative Proliferation. *Cell Rep, 12*(6), 1019-1031. doi:10.1016/j.celrep.2015.07.003

Narayanaswamy, P. B., Hodjat, M., Haller, H., Dumler, I., & Kiyan, Y. (2014). Loss of urokinase receptor sensitizes cells to DNA damage and delays DNA repair. *PLoS One, 9*(7), e101529. doi:10.1371/journal.pone.0101529

Nielsen, S. F., Nordestgaard, B. G., & Bojesen, S. E. (2013). Statin use and reduced cancer-related mortality. *N Engl J Med, 368*(6), 576-577. doi:10.1056/NEJMc1214827

Okada, N., Lin, C. P., Ribeiro, M. C., Biton, A., Lai, G., He, X., . . . He, L. (2014). A positive feedback between p53 and miR-34 miRNAs mediates tumor suppression. *Genes Dev, 28*(5), 438-450. doi:10.1101/gad.233585.113

Okar, D. A., & Lange, A. J. (1999). Fructose-2,6-bisphosphate and control of carbohydrate metabolism in eukaryotes. *Biofactors, 10*(1), 1-14.

Olson, K. A., Schell, J. C., & Rutter, J. (2016). Pyruvate and Metabolic Flexibility: Illuminating a Path Toward Selective Cancer Therapies. *Trends Biochem Sci, 41*(3), 219-230. doi:10.1016/j.tibs.2016.01.002

Osborne, T. F., & Espenshade, P. J. (2009). Evolutionary conservation and adaptation in the mechanism that regulates SREBP action: what a long, strange tRIP it's been. *Genes Dev, 23*(22), 2578-2591. doi:10.1101/gad.1854309

Ou, J., Tu, H., Shan, B., Luk, A., DeBose-Boyd, R. A., Bashmakov, Y., . . . Brown, M. S. (2001). Unsaturated fatty acids inhibit transcription of the sterol

regulatory element-binding protein-1c (SREBP-1c) gene by antagonizing ligand-dependent activation of the LXR. *Proc Natl Acad Sci U S A, 98*(11), 6027-6032. doi:10.1073/pnas.111138698

Owen, J. L., Zhang, Y., Bae, S. H., Farooqi, M. S., Liang, G., Hammer, R. E., . . . Brown, M. S. (2012). Insulin stimulation of SREBP-1c processing in transgenic rat hepatocytes requires p70 S6-kinase. *Proc Natl Acad Sci U S A, 109*(40), 16184-16189. doi:10.1073/pnas.1213343109

Owen, O. E., Kalhan, S. C., & Hanson, R. W. (2002). The key role of anaplerosis and cataplerosis for citric acid cycle function. *J Biol Chem, 277*(34), 30409-30412. doi:10.1074/jbc.R200006200

Padanad, M. S., Konstantinidou, G., Venkateswaran, N., Melegari, M., Rindhe, S., Mitsche, M., . . . Scaglioni, P. P. (2016). Fatty Acid Oxidation Mediated by Acyl-CoA Synthetase Long Chain 3 Is Required for Mutant KRAS Lung Tumorigenesis. *Cell Rep, 16*(6), 1614-1628. doi:10.1016/j.celrep.2016.07.009

Pampaloni, F., Reynaud, E. G., & Stelzer, E. H. (2007). The third dimension bridges the gap between cell culture and live tissue. *Nat Rev Mol Cell Biol, 8*(10), 839-845. doi:10.1038/nrm2236

Park, J. H., Zhuang, J., Li, J., & Hwang, P. M. (2016). p53 as guardian of the mitochondrial genome. *FEBS Lett, 590*(7), 924-934. doi:10.1002/1873-3468.12061

Parker, W. B., & Cheng, Y. C. (1990). Metabolism and mechanism of action of 5-fluorouracil. *Pharmacol Ther, 48*(3), 381-395.

Paton, C. M., & Ntambi, J. M. (2009). Biochemical and physiological function of stearoyl-CoA desaturase. *Am J Physiol Endocrinol Metab, 297*(1), E28-37. doi:10.1152/ajpendo.90897.2008

Patra, K. C., & Hay, N. (2014). The pentose phosphate pathway and cancer. *Trends Biochem Sci, 39*(8), 347-354. doi:10.1016/j.tibs.2014.06.005

Patra, K. C., Wang, Q., Bhaskar, P. T., Miller, L., Wang, Z., Wheaton, W., . . . Hay, N. (2013). Hexokinase 2 is required for tumor initiation and maintenance and its systemic deletion is therapeutic in mouse models of cancer. *Cancer Cell, 24*(2), 213-228. doi:10.1016/j.ccr.2013.06.014

Peck, B., & Schulze, A. (2016). Lipid desaturation - the next step in targeting lipogenesis in cancer? *FEBS J, 283*(15), 2767-2778. doi:10.1111/febs.13681

Perez-Escuredo, J., Van Hee, V. F., Sboarina, M., Falces, J., Payen, V. L., Pellerin, L., & Sonveaux, P. (2016). Monocarboxylate transporters in the brain and in cancer. *Biochim Biophys Acta, 1863*(10), 2481-2497. doi:10.1016/j.bbamcr.2016.03.013

Peterson, T. R., Sengupta, S. S., Harris, T. E., Carmack, A. E., Kang, S. A., Balderas, E., . . . Sabatini, D. M. (2011). mTOR complex 1 regulates lipin 1 localization to control the SREBP pathway. *Cell, 146*(3), 408-420. doi:S0092-8674(11)00709-4 [pii]
10.1016/j.cell.2011.06.034

Porstmann, T., Santos, C. R., Griffiths, B., Cully, M., Wu, M., Leevers, S., . . . Schulze, A. (2008). SREBP activity is regulated by mTORC1 and contributes to Akt-dependent cell growth. *Cell Metab, 8*(3), 224-236. doi:10.1016/j.cmet.2008.07.007

Punga, T., Bengoechea-Alonso, M. T., & Ericsson, J. (2006). Phosphorylation and ubiquitination of the transcription factor sterol regulatory element-binding protein-1 in response to DNA binding. *J Biol Chem, 281*(35), 25278-25286. doi:10.1074/jbc.M604983200

Qi, X. F., Kim, D. H., Yoon, Y. S., Kim, S. K., Cai, D. Q., Teng, Y. C., . . . Lee, K. J. (2010). Involvement of oxidative stress in simvastatin-induced apoptosis of murine CT26 colon carcinoma cells. *Toxicol Lett, 199*(3), 277-287. doi:10.1016/j.toxlet.2010.09.010

Qu, Q., Zeng, F., Liu, X., Wang, Q. J., & Deng, F. (2016). Fatty acid oxidation and carnitine palmitoyltransferase I: emerging therapeutic targets in cancer. *Cell Death Dis, 7*, e2226. doi:10.1038/cddis.2016.132

R. M. Sutherland, B. S., J. Bamat, H. Gabbert, B. BourrÃ¢t,and W. Mueller-Klieser. (1986). OxygÃ©nationand Differentiation in Multicellular Spheroids of Human

Colon Carcinoma1. *Cancer Research*.

Rabinovich, S., Adler, L., Yizhak, K., Sarver, A., Silberman, A., Agron, S., . . . Erez, A. (2015). Diversion of aspartate in ASS1-deficient tumours fosters de novo pyrimidine synthesis. *Nature, 527*(7578), 379-383. doi:10.1038/nature15529

Radhakrishnan, S. K., Lee, C. S., Young, P., Beskow, A., Chan, J. Y., & Deshaies, R. J. (2010). Transcription factor Nrf1 mediates the proteasome recovery pathway after proteasome inhibition in mammalian cells. *Mol Cell, 38*(1), 17-28. doi:10.1016/j.molcel.2010.02.029

Rankin, E. B., Rha, J., Selak, M. A., Unger, T. L., Keith, B., Liu, Q., & Haase, V. H. (2009). Hypoxia-inducible factor 2 regulates hepatic lipid metabolism. *Mol Cell Biol, 29*(16), 4527-4538. doi:10.1128/MCB.00200-09

Rauckhorst, A. J., & Taylor, E. B. (2016). Mitochondrial pyruvate carrier function and cancer metabolism. *Curr Opin Genet Dev, 38*, 102-109. doi:10.1016/j.gde.2016.05.003

Rawson, R. B. (2003). The SREBP pathway--insights from Insigs and insects. *Nat Rev Mol Cell Biol, 4*(8), 631-640. doi:10.1038/nrm1174

Reed, B. D., Charos, A. E., Szekely, A. M., Weissman, S. M., & Snyder, M. (2008). Genome-wide occupancy of SREBP1 and its partners NFY and SP1 reveals novel functional roles and combinatorial regulation of distinct classes of genes. *PLoS Genet, 4*(7), e1000133. doi:10.1371/journal.pgen.1000133

Reid, T., Oronsky, B., Scicinski, J., Scribner, C. L., Knox, S. J., Ning, S., . . . Infante, J. R. (2015). Safety and activity of RRx-001 in patients with advanced cancer: a first-in-human, open-label, dose-escalation phase 1 study. *Lancet Oncol, 16*(9), 1133-1142. doi:10.1016/S1470-2045(15)00089-3

Repa, J. J., Liang, G., Ou, J., Bashmakov, Y., Lobaccaro, J. M., Shimomura, I., . . . Mangelsdorf, D. J. (2000). Regulation of mouse sterol regulatory element-binding protein-1c gene (SREBP-1c) by oxysterol receptors, LXRalpha and LXRbeta. *Genes Dev, 14*(22), 2819-2830.

Ricoult, S. J., Yecies, J. L., Ben-Sahra, I., & Manning, B. D. (2016). Oncogenic PI3K and K-Ras stimulate de novo lipid synthesis through mTORC1 and SREBP. *Oncogene, 35*(10), 1250-1260. doi:10.1038/onc.2015.179

Ritzhaupt, A., Wood, I. S., Ellis, A., Hosie, K. B., & Shirazi-Beechey, S. P. (1998). Identification and characterization of a monocarboxylate transporter (MCT1) in pig and human colon: its potential to transport L-lactate as well as butyrate. *J Physiol, 513 (Pt 3)*, 719-732.

Robertson, H., Hayes, J. D., & Sutherland, C. (2018). A partnership with the proteasome; the destructive nature of GSK3. *Biochem Pharmacol, 147*, 77-92. doi:10.1016/j.bcp.2017.10.016

Robey, R. B., & Hay, N. (2009). Is Akt the "Warburg kinase"?-Akt-energy metabolism interactions and oncogenesis. *Semin Cancer Biol, 19*(1), 25-31. doi:10.1016/j.semcancer.2008.11.010

Robichon, C., Varret, M., Le Liepvre, X., Lasnier, F., Hajduch, E., Ferre, P., & Dugail, I. (2006). DnaJA4 is a SREBP-regulated chaperone involved in the cholesterol biosynthesis pathway. *Biochim Biophys Acta, 1761*(9), 1107-1113. doi:10.1016/j.bbalip.2006.07.007

Rodriguez-Colman, M. J., Schewe, M., Meerlo, M., Stigter, E., Gerrits, J., Pras-Raves, M., . . . Burgering, B. M. (2017). Interplay between metabolic identities in the intestinal crypt supports stem cell function. *Nature, 543*(7645), 424-427. doi:10.1038/nature21673

Rohrig, F., & Schulze, A. (2016). The multifaceted roles of fatty acid synthesis in cancer. *Nat Rev Cancer, 16*(11), 732-749. doi:10.1038/nrc.2016.89

Roongta, U. V., Pabalan, J. G., Wang, X., Ryseck, R. P., Fargnoli, J., Henley, B. J., . . . Rupnow, B. A. (2011). Cancer cell dependence on unsaturated fatty acids implicates stearoyl-CoA desaturase as a target for cancer therapy. *Mol Cancer Res, 9*(11), 1551-1561. doi:10.1158/1541-7786.MCR-11-0126

Ros, S., Floter, J., Kaymak, I., Da Costa, C., Houddane, A., Dubuis, S., . . . Schulze, A. (2017). 6-Phosphofructo-2-kinase/fructose-2,6-biphosphatase 4 is essential for p53-null cancer cells. *Oncogene, 36*(23), 3287-3299. doi:10.1038/onc.2016.477

Ros, S., Flöter, J., Kaymak, I., Da Costa, C., Houddane, A., Dubuis, S., . . . Schulze, A. (2017). 6-Phosphofructo-2-kinase/fructose-2,6-biphosphatase 4 is essential for p53-null cancer cells. *Oncogene*. doi:10.1038/onc.2016.477

Ros, S., Santos, C. R., Moco, S., Baenke, F., Kelly, G., Howell, M., . . . Schulze, A. (2012). Functional metabolic screen identifies 6-phosphofructo-2-kinase/fructose-2,6-biphosphatase 4 as an important regulator of prostate cancer cell survival. *Cancer Discov, 2*(4), 328-343. doi:10.1158/2159-8290.CD-11-0234

Ros, S., & Schulze, A. (2013). Balancing glycolytic flux: the role of 6-phosphofructo-2-kinase/fructose 2,6-bisphosphatases in cancer metabolism. *Cancer Metab, 1*(1), 8. doi:10.1186/2049-3002-1-8

Roth, G., Kotzka, J., Kremer, L., Lehr, S., Lohaus, C., Meyer, H. E., . . . Muller-Wieland, D. (2000). MAP kinases Erk1/2 phosphorylate sterol regulatory element-binding protein (SREBP)-1a at serine 117 in vitro. *J Biol Chem, 275*(43), 33302-33307. doi:10.1074/jbc.M005425200

Rutman, R. J., Cantarow, A., & Paschkis, K. E. (1954). Studies in 2-acetylaminofluorene carcinogenesis. III. The utilization of uracil-2-C14 by preneoplastic rat liver and rat hepatoma. *Cancer Res, 14*(2), 119-123.

Sakai, J., Nohturfft, A., Cheng, D., Ho, Y. K., Brown, M. S., & Goldstein, J. L. (1997). Identification of complexes between the COOH-terminal domains of sterol regulatory element-binding proteins (SREBPs) and SREBP cleavage-activating protein. *J Biol Chem, 272*(32), 20213-20221.

Sanchez, H. B., Yieh, L., & Osborne, T. F. (1995). Cooperation by sterol regulatory element-binding protein and Sp1 in sterol regulation of low density lipoprotein receptor gene. *J Biol Chem, 270*(3), 1161-1169.

Sanchez-Macedo, N., Feng, J., Faubert, B., Chang, N., Elia, A., Rushing, E. J., . . . Zaugg, K. (2013). Depletion of the novel p53-target gene carnitine palmitoyltransferase 1C delays tumor growth in the neurofibromatosis type I tumor model. *Cell Death Differ, 20*(4), 659-668. doi:10.1038/cdd.2012.168

Sansom, O. J., Meniel, V. S., Muncan, V., Phesse, T. J., Wilkins, J. A., Reed, K. R., . . . Clarke, A. R. (2007). Myc deletion rescues Apc deficiency in the small intestine. *Nature, 446*(7136), 676-679. doi:10.1038/nature05674

Santos, C. R., & Schulze, A. (2012). Lipid metabolism in cancer. *FEBS J, 279*(15), 2610-2623. doi:10.1111/j.1742-4658.2012.08644.x

Sarbassov, D. D., Guertin, D. A., Ali, S. M., & Sabatini, D. M. (2005). Phosphorylation and regulation of Akt/PKB by the rictor-mTOR complex. *Science, 307*(5712), 1098-1101. doi:10.1126/science.1106148

Sassano, A., & Platanias, L. C. (2008). Statins in tumor suppression. *Cancer Lett, 260*(1-2), 11-19. doi:10.1016/j.canlet.2007.11.036

Sato, R. (2009). SREBPs: protein interaction and SREBPs. *FEBS J, 276*(3), 622-627. doi:10.1111/j.1742-4658.2008.06807.x

Sato, R., Yang, J., Wang, X., Evans, M. J., Ho, Y. K., Goldstein, J. L., & Brown, M. S. (1994). Assignment of the membrane attachment, DNA binding, and transcriptional activation domains of sterol regulatory element-binding protein-1 (SREBP-1). *J Biol Chem, 269*(25), 17267-17273.

Sato, T., Stange, D. E., Ferrante, M., Vries, R. G., Van Es, J. H., Van den Brink, S., . . . Clevers, H. (2011). Long-term expansion of epithelial organoids from human colon, adenoma, adenocarcinoma, and Barrett's epithelium. *Gastroenterology, 141*(5), 1762-1772. doi:10.1053/j.gastro.2011.07.050

Sato, T., Vries, R. G., Snippert, H. J., van de Wetering, M., Barker, N., Stange, D. E., . . . Clevers, H. (2009). Single Lgr5 stem cells build crypt-villus structures in vitro without a mesenchymal niche. *Nature, 459*(7244), 262-265. doi:10.1038/nature07935

Saxton, R. A., & Sabatini, D. M. (2017). mTOR Signaling in Growth, Metabolism, and Disease. *Cell, 168*(6), 960-976. doi:10.1016/j.cell.2017.02.004

Scheid, M. P., & Woodgett, J. R. (2001). PKB/AKT: functional insights from genetic models. *Nat Rev Mol Cell Biol, 2*(10), 760-768. doi:10.1038/35096067

Schug, Z. T., Peck, B., Jones, D. T., Zhang, Q., Grosskurth, S., Alam, I. S., . . . Gottlieb, E. (2015). Acetyl-CoA synthetase 2 promotes acetate utilization and maintains cancer cell growth under metabolic stress. *Cancer Cell, 27*(1), 57-71. doi:10.1016/j.ccell.2014.12.002

Schug, Z. T., Vande Voorde, J., & Gottlieb, E. (2016). The metabolic fate of acetate in cancer. *Nat Rev Cancer, 16*(11), 708-717. doi:10.1038/nrc.2016.87

Schwartzenberg-Bar-Yoseph, F. (2004). The Tumor Suppressor p53 Down-Regulates Glucose Transporters GLUT1 and GLUT4 Gene Expression. *Cancer Research, 64*(7), 2627-2633. doi:10.1158/0008-5472.can-03-0846

Scortegagna, M., Cataisson, C., Martin, R. J., Hicklin, D. J., Schreiber, R. D., Yuspa, S. H., & Arbeit, J. M. (2008). HIF-1alpha regulates epithelial inflammation by cell autonomous NFkappaB activation and paracrine stromal remodeling. *Blood, 111*(7), 3343-3354. doi:10.1182/blood-2007-10-115758

Sehdev, A., Shih, Y. C., Huo, D., Vekhter, B., Lyttle, C., & Polite, B. (2014). The role of statins for primary prevention in non-elderly colorectal cancer patients. *Anticancer Res, 34*(9), 5043-5050.

Selak, M. A., Armour, S. M., MacKenzie, E. D., Boulahbel, H., Watson, D. G., Mansfield, K. D., . . . Gottlieb, E. (2005). Succinate links TCA cycle dysfunction to oncogenesis by inhibiting HIF-alpha prolyl hydroxylase. *Cancer Cell, 7*(1), 77-85. doi:10.1016/j.ccr.2004.11.022

Semenza, G. L. (2012). Hypoxia-inducible factors in physiology and medicine. *Cell, 148*(3), 399-408. doi:S0092-8674(12)00087-6 [pii]

10.1016/j.cell.2012.01.021
Semenza, G. L., Jiang, B. H., Leung, S. W., Passantino, R., Concordet, J. P., Maire, P., & Giallongo, A. (1996). Hypoxia response elements in the aldolase A, enolase 1, and lactate dehydrogenase A gene promoters contain essential binding sites for hypoxia-inducible factor 1. *J Biol Chem, 271*(51), 32529-32537.
Sengupta, S., & Harris, C. C. (2005). p53: traffic cop at the crossroads of DNA repair and recombination. *Nat Rev Mol Cell Biol, 6*(1), 44-55. doi:10.1038/nrm1546
Senkowski, W., Jarvius, M., Rubin, J., Lengqvist, J., Gustafsson, M. G., Nygren, P., . . . Fryknas, M. (2016). Large-Scale Gene Expression Profiling Platform for Identification of Context-Dependent Drug Responses in Multicellular Tumor Spheroids. *Cell Chem Biol, 23*(11), 1428-1438. doi:10.1016/j.chembiol.2016.09.013
Seo, Y. K., Jeon, T. I., Chong, H. K., Biesinger, J., Xie, X., & Osborne, T. F. (2011). Genome-wide localization of SREBP-2 in hepatic chromatin predicts a role in autophagy. *Cell Metab, 13*(4), 367-375. doi:10.1016/j.cmet.2011.03.005
Sermeus, A., & Michiels, C. (2011). Reciprocal influence of the p53 and the hypoxic pathways. *Cell Death Dis, 2*, e164. doi:10.1038/cddis.2011.48
Shadfan, M., Lopez-Pajares, V., & Yuan, Z. M. (2012). MDM2 and MDMX: Alone and together in regulation of p53. *Transl Cancer Res, 1*(2), 88-89.
Shah, S., Carriveau, W. J., Li, J., Campbell, S. L., Kopinski, P. K., Lim, H. W., . . . Wellen, K. E. (2016). Targeting ACLY sensitizes castration-resistant prostate cancer cells to AR antagonism by impinging on an ACLY-AMPK-AR feedback mechanism. *Oncotarget, 7*(28), 43713-43730. doi:10.18632/oncotarget.9666
Shamma, A., Takegami, Y., Miki, T., Kitajima, S., Noda, M., Obara, T., . . . Takahashi, C. (2009). Rb Regulates DNA damage response and cellular senescence through E2F-dependent suppression of N-ras isoprenylation. *Cancer Cell, 15*(4), 255-269. doi:10.1016/j.ccr.2009.03.001
Shao, W., & Espenshade, P. J. (2012). Expanding roles for SREBP in metabolism. *Cell Metab, 16*(4), 414-419. doi:10.1016/j.cmet.2012.09.002
Shaw, R. J., Bardeesy, N., Manning, B. D., Lopez, L., Kosmatka, M., DePinho, R. A., & Cantley, L. C. (2004). The LKB1 tumor suppressor negatively regulates mTOR signaling. *Cancer Cell, 6*(1), 91-99. doi:10.1016/j.ccr.2004.06.007
Shimano, H., Horton, J. D., Shimomura, I., Hammer, R. E., Brown, M. S., & Goldstein, J. L. (1997). Isoform 1c of sterol regulatory element binding protein is less active than isoform 1a in livers of transgenic mice and in cultured cells. *J Clin Invest, 99*(5), 846-854. doi:10.1172/JCI119248
Shimano, H., & Sato, R. (2017). SREBP-regulated lipid metabolism: convergent physiology - divergent pathophysiology. *Nat Rev Endocrinol, 13*(12), 710-730. doi:10.1038/nrendo.2017.91
Shimano, H., Shimomura, I., Hammer, R. E., Herz, J., Goldstein, J. L., Brown, M. S., & Horton, J. D. (1997). Elevated levels of SREBP-2 and cholesterol synthesis in livers of mice homozygous for a targeted disruption of the SREBP-1 gene. *J Clin Invest, 100*(8), 2115-2124. doi:10.1172/JCI119746
Siegel, R. L., Miller, K. D., & Jemal, A. (2016). Cancer statistics, 2016. *CA Cancer J Clin, 66*(1), 7-30. doi:10.3322/caac.21332
Sims, D., Mendes-Pereira, A. M., Frankum, J., Burgess, D., Cerone, M. A., Lombardelli, C., . . . Lord, C. J. (2011). High-throughput RNA interference

screening using pooled shRNA libraries and next generation sequencing. *Genome Biol, 12*(10), R104. doi:10.1186/gb-2011-12-10-r104

Singh, A., Boldin-Adamsky, S., Thimmulappa, R. K., Rath, S. K., Ashush, H., Coulter, J., . . . Biswal, S. (2008). RNAi-mediated silencing of nuclear factor erythroid-2-related factor 2 gene expression in non-small cell lung cancer inhibits tumor growth and increases efficacy of chemotherapy. *Cancer Res, 68*(19), 7975-7984. doi:10.1158/0008-5472.CAN-08-1401

Sorrentino, G., Ruggeri, N., Specchia, V., Cordenonsi, M., Mano, M., Dupont, S., . . . Del Sal, G. (2014). Metabolic control of YAP and TAZ by the mevalonate pathway. *Nat Cell Biol, 16*(4), 357-366. doi:10.1038/ncb2936

Soussi, T. (2007). p53 alterations in human cancer: more questions than answers. *Oncogene, 26*(15), 2145-2156. doi:10.1038/sj.onc.1210280

Stambolsky, P., Weisz, L., Shats, I., Klein, Y., Goldfinger, N., Oren, M., & Rotter, V. (2006). Regulation of AIF expression by p53. *Cell Death Differ, 13*(12), 2140-2149. doi:10.1038/sj.cdd.4401965

Steffen, J., Seeger, M., Koch, A., & Kruger, E. (2010). Proteasomal degradation is transcriptionally controlled by TCF11 via an ERAD-dependent feedback loop. *Mol Cell, 40*(1), 147-158. doi:10.1016/j.molcel.2010.09.012

Stockwell, B. R., Friedmann Angeli, J. P., Bayir, H., Bush, A. I., Conrad, M., Dixon, S. J., . . . Zhang, D. D. (2017). Ferroptosis: A Regulated Cell Death Nexus Linking Metabolism, Redox Biology, and Disease. *Cell, 171*(2), 273-285. doi:10.1016/j.cell.2017.09.021

Subramanian, A., Tamayo, P., Mootha, V. K., Mukherjee, S., Ebert, B. L., Gillette, M. A., . . . Mesirov, J. P. (2005). Gene set enrichment analysis: a knowledge-based approach for interpreting genome-wide expression profiles. *Proc Natl Acad Sci U S A, 102*(43), 15545-15550. doi:10.1073/pnas.0506580102

Sugimoto, Y., Whitman, M., Cantley, L. C., & Erikson, R. L. (1984). Evidence that the Rous sarcoma virus transforming gene product phosphorylates phosphatidylinositol and diacylglycerol. *Proc Natl Acad Sci U S A, 81*(7), 2117-2121.

Sullivan, L. B., Gui, D. Y., Hosios, A. M., Bush, L. N., Freinkman, E., & Vander Heiden, M. G. (2015). Supporting Aspartate Biosynthesis Is an Essential Function of Respiration in Proliferating Cells. *Cell, 162*(3), 552-563. doi:10.1016/j.cell.2015.07.017

Sun, L. P., Li, L., Goldstein, J. L., & Brown, M. S. (2005). Insig required for sterol-mediated inhibition of Scap/SREBP binding to COPII proteins in vitro. *J Biol Chem, 280*(28), 26483-26490. doi:10.1074/jbc.M504041200

Sun, R. C., & Denko, N. C. (2014). Hypoxic regulation of glutamine metabolism through HIF1 and SIAH2 supports lipid synthesis that is necessary for tumor growth. *Cell Metab, 19*(2), 285-292. doi:10.1016/j.cmet.2013.11.022

Sundqvist, A., Bengoechea-Alonso, M. T., Ye, X., Lukiyanchuk, V., Jin, J., Harper, J. W., & Ericsson, J. (2005). Control of lipid metabolism by phosphorylation-dependent degradation of the SREBP family of transcription factors by SCF(Fbw7). *Cell Metab, 1*(6), 379-391. doi:10.1016/j.cmet.2005.04.010

Sundqvist, A., & Ericsson, J. (2003). Transcription-dependent degradation controls the stability of the SREBP family of transcription factors. *Proc Natl Acad Sci U S A, 100*(24), 13833-13838. doi:10.1073/pnas.2335135100

Swamy, M. V., Patlolla, J. M., Steele, V. E., Kopelovich, L., Reddy, B. S., & Rao, C. V. (2006). Chemoprevention of familial adenomatous polyposis by low doses of atorvastatin and celecoxib given individually and in combination to

APCMin mice. *Cancer Res, 66*(14), 7370-7377. doi:10.1158/0008-5472.CAN-05-4619

Swinnen, J. V., Brusselmans, K., & Verhoeven, G. (2006). Increased lipogenesis in cancer cells: new players, novel targets. *Curr Opin Clin Nutr Metab Care, 9*(4), 358-365. doi:10.1097/01.mco.0000232894.28674.30

Tajan, M., Hock, A. K., Blagih, J., Robertson, N. A., Labuschagne, C. F., Kruiswijk, F., . . . Vousden, K. H. (2018). A Role for p53 in the Adaptation to Glutamine Starvation through the Expression of SLC1A3. *Cell Metab*. doi:10.1016/j.cmet.2018.07.005

Takaoka, A., Hayakawa, S., Yanai, H., Stoiber, D., Negishi, H., Kikuchi, H., . . . Taniguchi, T. (2003). Integration of interferon-alpha/beta signalling to p53 responses in tumour suppression and antiviral defence. *Nature, 424*(6948), 516-523. doi:10.1038/nature01850

Taylor, C. T. (2008). Interdependent roles for hypoxia inducible factor and nuclear factor-kappaB in hypoxic inflammation. *J Physiol, 586*(17), 4055-4059. doi:10.1113/jphysiol.2008.157669

Thewke, D. P., Panini, S. R., & Sinensky, M. (1998). Oleate potentiates oxysterol inhibition of transcription from sterol regulatory element-1-regulated promoters and maturation of sterol regulatory element-binding proteins. *J Biol Chem, 273*(33), 21402-21407.

Thorpe, L. M., Yuzugullu, H., & Zhao, J. J. (2015). PI3K in cancer: divergent roles of isoforms, modes of activation and therapeutic targeting. *Nat Rev Cancer, 15*(1), 7-24. doi:10.1038/nrc3860

Thurnher, M., Nussbaumer, O., & Gruenbacher, G. (2012). Novel aspects of mevalonate pathway inhibitors as antitumor agents. *Clin Cancer Res, 18*(13), 3524-3531. doi:10.1158/1078-0432.CCR-12-0489

Tomlinson, I. P., Alam, N. A., Rowan, A. J., Barclay, E., Jaeger, E. E., Kelsell, D., . . . Multiple Leiomyoma, C. (2002). Germline mutations in FH predispose to dominantly inherited uterine fibroids, skin leiomyomata and papillary renal cell cancer. *Nat Genet, 30*(4), 406-410. doi:10.1038/ng849

Valvezan, A. J., Turner, M., Belaid, A., Lam, H. C., Miller, S. K., McNamara, M. C., . . . Manning, B. D. (2017). mTORC1 Couples Nucleotide Synthesis to Nucleotide Demand Resulting in a Targetable Metabolic Vulnerability. *Cancer Cell, 32*(5), 624-638 e625. doi:10.1016/j.ccell.2017.09.013

Valvona, C. J., Fillmore, H. L., Nunn, P. B., & Pilkington, G. J. (2016). The Regulation and Function of Lactate Dehydrogenase A: Therapeutic Potential in Brain Tumor. *Brain Pathol, 26*(1), 3-17. doi:10.1111/bpa.12299

van der Vos, K. E., & Coffer, P. J. (2011). The extending network of FOXO transcriptional target genes. *Antioxid Redox Signal, 14*(4), 579-592. doi:10.1089/ars.2010.3419

Vander Heiden, M. G., Cantley, L. C., & Thompson, C. B. (2009). Understanding the Warburg effect: the metabolic requirements of cell proliferation. *Science, 324*(5930), 1029-1033. doi:10.1126/science.1160809

Vander Heiden, M. G., Locasale, J. W., Swanson, K. D., Sharfi, H., Heffron, G. J., Amador-Noguez, D., . . . Cantley, L. C. (2010). Evidence for an alternative glycolytic pathway in rapidly proliferating cells. *Science, 329*(5998), 1492-1499. doi:10.1126/science.1188015

Vanhaesebroeck, B., Stephens, L., & Hawkins, P. (2012). PI3K signalling: the path to discovery and understanding. *Nat Rev Mol Cell Biol, 13*(3), 195-203. doi:10.1038/nrm3290

Vassilev, L. T., Vu, B. T., Graves, B., Carvajal, D., Podlaski, F., Filipovic, Z., . . . Liu, E. A. (2004). In vivo activation of the p53 pathway by small-molecule antagonists of MDM2. *Science, 303*(5659), 844-848. doi:10.1126/science.1092472

Vegran, F., Rebucci, M., Chevrier, S., Cadouot, M., Boidot, R., & Lizard-Nacol, S. (2013). Only missense mutations affecting the DNA binding domain of p53 influence outcomes in patients with breast carcinoma. *PLoS One, 8*(1), e55103. doi:10.1371/journal.pone.0055103

Villunger, A., Michalak, E. M., Coultas, L., Mullauer, F., Bock, G., Ausserlechner, M. J., . . . Strasser, A. (2003). p53- and drug-induced apoptotic responses mediated by BH3-only proteins puma and noxa. *Science, 302*(5647), 1036-1038. doi:10.1126/science.1090072

Vivanco, I., & Sawyers, C. L. (2002). The phosphatidylinositol 3-Kinase AKT pathway in human cancer. *Nat Rev Cancer, 2*(7), 489-501. doi:10.1038/nrc839

Vousden, K. H., & Lane, D. P. (2007). p53 in health and disease. *Nat Rev Mol Cell Biol, 8*(4), 275-283. doi:10.1038/nrm2147

Vousden, K. H., & Prives, C. (2009). Blinded by the Light: The Growing Complexity of p53. *Cell, 137*(3), 413-431. doi:10.1016/j.cell.2009.04.037

Wade, M., Wang, Y. V., & Wahl, G. M. (2010). The p53 orchestra: Mdm2 and Mdmx set the tone. *Trends Cell Biol, 20*(5), 299-309. doi:10.1016/j.tcb.2010.01.009

Walker, A. K., Jacobs, R. L., Watts, J. L., Rottiers, V., Jiang, K., Finnegan, D. M., . . . Naar, A. M. (2011). A conserved SREBP-1/phosphatidylcholine feedback circuit regulates lipogenesis in metazoans. *Cell, 147*(4), 840-852. doi:10.1016/j.cell.2011.09.045

Walker, A. K., Yang, F., Jiang, K., Ji, J. Y., Watts, J. L., Purushotham, A., . . . Naar, A. M. (2010). Conserved role of SIRT1 orthologs in fasting-dependent inhibition of the lipid/cholesterol regulator SREBP. *Genes Dev, 24*(13), 1403-1417. doi:10.1101/gad.1901210

Wang, B. T., Ducker, G. S., Barczak, A. J., Barbeau, R., Erle, D. J., & Shokat, K. M. (2011). The mammalian target of rapamycin regulates cholesterol biosynthetic gene expression and exhibits a rapamycin-resistant transcriptional profile. *Proc Natl Acad Sci U S A, 108*(37), 15201-15206. doi:10.1073/pnas.1103746108

Wang, L., Xiong, H., Wu, F., Zhang, Y., Wang, J., Zhao, L., . . . Deng, Y. (2014). Hexokinase 2-mediated Warburg effect is required for PTEN- and p53-deficiency-driven prostate cancer growth. *Cell Rep, 8*(5), 1461-1474. doi:10.1016/j.celrep.2014.07.053

Wang, M., & Casey, P. J. (2016). Protein prenylation: unique fats make their mark on biology. *Nat Rev Mol Cell Biol, 17*(2), 110-122. doi:10.1038/nrm.2015.11

Wang, Y., & Hekimi, S. (2016). Understanding Ubiquinone. *Trends Cell Biol, 26*(5), 367-378. doi:10.1016/j.tcb.2015.12.007

Warburg, O. (1924). Über den Stoffwechsel der Carcinomzelle. *Die Naturwissenschaften, 12*(50), 1131-1137. doi:10.1007/bf01504608

Warburg, O. (1956). On the origin of cancer cells. *Science, 123*(3191), 309-314.

Webb, A. E., & Brunet, A. (2014). FOXO transcription factors: key regulators of cellular quality control. *Trends Biochem Sci, 39*(4), 159-169. doi:10.1016/j.tibs.2014.02.003

Weinberg, S. E., & Chandel, N. S. (2015). Targeting mitochondria metabolism for cancer therapy. *Nat Chem Biol, 11*(1), 9-15. doi:10.1038/nchembio.1712

West, M. J., Stoneley, M., & Willis, A. E. (1998). Translational induction of the c-myc oncogene via activation of the FRAP/TOR signalling pathway. *Oncogene, 17*(6), 769-780. doi:10.1038/sj.onc.1201990

Whitman, M., Kaplan, D. R., Schaffhausen, B., Cantley, L., & Roberts, T. M. (1985). Association of phosphatidylinositol kinase activity with polyoma middle-T competent for transformation. *Nature, 315*(6016), 239-242.

Williams, K. J., Argus, J. P., Zhu, Y., Wilks, M. Q., Marbois, B. N., York, A. G., . . . Bensinger, S. J. (2013). An essential requirement for the SCAP/SREBP signaling axis to protect cancer cells from lipotoxicity. *Cancer Res, 73*(9), 2850-2862. doi:10.1158/0008-5472.CAN-13-0382-T

Wilson, G. K., Tennant, D. A., & McKeating, J. A. (2014). Hypoxia inducible factors in liver disease and hepatocellular carcinoma: current understanding and future directions. *J Hepatol, 61*(6), 1397-1406. doi:10.1016/j.jhep.2014.08.025

Wise, D. R., Ward, P. S., Shay, J. E., Cross, J. R., Gruber, J. J., Sachdeva, U. M., . . . Thompson, C. B. (2011). Hypoxia promotes isocitrate dehydrogenase-dependent carboxylation of alpha-ketoglutarate to citrate to support cell growth and viability. *Proc Natl Acad Sci U S A, 108*(49), 19611-19616. doi:10.1073/pnas.1117773108

Wong, W. W., Dimitroulakos, J., Minden, M. D., & Penn, L. Z. (2002). HMG-CoA reductase inhibitors and the malignant cell: the statin family of drugs as triggers of tumor-specific apoptosis. *Leukemia, 16*(4), 508-519. doi:10.1038/sj.leu.2402476

Xiao, M., Yang, H., Xu, W., Ma, S., Lin, H., Zhu, H., . . . Guan, K. L. (2012). Inhibition of alpha-KG-dependent histone and DNA demethylases by fumarate and succinate that are accumulated in mutations of FH and SDH tumor suppressors. *Genes Dev, 26*(12), 1326-1338. doi:10.1101/gad.191056.112

Xiao, X., Huang, X., Ye, F., Chen, B., Song, C., Wen, J., . . . Xie, X. (2016). The miR-34a-LDHA axis regulates glucose metabolism and tumor growth in breast cancer. *Sci Rep, 6*, 21735. doi:10.1038/srep21735

Yabe, D., Brown, M. S., & Goldstein, J. L. (2002). Insig-2, a second endoplasmic reticulum protein that binds SCAP and blocks export of sterol regulatory element-binding proteins. *Proc Natl Acad Sci U S A, 99*(20), 12753-12758. doi:10.1073/pnas.162488899

Yahagi, N., Shimano, H., Hasegawa, K., Ohashi, K., Matsuzaka, T., Najima, Y., . . . Yamada, N. (2005). Co-ordinate activation of lipogenic enzymes in hepatocellular carcinoma. *Eur J Cancer, 41*(9), 1316-1322. doi:10.1016/j.ejca.2004.12.037

Yahagi, N., Shimano, H., Matsuzaka, T., Najima, Y., Sekiya, M., Nakagawa, Y., . . . Yamada, N. (2003). p53 Activation in adipocytes of obese mice. *J Biol Chem, 278*(28), 25395-25400. doi:10.1074/jbc.M302364200

Yalcin, A., Telang, S., Clem, B., & Chesney, J. (2009). Regulation of glucose metabolism by 6-phosphofructo-2-kinase/fructose-2,6-bisphosphatases in cancer. *Exp Mol Pathol, 86*(3), 174-179. doi:10.1016/j.yexmp.2009.01.003

Yamauchi, Y., & Rogers, M. A. (2018). Sterol Metabolism and Transport in Atherosclerosis and Cancer. *Front Endocrinol (Lausanne), 9*, 509. doi:10.3389/fendo.2018.00509

Yang, C., Ko, B., Hensley, C. T., Jiang, L., Wasti, A. T., Kim, J., . . . DeBerardinis, R. J. (2014). Glutamine oxidation maintains the TCA cycle and cell survival

during impaired mitochondrial pyruvate transport. *Mol Cell, 56*(3), 414-424. doi:10.1016/j.molcel.2014.09.025

Yang, J., Craddock, L., Hong, S., & Liu, Z. M. (2009). AMP-activated protein kinase suppresses LXR-dependent sterol regulatory element-binding protein-1c transcription in rat hepatoma McA-RH7777 cells. *J Cell Biochem, 106*(3), 414-426. doi:10.1002/jcb.22024

Yecies, J. L., Zhang, H. H., Menon, S., Liu, S., Yecies, D., Lipovsky, A. I., . . . Manning, B. D. (2011). Akt stimulates hepatic SREBP1c and lipogenesis through parallel mTORC1-dependent and independent pathways. *Cell Metab, 14*(1), 21-32. doi:10.1016/j.cmet.2011.06.002

Yeh, E., Cunningham, M., Arnold, H., Chasse, D., Monteith, T., Ivaldi, G., . . . Sears, R. (2004). A signalling pathway controlling c-Myc degradation that impacts oncogenic transformation of human cells. *Nat Cell Biol, 6*(4), 308-318. doi:10.1038/ncb1110

Yeung, S. J., Pan, J., & Lee, M. H. (2008). Roles of p53, MYC and HIF-1 in regulating glycolysis - the seventh hallmark of cancer. *Cell Mol Life Sci, 65*(24), 3981-3999. doi:10.1007/s00018-008-8224-x

Yokoyama, C., Wang, X., Briggs, M. R., Admon, A., Wu, J., Hua, X., . . . Brown, M. S. (1993). SREBP-1, a basic-helix-loop-helix-leucine zipper protein that controls transcription of the low density lipoprotein receptor gene. *Cell, 75*(1), 187-197.

Yoon, S., Woo, S. U., Kang, J. H., Kim, K., Kwon, M. H., Park, S., . . . Chwae, Y. J. (2010). STAT3 transcriptional factor activated by reactive oxygen species induces IL6 in starvation-induced autophagy of cancer cells. *Autophagy, 6*(8), 1125-1138.

Young, R. M., Ackerman, D., Quinn, Z. L., Mancuso, A., Gruber, M., Liu, L., . . . Simon, M. C. (2013). Dysregulated mTORC1 renders cells critically dependent on desaturated lipids for survival under tumor-like stress. *Genes Dev, 27*(10), 1115-1131. doi:10.1101/gad.198630.112

Zache, N., Lambert, J. M., Wiman, K. G., & Bykov, V. J. (2008). PRIMA-1MET inhibits growth of mouse tumors carrying mutant p53. *Cell Oncol, 30*(5), 411-418.

Zanet, J., Pibre, S., Jacquet, C., Ramirez, A., de Alboran, I. M., & Gandarillas, A. (2005). Endogenous Myc controls mammalian epidermal cell size, hyperproliferation, endoreplication and stem cell amplification. *J Cell Sci, 118*(Pt 8), 1693-1704. doi:10.1242/jcs.02298

Zaugg, K., Yao, Y., Reilly, P. T., Kannan, K., Kiarash, R., Mason, J., . . . Mak, T. W. (2011). Carnitine palmitoyltransferase 1C promotes cell survival and tumor growth under conditions of metabolic stress. *Genes Dev, 25*(10), 1041-1051. doi:10.1101/gad.1987211

Zhang, H. H., Lipovsky, A. I., Dibble, C. C., Sahin, M., & Manning, B. D. (2006). S6K1 regulates GSK3 under conditions of mTOR-dependent feedback inhibition of Akt. *Mol Cell, 24*(2), 185-197. doi:10.1016/j.molcel.2006.09.019

Zhang, N., Yin, Y., Xu, S. J., & Chen, W. S. (2008). 5-Fluorouracil: mechanisms of resistance and reversal strategies. *Molecules, 13*(8), 1551-1569.

Zhang, X., Fryknas, M., Hernlund, E., Fayad, W., De Milito, A., Olofsson, M. H., . . . Linder, S. (2014). Induction of mitochondrial dysfunction as a strategy for targeting tumour cells in metabolically compromised microenvironments. *Nat Commun, 5*, 3295. doi:10.1038/ncomms4295

Zhang, Y., & Manning, B. D. (2015). mTORC1 signaling activates NRF1 to increase cellular proteasome levels. *Cell Cycle, 14*(13), 2011-2017. doi:10.1080/15384101.2015.1044188

Zhang, Y., Nicholatos, J., Dreier, J. R., Ricoult, S. J., Widenmaier, S. B., Hotamisligil, G. S., . . . Manning, B. D. (2014). Coordinated regulation of protein synthesis and degradation by mTORC1. *Nature, 513*(7518), 440-443. doi:10.1038/nature13492

8 APPENDIX

8.1 Supplementary Tables

The following pages contain tables of selected gene sets that were significantly changed in the RNA-SEQ experiments.

A1: RNA-SEQ experiment that was performed in HCT116 p53+/+ and p53-/- cells cultured in monolayer, as spheroids and injected into xenograft mice subcutaneously

Table A1: Selected gene sets in the compared conditions HCT116 p53 +/+ monolayer vs spheroids

Regulation	Representative gene sets		
	Name (rank position)	NES	q-value
UP in MONOLAYER (p53 +/+)	Rosty Cervical cancer proliferation cluster (1)	3.73	<0.001
	Chang cycling genes(4)	3.56	<0.001
	Kegg cell cycle (136)	2.50	<0.001
UP in MCTS (p53 +/+)	Elvidge Hypoxia by DMOG up (1)	-3.40	<0.001
	Graham CML Quiscent vs Normal Dividing Up (162)	-2.40	<0.001
	Fridman Senescence Up (176)	-2.36	<0.001

Table A2: Selected gene sets in the compared conditions Compared conditions HCT116 p53 -/- monolayer vs spheroids

Regulation	Representative gene sets		
	Name (rank position)	NES	q-value
UP in MONOLAYER (p53 -/-)	Rosty Cervical cancer proliferation cluster (1)	3.26	<0.001
	Tang Senescence TP53 Targets Down (23)	2.87	<0.001
	Peng Glutamine Deprivation DN (129)	2.25	<0.001
UP in MCTS (p53 -/-)	Elvidge Hpoxia by DMOG Up (1)	-3.98	<0.001
	Harris Hypoxia (20)	-3.34	<0.001
	Dang Myc Targets DN (413)	-2.17	0.034

Table A3: Selected gene sets in the compared conditions HCT116 p53 +/+ monolayer vs subcutaneous tumours

Regulation	Representative gene sets		
	Name (rank position)	NES	q-value
UP IN P53 +/+ (MONOLAYER)	Hallmark E2F Targets (1)	5.67	<0.001
	Dang MYC Targets up (53)	3.82	<0.001
	Elvidge Hypoxia DN (215)	3.04	<0.001
UP IN P53 +/+ (TUMOUR)	Hecker IFNB1 Targets (1)	-2.42	<0.001
	Browne Interferon Responsive Genes (2)	-2.28	<0.001
	Zhang Interferon Response (12)	-2.13	<0.001

Table A4: Selected gene sets in the compared conditions HCT116 p53 -/- monolayer vs subcutaneous tumours

Regulation	Representative gene sets		
	Name (rank position)	NES	q-value
UP IN P53 -/- (MONOLAYER)	Hallmark E2F Targets (1)	5.40	<0.001
	Chang Cycling Genes (39)	3.93	<0.001
	Schuhmacher MYC Targets Up (72)	3.69	<0.001
UP IN P53 -/- (TUMOUR)	Reactome Interferon Alpha Beta Signaling (1)	-2.28	<0.001
	Fardin Hypoxia 11 (27)	-1.98	0.001
	Elvidge Hypoxia by DMOG UP	-1.97	0.001

Table A5: Selected gene sets in the compared conditions monolayer cultures of HCT116 p53 +/+ vs HCT116 p53 -/-

Regulation	Representative gene sets		
	Name (rank position)	NES	q-value
UP IN P53 +/+ (MONOLAYER)	Kerley Response to Cisplatin Up (1)	2.14	0.001
	PID P53 Downstream Pathway (8)	2.07	0.001
	Ongusaha TP53 Targets (11)	2.05	0.001
UP IN P53 -/- (MONOLAYER)	Gargalovic Response to Oxidized Phospholipids Yellow Up	-2.17	0.015
	Farmer Breast Cancer Cluster	-2.05	0.052
	Deposition of New Cenpa containing nucleosomes at the centromere	-2.03	0.043

Table A6: Selected gene sets in the compared conditions spheroid cultures of HCT116 p53 +/+ vs HCT116 p53 -/-

Regulation	Representative gene sets		
	Name (rank position)	NES	q-value
UP IN P53 +/+ (MCTS)	Browne Interferon Responsive genes (1)	2.38	<0.001
	Sana TNF Signaling Up (6)	2.20	<0.001
	Einav Interferon Signature in Cancer (14)	2.04	<0.001
UP IN P53 -/- (MCTS)	Horton SREBF Targets (5)	-2.64	<0.001
	Reactome Cholesterol Biosynthesis (9)	-2.49	<0.001
	Reactome Fatty Acyl Coa Biosynthesis (17)	-2.11	0.011

Table A7: Selected gene sets in the compared conditions subcutaneous tumours of HCT116 p53 +/+ vs HCT116 p53 -/-

Regulation	Representative gene sets		
	Name (rank position)	NES	q-value
UP IN P53 +/+ (TUMOUR)	Hallmark Interferon Alpha Response (1)	2.52	<0.001
	Browne Interferon Responsive Genes (2)	2.45	<0.001
	Der IFN Alpha Response Up (13)	2.03	<0.001
UP IN P53 -/- (TUMOUR)	Rickman Metastasis DN (1)	-2.30	0.001
	Reactome Cholesterol Biosynthesis (21)	-1.93	0.032
	Horton SREBF Targets (41)	-1.82	0.057

A2: RNA-SEQ experiment that was performed with HCT116 p53+/+ and p53-/- spheroids treated with control (DMSO), either with statin or statin and mevalonate

Table A8: Selected gene sets in the compared conditions HCT116 p53+/+ spheroids treated with statins compared to HCT116 p53 +/+ spheroids treated with DMSO

Regulation	Representative gene sets		
	Name (rank position)	NES	q-value
UP IN P53+/+	Hallmark Cholesterol Homeostasis (1)	2.96	<0.001
	Horton SREBP Targets (2)	2.89	<0.001
	Hallmark TNFA signaling via NFKB (26)	2.26	<0.001
DOWN IN P53+/+	Chang cycling (10)	3.26	<0.001
	KEGG Ribosome (14)	3.23	<0.001
	Hallmark MYC Targets (54)	2.82	<0.001

Table A9: Selected gene sets in the compared conditions HCT116 p53-/- spheroids treated with statins compared to HCT116 p53 -/- spheroids treated with DMSO

Regulation	Representative gene sets		
	Name (rank position)	NES	q-value
UP IN P53-/-	Horton SREBP Targets (3)	2.76	<0.001
	Hallmark Cholesterol Homeostasis (1)	2.74	<0.001
	Hallmark TNFA signaling via NFKB (19)	2.38	<0.001
DOWN IN P53-/-	Rosty Cervical Cancer Proliferation Cluster (2)	3.65	<0.001
	Reactome DNA Replication (35)	3.11	<0.001
	Yu MYC Targets up (103)	2.70	<0.001

Table A10: Selected gene sets in the compared conditions HCT116 p53+/+ spheroids treated with statins compared to HCT116 p53 -/- spheroids treated with spheroids

Regulation	Representative gene sets		
	Name (rank position)	NES	q-value
UP IN P53+/+	Browne Interferon Responsive Genes (1)	2.25	<0.001
	Hallmark Interferon Alpha Response (3)	2.20	<0.001
	Hallmark Interferon Gama Response (11)	2.12	<0.001
UP IN P53-/-	Reactome Respiratory Electron Transport (1)	2.76	<0.001
	KEGG Oxidative Phosphorylation (3)	2.59	<0.001
	SINGH NFE2L2 Targets (12)	2.25	<0.001

8.2 Abbreviations

4E-BP	eIF4E-binding protein
5-FU	5-Fluorouracil
ACC	acetyl-coA carboxylase
ACLY	ATP-citrate lyase
ACSS2	acetyl-coA synthetase 2
Akt/PBK	protein kinase B
AMP	adenosine mono-phosphate
AMPK	AMP-activated protein kinase
ATF6a	activating transcription factor 6
ATP	adenosine tri-phosphate
bHLH-Zip	basic helix-loop-helix-leucine zipper
BSA	bovine serum albumin
CA9	carbonic anhydrase
cDNA	complementary DNA
ChIP	chromatin immunoprecipitation
CoA	coenzyme A
CoQ10	ubiquinone
COPII	coat protein complex II
CPT1	carnitine palmitoyltransferase 1
DMEM	Dullbecco's modified eagle medium
DMSO	dimethylsulfoxide
EGF	epidermal growth factor
EGFR	EGF receptor
eIF4E	eukaryotic initiation factor 4E
ER	endoplasmic reticulum
EtOH	ethanol
FA	fatty acid
FABP	fatty acid binding protein
FASN	fatty acid synthase
FBS	foetal bovine serum
FFA	free fatty acids
flSREBP	full-length SREBP

FOXO	forkhead box other transcription factor
G6PD	glucose-6-phosphate dehydrogenase
GAP	GTPase activating protein
GBM	glioblastoma multiforme
GPAT	glycerol-3-phosphate acyltransferase
GPD1	glycerol-3-phosphate dehydrogenase 1
GSK3	glycogen synthase kinase 3
HDAC1	histone deacetylase complex 1
HIF1	hypoxia inducible factor 1
HMG-CoA	3-hydroxy-3-methylglutaryl-CoA
HMGCR	HMG-coA reductase
HMGCS	HMG-coA synthase
HRE	hypoxia response element
HRP	horseradish peroxidase
INSIG	insulin induced gene
LD	lipid droplet
LDH	lactate dehydrogenase
LDLR	low-density lipoprotein receptor
LXR	liver x receptor
MAPK	mitogen activated protein kinase
MCT	monocarboxylate transporter
ME	malic enzyme
MEV	mevastatin
mRNA	messenger RNA
MVL	mevalonate
mSREBP	mature SREBP
mTOR	mammalian target of rapamycin
mTORC1/2	mTOR complex 1/2
MUFA	monounsaturated fatty acid
NAC	N-Acetyl-Cysteine
NES	normalized enrichment score
OXPHOS	oxidative phosphorylation
PHD	prolyl hydroxylase
PI3K	phosphatidylinositol 3-kinase

PIP2	phosphatidylinositol-4,5-bisphosphate
PIP3	phosphatidylinositol-3,4,5-triphosphate
PPAR	peroxisome proliferator-activated receptor
PPP	pentose phosphate pathway
PRAS40	proline rich Akt substrate of 40kDA
PTEN	tensin homologue deleted on chromosome 10
PUFA	polyunsaturated fatty acid
qPCR	quantitative PCR
Rapa	rapamycin
Rheb	Ras homologue enriched in brain
RIP	regulated intramembrane proteolysis
RNAi	RNA interference
RPE	retinal pigment epithelial
ROS	reactive oxygen species
RT	room temperature
RTK	receptor tyrosine kinase
S1P	site-1 protease
S2P	site-2 protease
S6RB	ribosomal protein S6
S6K	ribosomal protein S6 kinase
SCAP	SREBP cleavage activating protein
SCD	stearoyl-coA desaturase
Seq	sequencing
SFA	saturated fatty acid
SH2	Src-homology 2
shRNA	short-hairpin RNA
siRNA	small interfering RNA
SIM	simvastatin
SIRT1	sirtuin 1
SRE	sterol regulatory element
SREBP	sterol regulatory element binding protein
SUMO	small ubiquitin-related modifier-1
TAG	triaclyglyceride
TCA cycle	tricarboxylic acid cycle

TSC1	tuberous sclerosis protein 1
TSC2	tuberous sclerosis protein 2
UMP	uridine monophosphate
VEGFA	vascular endothelial growth factor A
VHL	von Hippel Lindau

8.3 Acknowledgments

First of all, I would like to express my gratitude to Prof. Almut Schulze who gave me the opportunity to work in her group and guided me through my PhD with a lot of patience. Thanks for supporting me all the time and for the long discussions we had. I would also like to thank the members of my thesis committee, Dr. Mathias Rosenfeldt for supporting me for my scientific career and Prof. Thomas Rudel for agreeing to be in my thesis committee.
I acknowledge the Graduate School of Life Science (GSLS) for funding part of my PhD as a fellow student and Dr. Gabriele Blum-Oehler for giving me the opportunity to organise joyful events and supporting me as a female scientist.

This work would not be possible without help of Dr. Werner Schmitz. I really appreciate your help and your knowledge about biochemistry. I thank you a lot for all the great time in mass spec, for supporting me all the time when I get desperate about my favourite metabolite “Mevalonate” (?!).

Big thanks to the support of all present and past members of the Chair of Biochemistry and Molecular Biology.
I need to mention particularly some people:
Gabriele, I am really glad you found the way to the department, thanks for the time we spent together, for dealing with me all the time, for the antibodies, thanks my plus one, Therry for being crazy and especially for the zusammenfassung, guys Giacci, Carsten and Apo you will miss my complaining, Bea thanks for the help in the lab and listening to me all the time, Johanna, Sud, Master Markus thanks for the desperate-time discussions and help in calculations, Charis thanks for nothing☺, and Rosi for dealing with all the official tiring work and being so dynamic, lastly I will miss the FEIRABENDBIER a lot!!!
Special thanks to John for being English(!), critical proofreading and supporting me at the hardest part of this journey.

Annem, Babam, thank you very much for being my family and supporting me. I LOVE YOU!

8.4 Publications

1) Floter, J. *, **Kaymak, I. *,** Schulze, A. Regulation of Metabolic Activity by p53. *Metabolites* **7**, doi:10.3390/metabo7020021 (2017) *Contributed equally

2) Ros, S., Flöter, J., **Kaymak, I.**, Da Costa, C., Houddane, A., Dubuis, S., Griffiths, B., Mitter, R., Walz, S., Blake, S., Behrens, A., Brindle, KM., Zamboni, N., Rider, M.H. and *Schulze, A.*, (2017) 6-phosphofructo-2-kinase/fructose-2,6-biphosphatase4 is essential for p53-null cancer cells, Oncogene

3) **Kaymak, I.,** Schmitz, W., Dankworth, B., Maier C., Ade, C., Walz, S., Rosenfeldt, M., Kalogiouri, C., Campbell, A., Gay, D., McGregor, G., Sansom, O., Schulze, A. Mevalonate pathway provides ubiquinone to maintain pyrimidine synthesis and survival in p53-deficient cancer cells exposed to metabolic stress (in submission)

8.6 Affidavit

I hereby confirm that my thesis entitled 'Identification of metabolic liabilities in 3D models of cancer' is the result of my own work. I did not receive any help or support from commercial consultants. All sources and / or materials applied are listed and specified in the thesis.

Furthermore, I confirm that this thesis has not yet been submitted as part of another examination process neither in identical nor in similar form.

Place, Date Signature

Eidesstattliche Erklärung

Hiermit erkläre ich an Eides statt, die Dissertation "Untersuchung der Rolle von MYC als stress-reguliertes Protein" eigenständig, d.h. insbesondere selbständig und ohne Hilfe eines kommerziellen Promotionsberaters, angefertigt und keine anderen als die von mir angegebenen Quellen und Hilfsmittel verwendet zu haben.

Ich erkläre außerdem, dass die Dissertation weder in gleicher noch in ähnlicher Form bereits in einem anderen Prüfungsverfahren vorgelegen hat.

Ort, Datum Unterschrift